Modélisation et optimisation des procédés de polymérisation en émulsion et d'extrusion réactive pour le greffage sur polypropylène

Zheng-Hui Li

Ecole Doctorale Ressources
Procédés Produits
Environnement (RP2E)

Ecole Nationale
Supérieurs
des Industries Chimiqu

Laboratoire Réaction
et Génie des Procédés
(LRGP-CNRS)

Modélisation des Procédés de Polymérisation en Émulsion et d'Extrusion Réactive pour le Greffage sur Polypropylène

T H È S E

présentée in vue de l'obtention du

DOCTORAT DE L'UNIVERSITÉ DE LORRAINE

Spécialité: Génie des Procédés et des Produits

par

Zheng-Hui LI

Thèse soutenue publiquement le 7 Septembre 2012

Jury :

Président :	C A SERRA	-	Professeur (Université de Strasbourg)
Rapporteurs :	J-P PUAUX	-	Professeur (Université de Lyon)
	N S-OTHMAN	-	Chargée de recherches (CNRS (CR1))
Examinateurs :	G-H HU	-	Professeur (Université de Lorraine)
	J-P CORRIOU	-	Professeur (Université de Lorraine)

UNIVERSITÉ DE LORRAINE

Ecole Doctorale Ressources
Procédés Produits
Environnement (RP2E)

Ecole Nationale
Supérieurs
des Industries Chimiqu

ENSIC

Laboratoire Réaction
et Génie des Procédés
(LRGP-CNRS)

LRGP LABORATOIRE RÉACTIONS ET GÉNIE DES PROCÉDÉS

Modelling of Emulsion Polymerization and a Reactive Extrusion Process of Grafting of Polypropylene

P h D T H E S I S

In (Partial) Fulfillment of the Requirements for the Degree of

Doctor of Philosophy

at The University of Lorraine

Specialty : Chemical Engineering

Defended by

Zheng-Hui LI

defended on September, 2012

Jury :

Advisor :	Guo-Hua HU	-	University of Lorraine
	Jean-Pierre CORRIOU	-	University of Lorraine
President :	Christophe A. SERRA	-	University of Strasbourg
Reviewers :	Jean-Pierre PUAUX	-	University of Lyon
	Nida SHEIBAT-OTHMAN	-	CNRS (CR1)

Acknowledgement

I would like to thank all people who have helped and inspired me during my doctoral study.

I would like to express my deep and sincere gratitude to my advisor, Prof. Guo-Huo HU. His wide knowledge and his logical way of thinking have been of great value for me. His understanding, encouraging and personal guidance have provided a good basis for the present thesis.

I am deeply grateful to my advisor, Prof. Jean-Pierre CORRIOU. His perpetual energy and enthusiasm in research had motivated all his advisees, including me. In addition, he was always accessible and willing to help his students with their research. As a result, research life became smooth and rewarding for me.

I owe my most sincere gratitude to Prof. Christian FONTEIX, for his detailed and constructive comments, and for his important support throughout this work. His ideal and concept have had a remarkable influence on my entire research.

I wish to express my warm and sincere thanks to Prof. Liang-Fang Feng, Prof. Jia WU and Dr. Xiao-Ping HU, Zhejiang University China, who have been my teachers and mentors for many years. They offer advice and suggestions whenever I need them. Besides, without Prof. Liang-Fang Feng, I would not get the opportunity to join Ecole Nationale Supérieure des Industries Chimiques (ENSIC).

I warmly thank Dr. Sandrine HOPPE and Mr. Richard LAINE, for their valuable advice and friendly help. Their extensive discussions around my work and interesting explorations in operations have been very helpful for this study.

My sincere thanks are due to the official reviewers, Prof. Jean-Pierre PUAUX and Dr. Nida OTHMAN, for their detailed review, constructive criticism and excellent advice during the preparation of this thesis.

All my lab buddies at ENSIC made it a convivial place to work. In particular, I would like to thank Yuan Fang, Jin-Bai Zhang and Lei WANG for their friendship and help in the past three years. All other folks, including Tao-Tao FU, Jin-Biao Bao, Man LUO, Ahmed BHRAN, Sara RONASI, Itab YOUSSEF, have inspired me in research and life through our interactions during the long hours in the lab. Thanks. I cherished the friendships with Ming-Hui LEI, Ning YU, Ya-Jie LEI. I treasured all precious moments we shared and would really like to thank them.

My deepest gratitude goes to my family for their unflagging love and support throughout my life. I owe my loving thanks to my parents Tong-Hua LI and Xin-Jie ZHANG, my wife Ling-Li ZHANG, and my sister Xue LI. Without their encouragement and understanding, it would have been impossible for me to finish this work.

Furthermore, I especially want to thank DOW Corning Corporation, who provided the industrial project of grafting of silane onto polypropylene. The generous support of scholarship from China Scholarship Council (CSC) is greatly appreciated. Without their support, my ambition to study abroad can hardly be realized.

Résumé

Cette thèse se compose de deux parties, la Partie I, la modélisation théorique de la polymérisation en émulsion polymérisation et la Partie II, l'étude expérimentale et la modélisation de polypropylène greffé (PP) par extrusion réactive.

Dans la partie I, nous avons comparé les différences entre les polymérisations en macro- et mini- émulsion. Nous avons établi un modèle de polymérisation en macro-émulsion. Ce modèle peut prédire la distribution de la taille de la chaîne radicalaire pour une classe donnée de tailles des particules et la distribution des tailles des particules. Par comparaison, nous avons établi un modèle de polymérisation en mini-émulsion, fondé sur le bilan des potentiels chimiques du monomère dans le réacteur. Ce modèle peut fournir la distribution des tailles des particules et l'évolution des tailles des gouttelettes.

Dans la partie II, afin d'améliorer les propriétés du PP, deux types de monomères ont été utilisés pour être greffés sur PP par extrusion réactive. Ces monomères sont l'anhydride maléique MAH, qui peut modifier la polarité de la PP, et le silane, qui peut améliorer la résistance à la traction du PP. Pour améliorer le degré de greffage de MAH sur PP, la montmorillonite organiquement modifiée o-MMT a été utilisée comme un nanoréacteur. Les influences des quantités de MAH et d'initiateur ont été étudiées. Afin d'améliorer le degré de greffage du silane sur PP, les conditions opératoires ont été étudiées. Toutefois, une relation simple entre les propriétés du produit et les conditions de fonctionnement (vitesse d'alimentation Q, vitesse de la vis N, température du cylindre T) n'a pas pu être trouvée. Pour obtenir le montant le plus élevé de silane greffé sur PP, et en même temps, restreindre les deux réactions secondaires, c'est à dire la polymérisation du silane et la dégradation de la PP chaîne, une méthode d'optimisation multi-objectif a été essayée. Toutefois, en raison de la mauvaise répétabilité des expériences causée par des réactions complexes et les conditions opératoires dans l'extrudeuse, les modèles polynomiaux établis ne peuvent pas bien simuler le processus. Afin de réaliser l'optimisation multi-objectif de ce processus de manière satisfaisante, un procédé d'extrusion plus stable doit être mis au point.

Mots-Clefs: émulsion, polymérisation, mini-émulsion, modélisation, extrusion réactive, nanoréacteur, optimisation multi-objectif

Summary

This thesis consists of two parts: Part I, the theoretical modelling of emulsion polymerization and Part II, the experimental and modelling study of grafted polypropylene (PP) by reactive extrusion.

In Part I, the differences between macro-and mini-emulsion polymerization were compared. A model on macro-emulsion polymerization has been established. This model can predict the radical chain size distribution for a given class of particle sizes and the particle size distribution. By comparison, a model on mini-emulsion polymerization has been established, based on the balance of chemical potentials of the monomer in the reactor. This model can provide the particle size distribtution and the change of droplets size.

In Part II, in order to improve the properties of PP, two kinds of monomers were used to be grafted on PP by reactive extrusion. These monomers were maleic anhydride (MAH), which can modify the polarity of PP, and silane, which can improve the tensile strength of PP. To improve the grafting degree of MAH on PP, organically modified montmorillonite (MMT) was used as a nanoreactor. The effects of the amounts of MAH and the initiator was studied. In order to improve the grafting degree of silane on PP, the operating conditions were studied. However, a simple relation between the product properties and the operating conditions (feed rate Q, screw speed N, barrel temperature T) could not be found. To obtain the highest amount of silane grafted on PP, and meanwhile, restraining the two side reactions, i.e. the polymerization of silane and the PP chain degradation, a multi-objective optimization method was tried. However, because of the poor repeatability of experiments caused by the complex reactions and the operating conditions in the extruder, the polynomial models established could not well simulate the process. In order to obtain the multi-objective optimization of this process, a more stable extrusion process should be developed.

Keywords: emulsion polymerization, mini-emulsion polymerization, modelling, reactive extrusion, nanoreactor, Multi-objective optimization

Contents

Chapter 1

Résumé long

Les objectifs de ce travail sont:
1. la comparaison des macro- et mini- polymérisation en émulsion, et l'établissement d'un modèle théorique.
2. l'amélioration expérimentale des propriétés du polypropylène par extrusion réactive, puis la recherche des modèles statistiques de plan d'expérience.

1.1 Polymérisation en émulsion

Les émulsions sont des mélanges hétérogènes formés par un ou plusieurs composés organiques, l'eau, et des tensioactifs. Elles sont commercialisées depuis plus d'un demi-siècle. Les macro-émulsions, plus communément appelées émulsions, sont des émulsions classiques qui ont des tailles de gouttelettes de l'ordre de 1-10 microns. Elles sont rapidement séparés après repos. Les mini-émulsions sont constituées de gouttelettes submicroniques qui sont stabilisées par l'utilisation de co-stabilisants (également connus comme co-tensioactifs) et/ou des agents gonflants qui sont généralement des alcanes à chaîne longue ou des alcools gras. Les mini-émulsions peuvent être stables pendant des mois. En raison de la présence de co-stabilisant dans des mini-émulsions, la polymérisation en mini-émulsion suit un mécanisme différent de la polymérisation en macro-émulsion, car dans des mini-émulsions, les gouttelettes de monomères sont la source des particules, tandis que, dans la polymérisation en macro-émulsion, c'est le rôle de micelles ou de la phase aqueuse, et les gouttelettes sont considérées comme le réservoir du monomère.

Quantité d'efforts de recherche ont montré la différence entre ces deux types de polymérisations [Delgado and El-Aasser, 1990, Tang et al., 1991, Miller et al., 1995]. On a publié de nombreux modèles pour les polymérisations en émulsion et les polymérisations continues [Edouard et al., 2005, Sood and Awasthi, 2004a,b], mais en raison de l'absence de mesure complète de la distribution de taille des gouttelettes initiale dans le cas de la polymérisation en mini-émulsion, la plupart des modèles ont été développés pour la classique polymérisation en macro-émulsion, cependant que peu de modèles représentent le procédé de polymérisation en mini-émulsion.

Dans ce travail, les différences entre les polymérisations en macro- et mini-émulsion ont été comparées. Un modèle de polymérisation en macro-émulsion a été établi. Ce modèle peut prédire la distribution des tailles de radicaux pour une classe donnée de tailles de particules et la distribution de tailles de particules. Par comparaison, nous avons établi un modèle de polymérisation en mini-émulsion a été établi en utilisant le bilan des potentiels

chimiques du monomère dans le réacteur. Ce modèle peut prédire la distribtution de taille des particules et la variation de taille des gouttelettes.

1.1.1 Caractéristiques principales de la polymérisation en émulsion et différences entre les polymérisations en macro- et mini-émulsion

La polymérisation en émulsion (macro- et mini- émulsion) est essentiellement un procédé dans lequel une dispersion aqueuse d'un monomère ou un mélange de monomères est convertie par polymérisation radicalaire libre, superposée à des lieux ségrégés de polymérisation, en une dispersion stable de particules de polymère. Dans un environnement typique de réacteur, les gouttelettes de monomère, les micelles gonflés de monomère, le monomère dissous dans la phase aqueuse et les particules gonflées par le monomère rentrent en compétition pour les radicaux libres en phase aqueuse. Dans la polymérisation en macro-émulsion, en raison de leur grande taille (1000nm-10000nm), et par conséquent de leur petite surface totale, les gouttelettes de monomère ne rivalisent pas favorablement avec d'autres sites de nucléation des particules et on ne considère pas qu'elles contribuent de manière significative à la nucléation des particules. Elles servent principalement comme des réservoirs qui alimentent en monomère les particules en croissance qui sont formées principalement sous forme de nucléation dans les micelles gonflés de monomère et la phase aqueuse. Dans la polymérisation en mini-émulsion, en raison de leur petite taille (50-500nm), les gouttelettes de monomère deviennent les sites prédominants de nucléation des particules et de la polymérisation qui s'ensuit. Dans ce domaine de taille, la surface totale des gouttelettes est telle que la quantité de tensioactif généralement utilisée est adsorbée principalement sur les gouttelettes, d'où son indisponibilité pour former des micelles. On stabilise généralement ces systèmes en utilisant un composé anionique, par exemple le dodécyl sulfate de sodium et un co-stabilisant qui n'est soluble que dans la phase organique. La seule différence entre les recettes de polymérisation en mini-émulsion et en macro-émulsion est la présence du co-stabilisant. Les co-stabilisants doivent être insolubles dans l'eau et de faible masse molaire. La petite taille des gouttelettes est le résultat de l'homogénéisation du mélange monomère-eau par fort cisaillement qui brise les gouttelettes en nano-dimension et ces gouttelettes sont stabilisées contre la coalescence et la dégradation par diffusion à longue échéance par une combinaison appropriée de tensioactif/co-stabilisant. On peut éviter la coalescence par addition d'un tensioactif approprié. La dégradation par diffusion ou maturation d'Ostwald ("Ostwald ripening") peut être éliminée par addition d'une petite quantité de co-stabilisant. Dans des travaux récents, la stabilité de la distribution des tailles de gouttelettes en mini-émulsion et la nature de la distribution initiale des tailles de gouttelettes sont discutées. La conclusion est que la distribution initiale de la taille des gouttelettes en polymérisation en mini-émulsion est large et peut être bi-modale. La distribution résultante de tailles de particules est également très large et bi-modale. La formation et la stabilisation de gouttelettes dans le domaine nano incluent les étapes de pré-émulsification et d'émulsification. La pré-émulsification se réfère à la préparation du mélange homogène de monomère, tensioactif, co-tensioactif et d'eau, qui sont cassés ensuite sous un cisaillement élevé en gouttelettes au cours de l'étape d'émulsification. La polymérisation en mini-émulsion suit la cinétique de la polymérisation radicalaire libre superposée à un milieu compartimenté. Une caractéris-

tique cinétique que la polymérisation en mini-émulsion partage avec tous les processus de polymérisation en émulsion est que les radicaux libres entrent dans une particule par intermittence. Le nombre de radicaux dans une particule est déterminé par le bilan entre les vitesses d'entrée, de sortie et la terminaison des radicaux à l'intérieur de la particule. Une autre caractéristique cinétique que la polymérisation en mini-émulsion partage avec l'émulsion conventionnelle en polymérisation est que le transport de monomère est gouverné thermodynamiquement. Le transport de monomère dans les particules est très rapide par rapport à la vitesse à laquelle il est consommé à l'intérieur de la particule en raison de la polymérisation. Cela ne signifie pas que la particule continuera à gonfler en dépit du fait que le monomère est un bon solvant pour son polymère. Le point auquel une particule peut gonfler est gouverné par la thermodynamique, car la variation de l'énergie libre de mélange est équilibrée par le changement d'énergie libre de l'expansion de la surface interfaciale. Les différences des moments auxquels les particules sont nucléées à partir des gouttelettes, et la vitesse à laquelle elles grandissent ensuite, conduisent à des différences dans leurs tailles. Cela induit l'évolution de la distribution de tailles de particules.

1.1.2 Cinétique de polymérisation en émulsion

Réactions de polymérisation en émulsion

On considère généralement que la polymérisation en mini-émulsion diffère de la polymérisation en macro-émulsion par le mécanisme de nucléation. Le processus de polymérisation commence par la décomposition de l'amorceur I dans la phase aqueuse produisant des radicaux $I^{\bullet}$, Dans la polymérisation en macro-émulsion, une partie des radicaux entrent dans les micelles, ce qui signifie une nucléation micellaire, et dans la polymérisation en mini-émulsion, une partie des radicaux entrent dans les gouttelettes, ce qui signifie une nucléation dans les gouttelettes. Une partie des radicaux est capturée par des particules. Les réactions dans les particules sont les mêmes, c'est-à-dire la propagation, le transfert de chaîne au monomère, et la terminaison. Les principales réactions qui ont lieu sont illustrées dans le tableau 1.1

Table 1.1: Réactions de polymérisation en émulsion

	Macro-émulsion	Mini-émulsion
Réactions en phase aqueuse		
Initiation	$I \xrightarrow{f,k_{dc}} 2R^{\bullet}_w$	
Nucléation	Nucléation micellaire $R^{\bullet}_w \xrightarrow{k_{cmm}} R^{\bullet}_1$	Nucléation dans les gouttelettes $R^{\bullet}_w \xrightarrow{k_{cmd}} R^{\bullet}_1$
	Nucléation homogène $R^{\bullet}_w \xrightarrow{k_{cmh}} R^{\bullet}_1$	
Réactions dans les particules		
Propagation	$\begin{cases} R^{\bullet}_1 + M \xrightarrow{k_{pr}} R^{\bullet}_2 \\ R^{\bullet}_i + M \xrightarrow{k_{pr}} R^{\bullet}_{i+1} \end{cases}$	
Transfert de chaîne du radical au monomère	$R^{\bullet}_i + M \xrightarrow{k_{trM}} P_i + M^{\bullet}$	
Capture des radicaux dans la phase aqueuse par les particules	$R^{\bullet}_w \xrightarrow{k_{cp}} R^{\bullet}_1$	
Terminaison instantanée	$R^{\bullet}_i + R^{\bullet}_1 \xrightarrow{k_{pr}} P_{i+1}$	

Diffusion du monomère

Dans la polymérisation en émulsion, le nombre et la taille des particules dépendent des sites de nucléation des particules. Pendant le processus de polymérisation, chaque particule est un mini- ou nano-réacteur où la concentration de monomère détermine la vitesse de réaction, puis influence la distribution finale de tailles de particules. Les monomères diffusent dans la phase aqueuse, les particules, les gouttelettes et les micelles (dans la polymérisation en macro-émulsion) et on peut écrire le bilan fondé sur l'hypothèse thermodynamique. Dans la polymérisation en mini-émulsion, en raison du co-stabilisant, la diffusion du monomère et la concentration de monomère dans chaque phase sont très différentes de celles dans la polymérisation en macro-émulsion, Ceci constitue la principale différence dans le développement du modèle.

Dans la polymérisation en macro-émulsion, la majeure partie du monomère est stockée dans les gouttelettes bien que le nombre des gouttelettes soit beaucoup plus petit que celui des micelles. Quand les conditions initiales sont déterminées, la taille des micelles et des micelles gonflées est fixées, ainsi que les tailles initiales des gouttelettes. Avant les gouttelettes disparaissent, elles servent principalement comme réservoirs qui alimentent en monomère les particules en croissance qui sont formées essentiellement par nucléation dans les micelles gonflés en monomère et dans la phase aqueuse, et la concentration de

monomère dans les particules est la concentration de saturation.

De l'autre côté, dans la polymérisation en mini-émulsion, il n'y a pas de micelles, et les gouttelettes sont des sites prédominants de nucléation de particules et de la polymérisation qui s'ensuit. Le rapport entre les monomères et tensioactif/co-stabilisateur et les effets physiques et/ou mécanique, de cisaillement élevé, sonicateur ou un homogénéisateur mécanique, etc, modifient la distribution initiale de tailles des gouttelettes. En absence de connaissance de la distribution complète de tailles des gouttelettes, la définition de la distribution en termes de fonctions analytiques apparaît comme un recours convenable. De loin, la distribution normale ou gaussienne est utilisée le plus souvent et elle est valable quand un grand nombre de facteurs purement aléatoires sont responsables de la distribution. Dans ce travail, la DSD (Droplet Size Distribution) pré-spécifiée est représentée par une distribution log-normale, est définie par une moyenne et un écart-type pré-déterminés. La fonction de densité de probabilité de la distribution normale $P(d)$ s'exprime comme:

$$P(d) = \frac{1}{\sqrt{(2\pi)\sigma}} \cdot \exp\left[-\left(\frac{d-d_m}{2\sigma^2}\right)^2\right] \tag{1.1}$$

Deux gouttelettes de taille différente peuvent modifier leur taille, sans rentrer en contact, mais par diffusion moléculaire, la plus petite gouttelette diminuant en taille et la plus grande gouttelette augmentant en taille (maturation d'Ostwald). On peut retarder et arrêter cela par addition d'un composant de faible masse molaire et moins soluble dans l'eau. En polymérisation en mini-émulsion, le co-stabiliseur joue ce rôle. En général, le processus de diffusion moléculaire est gouverné par la différence entre les potentiels chimiques des substances diffusantes (un monomère dans notre cas) dans les deux phases. Le potentiel chimique μ du monomère dans une gouttelette de monomère de diamètre d, avec la fraction volumique de co-stabilisant ϕ_c est égal à:

$$\mu = \ln(1-\phi_c) + (1-m_{mc})\,\phi_c + \chi_{mc}\phi_c^2 + \frac{4\gamma V_m}{dRT} \tag{1.2}$$

où m_{mc} est le rapport du nombre équivalent du segment moléculaire, χ le paramètre d'interaction, V_m le volume molaire du monomère, γ la tension interfaciale, R la constante des gaz parfaits et T la température. Cette équation est basée sur la théorie des réseaux de Flory-Huggins des solutions de polymères. Les trois premiers termes de cette équation représentent l'énergie libre molaire partielle de mélange et les deux premiers termes représentant l'enthalpie de mélange, utilisés pour tenir compte de la non-idéalité du système. Plus χ est grand, plus la non-idéalité est importante. Le quatrième terme représente l'énergie libre molaire partielle du gonflement. En présence de co-stabilisant, le transfert de matière du monomère à partir des gouttelettes plus petites vers les gouttelettes plus grandes modifie leur composition. Finalement, l'équilibre sera atteint lorsque le second terme provenant du mélange des deux composants compense le premier terme lié au gonflement, et donc l'égalité des potentiels chimiques du monomère de toutes des gouttelettes en résulte.

Pendant la polymérisation, en raison de l'insolubilité dans l'eau du co-stabilisant, chaque particule contient une quantité donnée de co-stabilisant, qui affectera la diffusion du monomère dans la phase aqueuse, les particules et les gouttelettes. Chaque taille de particules est déterminée par la quantité de co-stabilisant, de polymère et des monomères. Chaque taille de particules est déterminée par la quantité de co-stabilisant, de polymère

et de monomères. Cela signifie que la concentration de monomère dans chaque particule n'est pas identique. Le potentiel chimique du monomère dans les différentes phases est donné par les équations étendues de Flory-Huggins:
Phase de gouttelettes:

$$\mu_d = \ln\left(1-\phi_{c,d}\right) + \left(1-m_{mc}\right)\phi_{c,d} + \chi_{mc}\phi_{c,d}^2 + \alpha/d_d \tag{1.3}$$

Phase aqueuse:

$$\mu_w = \ln\phi_{m,w} + \left(1-m_{mw}\right)\left(1-\phi_{m,w}\right) + \chi_{mw}\left(1-\phi_{m,w}\right)^2 \tag{1.4}$$

Phase des particules:

$$\begin{aligned}\mu_{p,i,j} = \quad & \ln\phi_{m,p} + \left(1-m_{mc}\right)\phi_{c,p} + \left(1-m_{mp}\right)\phi_{p,p} \\ & +\chi mp\phi_{p,p}^2 + \phi_{c,p}\phi_{p,p}(\chi_{mc}+\chi_{mp}-\chi_{cp}m_{cp}) + a/d_p\end{aligned} \tag{1.5}$$

où on définit $a = 4\gamma V_m/RT$.

1.1.3 Modélisation

Dans la polymérisation en émulsion, on utilise souvent le modèle zéro-un et nous l'utiliserons également dans cette étude. Dans ce modèle, on suppose qu'il n'y a qu'un seul ou aucun radical dans une particule.

Cadre des bilans de population

Un bilan de population est un bilan sur un ensemble défini d'entités distribuées (dans le cas de la polymérisation, par leur taille) qui représente l'accumulation nette de ces entités dans un système donné comme le résultat de tous les phénomènes qui ajoutent ou suppriment des entités de l'ensemble. Le bilan de population tient compte de toutes les manières les plus importantes selon lesquelles la valeur de chaque coordonnée de phase change avec le temps. On peut subdiviser ces manières en trois types:
(1) Evolution: c'est l'événement par lequel une phase de coordonnée associée au changement des entités distribuées dépend du temps,
(2) Naissance et mort: ce sont les événements par lesquels le nombre des entités distribuées change, soit par la naissance de nouvelles entités ou le décès d'entités existantes,
(3) Accumulation: c'est le bilan net des événements à la fois d'évolution et de naissance/décès sur le nombre d'entités distribuées avec des valeurs données des coordonnées des phases.
Les termes de ces trois types sont rassemblés pour donner les équations de bilan de population: Accumulation = Evolution + Naissance + Décès.

Modèle de polymérisation en macro-émulsion

Dans une particule, en raison de la terminaison, du transfert, de la capture du radical de la phase aqueuse, il y a plus d'une chaîne polymère. On suppose que le nombre d'unités monomères de tous les polymères dans une particule est j, et le nombre d'unités monomères du radical polymère est i.
Ainsi, $w_{i,j}$ est le pourcentage en moles de radical polymère avec i unités monomères dans

la particule de j unités monomères de tous les polymères avec 1 radical.
$sigma_j$ est le pourcentage en moles de tous les polymères avec j unités monomères dans la particule avec 0 radical.
et $i \leq j$.

Les équations de bilan de population sont:

- En phase aqueuse

$$\begin{aligned} \frac{d[\mathrm{I}]}{dt} &= -k_d[\mathrm{I}] \\ \frac{d[\mathrm{R}_w^\bullet]}{dt} &= 2k_d f[\mathrm{I}] - \mathcal{R}_{cm} - \mathcal{R}_{cp} \end{aligned} \tag{1.6}$$

- Particules avec 1 radical
  Quand $i = 1$ pour $j = j_{crit}$

$$\begin{aligned} \frac{dN_{p,1}w_{1,j}}{dt} &= \mathcal{R}_{cm} - \mathcal{R}_{pr,1,j} - \mathcal{R}_{cp,1,j,1} \\ &= \mathcal{R}_{cm} - \mathcal{R}_{pr} \cdot w_{1,j} - \mathcal{R}_{cp} \cdot \frac{d_{p,j}}{\overline{d}_{p,n}} \cdot \overline{n} \cdot w_{1,j} \end{aligned} \tag{1.7}$$

pour $j = j_{crit} + 1$

$$w_{1,j} = 0 \tag{1.8}$$

pour $j > j_{crit} + 1$

$$\begin{aligned} \frac{dN_{p,1}w_{1,j}}{dt} &= \sum_{i=2}^{j-1} \mathcal{R}_{trM,i,j-1} - \mathcal{R}_{pr,1,j} - \mathcal{R}_{cp,1,j,1} + \mathcal{R}_{cp,j-1,0} \\ &= \mathcal{R}_{trM} \cdot \sum_{i=2}^{j-1} w_{i,j-1} - \mathcal{R}_{pr} \cdot w_{1,j} - \mathcal{R}_{cp} \cdot \frac{d_{p,j}}{\overline{d}_{p,n}} \cdot \overline{n} \cdot w_{1,j} + \mathcal{R}_{cp} \cdot \frac{d_{p,j-1}}{\overline{d}_{p,n}} \cdot (1-\overline{n}) \cdot \sigma_{j-1} \end{aligned} \tag{1.9}$$

Quand $i \in [2, j]$

$$\begin{aligned} \frac{dN_{p,1}w_{i,j}}{dt} &= \mathcal{R}_{pr,i-1,j-1} - \mathcal{R}_{pr,i,j} - \mathcal{R}_{cp,i,j,1} - \mathcal{R}_{trM,i,j} \\ &= \mathcal{R}_{pr} \cdot w_{i-1,j-1} - \mathcal{R}_{pr} \cdot w_{i,j} - \mathcal{R}_{cp} \cdot \frac{d_{p,j}}{\overline{d}_{p,n}} \cdot \overline{n} \cdot w_{i,j} - \mathcal{R}_{trM} \cdot w_{i,j} \end{aligned} \tag{1.10}$$

- Particules avec 0 radical
  pour $j = j_{crit}$

$$\sigma_j = 0 \tag{1.11}$$

pour $j > j_{crit}$

$$\begin{aligned} \frac{dN_{p,0}\sigma_j}{dt} &= \sum_{i=1}^{j-1} \mathcal{R}_{cp,i,j-1,1} - \mathcal{R}_{cp,j,0} \\ &= \mathcal{R}_{cp} \cdot \frac{d_{p,j-1}}{\overline{d}_{p,n}} \cdot \overline{n} \cdot \sum_{i=1}^{j-1} w_{i,j-1} - \mathcal{R}_{cp} \cdot \frac{d_{p,j}}{\overline{d}_{p,n}} \cdot (1-\overline{n}) \cdot \sigma_j \end{aligned} \tag{1.12}$$

Modèle de polymérisation en mini-émulsion

Par comparaison avec la polymérisation en macro-émulsion, la composition dans la polymérisation en mini-émulsion est beaucoup plus complexe en raison de l'existence du co-stabilisant qui est insoluble dans la phase aqueuse. Dans la polymérisation en mini-émulsion, les tailles des gouttelettes ont une distribution, que l'on considère comme constante dans la polymérisation en macro-émulsion, et les concentrations de monomère dans les particules sont différentes en fonction de la taille de la gouttelette et la quantité du co-stabilisant qu'elle contient. En raison de ces phénomènes complexes, dans cette étude, pour simplifier, nous avons créé un modèle qui peut simplement prédire la distribution des tailles des particules, par comparaison avec le modèle de polymérisation en macro-émulsion, qui peut prédire la distribution des tailles de radicaux des polymères pour une classe donnée de tailles de particules.

Le volume d'une particule est composé de trois parties: le volume de monomère dans la particule, le volume du polymère dans la particule et celui du co-stabilisant. La quantité de polymère dans une particule est obtenue en suivant la variation de la masse de polymère formé dans la particule par la polymérisation. Le volume de monomère dans la particule est déterminé par le bilan du potentiel chimique du monomère dans les différentes phases. On considère que la quantité de co-stabilisant dans la particule est la même que la quantité de co-stabilisant dans la gouttelette à partir de laquelle cette particule est nucléée. Ainsi, le montant de co-stabilisant dans les particules est inchangée au cours du processus de polymérisation. Nous définissons:
• $w_{i,j}$ pourcentage de moles de particules avec 1 radical de la $i$ème classe des gouttelettes (sur la base du volume de co-stabilisant), dans la j ème unité (toutes les unités monomères des polymères dans la particule).
• $\sigma_{i,j}$ pourcentage de moles de particules avec 0 radical de la $i$ème classe des gouttelettes (sur la base du volume de co-stabilisant), dans la j ème unité (toutes les unités monomères des polymères dans la particule).

Les équations de bilan de population sont:

- En phase aqueuse

$$\begin{aligned} \frac{d[\mathrm{I}]}{dt} &= -k_{dc}[\mathrm{I}] \\ \frac{d[\mathrm{R}^{\bullet}]_w}{dt} &= 2k_{dc}f[\mathrm{I}] - \mathcal{R}_{cm} - \mathcal{R}_{cp} \end{aligned} \tag{1.13}$$

- Particules avec 1 radical
  Pour $j = j_{crit} = 1$

$$\begin{aligned} \frac{dN_{p,1}w_{1,j}}{dt} &= \mathcal{R}_{cm,j} - \mathcal{R}_{pr,1,j} - \mathcal{R}_{cp,1,j,1} \\ &= \mathcal{R}_{cmh} - \mathcal{R}_{pr} \cdot w_{1,j} \frac{[\mathrm{M}]_{p,1,j}}{\overline{[\mathrm{M}]}_{p,1}} - \mathcal{R}_{cp} \cdot \frac{d_{p,1,j}}{\overline{d}_{p,n}} \cdot \overline{n} \cdot w_{1,j} \\ \frac{dN_{p,1}w_{i,j}}{dt} &= \mathcal{R}_{cm,i} - \mathcal{R}_{prr,i,j} - \mathcal{R}_{cp,i,j,1} \\ &= \mathcal{R}_{cmd,i} - \mathcal{R}_{pr} \cdot w_{i,j} \frac{[\mathrm{M}]_{p,i,j}}{\overline{[\mathrm{M}]}_{p,j}} - \mathcal{R}_{cp} \cdot \frac{d_{p,i,j}}{\overline{d}_{p,n}} \cdot \overline{n} \cdot w_{i,j} \end{aligned} \tag{1.14}$$

Pour $j = j_{crit} + 1$

$$\begin{aligned}\frac{dN_{p,1}w_{i,j}}{dt} &= \mathcal{R}_{pr,i,j-1} - \mathcal{R}_{pr,i,j} - \mathcal{R}_{cp,i,j,1} - \mathcal{R}_{trM,i,j} \\ &= \mathcal{R}_{pr} \cdot w_{i,j-1} \frac{[\mathrm{M}]_{p,i,j-1}}{\overline{[\mathrm{M}]}_{p,1}} - \mathcal{R}_{pr} \cdot w_{i,j} \frac{[\mathrm{M}]_{p,i,j}}{\overline{[\mathrm{M}]}_{p,1}} - \mathcal{R}_{cp} \cdot \frac{d_{p,i,j}}{\overline{d}_{p,n}} \cdot \overline{n} \cdot w_{i,j} \\ &-\mathcal{R}_{trM} \cdot w_{i,j} \frac{[\mathrm{M}]_{p,i,j}}{\overline{[\mathrm{M}]}_{p,1}}, (i \in [1,n])\end{aligned} \tag{1.15}$$

Pour $j > j_{crit} + 1$

$$\begin{aligned}\frac{dN_{p,1}w_{i,j}}{dt} &= \mathcal{R}_{prr,i,j-1} + \mathcal{R}_{trM,i,j-1} - \mathcal{R}_{prr,i,j} + \mathcal{R}_{cp,i,j-1,0} - \mathcal{R}_{cp,i,j,1} - \mathcal{R}_{trM,i,j} \\ &= \mathcal{R}_{pr} \cdot w_{i,j-1} \frac{[\mathrm{M}]_{p,i,j-1}}{\overline{[\mathrm{M}]}_{p,1}} + \mathcal{R}_{trM} \cdot w_{i,j} \frac{[\mathrm{M}]_{p,i,j-1}}{\overline{[\mathrm{M}]}_{p,1}} - \mathcal{R}_{pr} \cdot w_{i,j} \frac{[\mathrm{M}]_{p,i,j}}{\overline{[\mathrm{M}]}_{p,1}} \\ &+\mathcal{R}_{cp} \cdot \frac{d_{p,i,j-1}}{\overline{d}_{p,n}} \cdot (1-\overline{n}) \cdot \sigma_{i,j-1} - \mathcal{R}_{cp} \cdot \frac{d_{p,i,j}}{\overline{d}_{p,n}} \cdot \overline{n} \cdot w_{i,j} \\ &-\mathcal{R}_{trM} \cdot w_{i,j} \frac{[\mathrm{M}]_{p,i,j}}{\overline{[\mathrm{M}]}_{p,1}}, (i \in [1,n])\end{aligned} \tag{1.16}$$

- Particules avec 0 radical

  Pour $j = j_{crit}$

$$\sigma_{i,j} = 0 \tag{1.17}$$

  Pour $j > j_{crit}$

$$\begin{aligned}\frac{dN_{p,0}\sigma_{i,j}}{dt} &= \mathcal{R}_{cp,i,j-1,1} - \mathcal{R}_{cp,i,j,0} \\ &= \mathcal{R}_{cp} \cdot \frac{d_{p,i,j-1}}{\overline{d}_{p,n}} \cdot \overline{n} \cdot w_{i,j-1} - \mathcal{R}_{cp} \cdot \frac{d_{p,i,j}}{\overline{d}_{p,n}} \cdot (1-\overline{n}) \cdot \sigma_{i,j}\end{aligned} \tag{1.18}$$

1.1.4 Validation

Dans ce travail, le système choisi pour la validation comprend le styrène (monomère), le dodécylsulfate de sodium (émulsifiant), le persulfate de potassium (amorceur) et le hexadécanol (co-stabilisant) (pour les polymérisations en mini-émulsion). Nous utilisons les données expérimentales de [Massebeuf, 1997], qui est diplômé de notre laboratoire, dans le but de valider la simulation de la polymérisation en macro-émulsion. Les données expérimentales de la littérature [Choi et al., 1985] sont utilisées pour la validation des polymérisations en mini-émulsion. Par souci de simplicité, nous ne tenons pas compte pas de la désorption des radicaux monomères dans les particules entrant dans la phase aqueuse dans les modèles et la simulation.

Les figures 1.1 et 1.2 comparent les conversions expérimentales et simulées de polymérisation en macro-émulsion. On vérifie l'influence de la concentration initiale de tensioactif et de l'amorceur. La figure 1.3 compare les conversions expérimentales et simulées de polymérisation en mini-émulsion. On vérifie l'influence de la concentration initiale de l'amorceur. En général, on observe un bon accord entre les modèles et les expériences.

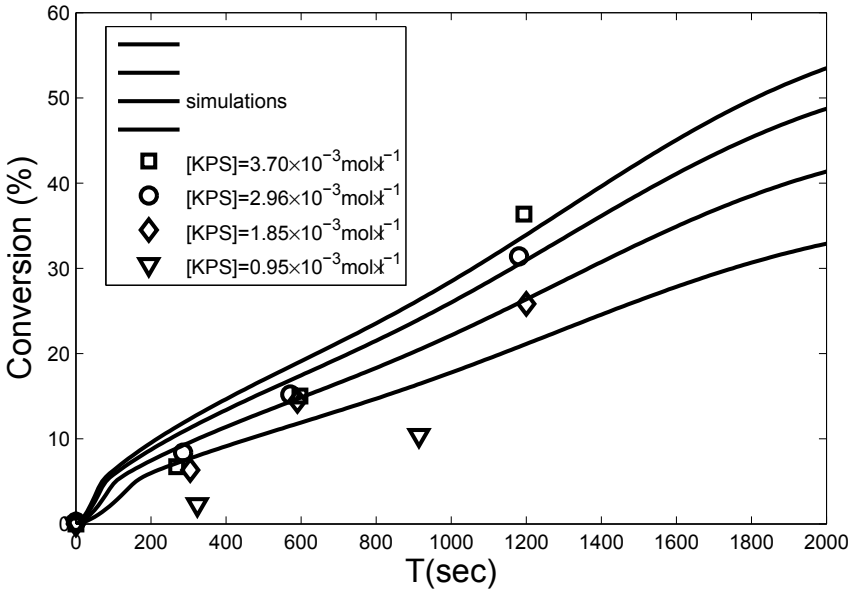

Figure 1.1: Polymérisation en macro-émulsion: Comparaison de l'évolution des conversions expérimentales et simulées en fonction du temps pour une concentration initiale de tensioactif $= 3,70\,10^{-3}$mol.l^{-1} au-dessus de la cmc et différentes concentrations initiales de l'amorceur

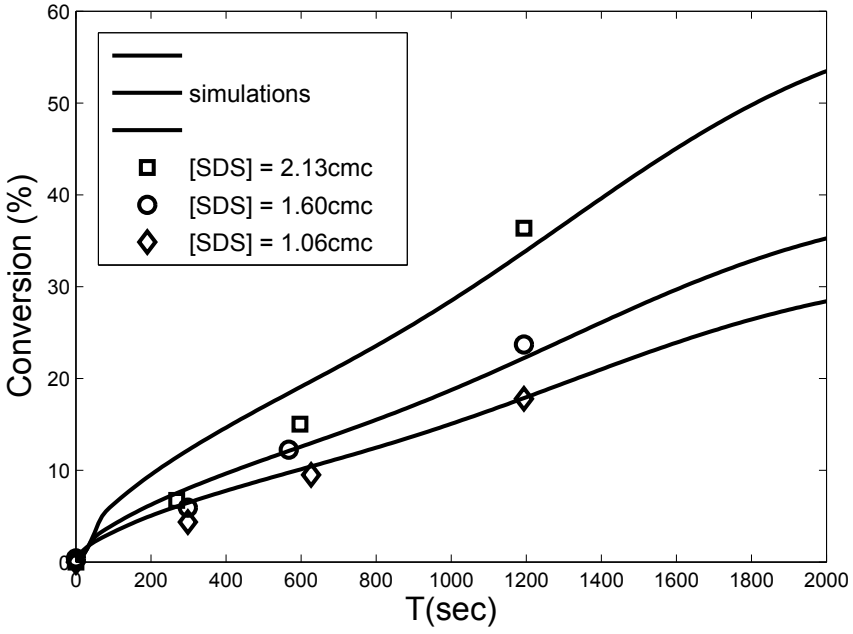

Figure 1.2: Polymérisation en macro-émulsion: Comparaison de l'évolution des conversions expérimentales et simulées en fonction du temps pour une concentration initiale d'amorceur $=$ 2.13cmc et différentes concentrations initiales de surfactant

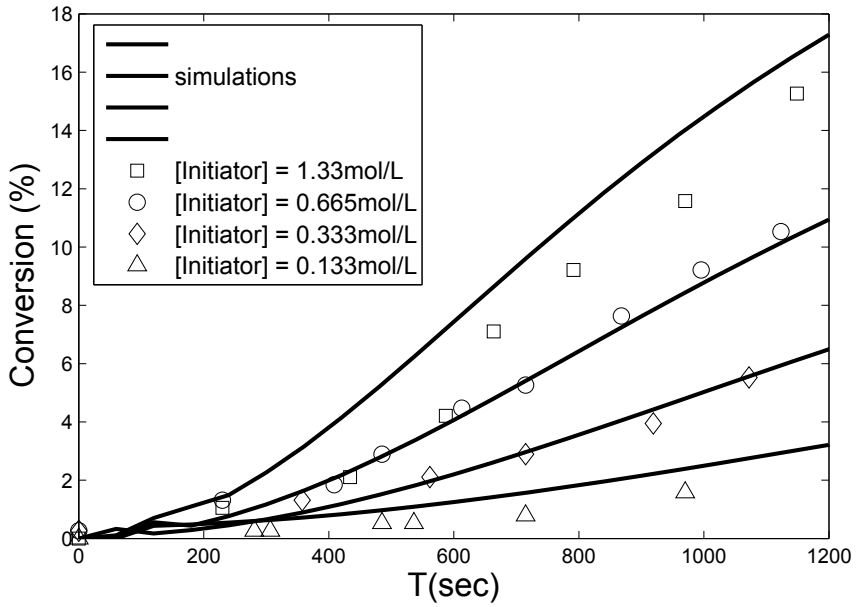

Figure 1.3: Polymérisation en mini-émulsion: Comparaison de l'évolution des conversions expérimentales et simulées en fonction du temps pour différentes concentrations initiales en amorceur

1.1.5 Résultats et discussion

Polymérisation en macro-émulsion

Nous avons choisi comme condition initiale la concentration en tensioactif $[SDS] = 2.13\text{cmc}$ et la concentration de l'amorceur $[KPS]_0 = 3,70\,10^{-3}\text{mol.l}^{-1}$. Le résultat de la simulation indique que les gouttelettes dans le système sont épuisées après 1240sec.

- Distribution de la taille des particules

  Les figures 1.4 et 1.5 illustrent l'évolution temporelle de la PSD (Particle Size Distribution). Au début de la polymérisation, bien que l'entrée des radicaux dans les micelles soit plus lente que celle dans les particules de plusieurs ordres de grandeur (le rapport entre le coefficient de vitesse d'entrée de micelles et celui des particules est de 0.08 [Sood and Awasthi, 2004b]), cependant le nombre de micelles est beaucoup plus grand que celui des particules, ainsi, le nombre des particules et la taille des particules augmentent. Au cours du temps, le nombre des particules est suffisamment grand pour rentrer en concurrence avec les micelles pour capturer les radicaux, et l'entrée des radicaux dans les micelles est plus lente que celle dans les particules, donc la plupart des radicaux sont capturés par des particules. Le nombre des particules est pratiquement inchangé et la taille des particules augmente en raison de la propagation dans les particules.

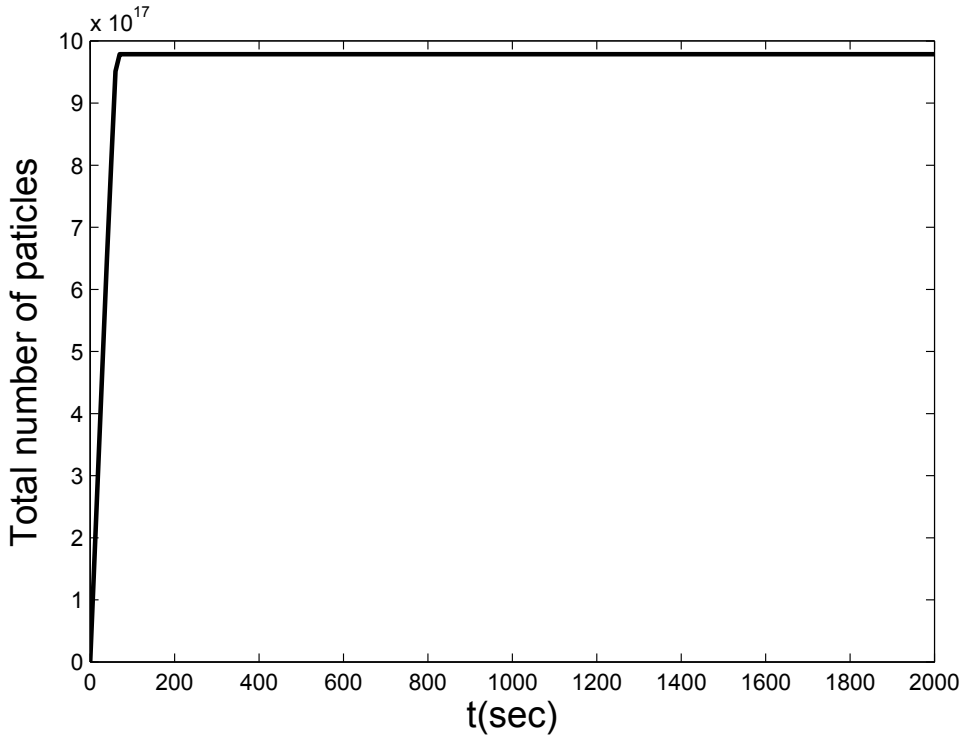

Figure 1.4: Polymérisation en macro-émulsion: Evolution du nombre de particules en fonction du temps

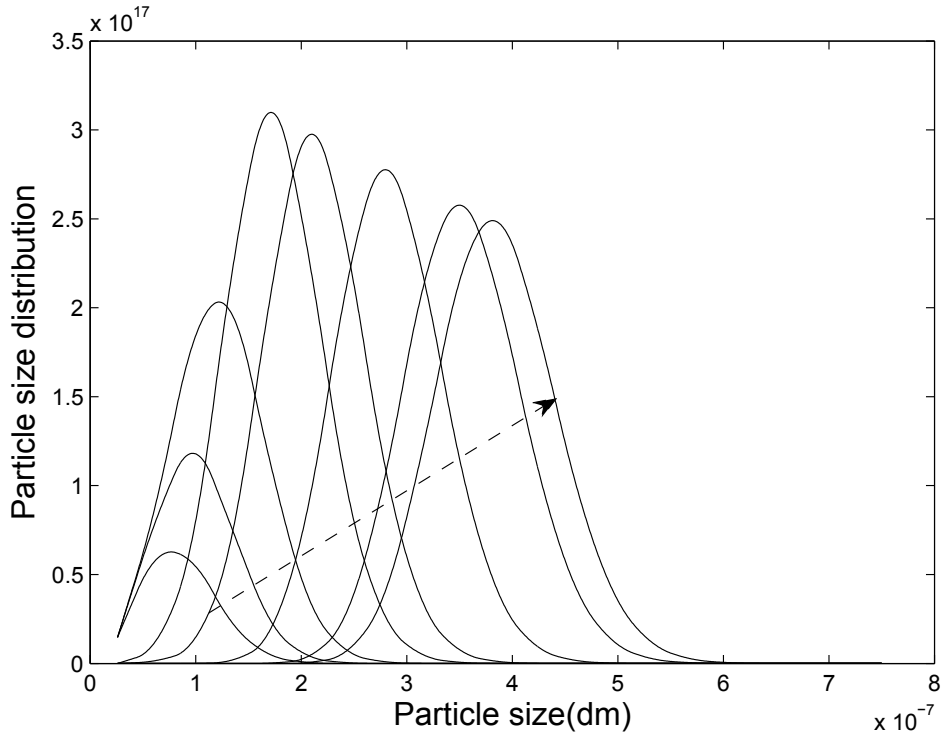

Figure 1.5: Polymérisation en macro-émulsion: Distribution de tailles des particules (le temps augmente selon la flèche, t = 10sec, 20sec, 40sec, 110sec, 210sec, 510sec, 1010sec and 1310sec)

- Distribution de la taille des radicaux dans les particules

  La figure 1.6 donne la distribution des tailles de radicaux dans la particule avec les rayons des particules de 9.8nm, 31.6nm, 46.4nm et 64.1nm à 10 secondes, lorsque la polymérisation commence à peine. La figure 1.7 donne la distribution des tailles de radicaux dans la particule avec les rayons des particules de 9.8nm, 31.6nm, 46.4nm et 64.1nm à 510 secondes, quand le nombre total de particules est stable. La figure 1.8 donne la distribution des tailles de radicaux dans la particule avec les rayons des particules de 9.8nm, 31.6nm, 46.4nm et 64.1nm à 1310 secondes, quand les gouttelettes dans le système sont épuisées. Dans notre modèle, nous prenons en compte le transfert de radicaux polymères aux monomères dans les particules considérées, mais nous ne considérons pas la désorption de radicaux monomères dans les particules dans la phase aqueuse. Le premier va augmenter le nombre de radicaux de petite taille, mais le dernier va diminuer le nombre de radicaux de petite taille. Ceci entraîne l'augmentation du nombre des radicaux de petite taille, ainsi, quelle que soit l'étape de polymérisation, et quelle que soit la taille de particules, les tailles des chaînes radicalaires sont centrées dans les radicaux oligomères. Pour obtenir une description plus précise de la distribution des tailles de la chaîne radicalaire, on devrait développer un modèle faisant intervenir le transfert des radicaux polymères aux monomères dans les particules et la désorption des radicaux monomères dans les particules dans la phase aqueuse.

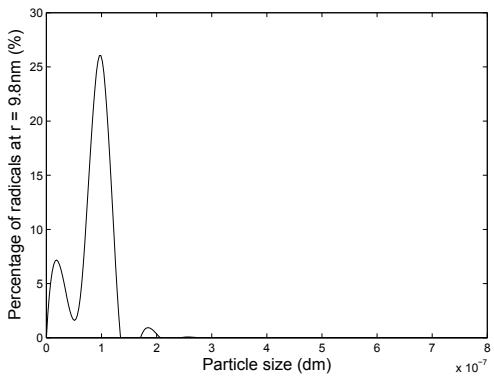

(a) r = 9.8nm, t = 10sec

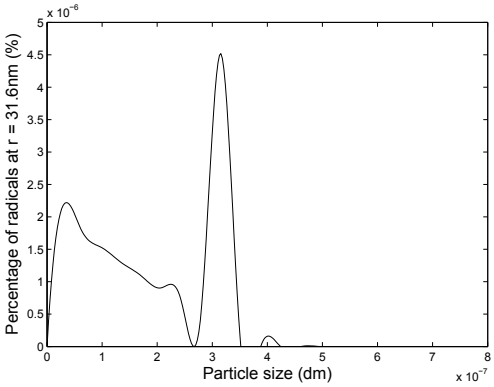

(b) $r = 31.6$nm, $t = 10$sec

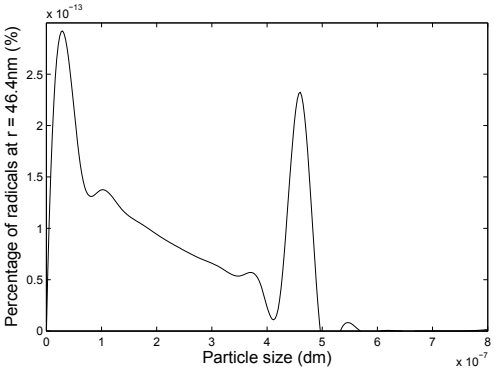

(c) $r = 46.4$nm, $t = 10$sec

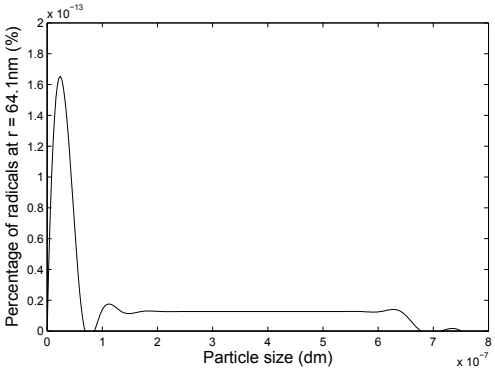

(d) $r = 64.1$nm, $t = 10$sec

Figure 1.6: Polymérisation en macro-émulsion: Distribution des tailles de radicaux dans les particules d'une certaine taille à $t = 10$sec

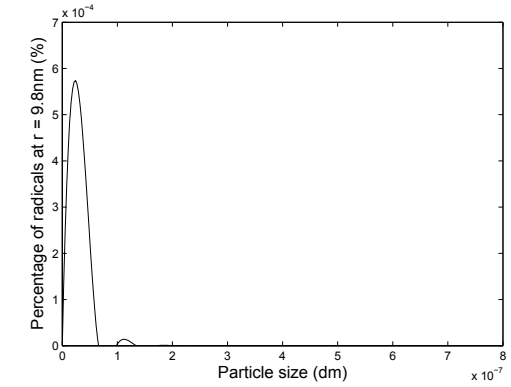

(a) r = 9.8nm, t = 510sec

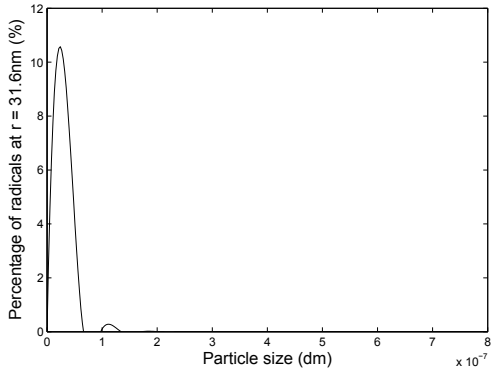

(b) $r = 31.6$nm, $t = 510$sec

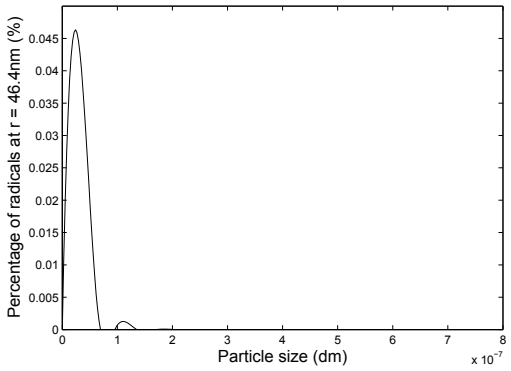

(c) $r = 46.4$nm, $t = 510$sec

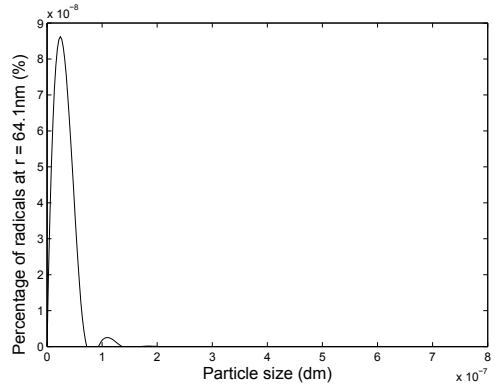

(d) $r = 64.1$nm, $t = 510$sec

Figure 1.7: Polymérisation en macro-émulsion: Distribution des tailles de radicaux dans les particules d'une certaine taille à $t = 510$ sec

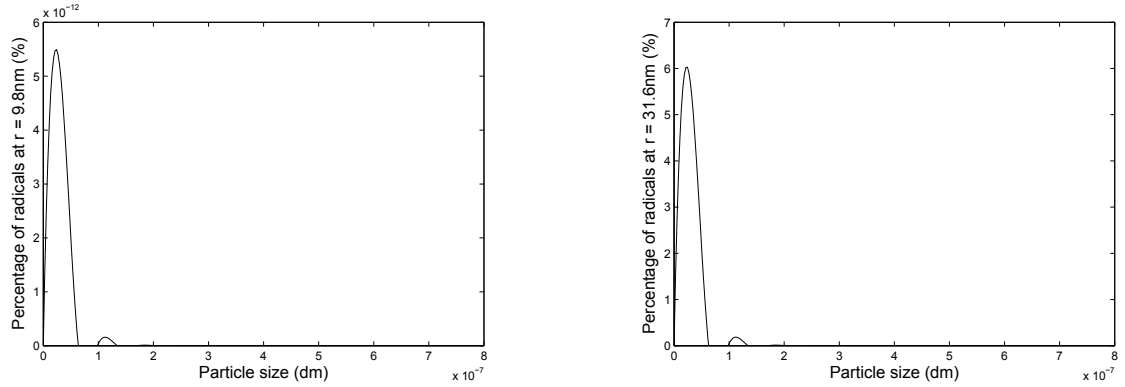

(a) r = 9.8nm, t = 1310sec (b) $r = 31.6$nm, $t = 1310$sec

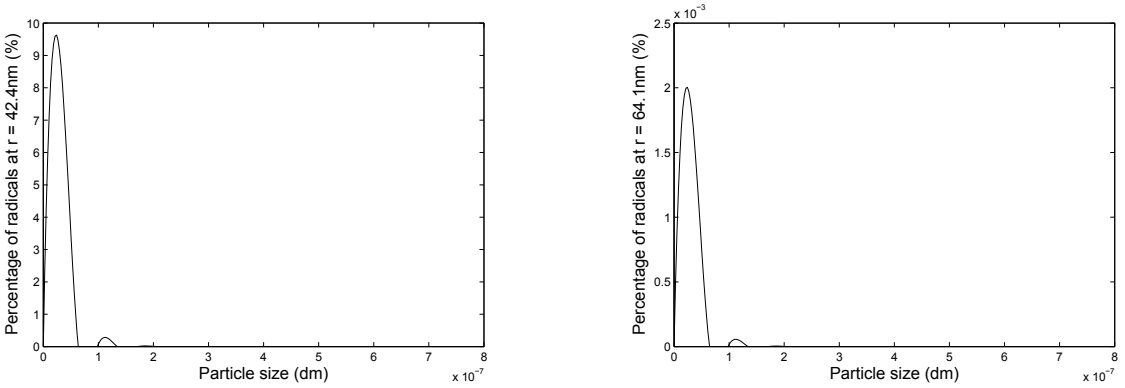

(c) $r = 42.4$nm, $t = 1310$sec (d) $r = 64.1$nm, $t = 1310$sec

Figure 1.8: Polymérisation en macro-émulsion: Distribution des tailles de radicaux dans les particules d'une certaine taille à $t = 1310$sec

Polymérisation en mini-émulsion

Nous avons choisi comme condition initiale la concentration de l'amorceur $1.33\,10^{-3}$mol.l^{-1}.

- Distribution de la taille des particules

  Nous montrons l'évolution de la distribution des tailles des particules en fonction du temps dans la figure 1.9. Initialement, la vitesse de croissance est très élevée à cause de la fraction volumique en monomère importante dans les particules, cela dure environ 100s. Ensuite, la vitesse de croissance diminue nettement à cause de la diminution de la concentration de monomère dans les particules. Comme la vitesse de croissance du nombre total de particules dépend uniquement de la vitesse de nucléation, avec l'augmentation du temps, le nombre de gouttelettes diminue, et pendant ce temps, les particules nouvellement formées seront en concurrence avec les gouttelettes pour capturer les radicaux, d'où une diminution de la vitesse de nucléation. Ainsi, la vitesse de croissance du nombre total de particules diminue avec le temps. On peut voir que le nombre de particules d'un diamètre sec proche de 80nm augmente plus vite que celle des particules avec les autres diamètres secs.

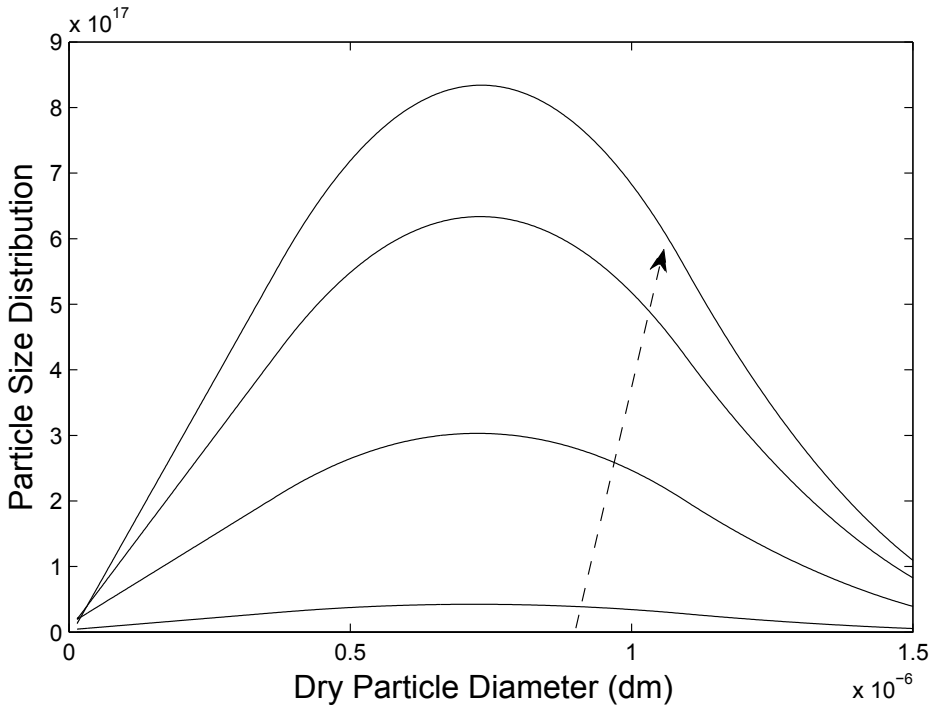

Figure 1.9: Polymérisation en mini-émulsion: Distribution des tailles de particules (le temps augmente avec la flèche, t = 1sec, 50sec, 100sec, 500sec, 1000sec et 1500sec)

- Variations des tailles des gouttelettes

  Nous montrons les changements des tailles des gouttelettes de cinq classes différentes de gouttelettes en fonction du temps dans la figure 1.10 et les tailles de gouttelettes initiales dans le tableau 1.2. A t = 0s, les tailles des gouttelettes des cinq classes différentes sont 48, 74, 100, 127, 153nm. Il convient de noter que, dans la validation du modèle, basée sur les données qui doivent être validées, nous avons supposé une distribution mono-disperse de la taille des gouttelettes. Avec l'augmentation du temps de polymérisation, les différences des tailles des gouttelettes des différentes classes de gouttelettes ont tendance à être faibles, ce qui signifie que la distribution de la taille des gouttelettes devient plus étroite. Ainsi, plus de monomère va être transféré des gouttelettes plus grosses aux particules que des plus petites. Cela montre aussi que notre modèle est général suffisant pour incorporer une distribution complète des tailles des gouttelettes.

Table 1.2: Résultats de thermodynamique de grossissement (équilibre)

Fraction de gouttelettes	Diamètre initial (nm)	Diamètre final (nm)
0.03	50	48
0.24	75	74
0.46	100	100
0.24	125	127
0.03	150	153
diamètre moyen	100	100

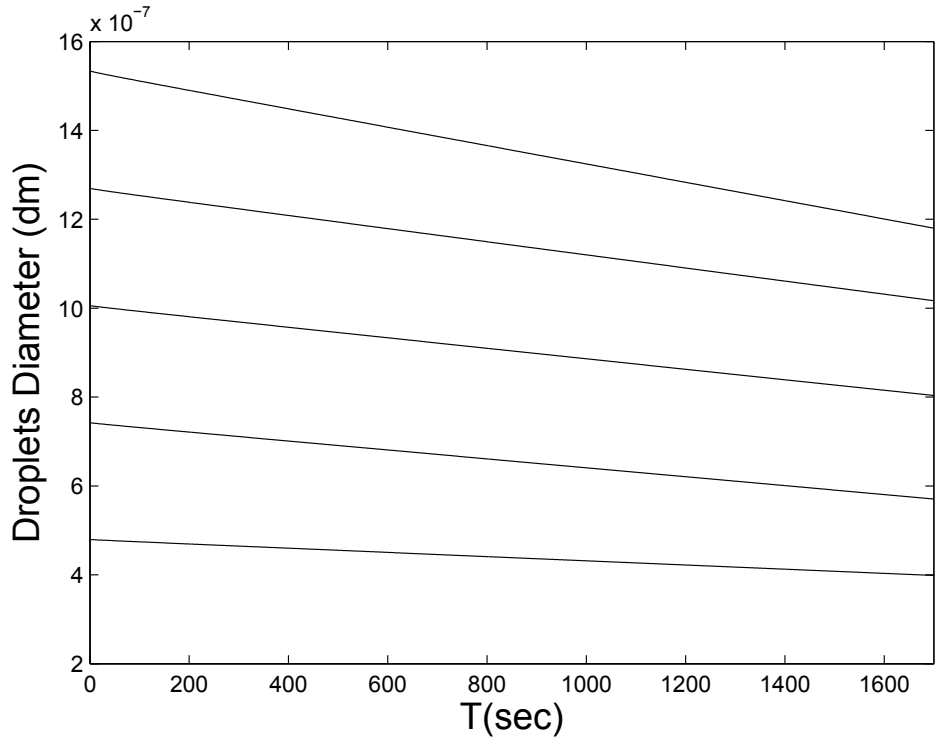

Figure 1.10: Polymérisation en mini-émulsion: Variations des tailles de gouttelettes de cinq classes différentes de gouttelettes. Les tailles initiales des gouttelettes sont données dans le tableau 1.2 et respectivement égales à 48, 74, 100, 127, 153nm.

1.2 Polypropylène greffé par extrusion réactive

Les polyoléfines (OP) sont devenues et sont restées les thermoplastiques les plus utilisés dans le monde depuis leur découverte dans les années 1950. De l'homopolyéthylène à l'homopolypropylène isotactique et les copolymères apparentés, on peut obtenir un large spectre de matériaux chimiquement stables et respectueux de l'environnement avec de très intéressantes propriétés thermiques et mécaniques.

L'inertie des polyoléfines a été une de leurs caractéristiques importantes dans de nombreuses applications, mais en même temps un inconvénient pour les applications pour lesquelles la mouillabilité de la surface ou l'interaction avec des produits polaires est nécessaire.

Dans le 1970-1980, on a greffé avec succès l'anhydride maléique (MAH) et ses dérivés sur le squelette paraffinique de macromolécules constituant une polyoléfine. [Kaufman and Falcetta, 1977, Gaylord and Mishra, 1983, Gloor et al., 1994, Ruggeri et al., 1983] ont ouvert la voie à des polyoléfines modifiées, caractérisées par une affinité acceptable avec des molécules organiques polaires, du métal et des minéraux, agissant ainsi comme un agent de compatibilité efficace pour un grand nombre de mélanges [Feldman, 2005, Koning et al., 1998, Liu and Baker, 1992, Xanthos and Dagli, 1991], de composites [Vasile, 2000] et de nanocomposites [Alexandre and Dubois, 2000, Ray and Okamoto, 2003, Ciardelli et al., 2008]. Cependant, pour atteindre la faible viscosité nécessaire pour la modification chimique diffusée de manière homogène, des températures élevées sont utilisées (bien au-dessus du point de fusion des polyoléfines) et un peroxyde est ajouté comme générateur de radicaux libres pour activer la réaction de greffage. Les contraintes thermique et mécanique et la présence de radicaux libres ont rendu le processus très difficile à contrôler d'autant plus que la réaction de greffage principale est concernée, tandis qu'en même temps, différentes réactions secondaires se produisent en particulier la dégradation et l'extension de la chaîne de réticulation/ramification des macromolécules de polyoléfine.

Le polypropylène PP est l'un des trois plus grandes plastiques considérés comme appartenant à des matières plastiques de commodité en raison de sa relative basse performance mécanique, sa haute résistance à la traction, sa rigidité et sa résistance chimique [Moore and A.Larson, 1996]. Cependant, certaines de ses propriétés doivent encore être améliorées, telles que sa relativement faible résistance à la fusion, sa résistance à la chaleur et sa résistance chimique. Dans les dernières décennies, on a prêté beaucoup attention à la fonctionnalisation du PP par greffage de monomères insaturés tels que l'anhydride maléique (MAH), l'acide acrylique et ses dérivés, en présence de peroxyde organique comme amorceur, Le PP modifié a été utilisé intensivement pour la compatibilisation de polypropylène-polyamide non miscibles et des mélanges de polypropylène-polyester, ainsi que pour améliorer l'adhérence interfaciale de PP avec des fibres de verre et de carbone, et même comme une aide à la transformation du plastique dégradable [Paul and Newman, 1978, Gaylord, 1989]. Toutefois, le degré de greffage de MAH sur PP est faible. Au cours des dernières décennies, afin de trouver un moyen d'améliorer le degré de greffage de MAH, de nombreuses études ont mis l'accent sur le mécanisme de greffage [Minoura et al., 1969, Gaylord et al., 1983, Al-Malaika, 1996, Russell and Kelusky, 1988, De Roover et al., 1995, Heinen et al., 1996, Moad, 1999, Russell, 2002]. Le préconfinement de l'amorceur dans les passages à l'échelle nanométrique d'une montmorillonite organiquement modifiées (o-MMT) a permis la concentration MAH molécules sur sa surface extérieure et en ralentissant la libération de radicaux primaires au volume de réaction de greffage. Par conséquent, la sélectivité du greffage de MAH sur PP a été considérablement augmentée, et l'effet d'encapsulation d'espèces actives preconfined dans l'o-MMT est considéré comme la principale raison.

Pour préparer du polypropylène (HMSPP) à haute résistance à la fusion, les scientifiques ont exploré de nombreuses méthodes. Cross-linking of polyolefin is simple, appropriate and souvent utilisé pour des applications. Le greffage du silane et la réticulation du PP est une autre approche développée récemment pour préparer du HMSPP [An et al., 2008, Demjen et al., 1999, Huang and Liu, 1998, Zhou et al., 2009, Beltran and Mijangos, 2000, Jain et al., 2006]. La manière de faire du PP réticulable par greffage de silane puis suivi par réticulation à l'eau présente divers avantages, tels qu'un procédé facile, un faible coût et investissement en capital, et des propriétés favorables dans les matériaux réalisés.

Dans ce travail, nous avons utilisé deux types de monomères afin d'améliorer les propriétés du PP par extrusion eactive. Ces monomères sont l'anhydride maléique (MAH), qui peut modifier la polarité de la PP, et le silane, qui peut améliorer la résistance à la traction de la PP.

1.2.1 Montmorillonite organiquement modifiée comme nanoréacteur pour améliorer le degré de greffage de l'anhydride maléique sur du polypropylène

Dans cette recherche, nous avons utilisé la montmorillonite organiquement modifiées (o-MMT) comme nanoréacteur. Nous avons étudié l'effet de préconfinement du MMT et la relation entre MMT et MAH, ainsi que la méthode de greffage.

Expérimentation

- Confinement du peroxyde dans l'o-MMT

  Une quantité donnée de o-MMT a été chargée dans 100 ml d'acétone. et homogénéisé le mélange o-MMT/acétone sous ultrasons pendant 1 h. En parallèle, une quantité prescrite de DCP a été dissoute dans 10 ml d'acétone. Ensuite, la solution de DCP dans de l'acétone a été ajoutée lentement au mélange o-MMT/acétone précédemment mentionné sous agitation continue. Le rapport massique de o-MMT et DCP était de 1:1. L'ensemble a été remué pendant 3 h à température ambiante avant d'être coulé sur une plaque de polytétrafluoroéthylène. Le DCP confiné avec o-MMT est noté DCP/o-MMT et est obtenu après évaporation complète de l'acétone à la température ambiante. Ensuite, la poudre DCP/o-MMT est sèchée dans une étuve sous vide à 50°C pendant 24h avant utilisation pour des réactions de greffage des radicaux libres à venir.

- Greffage de MAH fondu de radicaux libres sur PP

  On a effectué la réaction de greffage dans un mélangeur discontinu Haake (HBI 90) équipé d'une chambre de mélange et de deux rotors à l'intérieur à 190°C pendant 7 minutes. La vitesse de rotation du mélangeur était 65 rpm. Les matériaux (MAH, PP poudre et (DCP / o-MMT) poudre) étaient pré-mélangés et ensuite chargés simultanément dans le mélangeur. A titre de comparaison, la même réaction de greffage a été effectuée d'une manière classique, c'est à dire que le DCP n'a pas été pré-confiné dans o-MMT. Les concentrations de DCP étaient identiques dans les deux systèmes. Après le greffage, les produits PP-g-MAH produits ont été dissous dans le xylène chaud, puis précipités dans de l'acétone. Ensuite, le précipité a été lavé deux fois avec de l'acétone pour éliminer complètement les résidus MAH. Les produits PP-g-MAH purifiés ont été séchés dans un four sous vide à 80°C pendant 12 h pour les analyses ultérieures.

- Mesures

  Le degré de greffage, défini comme le pourcentage en poids de MAH en PP-g-MAH, est mesuré par une méthode de titrage chimique. Les masses molaires des échantillons de PP-g-MAH échantillons ont été mesurées en utilisant un GPC à haute

température V2000 Waters. La caractérisation des particules de o-MMT particules ou la dispersion de plaquettes a été effectuée en utilisant la microscopie électronique à transmission (TEM).

Résultats et discussion

Le tableau 1.3 rassemble les compositions de tous les essais effectués dans ce travail et des caractéristiques choisies du PP-g-MAH. Deux types d'expériences sont rapportés:
Système 1: système de greffage PP/ DCP/MAH sans o-MMT (n°1-10).
Système 2: système de greffage PP/(DCP/o-MMT)/MAH (n°11-20).

Table 1.3: Compositions de tous les essais effectués dans ce travail et certaines caractéristiques du PP-g-MAH

Trial ♯	PP(g):o-MMT/DCP(DCP)(g):MAH(g)	DG wt%	M_n(kg/mol)	M_w(kg/mol)
0	PP/o-MMT*=40:1	-	-	-
System 1.(PP/(DCP)/MAH)				
1	40: (0.25): 1	0.422	42.3	110.7
2	40: (0.50): 1	0.458	43.8	113.9
3	40: (1.00): 1	0.532	39.9	94.6
4	40: (1.50): 1	0.528	50.0	122.5
5	40: (1.00): 2	0.375	55.8	211.1
6	40: (1.00): 3	0.367	61.8	221.4
7	40: (1.00): 4	0.369	55.6	224.6
8	40: (0.50): 2	0.375	53.2	155.8
9	40: (0.50): 3	0.368	50.9	202.2
10	40: (0.50): 4	0.377	46.6	170.5
System 2. (PP/(o-MMT/DCP)/MAH)				
11	40: 0.50: 1	0.471	47.2	113.1
12	40: 1.00: 1	0.510	42.2	118.7
13	40: 2.00: 1	0.599	36.2	93.7
14	40: 3.00: 1	0.578	38.0	98.3
15	40: 2.00: 2	0.494	46.3	135.1
16	40: 2.00: 3	0.438	41.1	128.3
17	40: 2.00: 4	0.399	51.5	194.0
18	40: 1.00: 2	0.394	55.7	189.1
19	40: 1.00: 3	0.399	55.3	162.4
20	40: 1.00: 4	0.382	49.9	187.9
System 3. (PP/o-MMT*/DCP/MAH)				
26	40: 1: 1: 3	0.412	-	-

o-MMT* n'a pas été pré-traitée par de l'acétone et les ultrasons

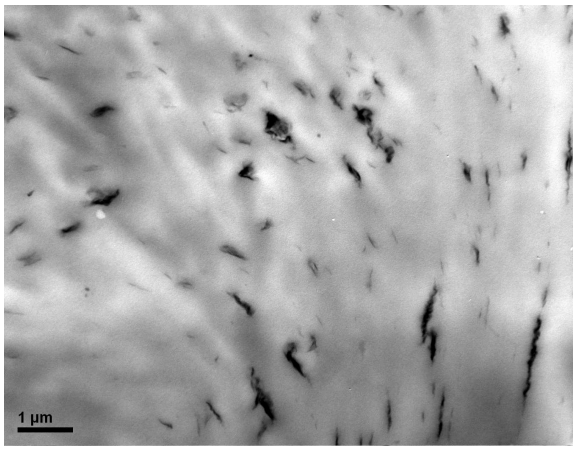

(a) essai 0 (PP/o-MMT=40: 1wt, o-MMT sans pré-traitement)

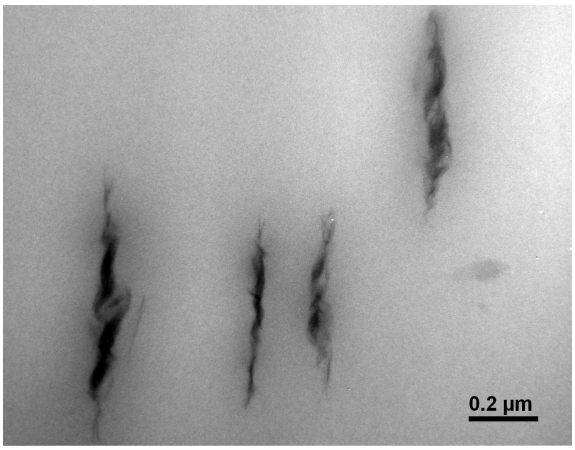

(b) essai 0 (PP/o-MMT=40: 1wt, o-MMT sans pré-traitement)

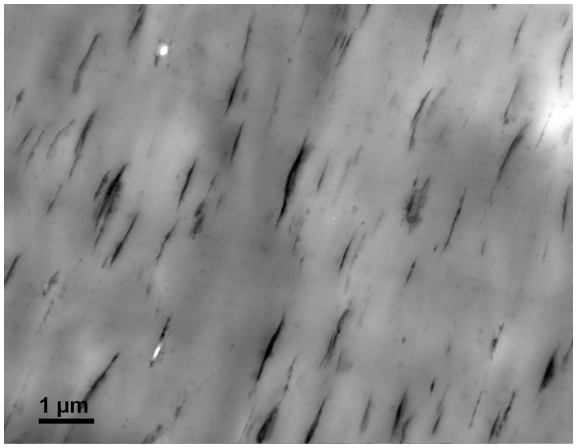

(c) essai 26 (PP/o-MMT/DCP/MAH=40: 1: 1: 3wt, o-MMT sans pré-traitement)

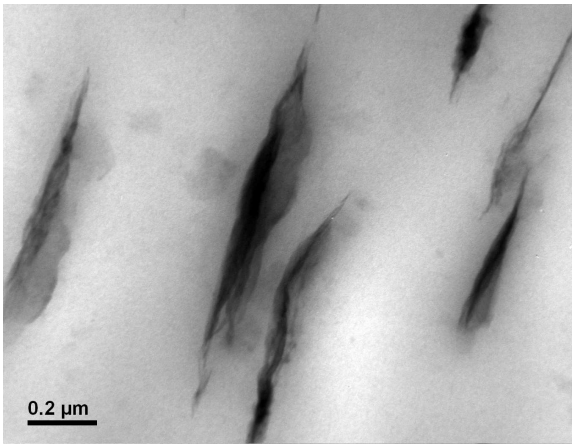

(d) essai 26 (PP/o-MMT/DCP/MAH=40: 1: 1: 3wt, o-MMT sans pré-traitement)

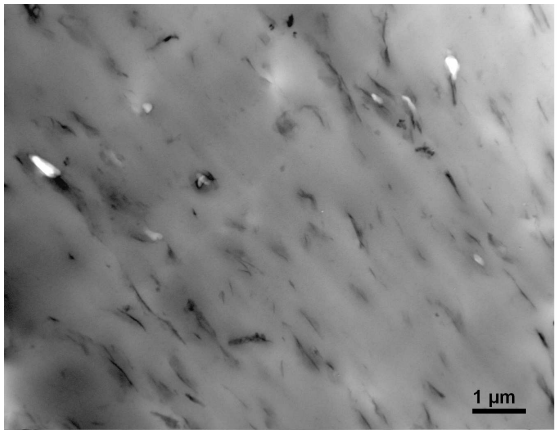

(e) essai 16 (PP/(o-MMT/DCP)/MAH=40:2:3wt, DCP pré-confiné dans l'o-MMT avec le ratio 1:1 en poids)

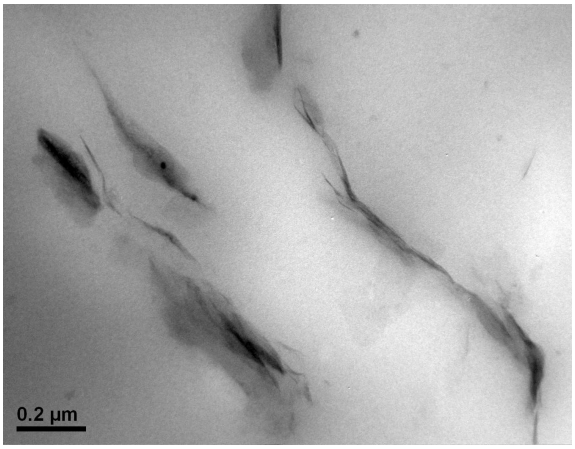

(f) essai 16 (PP/(o-MMT/DCP)/MAH=40:2:3wt, DCP pré-confiné dans l'o-MMT avec le ratio 1:1 en poids)

Figure 1.11: Micrographies TEM de PP/o-MMT des essais 0, 16, 26.

Les figures 1.11(a), 1.11(b), 1.11(c), 1.11(d), 1.11(e), 1.11(f) montrent la dispersion des particules de o-MMT ou de plaquettes dans le PP ou le PP et la phase PP-g-MAH. Les échantillons utilisés dans la Figure 1.11(a) étaient les produits de l'essai 0 composés par PP: o-MMT = 40:1 (en poids), sans réaction, mais juste avec mélange dans le mélangeur Haake. et l'o-MMT n'a pas été pré-traitée par de l'acétone et les ultrasons. Les échantillons utilisés dans la Figure 1.11(b) étaient les produits qui ont la même composition que l'essai 16 mais avec o-MMT non pré-traitée par de l'acétone et les ultra-sons, ce qui signifie que le DCP n'a pas été pré-confiné dans l'o-MMT. Les échantillons utilisés dans la figure 1.11(c) était les produits de l'essai 16. Peu importe si elle a été pré-traitée, l'o-MMT peuvent être dispersée de façon homogène dans la phase PP, et par pré-traitement de l'acétone et l'échographie, la largeur des galeries de MMT est devenu plus grande, ce qui a été prouvé par [Shi et al., 2006] par diffraction X à grand angle (XAXD).

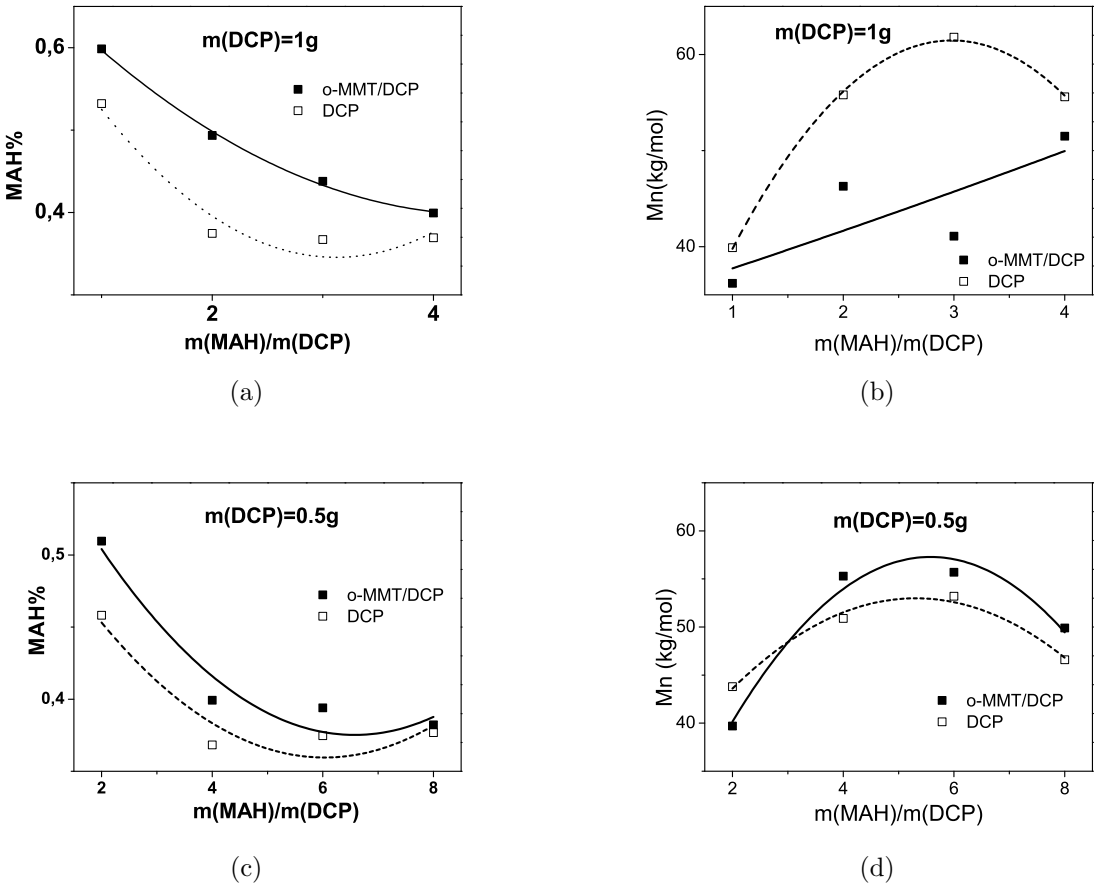

Figure 1.12: Comparaison entre les systèmes de greffage PP/DCP/MAH, PP/(DCP/o-MMT)/MAH en termes d'évolution du degré de greffage et de la masse molaire du PP-g-MAH en fonction de la MAH pour une quantité donnée de DCP.

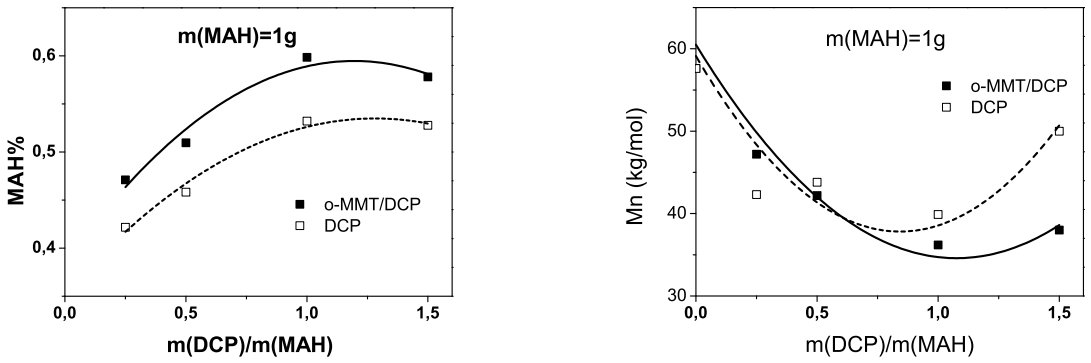

(a) (b)

Figure 1.13: Comparaison entre les systèmes de greffage PP/DCP/MAH, PP/(DCP/o-MMT)/MAH en termes d'évolution du degré de greffage et de la masse molaire du PP-g-MAH en fonction de la DCP pour une quantité donnée de MAH.

La Figure 1.12 compare l'évolution du degré de greffage de MAH et de la masse molaire moyenne en nombre de la PP-g-MAH, M_n, en fonction de la teneur en MAH dans les systèmes de greffage. La Figure 1.13 compare l'évolution du degré de greffage de MAH et de la masse molaire moyenne en nombre de la PP-g-MAH, M_n, en fonction de la teneur en DCP dans les systèmes de greffage. Le degré de greffage dans le système de greffage du nanoréacteur o-MMT est toujours plus élevé que dans le système de greffage classique, mais les masses molaires moyenness en nombre dans le système greffage du nanoréacteur de o-MMT ne sont pas plus élevées que celles dans le système de greffage classique.

[Shi et al., 2001] explique les mécanismes de réaction de PP-g-MAH greffage comme suit:

le système classique de greffage doit suivre plus ou moins le schéma réactionnel de la figure 1.14. Selon ce mécanisme de réaction, un radical libre primaire RO$^\bullet$ formé par la décomposition d'une molécule de peroxyde peut suivre l'une des deux voies réactionnelles suivantes:
Voie A: RO$^\bullet$ réagit avec un monomère insaturé MAH pour former un radical libre saturé RM$^\bullet$. Ce dernier ne participera pas à des réactions de greffage car il ne peut plus se propager, mais peut seulement subir la terminaison par dismutation.
Voie D: RO$^\bullet$ réagit avec un atome d'hydrogène du polymère PP, de préférence un tertiaire, pour former le macroradical correspondant PP$^\bullet$. Ce dernier peut aussi suivre l'un des deux voies réactionnelles suivantes:
Voie E: fragmentation en deux segments plus courts par β-scission.
Voie F: greffage

Peu importe quelle voie est suivie, quand plus le greffage a lieu, plus la terminaison par disproportionation va se produire. ce qui résulte en une réduction de la masse molaire moyenne des produits. Ainsi, plus le degré de greffage sera élevé, plus la masse molaire moyenne des produits sera faible.

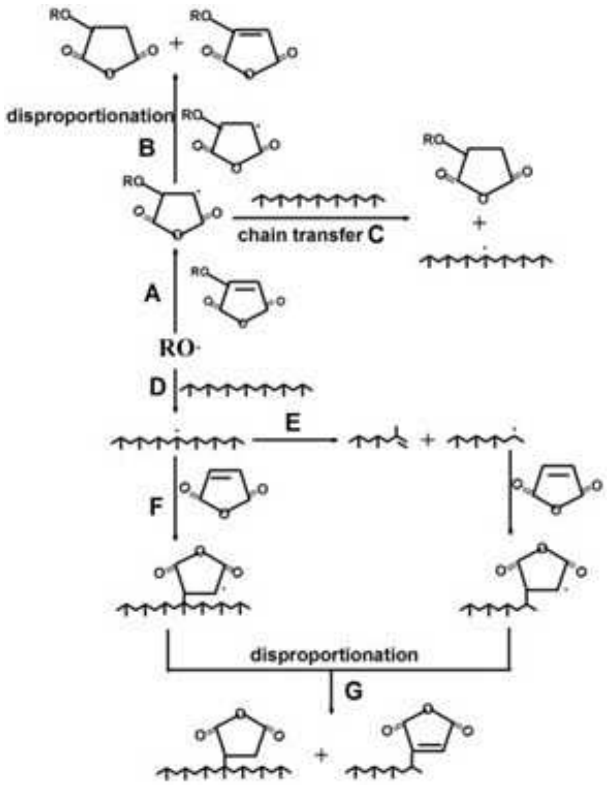

Figure 1.14: Un schéma simplifié de la réaction de greffage de PP-g-MAH système (selon [Shi et al., 2006]).

Pourquoi la performance du système de greffage du nanoréacteur o-MMT est-elle supérieure au système classique? Tout d'abord, parce que PP n'est pas miscible avec MAH, dans les systèmes classiques de greffage, lorsque le PP moléculaire est élevé, sa viscosité en phase fondue doit être également élevée, et ainsi les MAH monomères diffusent difficilement dans les chaînes de PP. Donc MAH peut rencontrer et réagir avec PP$^{\bullet}$ avec une faible probabilité. Mais dans les systèmes avec o-MMT comme nanoréacteurs, les interactions entre MAH et MMT en surface sont relativement fortes (PP-g-MAH est souvent utilisé comme compatibilisant entre le PP et MMT dans la préparation de PP/MMT nanocomposites [Kawasumi et al., 1997, Hasegawa et al., 2000b,a, Nam et al., 2001]), MAH sera enrichie autour o-MMT. En outre, la dispersion de la o-MMT dans la phase PP est homogène (Figure 1.11), quand PP ^{bullet} se forme autour de o-MMT, MAH va réagir immédiatement avec elle. Pour cette raison, avec les mêmes contenus initiaux de MAH et DCP, le degré de greffage de MAH sur PP de l'essai 16 et celui de l'essai 26 sont plus élevés que celui de l'essai 6. Une autre différence évidente et importante entre le système de greffage classique et celui avec les nanoréacteurs de o-MMT est que dans le premier cas, des radicaux primaires RO$^{\bullet}$ sont formés de façon uniforme sur l'ensemble du volume réactionnel. Dès qu'ils sont formés, ils sont en contact direct et immédiat avec MAH et/ou PP. Cependant, dans le dernier cas, ils sont formés uniquement à l'intérieur des galeries de l'o-MMT (Figure 1.15). Ils ne peuvent pas réagir avec le PP et/ou MAH avant d'avoir diffusé hors des galeries d'o-MMT. Comme la décomposition de ROOR en RO$^{\bullet}$ est une réaction réversible, la vitesse avec laquelle les radicaux primaires RO$^{\bullet}$ sont générés dans le système de greffage de PP/MAH(DCP/o-MMT) devrait être beaucoup plus faible que dans le système PP/MAH/DCP. Ainsi, le rôle de l'o-MMT est de ralentir

la vitesse de libération de RO ^{bullet} de l'intérieur des galeries de o-MMT dans le volume réactionnel externe occupé par le PP et le MAH. Ceci est semblable à l'encapsulage d'espèces actives. De cette manière, la vitesse de formation de radicaux primaires n'est plus contrôlée par la température seule, mais par la température et la diffusion. Sans pré-traitement à l'acétone et ultrasons, la largeur des galeries d'o-MMT est inférieure à celle avec pré-traitement, qui n'est pas assez large pour que le DCP y soit dispersé [Shi et al., 2006], si bien qu'il n'y a donc aucun effet d'encapsulation dans l'essai 26, ce qui est la principale raison pour laquelle degré de greffage de MAH sur PP de l'essai 26 est inférieur à celui de l'essai 16.

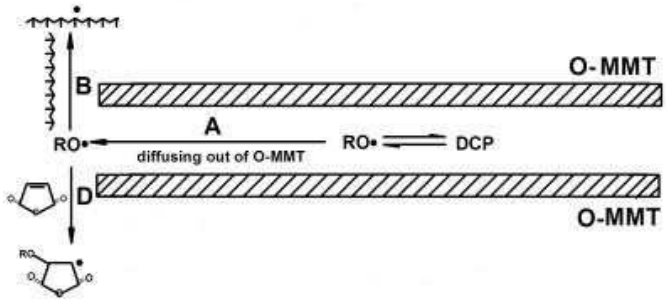

Figure 1.15: Schéma réactionnel simplifié de la fragmentation homolytique DCP et diffusion dans l'o-MMT

Dans le système PP /MAH/DCP sans o-MMT, à quantité initiale de DCP constante, lorsque le rapport entre MAH et DCP est assez grand, en augmentant la teneur des MAH, la voie A de la figure 1.14 est favorisée et le nombre de radicaux attaquant la chaîne PP diminue, de même que pour la scission de la chaîne PP, le degré de greffage diminue. La même situation se produira dans le système PP/MAH/(DCP/o-MMT), dans laquelle MAH sera enrichi autour de l'o-MMT. En augmentant la teneur en MAH, l'o-MMT sera isolée avec PP, ce qui signifie que RO$^{\bullet}$ dispersé à partir de l'o-MMT ne peut pas entrer en contact avec le PP, la plupart des radicaux libres dans le système de greffage sont sous la forme RM$^{\bullet}$. Ainsi, la plupart des molécules MAH serait consommée par RO$^{\bullet}$ avant qu'ils puissent réagir avec PP$^{\bullet}$ pour former PP-g-MAH, et la voie A sera la réaction principale. Donc dans la figure 1.13, avec la quantité initiale de DCP constante, le degré de greffage est réduit en augmentant la teneur de MAH dans le système avec de l'o-MMT et sans elle.

Lorsque la quantité initiale de MAH est constant, avec une quantité de DCP de petite à grande, lorsque la quantité de DCP est petite, la voie A de la figure 1.14 est favorisée, le degré de greffage est faible. Avec l'augmentation de la quantité de DCP, la degré de greffage augmente. Mais lorsque la quantité de DCP est assez grande, les voies A et B dans la figure 1.14 peuvent être négligées, et les radicaux primaires formés par la décomposition de la DCP sont principalement utilisés pour générer des macroradicaux PP (voie D), mais sans assez de MAH pour greffer sur les macroradicaux PP. Les macroradicaux subissent une β-scission et une terminaison. Ainsi, dans la figure 1.13, le degré de greffage augmente tout d'abord, puis diminue avec l'augmentation de la quantité de DCP. En outre, il semble quand le ratio initial entre MAH et DCP est égal à 1, le degré de greffage est le plus grand.

1.2.2 Greffage de silane sur du polypropylène par extrusion réactive

Dans cette recherche, nous avons étudié le processus de réaction radicalaire libre de greffage par le silane du PP par extrusion réactive. Nous avons utilisé la transformée de Fourier à infrarouge (FTIR) pour confirmer le greffage du silane sur le PP. La quantité de silane polymérisé, la masse molaire du PP résultant greffé par le silane et sa viscosité ont été mesurées. On a examiné les influences des conditions opératoires de l'extrusion réactive sur la qualité du PP silane greffé. L'objectif est de maximiser la quantité de silane greffé sur le PP, et dans le même temps de minimiser la quantité de silane polymérisée et la scission de la chaîne PP. Pour atteindre cet objectif, nous avons essayé la méthode d'optimisation multi-objectif.

Expérimentation

- Greffage de silane de radicaux libres sur PP par extrusion réactive

Le processus de greffage du silane a été effectué dans une extrudeuse à double vis. Deux profils de vis ont été utilisés (Figure 1.16). On a introduit le PP à la trémie et ajouté le mélange de quantités requises de silane, co-agent, peroxyde et additif antioxydant à l'extrudeuse à la zone 4. La principale différence entre ces deux profils de vis, c'est que la deuxième zone de malaxage du premier profil de la vis était plus proche du port d'injection des molécules de petite taille que le second. Pour toutes les essais, la composition du système de greffage a été constante.

Les extrudats obtenus à la sortie de l'extrudeuse étaient sous la forme de pastilles de 2 mm de diamètre et 4 mm de longueur. Ils ont été notés comme *original samples*. Ces derniers ont été séchés dans un four sous vide à 120°C pendant 20 heures afin d'éliminer les résidus de silane et de coagent. Ils ont été alors notés comme *dried samples*. Ces derniers ont été dissous dans le xylène bouillant, puis précipités dans l'acétone à température ambiante pour éliminer davantage silane n'ayant pas réagi et les résidus de coagent, de silane et silane polymérisé. Ils ont été notés comme *extracted samples*.

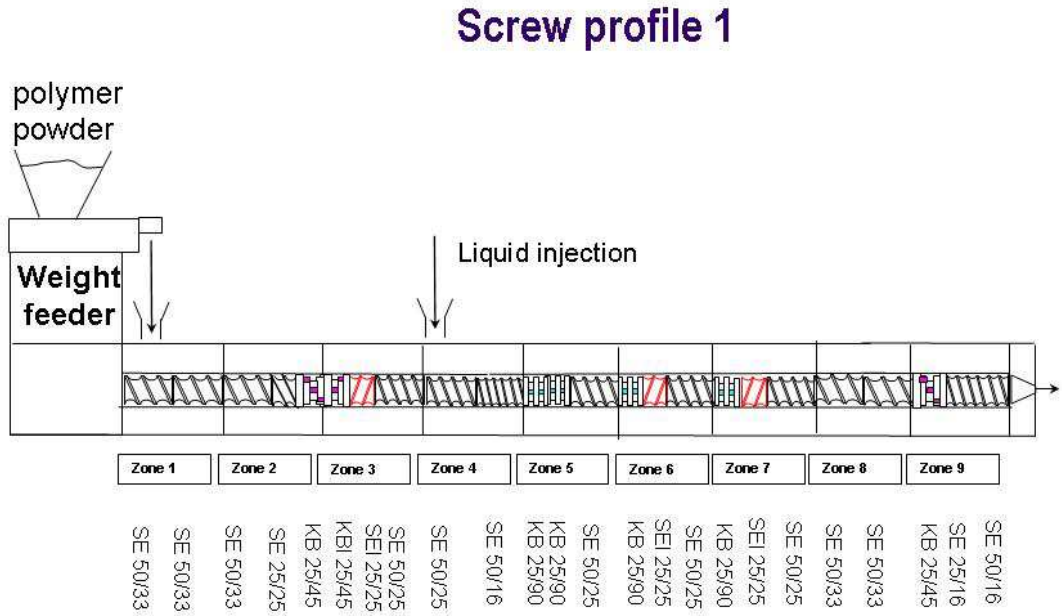

(a) Profils de la vis 1

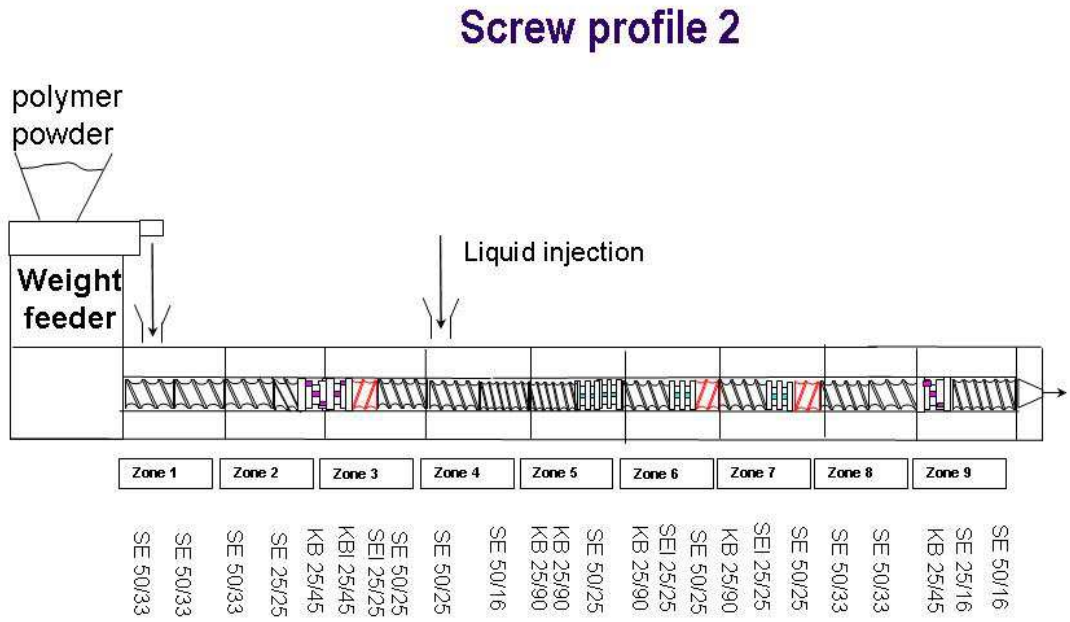

(b) Profils de la vis 2

Figure 1.16: Profils de la vis pour le greffage de silane sur du polypropylène

- Mesures

  Nous avons utilisé un spectrophotomètre FTIR de type Thermo-Nicolet Avatar 370 FTIR spectromètre pour vérifier si oui ou non le greffage de silane avait eu lieu au cours du processus d'extrusion réactive, et pour mesurer le degré de greffage et la polymérisation du silane. On a utilisé une chromatographie par perméation sur gel à haute température (Viscotek 350A HT-GPC System, US) à triple détecteur pour mesurer la masse molaire du PP modifié par le silane. Nous avons caractérisé

les propriétés rhéologiques de PP modifié par silane à l'état fondu en utilisant un rhéomètre à contrainte imposée Rheometric scientifique RDA3 avec une géométrie de plaques parallèles (diamètre de 15 mm et écart de 1.0 mm).

- Réticulation et résistance à la traction

Les "dried samples" ont été fondus dans un préparateur bi-vis micro de 15cc (DSM Xplore, Netherlands) à 190°C, puis injectés dans le moule pour obtenir des barres en forme d'haltère avec la partie test dans le milieu (dimension de la section transversale = 10 mm×4 mm, longueur de la partie de test = 80 mm). Ces derniers ont été notés *uncross-linked specimens*. Ces derniers ont ensuite été réticulés dans une solution aqueuse d'acide acétique 1% bouillant pendant 24 heures, et notés alors *cross-linked specimens*. Nous avons mesuré la résistance à la traction selon la Zwick/Roell Z020 à 23°C, avec une vitesse transverse de 50 mm/min.

Résultats et discussion

La Figure 1.17 compare les spectres IR des *origininal, dried* et *extracted samples* avec ceux de PP vierge. Le Tableau 1.4 indique les affectations des pics principaux. Les spectres de *extracted sample* affiche de nouveaux pics à 1191, 1086, 770 cm^{-1}, respectivement, indiquant que la réaction prévue de greffage de silane s'est produite. Le pic à 1060 cm^{-1} caractéristique de la liaison de Si-O-Si ([Ahmed et al., 2009]) n'est pas significatif, ce qui implique que aucune réaction significative de réticulation ne s'était passée.

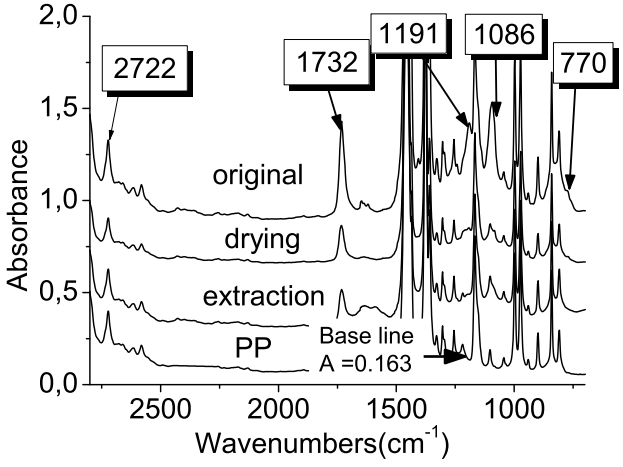

Figure 1.17: Spectres FT-IR de PP et de l'échantillon sélectionné

Table 1.4: Caractéristiques des spectres IR

Longueur d'onde (cm^{-1})	Groupe	Remarque
770	Si-O-CH_3	Si-O-CH_3 (CH3 rocking)
1086	Si-O-C	O-C stretching vibration of reacted or unreacted silane
1191	Si-O-C	O-CH_3 rocking vibration
1732	-C=O	C=O stretching vibration
2722	-C-H	-C-H stretching vibration

La Figure 1.18 montre des tracés typiques de GPC de PP vierge, *dried* et *extracted samples* à l'aide d'un détecteur de diffusion de lumière à angle droit 90° (RALS). Il y a un pic supplémentaire faible pour *dried sample*, correspondant à des molécules de grandes masses molaires. Il disparaît après l'extraction, ce qui indique que ces grosses molécules peuvent être solubilisées dans le xylène ou l'acétone. De ce fait, ce n'est pas le PP vierge ou le PP greffé par silane, mais le silane polymérisé. La polymérisation du silane est une réaction secondaire qui est en compétition avec son greffage sur PP.

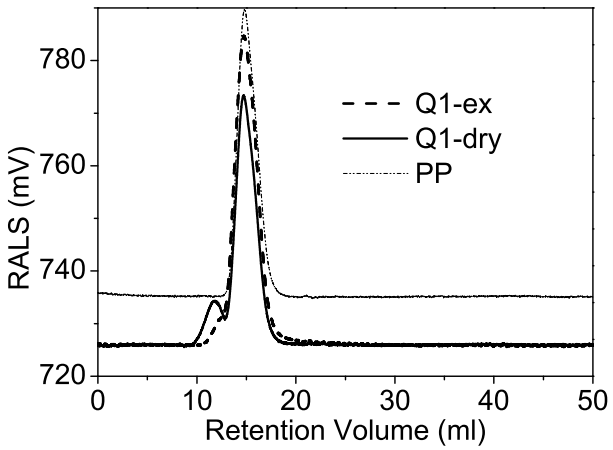

Figure 1.18: Courbes typiques de GPC pour *dried* et *extracted samples* (Q1-1)

La Figure 1.19 montre les courbes de viscosité complexes de PP vierge, de *dried* et *extracted samples* à l'état fondu. Par rapport à PP vierge, une plus grande viscosité complexe à basse fréquence de *dried sample* indique une ramification de chaîne PP et/ou les mélanges des molécules de grandes masses molaires, qui sont du silane polymérisé (prouvé par des traces GPC). Ainsi, les *dried samples* sont des mélanges de silane polymérisé, PP et de PP greffé par silane (PP-g-ATM). Après extraction, le silane polymérisé est retiré. Une plus grande viscosité complexe à basse fréquence est probablement causée par une rare réticulation au cours du processus d'extraction. On admet actuellement que les polymères fondus remplis des par des particules présentent une transition sol-gel (également nommée liquide-solide) due à la formation d'une structure de type gel par des particules solides

[Jain et al., 2006]. Ce comportement de gel est caractérisée par l'apparition d'un module élastique constant à des fréquences basses correspondant à un comportement de la contrainte d'écoulement de la viscosité. Les *extracted samples* présentent un comportement de type gel ou plus précisément un comportement de la contrainte d'écoulement, qui représente la ramification de chaîne. Cependant, la diminution importante de la viscosité complexe indique que, durant la réaction radicalaire du processus de réticulation par le silane, la scission de chaîne PP intervient comme une réaction secondaire.

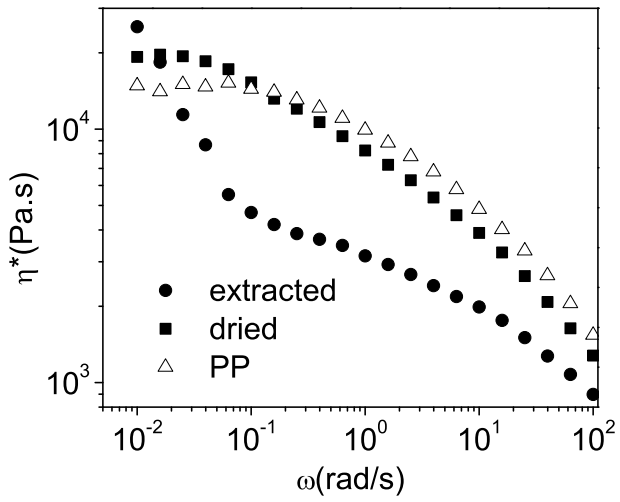

Figure 1.19: Variation de la viscosité de cisaillement complexe de PP vierge et de l'échantillon représentatif (Q=10kg/h, T=200°C, N=100rpm, profil de vis 1). (a) PP vierge (triangles) (b) *dried sample* (carrés) and (c) *extracted sample* (cercles).

La Figure 1.20 montre les courbes de contrainte-déformation d'un échantillon représentatif (Q=5.5kg/h, T=200°C, N=300rpm). Par rapport à PP vierge, le *uncross-linked specimen* (fait par *dried sample*) montre une plus grande contrainte de traction, avec un module comparable. Cela signifie que le PP greffé par silane et/ou les mélanges de PP greffé par silane, silane polymérisé et PP peuvent améliorer la résistance à la traction du matériau. Ceci peut s'expliquer car une plus faible interaction entre les particules rigides et la matrice polymère conduit à une plus grande dureté. [Thio et al., 2004] et [Jain et al., 2006] ont fait des observations similaires dans le cas de PP remplie par des billes de verre et dans le cas de (PP greffé par vinyl-triéthoxy silane)/silice nanocomposites. On peut trouver une augmentation supplémentaire de cette propriété dans le spécimen réticulé, ce qui prouve la formation d'une structure en réseau réticulé. De plus, le réseau réticulé peut ensuite augmenter la force de tension.

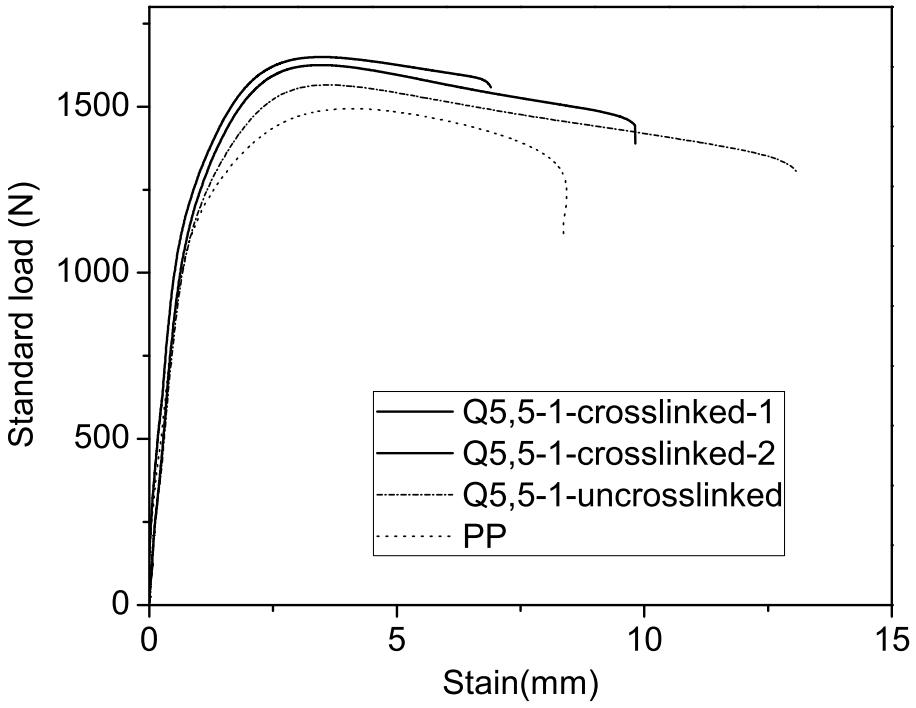

Figure 1.20: Courbes de contrainte-déformation de PP et Q5.5-1

Pour obtenir du polypropylène réticulé par un silane, l'étape-clé est le greffage du silane sur le polypropylène. Les réactions secondaires compétitives complexes et les transferts complexes de masse et de chaleur dans une extrudeuse rendent le processus d'extrusion réactive difficile à contrôler. Les conditions de fonctionnement, telles que le débit d'alimentation en matière Q, vitesse de la vis N, la température du cylindre T, même le profil de vis de l'extrudeuse, affecteront grandement les propriétés des produits.

Comme la composition du système de greffage est constante, le pourcentage de silane greffé sur PP et celui du silane polymérisé ont été utilisés pour représenter l'efficacité de greffage de silane et la quantité de silane polymérisé. Comme cela a été mentionné précédemment, les propriétés rhéologiques linéaires dynamiques peuvent fournir des informations précises sur les mélanges de polymères et/ou polymère greffé, et en même temps, la viscosité complexe peut également fournir l'information sur la masse molaire. Une faible viscosité complexe correspond à un faible masse molaire. Dans cette étude, nous avons utilisé la viscosité complexe pour étudier le degré de la dégradation de la chaîne de PP. Plus la viscosité complexe est faible, plus le degré de la dégradation de la chaîne de PP est sévère. Ainsi, l'objectif est d'obtenir le plus haut pourcentage de silane greffé avec le plus faible pourcentage de silane polymérisé et la plus haute viscosité complexe.

Le tableau 1.5 compare les deux profils de vis en termes de pourcentages de silane greffé et polymérisé. La principale différence entre les deux profils de vis est que la seconde zone de malaxage du profil 1 est plus proche du port d'injection des petites molécules que le profil 2. On peut voir que le profil de vis 1 surpasse systématiquement le profil de vis 2 en termes de pourcentage de silane greffé, sauf pour les échantillons Q5.5-3 et Q5.5-8-p2.

Ainsi, les pourcentages de silane greffé obtenus avec le profil de vis 1 sont toujours plus élevés que ceux obtenus avec le profil de vis 1, et cela indique que le profil de vis 1 est plus efficace pour le greffage de silane. Il en est de même pour le pourcentage de silane ayant réagi (greffé et polymérisé) et cela indique qu'il y a moins de silane non-réagi restant dans le produit PP-g-ATM pour le profil de vis 1. Les pourcentages de silane polymérisé obtenus avec le profil de vis 1 sont également toujours plus élevés que ceux obtenus avec le profil de vis 2. Ces résultats montrent que la qualité du mélange local entre le PP fondu et les réactifs liquides est un point clé pour la réaction de greffage. Afin d'assurer un bon mélange local, il est important que le lieu où les réactifs liquides sont injectés soit situé aussi proche que possible du bloc de mélange en aval.

Table 1.5: Comparaison des profils 1 et 2

Echantillon		$Q5.5-1$ $Q5.5-2-p2$	$Q5,5-2$ $Q5,5-4-p2$	$Q5,5-3$ $Q5,5-8-p2$	$Q5.5-4$ $Q5.5-6-p2$
Débit d'alimentation	kg/h	5.5	5.5	5.5	5.5
Température	°C	200	220	240	220
Vitesse de vis	rpm	300	100	300	500
Profil 1	Silane greffé %	37.76	19.85	30.37	25.72
	Silane polymérisé %	14.88	41.80	24.69	31.17
	Silane réagi %	52.64	61.64	55.07	56.89
Profil 2	Silane greffé %	22.68	17.62	37.76	19.04
	Silane polymérisé %	22.77	31.27	20.65	27.53
	Silane réagi %	45.45	48.89	58.41	46.56
Différence entre Profils 1 et 2	Silane greffé %	15.08	2.23	−7.39	6.68
	Silane polymérisé %	−7.89	10.53	4.04	3.64
	Silane réagi %	7.19	12.75	−3.34	10.33

Le rapport entre le débit d'alimentation et la vitesse de la vis, Q/N, caractérise le degré global de remplissage et de l'intensité du mélange dans une extrudeuse à double vis. Le Tableau 1.6 représente les pourcentages de silane greffé, polymérisé et ayant réagi, ainsi que la viscosité de fusion des *dried samples* PP-g-ATM pour un rapport Q/N de 1.1/60 kg/tour de vis et pour le profil de vis 2 qui est plus sensible aux paramètres de traitement. Nous pouvons voir qu'un débit d'alimentation élevé et de façon concomitante une vitesse de vis élevée entraînera un faible pourcentage de silane greffé de même que pour le pourcentage de silane ayant réagi, à l'intérieur des erreurs expérimentales. Par contraste, le pourcentage de silane polymérisé suit plus ou moins la tendance inverse. Lorsque Q/N est fixé, le degré global de remplissage et l'intensité de mélange sont fixés, quels que soient Q et N. Une augmentation Q avec une augmentation concomitante de N ne change pas le degré de remplissage ou de l'intensité de mélange mais réduit le temps de séjour. En conséquence, le temps disponible pour la polymérisation du silane est diminué et les pourcentages de silane greffés et polymérisés sont réduits. Cela indique que, indépendamment du mélange local entre PP et monomères à l'endroit de l'injection, le temps de séjour est également un paramètre important.

Table 1.6: Effet de Q et N sur les pourcentages de silane greffé, polymérisé et ayant réagi pour une valeur donnée de Q/N égale à 1.1/60 kg/tour de vis

Echantillon	Vitesse d'alimentation (kg/hr)	Température (°C)	Vitesse de vis (rpm)	Silane greffé %	Silane polymérisé %	Silane réagi %	$\eta_{0.063}$(10^4Pa.s) Sec	extr
Q5.5-Q/N-1s	5.5	220	300	26.83	34.76	61.59	0.442	0.077
Q8-Q/N-1s	8	220	440	19.10	24.21	43.31	0.166	0.094
Q10-Q/N-1s	10	220	545	16.40	27.68	44.07	0.185	0.080
Q2-Q/N-2s	2	220	109	29.13	16.66	45.80	0.229	0.091
Q8-Q/N-2s	8	220	440	18.10	23.79	41.89	0.170	0.058
Q/N	Débit d'alimentation/vitesse de vis = 1.1/60 kg/tour de vis							
1s	Un silane (ATM)							
2s	Un mélange de deux silanes (ATM + un autre silane)							

Les Figures 1.21, 1.22, 1.23, et le Tableau 1.7 montrent les influences des conditions opératoires (débit d'alimentation en matériau Q, température du cylindre T, vitesse de vis N) sur les pourcentages de silane greffé, polymérisé et ayant réagi (greffé et polymérisé), et la viscosité complexe à w=0.063 s^{-1}, en utilisant le profil de vis 1, qui est plus efficace pour le mélange de PP et de silane, amorceur. La dégradation de la chaîne PP et de la réaction du silane sont deux réactions compétitives. Parmi les expériences réalisées, les meilleures conditions pour empêcher la dégradation de la chaîne PP (la plus haute viscosité complexe) étaient Q=10 kg/h, T=220°C et N=100rpm, qui ont également fourni un faible pourcentage de silane ayant réagi. Les pires conditions pour la limitation de la dégradation de la chaîne PP (basse viscosité complexe) étaient Q=1kg/h, T =240°C et N =500rpm. Les conditions pour obtenir le montant le plus élevé de silane ayant réagi étaient Q=1kg/h, T=200°C and N=500rpm, correspondant également à l'obtention d'une faible viscosité complexe (soit une grave dégradation de la chaîne PP). On peut conclure qu'un faible débit d'alimentation, une température de cylindre élevée et/ou une vitesse de vis haute auront tendance à provoquer une sérieuse dégradation de la chaîne PP. De plus, le débit d'alimentation et la température du cylindre auront une influence plus grande que la vitesse de la vis. Un débit d'alimentation faible et une température du cylindre basse augmenteront aussi le pourcentage de silane ayant réagi. Cependant, la vitesse de vis a peu d'effet sur la réaction du silane, sauf dans les conditions de faible débit d'alimentation et température du cylindre basse. La réaction de dégradation de la chaîne PP sera plus compétitive que la réaction du silane à température du cylindre plus élevée. Dans des conditions de faible débit d'alimentation et la température du cylindre basse, comme un débit d'alimentation faible correspond à une durée suffisante pour la réaction et une température du cylindre faible correspond à une faible viscosité dans l'extrudeuse, par conséquent la vitesse de la vis déterminera grandement le degré de mélange des matériaux et modifiera le pourcentage de silane ayant réagi.

Cependant, le silane ayant réagi est constitué de deux parties, silane greffé et polymérisé. Un pourcentage élevé de silane ayant réagi ne signifie pas une grande quantité de silane greffé sur PP. Comme le montrent les figures 1.21, 1.22, 1.23 et le tableau 1.7, les conditions opératoires ont des effets opposés sur les pourcentages de silane greffé et polymérisé, ce qui indique que ce sont des réactions compétitives. Dans les expériences

réalisées, les conditions pour obtenir la quantité la plus élevée de silane greffé étaient avec Q=1kg/h, T=200°C, N=100rpm, ce qui a également fourni un faible pourcentage de silane polymérisé. A l'opposé, les conditions pour obtenir le pourcentage le plus élevé de silane polymérisé étaient Q=10kg/h, T=200°C, N=100rpm, qui corerspondait aussi aux plus mauvaises conditions pour le greffage de silane. Ainsi, un débit d'alimentation faible favorise le greffage du silane et, en même temps, une vitesse de vis faible favorise la polymérisation du silane. Ainsi, un débit d'alimentation faible, ce qui signifie un temps de séjour long, conduit à un temps suffisant pour la réaction. Une vitesse de vis faible, ce qui signifie une faible intensité de mélange, conduit à un mauvais contact entre le PP et le liquide (silane et amorceur) et l'enrichissement du silane et de l'amorceur. Ceci est favorable à la polymérisation du silane.

Cependant, les effets des conditions opératoires sur les pourcentages de silane greffé et polymérisé sont complexes. Les conclusions fondées sur ces figures sont difficiles à tirer.

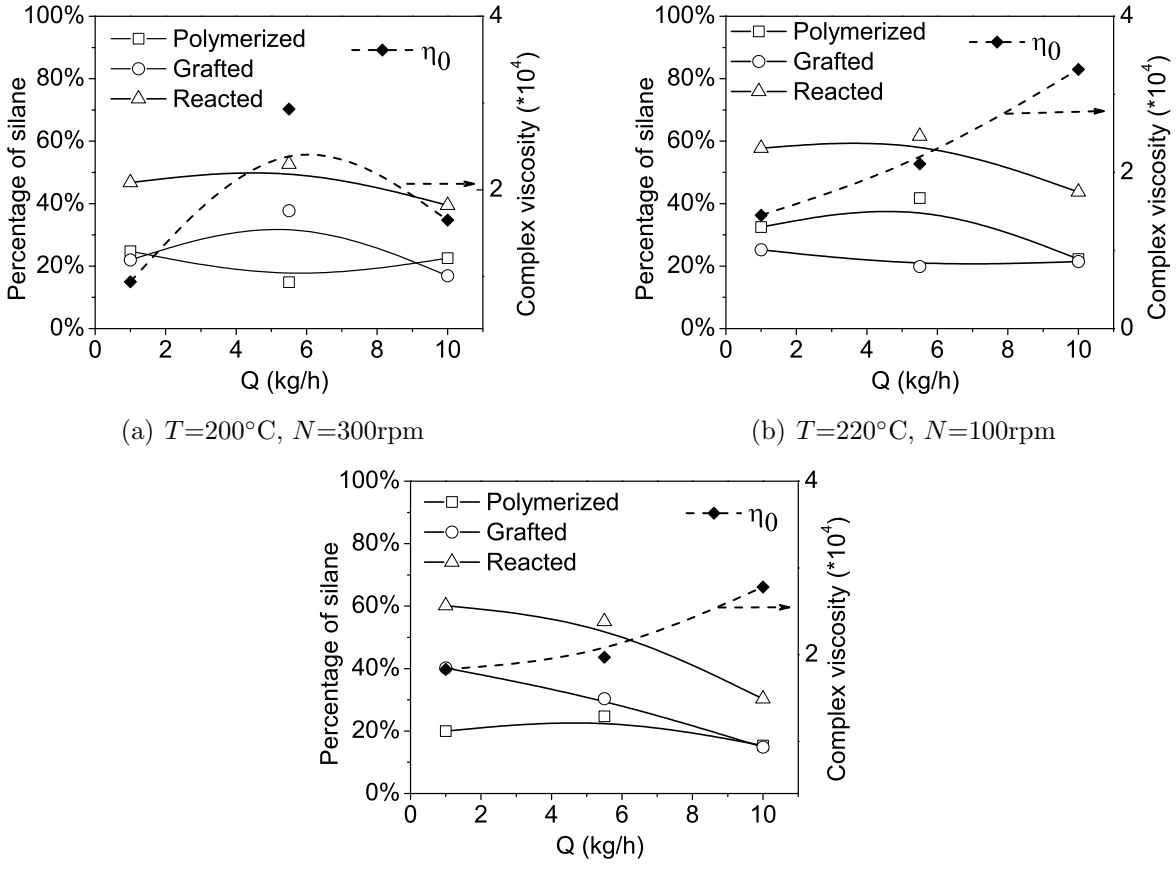

(a) T=200°C, N=300rpm

(b) T=220°C, N=100rpm

(c) T=220°C, N=300rpm

Figure 1.21: Effet du débit d'alimentation sur les propriétés du produit

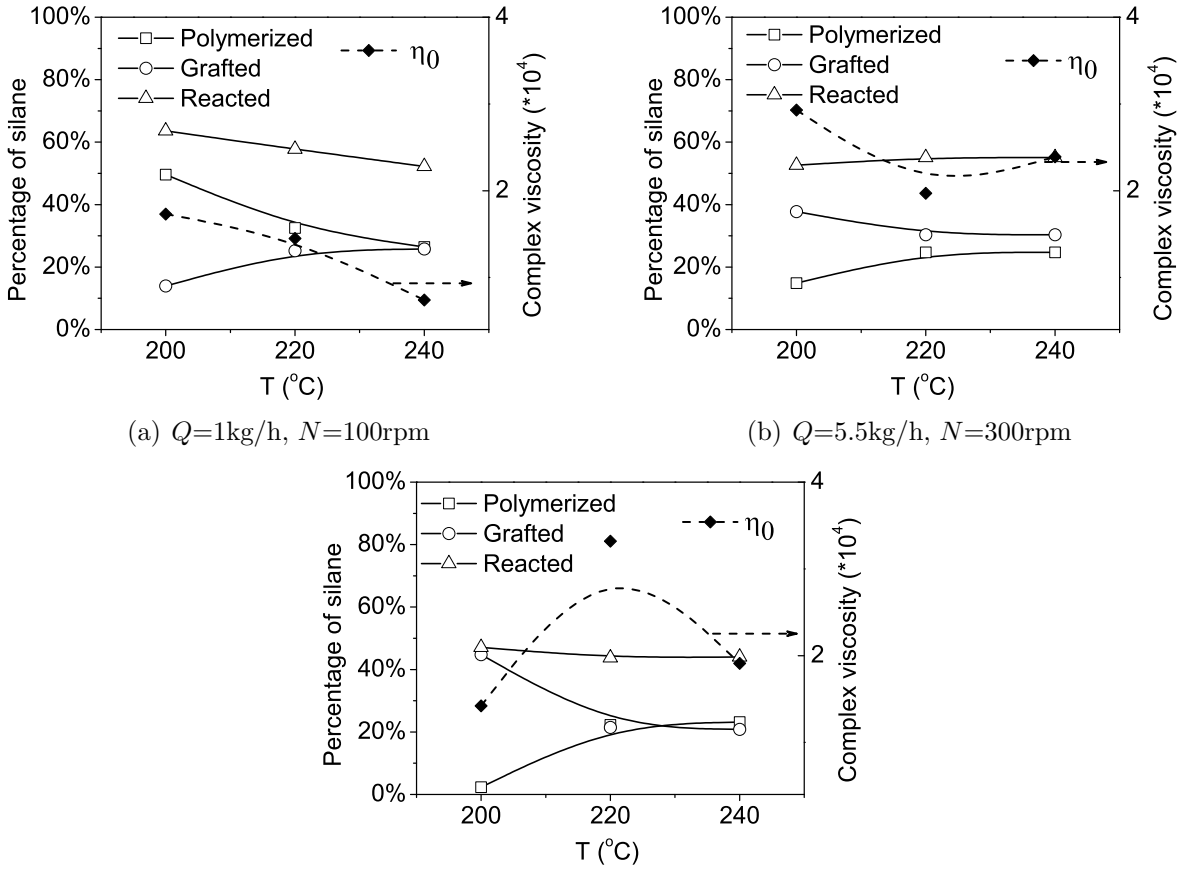

(a) Q=1kg/h, N=100rpm

(b) Q=5.5kg/h, N=300rpm

(c) Q=10kg/h, N=100rpm

Figure 1.22: Effet de la température du cylindre sur les propriétés du produit

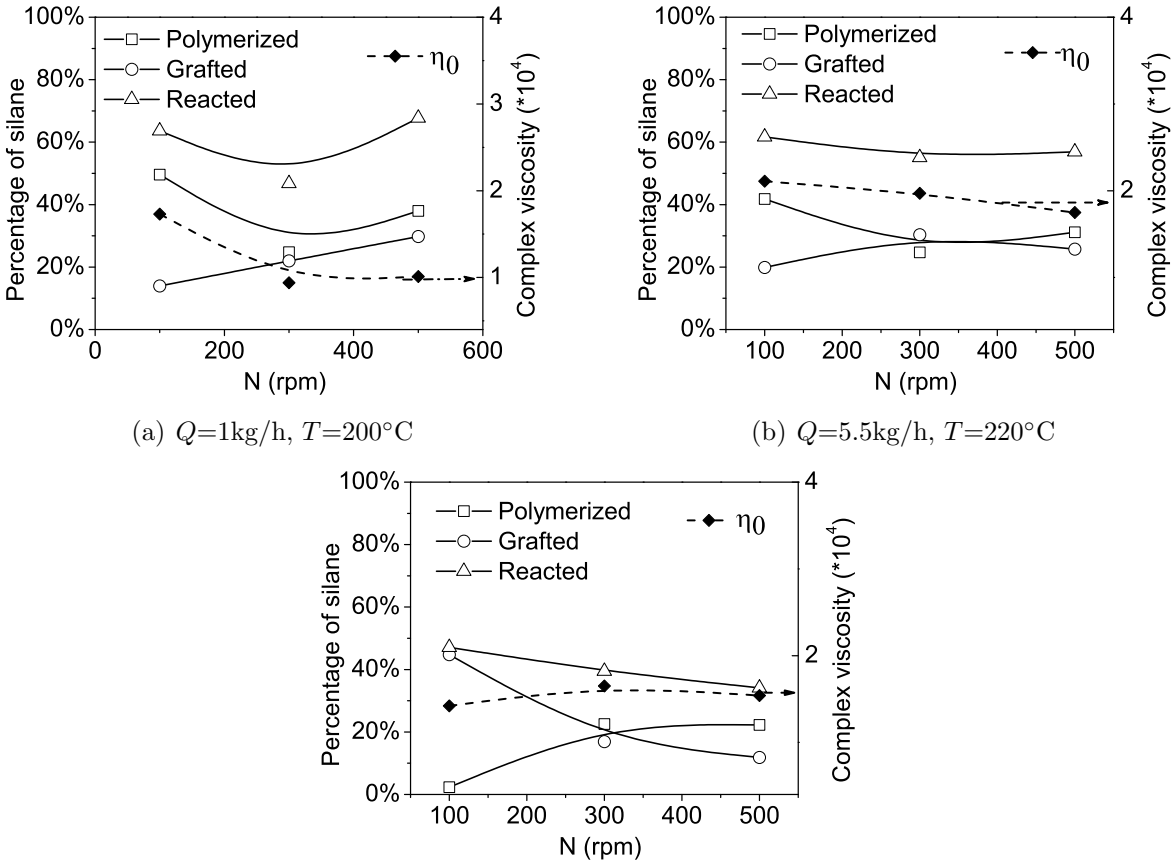

(a) Q=1kg/h, T=200°C

(b) Q=5.5kg/h, T=220°C

(c) Q=10kg/h, T=200°C

Figure 1.23: Effet de la vitesse de la vis sur les propriétés du produit

Table 1.7: Pourcentage de silane ayant réagi et viscosité complexe de PP-g-ATM

Echantillon	Débit d'alimentation (kg/h)	Température (°C)	Vitesse de vis (rpm)	Silane greffé %*	Silane polymérisé %*	Couple	$\eta_{0.063}$ (10^4Pa.s)	
							dry	extr
PP	-	-	-	-	-	-	1.52	
Q10-1	10	200	100	2.33	44.74	>110	1.42	0.33
Q10-2	10	200	300	22.57	16.91	75	1.65	0.58
Q10-3	10	200	500	22.26	11.85	74	1.54	0.40
Q10-4	10	220	100	22.26	21.47	91	3.32	0.29
Q10-5	10	220	300	15.38	14.89	75	2.78	0.23
Q10-6	10	240	100	23.18	20.86	98	1.91	0.33
Q10-7	10	240	500	27.93	16.71	67	1.89	0.19
Q5.5-1	5.5	200	300	14.88	37.76	66	2.93	0.38
Q5.5-2	5.5	220	100	41.80	19.85	65	2.11	0.21
Q5.5-3	5.5	240	300	24.69	30.37	58	2.39	0.41
Q5.5-4	5.5	220	500	31.17	25.72	63	1.75	0.18
Q1-1	1	200	100	49.62	13.98	51	1.73	0.45
Q1-2	1	200	300	24.79	21.97	63	0.94	0.17
Q1-3	1	200	500	37.96	29.76	53	1.01	0.20
Q1-4	1	200	300	37.66	22.68	-	-	-
Q1-5	1	220	100	32.52	25.21	50	1.45	0.41
Q1-6	1	220	300	19.98	40.19	54	1.83	0.36
Q1-7	1	240	100	26.40	25.82	50	0.74	0.14
Q1-8	1	240	500	33.50	18.83	52	0.44	0.19
Q5.5-t1-re	5.5	220	300	36.64	28.35	60	3.66	-
Q5.5-t2-re	5.5	220	300	18.93	42.52	60	2.56	-
Q5.5-t3-re	5.5	220	300	22.87	54.46	61	1.42	-
Q5.5-t4-re	5.5	220	300	18.22	40.49	60	1.93	-
Q5.5-1-p2	5.5	200	100	12.75	34.22	-	3.23	1.70
Q5.5-2-p2	5.5	200	300	22.77	22.68	60	3.27	0.94
Q5.5-3-p2	5.5	200	500	19.55	22.67	-	1.27	0.68
Q5.5-4-p2	5.5	220	100	31.27	17.62	61	1.75	0.38
Q5.5-5-p2	5.5	220	300	28.34	22.07	-	1.42	0.49
Q5.5-6-p2	5.5	220	500	27.53	19.04	57	1.02	0.39
Q5.5-7-p2	5.5	240	100	15.59	33.41	-	1.03	0.72
Q5.5-8-p2	5.5	240	300	20.65	37.76	54	3.26	0.36
Q5.5-9-p2	5.5	240	500	28.64	26.02	-	0.64	0.41
Q5.5-Q/N-1s	5.5	220	300	34.76	26.83	-	0.44	0.077
Q8-Q/N-1s	8	220	440	24.21	19.10	-	0.17	0.094
Q10-Q/N-1s	10	220	545	27.68	16.40	-	0.19	0.080
Q2-Q/N-2s	2	220	109	16.66	29.13	-	0.23	0.091
Q8-Q/N-2s	8	220	440	23.79	18.10	-	0.17	0.058

'sec'	Echantillons originaux séchés dans un four sous vide
'extr'	Echantillons après extraction
'p2'	Profil 2
Q5,5-t'n'-re	$n$ème échantillon répété avec la même condition
Q/N	Débit d'alimentation/vitesse de vis = 1.1 kg/tour de vis
1s	Un silane (ATM)
2s	Mélange de deux silanes (ATM + un autre silane)

Table 1.8: Propriétés de résistance à la traction de PP-g-ATM

Echantillon	Contrainte d'écoulement (MPa)		Allongement à contrainte d'écoulement (mm)		Contrainte à rupture (N)		Module de Young (kPa)		Allongement à rupture (%)	
	cr	un	cr	un	cr	un	cr	un	cr	un
PP	37.7		4.2		1050		1990		19.4	
Q10-1	45.6	39.7	2.9	3.3	1630	1210	2240	2080	17.5	22.5
Q10-2	45.6	41.3	2.7	2.9	1560	1280	3060	2230	18.6	13.9
Q10-3										
Q10-4	43.4	40.6	3.4	3.4	1570	1330	2340	2980	18.1	32.1
Q10-5	40.8	38.4	2.9	3.2	1480	1350	2580	1740	9.8	12.7
Q10-6	40.3	37.9	2.9	2.9	1330	1100	2120	2140	24.4	10.0
Q10-7	40.1	36.4	2.7	3.6	1460	1280	2810	2210	10.0	17.7
Q5.5-1	41.7	40.2	3.4	3.6	1470	1300	2460	1890	16.7	26.2
Q5.5-2	42.5	39.4	3.1	3.3	1490	1340	2380	1890	18.0	24.5
Q5.5-3	43.9	38.3	2.8	3.1	1570	1180	2550	2200	11.6	18.6
Q5.5-4	40.4	37.2	3.1	3.2	1360	1160	2130	2000	12.7	10.5
Q1-1	41.0	36.2	2.5	3.0	1450	1170	2090	2100	9.9	9.8
Q1-2	41.8	38.6	3.0	3.0	1400	1150	2490	2250	20.6	15.2
Q1-3	40.4	40.8	3.2	4.0	1530	1240	2110	1900	10.1	18.8
Q1-4										
Q1-5	44.5	39.4	3.3	3.9	1530	1300	2180	2060	23.4	20.5
Q1-6	40.3		3.0		1440		2030		14.0	
Q1-7	39.9	37.9	3.3	3.0	1470	1270	1880	2360	14.2	16.1
Q1-8										
Q5.5-t1-re	44.5	41.8	3.2	3.5	1500	1470	2540	2410	16.6	20.3
Q5.5-t2-re	44.4	45.5	3.2	2.9	1540	1590	2280	2670	16.5	79.2
Q5.5-t3-re	44.4	42.5	3.0	2.9	1570	1410	2510	2440	19.7	14.3
Q5.5-t4-re	42.9	44.1	3.3	2.8	1440	1490	2770	2480	22.1	19.9
Q5.5-1-p2	43.5	41.6	3.3	3.1	1580	1340	2500	2430	23.9	742.3
Q5.5-2-p2	45.2	42.9	2.9	3.0	1610	1510	2230	2190	15.8	9.9
Q5.5-3-p2	42.9	39.6	3.0	3.1	1550	1290	2170	2180	16.3	29.8
Q5.5-4-p2	45.6	43.9	2.7	2.7	1660	1520	2670	2880	15.6	14.3
Q5.5-5-p2	42.7	42.5	3.3	3.7	1520	1520	2340	2120	15.2	14.0
Q5.5-6-p2	43.0	42.7	3.7	3.0	1560	1570	2270	2320	16.3	712.4
Q5.5-7-p2	43.9	42.8	3.7	2.9	1390	1500	2110	2120	32.3	10.9
Q5.5-8-p2	40.5		2.7		1430		2330		12.6	
Q5.5-9-p2	43.0		3.7		1530		2230		16.5	
Q5.5-Q/N-1s	42.4	41.2	4.1	4.0	1480	1520	2200	2040	20.1	13.2
Q8-Q/N-1s	42.0	38.9	3.9	4.0	1560	1470	2360	2150	13.0	10.6
Q10-Q/N-1s	40.0	39.8	3.0	3.5	1540	1550	1980	2340	8.2	8.2
Q2-Q/N-2s	43.8	41.5	4.0	3.3	1540	1440	1910	2380	16.6	15.5
Q8-Q/N-2s	42.2	36.8	3.7	3.4	1530	1350	1940	1670	14.3	10.8

'dry'	Echantillons originaux séchés dans un four sous vide
'extr'	Echantillons après extraction
'p2'	Profil 2
Q5,5-t'n'-re	$n$ème échantillon répété avec la même condition
Q/N	Débit d'alimentation/vitesse de vis = 1.1 kg/tour de vis
1s	Un silane (ATM)
2s	Mélange de deux silanes (ATM + un autre silane)
cr	réticulé
un	non réticulé

Le Tableau 1.8 montre des propriétés de traction. Au cours de la réaction de greffage de silane, les réactions de greffage de silane et de scission de la chaîne de PP se produisent en même temps. Le silane et la réticulation peuvent améliorer les propriétés de traction du matériau, mais une scission de chaîne PP l'affectera de manière compliquée. Ainsi, nous ne pouvons pas trouver des relations simples entre les propriétés de traction et le pourcentage de silane greffé/réagi ou entre les propriétés de traction et de la viscosité complexe.

De ce fait, nous utiliserons des modèles de simulation assistée par ordinateur et d'autres outils de conception pour concevoir, simuler et optimiser ce processus chimique. En se fondant sur une conception expérimentale, nous pouvons établir des modèles polynomiaux, qui peuvent fournir la relation quantitative entre les propriétés du produit et les conditions opératoires, et ensuite, le décideur peut obtenir la meilleure solution en utilisant une méthode d'optimisation multi-objectif.

Stratégie de modélisation

La procédure appliquée de l'optimisation des processus comprend la définition du modèle, l'analyse et l'optimisation (Figure 1.24).

En raison des réactions complexes dans l'extrudeuse, il est difficile d'établir un modèle basé sur le mécanisme de réaction. La possibilité est de considérer le réacteur comme une boîte noire et de développer des relations empiriques entre les variables de processus et les propriétés des produits. La seule restriction est de choisir un degré assez élevé pour obtenir une représentation satisfaisante de ce phénomène et assez petit pour éviter un trop grand nombre de paramètres. Afin de déterminer un modèle polynomial, nous commençons par un modèle de premeir degré pour la première étape. Mais un tel modèle ne permet pas de représenter les phénomènes non linéaires. Pour cette raison, deux types de modèles polynomiaux du second degré ont été choisis de manière à être en mesure de les représenter d'une manière satisfaisante. En fait, pour trois facteurs, les structures des modèles polynomiaux sont les suivantes:

1. Modèle I

$$y_i = a_0 + a_1\,Q_i + a_2\,T_i + a_3\,N_i + a_{11}\,Q_i^2 + a_{22}\,T_i^2 + a_{33}\,N_i^2 + a_{12}\,Q_iT_i + a_{13}\,Q_iN_i + a_{23}\,T_iN_i + \epsilon_i \tag{1.19}$$

2. Modèle II

$$y_i = a_0 + a_1\,Q_i + a_2\,T_i + a_3\,N_i + a_{12}\,Q_iT_i + a_{13}\,Q_iN_i + a_{23}\,T_iN_i + a_{123}\,Q_iT_iN_i + \epsilon_i \tag{1.20}$$

où y est la valeur du critère pour le numéro de l'expérience i, Q, T et N représentent, dans le même ordre, les valeurs normalisées du débit d'alimentation Q, la température du cylindre T, la vitesse de vis N. Les paramètres a_i sont les coefficients du polynôme à déterminer. ϵ est l'erreur inconnue expérimentale supposée gaussienne. De manière évidente, le modèle I contient des termes quadratiques tandis que le modèle II contient un terme d'interaction triple.

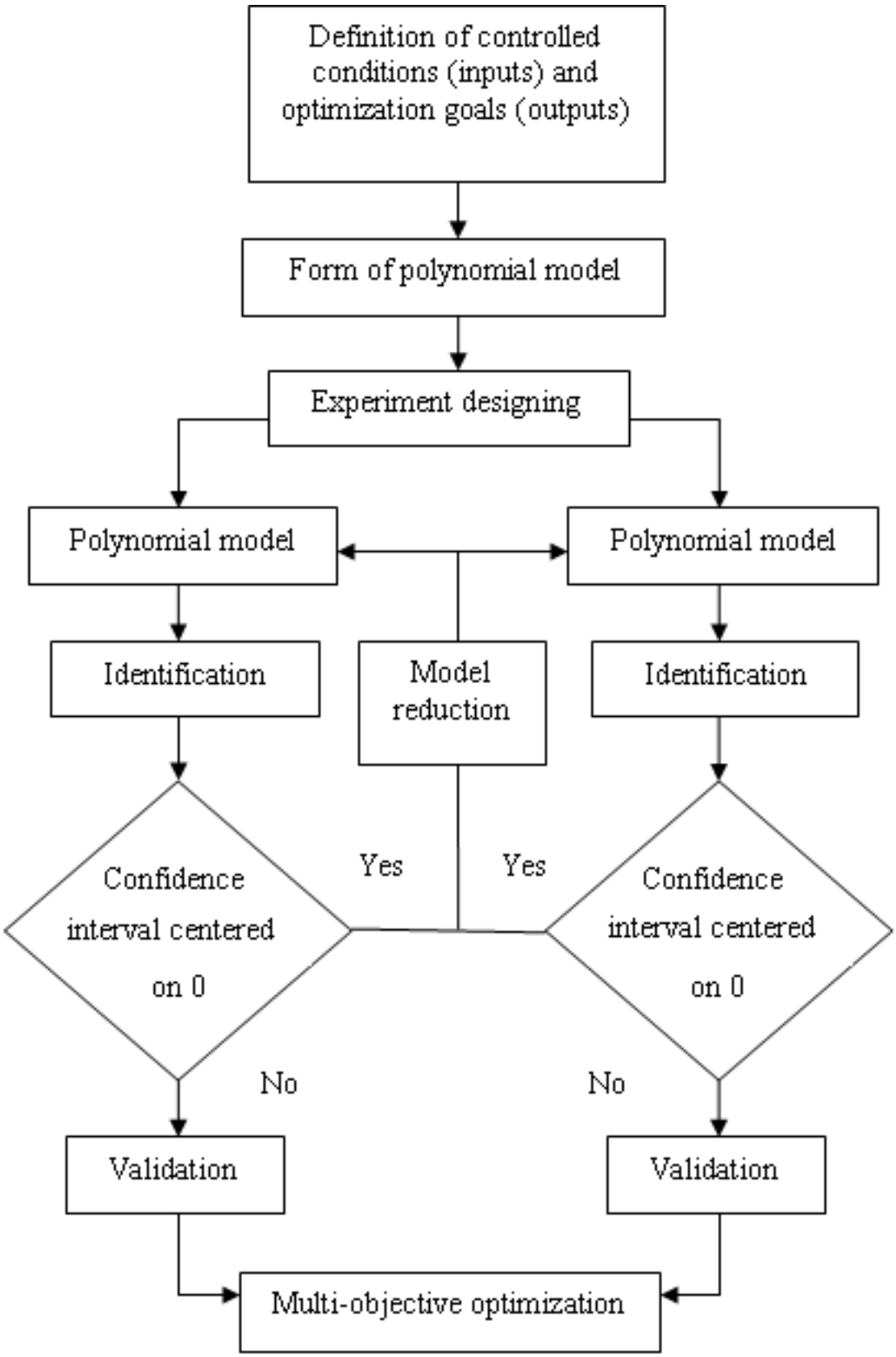

Figure 1.24: Structure de la méthodologie pour l'optimisation des processus.

Nous avons estimé les coefficients par régression multilinéaire. Toutefois, la validation

du modèle n'est possible que si le nombre de degrés de liberté est supérieur à zéro, le nombre de degrés de liberté étant égal au nombre d'expériences choisies pour l'estimation moins le nombre de coefficients du modèle. La méthodologie utilisée est résumée dans la figure 1.25.

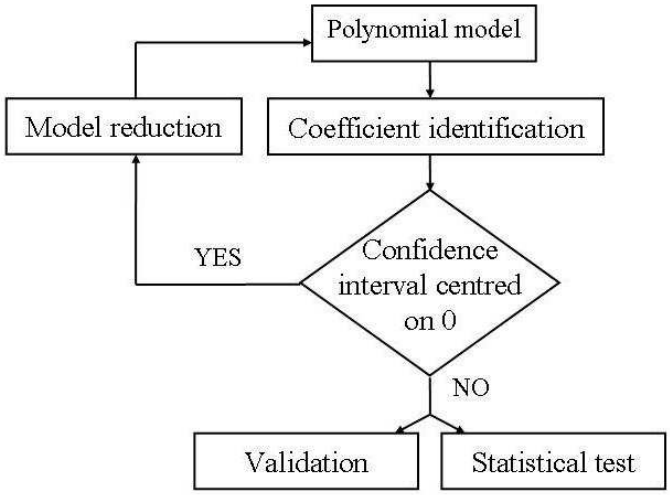

Figure 1.25: Etapes de la modélisation polynomiale

Après avoir calculé les coefficients, il est nécessaire de vérifier s'ils sont significatifs ou si les écarts des données à partir d'une valeur constante sont simplement dûs à une variation aléatoire de la réponse, à cause d'erreurs de mesure ou de la dérive de facteurs non contrôlés. Nous pouvons utiliser le test de Fisher-Snedecor et l'écart-type des coefficients.

Les réactions complexes et les conditions opératoires dans le processus de greffage du silane sur du polypropylène par extrusion réactive dans l'extrudeuse causent une mauvaise répétabilité des expériences. Ceci a causé l'échec du processus de modélisation. Les résultats de la modélisation des échantillons sont présentés dans la figure 1.26 et les tables 1.9, 1.10 and 1.11.

Table 1.9: Test de Fisher-Snedecor pour le pourcentage de silane greffé

Ratio	$F = \sigma_1^2/\sigma_2^2$	$(n_1; n_2)$	$1/F_{0.025}(n_2, n_1)$	$F_{0.025}(n_1, n_2)$	Validation
Modèle I					
Validation/Identification	1.390	(6 ; 5)	0.228	4.950	Oui
Validation/Répétition	1.522	(6 ; 3)	0.210	8.941	Oui
Identification/Répétition	1.094	(5 ; 3)	0.185	9.014	Oui
Modèle II					
Validation/Identification	2.783	(6 ; 7)	0.238	3.866	Oui
Validation/Répétition	0.893	(6 ; 3)	0.210	8.941	Oui
Identification/Répétition	0.321	(7 ; 3)	0.230	8.887	Oui

Table 1.10: Intervalle de confiance apparent des coefficients du modèle initial avec un risque de 5% pour le pourcentage de silane greffé

Coefficients	Values of $\hat{a}$	$\hat{a}_{min}$	$\hat{a}_{max}$	$\hat{a}^{red}_{min}$	$\hat{a}^{red}_{max}$	Θ	Significatif
Model I							
a_0	0.2755	-0.5049	1.0559	-0.0131	0.5641	2.0915	Oui
a_1	-0.0195	-0.3486	0.3095	-0.3486	0.3095	1.1262	Oui
a_2	-0.0255	-0.3545	0.3035	-0.3545	0.3035	1.1680	Oui
a_3	0.0353	-0.4032	0.3326	-0.3822	0.3115	1.2124	Oui
a_{11}	-0.0001	-0.7805	0.7803	-0.3292	0.3289	1.0003	Non
a_{22}	0.0651	-0.7153	0.8455	-0.2639	0.3942	1.1821	Oui
a_{33}	-0.1123	-0.8927	0.6681	-0.4592	0.2345	1.3363	Oui
a_{12}	-0.0249	-0.3928	0.3430	-0.3928	0.3430	1.1453	Oui
a_{13}	-0.0573	-0.4252	0.3106	-0.4252	0.3106	1.3689	Oui
a_{23}	0.0075	-0.3604	0.3753	-0.3604	0.3753	1.0414	Non
Model II							
a_0	0.2247	0.1212	0.3282	0.1232	0.3262	2.7081	Oui
a_1	-0.0129	-0.1223	0.0965	-0.1186	0.0928	1.2668	Oui
a_2	-0.0038	-0.1145	0.1070	-0.1141	0.1066	1.0705	No
a_3	-0.0300	-0.1476	0.0876	-0.1458	0.0858	1.6847	Oui
a_{12}	-0.0174	-0.1353	0.1004	-0.1332	0.0983	1.3476	Oui
a_{13}	-0.0447	-0.1625	0.0731	-0.1604	0.0711	2.2212	Oui
a_{23}	0.0075	-0.1220	0.1369	-0.1220	0.1369	1.1224	Non
a_{123}	0.0644	-0.0650	0.1938	-0.0650	0.1938	2.9799	Oui

Table 1.11: Ecart-type et intervalle de confiance des coefficients du modèle polynomial des deux modèles polynomiaux avec un risque de 5% pour le pourcentage de silane greffé

Coefficients	Values of $\hat{a}$	$\hat{a}_{min}$	$\hat{a}_{max}$	$\hat{a}^{red}_{min}$	$\hat{a}^{red}_{max}$
Model I: $y = a_0 + a_1Q + a_2T + a_3N + a_{22}T^2 + a_{33}N^2 + a_{12}QT + a_{13}QN$					
a_0	0.2755	-0.0850	0.6359	0.1151	0.4358
a_1	-0.0195	-0.2023	0.1633	-0.2023	0.1633
a_2	-0.0255	-0.2083	0.1573	-0.2083	0.1573
a_3	-0.0353	-0.2339	0.1633	-0.2280	0.1574
a_{22}	0.0651	-0.3657	0.4960	-0.1177	0.2479
a_{33}	-0.1124	-0.5008	0.2760	-0.3051	0.0803
a_{12}	-0.0249	-0.2293	0.1795	-0.2293	0.1795
a_{13}	-0.0573	-0.2617	0.1471	-0.2617	0.1471
Model II: $y = a_0 + a_1Q + a_3N + a_{12}QT + a_{13}QN + a_{123}QTN$					
a_0	0.225	0.1547	0.2953	0.1558	0.2942
a_1	-0.0129	-0.0874	0.0617	-0.0849	0.0591
a_3	-0.0299	-0.1101	0.0502	-0.1088	0.049
a_{12}	-0.0174	-0.0977	0.0628	-0.0963	0.0614
a_{13}	-0.0447	-0.125	0.0356	-0.1236	0.0342
a_{123}	0.0644	-0.0238	0.1526	-0.0238	0.1526

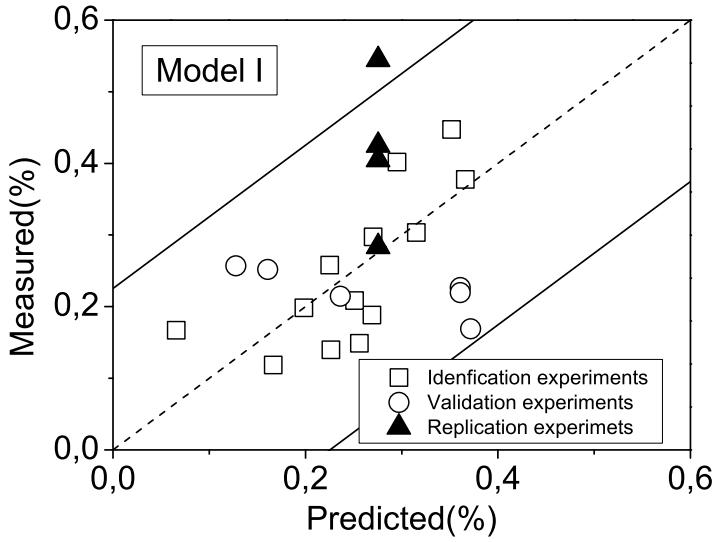

(a) model I

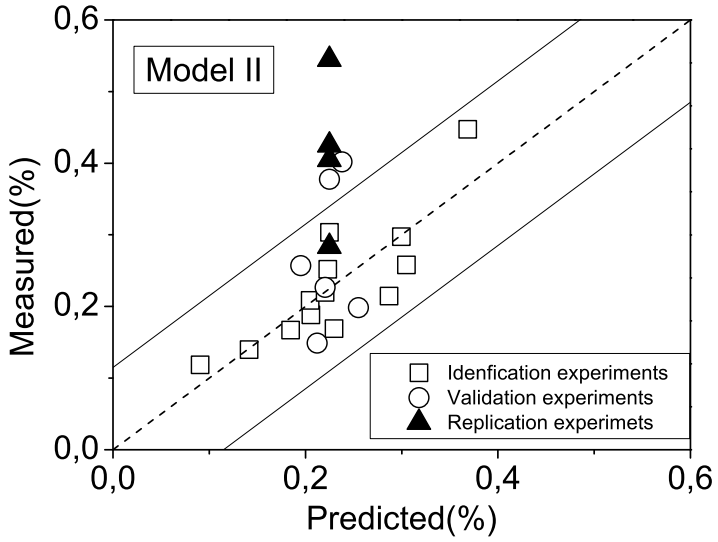

(b) model II

Figure 1.26: Comparaison entre les pourcentages de silane greffé expérimental et calculé

Après la validation du modèle, les modèles utilisés pour l'optimisation multi-objectif sont définis. On peut obtenir l'optimisation à l'aide d'un algorithme génétique diploïde en codage réel, qui est développé dans notre laboratoire [Fonteix et al., 1995, 2004], afin de déterminer une représentation finie du domaine de Pareto.

Les réactions complexes et les conditions opératoires dans le processus de greffage du silane sur du polypropylène par extrusion réactive dans l'extrudeuse provoquent une mauvaise répétabilité des expériences, qui est la raison principale pour laquelle presque tous les modèles polynomiaux établis ci-dessus ne peuvent pas être utilisé. Afin d'optimiser ce processus, nous devrions améliorer les conditions de fonctionnement pour rendre le procédé d'extrusion plus stable pour obtenir une bonne reproductibilité des expériences.

C'est le travail que nous devrons faire par la suite.

1.3 Conclusion

La partie I traite des modèles théoriques de polymérisations en émulsion. Sa principale conclusion est que les différences entre les macro-et mini- polymérisation en émulsion sont liés au mécanisme de nucléation. La nucléation micellaire est le processus dominant de nucléation de particules dans les polymérisation en macro-émulsion, et par comparaison, la nucléation des gouttelettes est dominante dans les polymérisations en mini-émulsion. L'établissement d'un modèle dans la polymérisation en mini-émulsion est plus difficile que dans la polymérisation en macro-émulsion, car dans la polymérisation en mini-émulsion, le nombre des sites de nucléation est plus complexe à calculer. Nous avons établi un modèle de polymérisation en macro-émulsion basé sur le modèle 0-1, et par comparaison, un modèle de polymérisation en mini-émulsion sur la base des bilan des potentiels chimiques du monomère dans le réacteur. En général, on observe une bonne concordance entre les modèles et les données expérimentales de la littérature. Le modèle de polymérisation en macro-émulsion nous permet de prédire la distribution des tailles de de radicaux pour une classe donnée de tailles de particules et la distribution de taille des particules, et le modèle de polymérisation en mini-émulsion nous permet de prédire la distribution de taille des particules et la variation des tailles de gouttelettes. Cependant, pour obtenir une distribution plus précise des tailles de radicaux, il faut développer les modèles incluant le transfert des radicaux polymères aux monomères dans les particules et la désorption des radicaux monomères dans les particules à la phase aqueuse.

La partie II traite de l'amélioration des propriétés de polypropylène par extrusion réactive, Pour améliorer le degré de greffage de la MAH de PP, nous avons utilisé la montmorillonite organiquement modifiée o-MMT comme un nanoréacteur. Nous avons étudié les effets des quantités de MAH et de l'amorceur. Des interactions fortes entre la surface de MMT et MAH et l'encapsulation d'espèces actives améliorent le degré de greffage. Avec MAH en excès, il se formera une cage autour de MMT qui empêchera la formation de $PP^{\bullet}$ et réduira le degré de greffage. Pour améliorer le degré de greffage du silane sur PP, nous avons étudié les conditions de fonctionnement. Le silane a en effet été greffé sur le PP et la réticulation ne s'est pas produite pendant le processus d'extrusion réactive, comme cela est prouvé par spectroscopie FTIR. Le greffage de silane sur PP et/ou des mélanges de PP greffé par silane, de silane polymérisé et de PP peuvent améliorer la résistance à la traction des matériaux, et cette propriété peut encore être améliorée par la formation de la structure du réseau réticulé par réticulation en phase aqueuse. D'après le GPC avec un détecteur RALS et les mesures rhéologiques au fondu en condition dynamique, la polymérisation du silane et de la scission de la chaîne PP sont les deux principales réactions secondaires compétitives dans l'extrudeuse. Cependant, de nombreux éléments, en particulier les conditions opératoires, peuvent affecter le processus d'extrusion réactive. Le bon mélange entre le PP fondu et les petites molécules liquides (essentiellement silane et amorceur) après l'injection est un élément clé de la réaction de greffage. Le temps de séjour est également un paramètre important du processus. Un long temps de séjour, une température de cylindre de haute et/ou une forte intensité de mélange entraîneront la dégradation de la chaîne de PP. Un long temps de séjour favorise le greffage de silane et une vitesse de vis faible favorise la polymérisation de

silane. Toutefois, on ne peut pas obtenir l'objectif de la plus grande quantité de silane greffé avec le plus bas taux de silane polymérisé et la dégradation de la chaîne de PP ne peut pas être obtenue uniquement par une méthode expérimentale. Nous devrions développer un procédé d'extrusion plus stable pour obtenir une bonne reproductibilité des expériences. Ensuite, nous pouvons utiliser des modèles polynomiaux et optimisation multi-objectif d'atteindre l'objectif précédent. Cela peut même aider le décideur dans l'industrie pour obtenir la meilleure solution.

Bibliography

G. S. Ahmed, M. Gilbert, S. Mainprize, and M. Rogerson. Ftir analysis of silane grafted high density polyethylene. *Plastics, Rubber and Composites*, 38:13–20, 2009.

S. Al-Malaika, editor. *Reactive modifiers for polymers*. Blackie Academic and Professional Chapman and Hall, London, 1996.

M. Alexandre and P. Dubois. Polymer-layered silicate nanocomposites: preparation, properties and uses of a new class of materials. *Mater. Sci. Eng.*, 28:1–63, 2000.

Y. J. An, Z. J. Zhang, and W. G. Bi. Characterization of high melt strength polypropylene synthesized via silane grafteing initiated by in situ heat induction reaction. *J. Appl. Polym. Sci.*, 110:3727–3732, 2008.

M. Beltran and C. Mijangos. Silane grafting and moisture cross - linking of polypropylene. *Polym. Eng. Sci.*, 40:1534–1541, 2000.

Y. T. Choi, M. S. El-Aasser, E. D. Sudol, and J. W. Vanderhoff. Polymerization of styrene miniemulsions. *J. Polym. Sci. Pol. Chem.*, 23:2973–2987, 1985.

F. Ciardelli, S. Coiai, E. Passaglia, A. Pucci, and G. Ruggeri. Nanocomposites based polyolefins and functional thermoplastic materials. *Polym. Int.*, 57:805–836, 2008.

B. De Roover, M. Sciavons, V. Carlier, J. Devaux, R. Legras, and A. Momtaz. Molecular characterization of maleic anhydride-functionalized polypropylene. *J. Polym. Sci. Part A: Polym. Chem.*, 33:829–842, 1995.

J. Delgado and M. S. El-Aasser. Kinetic and thermodynamic aspects of miniemulsion copolymerization. *Makromol. Chem. Macromol. Symp.*, 31:63–67, 1990.

Z. Demjen, B. Pukanszky, and J. Nagy. Possible coupling reactions of functional silanes and polypropylene. *Polymer*, 40:1763–1773, 1999.

D. Edouard, N. Sheibat-Othman, and H. Hammouri. Observer design for particle size distribution in emulsion polymerization. *AIChE J.*, 51:3167–3185, 2005.

D. Feldman. Polyblend compatibilization. *J. Macromol. Sci. Part A: Pure Appl. Chem.*, 42:587–605, 2005.

C. Fonteix, F. Bicking, E. Perrin, and I. Marc. Haploid and diploid algorithms, a new approach for global optimization: compared performances. *Int. J. Syst. Sci.*, 26:1919–1933, 1995.

C. Fonteix, S. Massebeuf, F. Pla, and L. N. Kiss. Multicriteria optimization of an emulsion polymerization process. *Eur. J. Oper. Res.*, 153:350–359, 2004.

N. G. Gaylord. Use Surfactants to Blend Polymers. *Chem. tech.*, 19:435, 1989.

N. G. Gaylord and M. K. Mishra. Nondegradative reaction of maleic anhydride and molten polypropylene in the presence of peroxides. *J. Polym. Sci. Polym. Lett. Ed.*, 21:23–30, 1983.

N. G. Gaylord, M. Mehta, and V. Kumar. Graft copolymerization of maleic anhydride onto polyethylene. *Polym. Sci. Technol.*, 21:171–182, 1983.

P. E. Gloor, Y. Tang, A. E. Kostanska, and A. E. Hamielec. Chemical modification of polyolefins by free radical mechanisms: a modeling and experimental study of simultaneous random scission, branching and crosslinking. *Polymer*, 35:1012–1030, 1994.

N. Hasegawa, H. Okamoto, M. Kato, A. Tsukigase, and A. Usuki. Polyolefin-clay hybrids based on modified polyolefins and organophilic clay. *Macromol. Mater. Eng.*, 76:76–79, 2000a.

N. Hasegawa, H. Okamoto, M. Kato, and A. Usuki. Preparation and mechanical properties of polypropylene-clay hybrids based on modified polypropylene and organophilic clay. *J. Appl. Polym. Sci.*, 78:1918–1922, 2000b.

W. Heinen, C.H. Rosenmolle, C.B. Wenzel, H.J.M. de Groot, J. Lurtenburg, and M.van Duin. 13C NMR study of the grafting of maleic anhydride onto polyethene, polypropene, and ethene-propene copolymers. *Macromolecules*, 29:1151–1157, 1996.

H. Huang and N. C. Liu. Nondegradative melt functionalization of polypropylene with glycidyl methacrylate. *J. Appl. Polym. Sci.*, 67:1957–1963, 1998.

S. Jain, J. G. P. Goossens, and M. van Duin. Synthesis, characteriztion and properties of (vinyl triethoxy silane-grafted pp)/silica nanocomposites. *Macromol. Symp.*, 233: 225–234, 2006.

H. S. Kaufman and J. J. Falcetta, editors. *Introduction to polymer science and technology: an SPE Text-book.* Wiley, New York, 1977.

M. Kawasumi, N. Hasegawa, M. Kato, A. Uski, and A. Okada. Preparation and mechanical properties of polypropylene-clay hybrids. *Macromolecules*, 30:6333–6338, 1997.

C. Koning, M. Van Duin, C. Pagnoulle, and R. Jerome. Strategies for compatibilization of polymer blends. *Prog. Polym. Sci.*, 23:707–757, 1998.

N. C. Liu and W. E. Baker. Reactive polymers for blend compatibilization. *Adv. Polym. Technol.*, 11:149–262, 1992.

S. Massebeuf. *Optimisation Multicritère de Procédés Discontinus d'Homopolymérisation et de Copolymérisation en Emulsion.* PhD thesis, Institut National Polytechnique de Lorraine, Nancy, France, 1997.

C. M. Miller, E. D. Sudol, C. A. Silebi, and M. S. El-Aasser. Miniemulsion polymerization of styrene: evolution of the particle size distribution. *J. Polym. Sci. Part A : Polym. Chem.*, 33:1391–1408, 1995.

Y. Minoura, M. Ueda, S. Mizunuma, and M. Oba. The reaction of polypropylene with maleic anhydride. *J. Appl. Polym. Sci.*, 13:1625–1640, 1969.

G. Moad. The synthesis of polyolefin graft copolymers by reactive extrusion. *Prog. Polym. Sci.*, 24:1527–1528, 1999.

Jr. E. P. Moore and G. A.Larson, editors. *Polypropylene Handbook.* Hanser, Munich, 1996.

P.H. Nam, P. Maiti, M. Okamoto, T. Kotaka, N. Hasegawa, and A. Usuki. A hierarchical structure and properties of intercalated polypropylene/clay nanocomposites. *Polymer*, 42:9633–9640, 2001.

J. R. Paul and S. Newman, editors. *Polymer blends.* Academic Press, New York, 1978.

S. Sinha Ray and M. Okamoto. Polymer/layered silicate nanocomposites: a review from preparation to processing. *Prog. Polym. Sci.*, 28:1539–1641, 2003.

G. Ruggeri, M. Aglietto, A. Petragnani, and F. Ciardelli. Some aspects of polypropylene functionalization by free radical reactions. *Chem. Eng. Sci.*, 19:863–866, 1983.

K. E. Russell. Free radical graft polymerization and copolymerization at higher temperature. *Prog. Polym. Sci.*, 27:1007–1038, 2002.

K. E. Russell and E.C. Kelusky. Grafting of maleic anhydride to n-eicosane. *J. Polym. Sci. Part A: Polym. Chem.*, 26:2273–2280, 1988.

D. Shi, J. Yang, Z. Yao, Y Wang, H. Huang, W. Jing, J. Yin, and G. Costa. Functionalization of isotactic polypropylene with maleic anhydride by reactive extrusion: mechanism of melt grafting. *Polymer*, 42:5549–5557, 2001.

D. Shi, G.-H. HU, and R. K. Y. Li. Concept of nano-reactor for the control of the selectivity of the free radical grafting of maleic anhydride onto polypropylene in the melt. *Chem. Eng. Sci.*, 61:3780–3784, 2006.

A. Sood and S. K. Awasthi. Population balance model for miniemulsion polymerization.2. Model solution and validation. *Macromol. Theory Simul.*, 13:615–628, 2004a.

A. Sood and S. K. Awasthi. Population balance model for miniemulsion polymerization.1. Model development. *Macromol. Theory Simul.*, 13:603–614, 2004b.

P. L. Tang, E. D. Sudol, C. A. Silebi, and M. S. El-Aasser. Miniemulsion polymerization - a comparative study of preparative variable. *J. Appl. Polym. Sci.*, 43:1059–1066, 1991.

Y. S. Thio, A. S. Argon, and R. E. Cohen. Role of interfacial adhesion strength on toughening polypropylene with rigid particles. *Polymer*, 45:3139–3147, 2004.

C. Vasile, editor. *Handbook of polyolefins. 2nd ed.* Marcel Dekker, New York, 2000.

M. Xanthos and S. S. Dagli. Compatibilization of polymer blends by reactive processing. *Polym. Eng. Sci.*, 31:926–935, 1991.

H. Zhou, M. Hu, and Y. Hu. Influence of coagents on the silane grafting and cross-linking of polypropylene. *Polym. Plast. Tech. Eng.*, 48:193–200, 2009.

Chapter 2

Introduction on Modelling of Emulsion Polymerization

Emulsion polymerization is the most common way of forming polymer latexes; in the simplest system, the ingredients comprise water, a monomer of low water solubility (e.g. styrene), water-soluble initiator (e.g. persulfate) and surfactant (latexes can also be synthesized without added surfactant and/or initiator, but this is not common). A new phase is quickly formed: a polymer colloid, comprising a discrete phase of colloidally stable latex particles, dispersed in an aqueous continuous phase. Virtually all polymerization occurs within these nanoreactors. By the end of the reaction, they are typically 100 nm in size, each containing many polymer chains. Colloidal stabilizers may be electrostatic (e.g. with an ionic surfactant such as sodium dodecyl sulfate), steric (with a steric, or polymeric, stabilizer such as poly(ethylene oxide) nonylphenyl ether), or electrosteric, displaying both stabilizing mechanisms, such as a 'hairy layer' of poly(acrylic acid) grafted to long hydrophobic chains within the particles. Polymer latexes are used in the production of a wide range of specialty polymers including adhesives, paints, binders for nonwoven fabrics, additives for paper, textiles and construction materials, impact modifiers for plastic matrices, diagnostic tests, and drug-delivery systems [Lovell and El-Aasser, 1997, Warson and Finch, 2001, Urban and Takamura, 2002, Asua, 2004]. The development of this industry has been due to both the possibility of producing polymers with unique properties and the environmental concerns and governmental regulations to substitute solvent-based systems by waterborne products.

The term emulsion polymerization encompasses several related processes:
(1) conventional emulsion polymerization (macro-emulsion polymerization),
(2) inverse emulsion polymerization,
(3) mini-emulsion polymerization, [Ugelstad et al., 1973a, Antonietti and Landfester, 2002, Asua, 2002]
(4) dispersion polymerization, [Barrett, 1975, Saenz and Asua, 1995, 1998] and micro-emulsion polymerization.[Asua, 1997, de Buruaga et al., 1998].

Commonly, the products mentioned above are produced by means of macro-emulsion polymerization. Batch emulsion polymerization is commonly used in the laboratory to study reaction mechanisms, develop new latex products and obtain kinetic data for process development and reactor scale-up. In this process, monomer is dispersed in an aqueous solution of surfactant with a concentration exceeding the critical micelle concentration (CMC) and polymerization is started by means of an (most often water-soluble) initiator

system. In principle, polymer particles can be formed by entry of radicals into the micelles (heterogeneous nucleation), precipitation of growing oligomers in the aqueous phase (homogeneous nucleation), and radical entry in monomer droplets. However, monomer droplets are relatively large (1-10μm) compared to the size of monomer-swollen micelles (10-20 nm), and hence the surface area of the micelles is several orders of magnitude greater than that of the monomer droplets. Consequently, the probability for a radical to enter into the monomer droplets is very low, and most particles are formed by either homogeneous or heterogeneous nucleation.

Once they are nucleated, the polymer particles undergo substantial growth by polymerization. The monomer required for the polymerization must be transported from the monomer droplets by diffusion through the aqueous phase. In some cases, this represents a severe limition of the macro-emulsion polymerization. Thus, water resistance of coatings prepared from dispersed polymers is significantly improved if very hydrophobic monomers, e.g. lauryl and stearyl methacrylates, are incorporated into the polymer backbone. However, mass transfer of these monomers from monomer droplets to polymer particles through the aqueous phase is diffusionally controlled, and hence they cannot be readily incorporated into the polymer in macro-emulsion polymerization.

The need of mass transport of monomer through the aqueous phase would be greatly diminished if all (or at least a large fraction) monomer droplets were nucleated. Prevalent droplet nucleation can only occur if the surface area of the monomer droplets is large compared with that of the micelles, and this requires submicron droplet size. The word mini-emulsion was coined [Chou et al., 1980] to describe submicron oil-in-water dispersions that are stable for a period ranging from hours to months.

[Ugelstad et al., 1973a] were the first to demonstrate that under conditions in which the droplet size is small enough, nucleation of monomer droplets could account for an important part of the particles formed. The method used to produce the small droplet size was inspired in previous reports showing that the presence of long chain fatty alcohols drastically increased the capacity of anionic surfactants to disperse and stabilize oil-in-water emulsions [Schulman and Cockbain, 1940, Barry, 1968, Prince, 1969, Friberg and Rydhag, 1971]. In those works, it was reported that the presence of fatty alcohols led to the reduction of the interfacial energy and to the formation of ordered structures far exceeding the molecular size at the oil-water interface. [Ugelstad et al., 1973a] stirred cetyl alcohol (CA) with water and sodium lauryl surfate (SLS) at 60℃ and then styrene was added under stirring. It was found that the mini-emulsions were stable for 2 weeks. The monomer mini-emulsions were polymerized at 60℃ and it was found that a large fraction of polymer particles were formed by droplet nucleation when a relatively modest amount of surfactant was used. The existence of droplet nucleation had been previously suggested by [Ugelstad et al., 1973b] for the emulsion polymerization of vinyl chloride stabilized with a combination of anionic surfactants and fatty alcohols.

Early work also reported on the key role of both formulation and emulsification process on droplet size and stability. [Ugelstad et al., 1974] prepared styrene mini-emulsions by stirring sodium hexadecyl sulfate/hexadecanol mixtures with water at 70℃, then the system was cooled to 60℃ and monomer added under stirring at 600 rpm. It was found that the droplet size decreased and the stability increased as the sufactant/fatty alcohol ratio increased from 1 to 3. Mini-emulsions degrade with time, the degradation being faster at higher temperatures. A mechanism for emulsification was proposed. In the first stage, a temporary complex surfactant/fatty alcohol layer is formed which helps

to emulsify the monomer. Later, the fatty alcohol diffuses towards the interior of the droplets reducing the stability of the droplets. According to this mechanism, a minimum amount of fatty alcohol is needed to saturate the droplets and have enough fatty alcohol to form the complex at the interface. This idea was supported by experiments in which the fatty alcohol was dissolved in styrene prior emulsification and only coarse unstable systems were obtained. However, the mechanism is based on the idea that the only role of the fatty alcohol is to modify the droplet surface, and it has been proved that this is not the case. Polymerization of the styrene mini-emulsions yielded bimodal particle size distributions (PSD), the large particles being produced through droplet nucleation. Only large fatty alcohol/surfactant ratios led to a generalized droplet nucleation. Because the fatty alcohols led to the reduction of the interfacial energy and to the formation of ordered structures, these compounds were called cosurfactants.

[Azad and Fitch, 1980] found that the longer the fatty alcohol, the more stable the mini-emulsion. These authors introduced two new key aspects in the process. Inspired by the works of [Carless and Hallworth, 1968, Hallworth and Carless, 1972, 1973] and [Smith, 1976] who had found that the stability of light petroleum, benzene and hexane emulsions was strongly improved by small amounts of hexadecane (HD: water solubility estimated at $1\,10^{-9}$, [Chern and Chen, 1998]), they decided to use this compound instead of a fatty alcohol to stabilize the monomer mini-emulsion. It was found that with ordinay stirring equipment, addition of hexadecane did not give the rapid emulsification that could be obtained with the long chain fatty alcohols. Therefore, a more effient homogenization system was used. It was found that when the hexadecane containing emulsions were homogenized with a Manton-Gualin high pressure laboratory homogenizer, extremely stable monomer nimi-emulsions were obtained. The use of Mantton-Gaulin homogenizer did not lead to any improvement in the stability of fatty alcohol containing mini-emulsions, but in this case, the stability of the mini-emulsion was independent of the order in which the components of the formulation were mixed.

[Smith, 1976] had suggested that the effect of the addition of small amount of hexadecane might be due to the prevention of mini-emulsion degradation by molecular diffusion (Ostwald ripening effect). This approach to emulsion stability was first presented by [Higuchi and J.Misra, 1962], and it was based on the fact that due to the surface energy, the chemical potential of the monomer in small dropolets is higher than in large droplets or plane surfaces. consequently, monomer diffused from small to large droplets leading to larger droplets and emulsion destabilization. [Higuchi and J.Misra, 1962] predicted that the addition of a small amount of a water-insoluble compound would retard the emulsion degradation by molecular diffusion because the slow rate of diffusion of the water-insoluble compound would permit the monomer to remain essentially equilibrated among the droplets. Therefore, changes in the system would occur only at the same velocity as the change in distribution of the slowest diffusing compound.

[Durbin et al., 1979] applied different degrees of emulsification (no emulsification, hand shaking, homogenization with a hand-homogenizer (Fisher Scientific), and ultrasonication) to a styrene-anionic surfactant-water system. It was found that in the absence of cetyl alcohol or hexadecane, droplet nucleation was negligible.

This early work established the basis for the mini-emulsion polymerization process, namely, that energetic homogenization should be applied to reduce the size of the monomer droplets, and that these droplets should be protected against both diffusional degradation and droplet coagulation by suing a water-insoluble compound and an efficient surfactant.

The early work also influenced nomenclature. Thus, the water-insoluble low-molecular weight compound is often referred to as a co-surfactant in mini-emulsion polymerization publications. However, with the exception of the long chain alcohols, this is a misnamed because compounds like hexadecane have no surface activity. In addition, the main stabilizing effect of these compounds (including cetyl alcohol (CA: water solubility estimated at $6\,10^{-8}$, [Chern and Chen, 1998]) is not a surface effect but a bulk effect. The compound responsible for stabilizing the monomer droplets against Ostwald ripening has also been called a hydrophobe to account for its water-insolubility. However, although any water-insoluble compound may retard diffusional degradation, its efficiency strongly depends on the molecular weight. Thus low-molecular weight water-insoluble compounds are much more efficient than high-molecular weight water-insoluble compounds. Therefore, the term co-stabilizer is used in this thesis to refer to low-molecular weight water-insoluble compounds, which are highly efficient in stabilizing monomer droplets against diffusional degradation.

2.1 The mechanism of macro-emulsion polymerization and mini-emulsion polymerization

2.1.1 The mechanism of macro-emulsion polymerization

Macro-emulsion polymerization is a complex process. The literature contains extensive reviews of emulsion polymerization theory [Garden, 1970, Piirma, 1982, Poehlein, 1985, Poehlein and Dougherty, 1977, Ugelstad and Hansen, 1976]. The earliest qualitative theory of emulsion polymerization was developed by Harkins [Harkins, 1947] and was quickly quantified by [Smith and Ewart, 1948] (SE). Although this theory only holds for the special case of water-insoluble monomers, it is the typical starting point for most other theories. This theory is based on the batch emulsion polymerization of styrene. It includes three intervals, as depicted in the left half of Figure 2.1. The first interval begins with the initiation of the reaction and continues until all micelles become nucleated or are used up as surface stabilizing agents. At this point, particle formation ceases. During Interval II, the particles grow at a constant rate in the presence of monomer droplets. Once the monomer droplets disappear, interval III begins. The monomer concentration in the particle decreases and the reaction within the particles becomes diffusion-limited throughout the remainder of the polymerization.

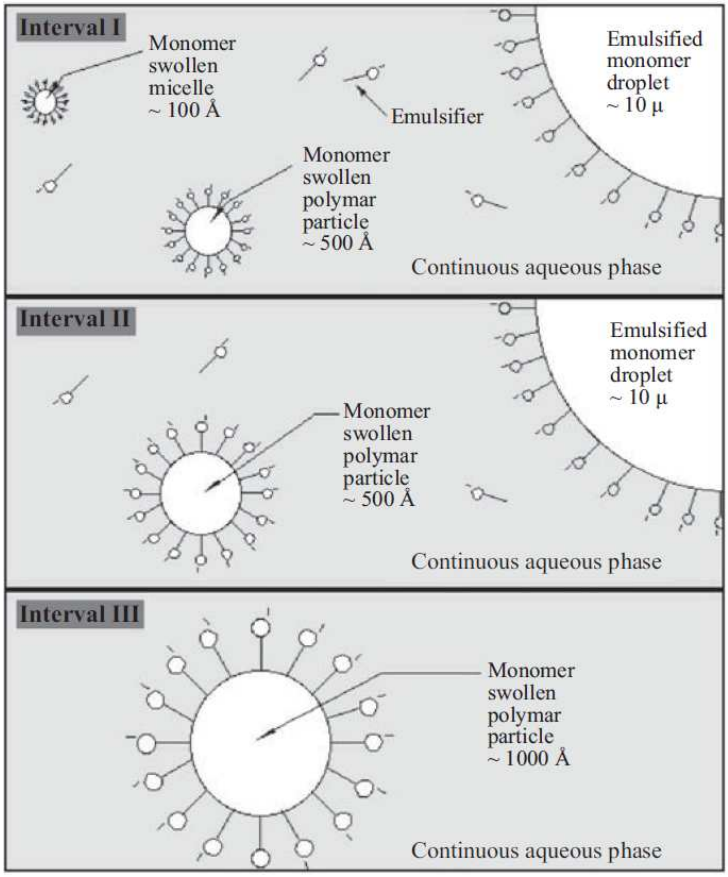

(a) Macro-emulsion polymerization

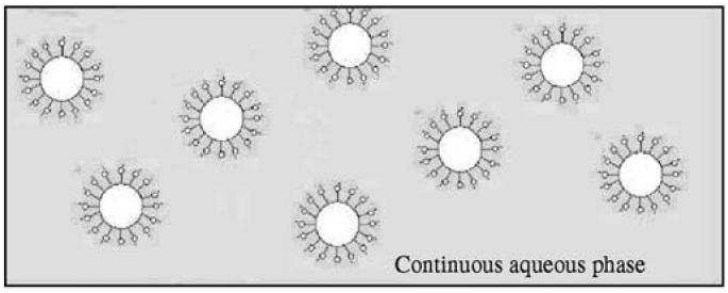

(b) Mini-emulsion polymerization

Figure 2.1: Macro-emulsion polymerization versus mini-emulsion polymerization

Interval I - Particle Nucleation

Nucleation mechanisms are generally divided into three types: micellar, homogeneous and droplet. Statistically, all three types can occur simultaneously in every reaction. However, it is the preponderance of one mechanism with respect to the others in a given system that causes authors to consider only one in their studies. Numerous extensions have been made to the SE [Smith and Ewart, 1948] micellar nucleation theory in an effort to furnish explanations for experimental results observed for monomers with slight water solubilities. Detailed reviews of these extensions are readily available [Ugelstad and Hansen, 1976, Harkins, 1947, Alexander and Napper, 1971, Blackley, 1982]. Monomer droplet nucleation is normally neglected, except when considering mini- and micro- emulsions, due to its

insignificant contribution to the particle number and the size distribution.

1. Micellar Nucleation

   All quantitative theories based on micellar nucleation can be developed from balances of the number concentrations of particles and of the concentrations of aqueous radicals. [Smith and Ewart, 1948] solved these balances for two limiting cases:
   (i) all free radicals generated in the aqueous phase assumed to be absorbed by surfactant micelles,
   (ii) micelles and existing particles competing or compete for aqueous phase radicals.
   In both cases, the number of particles at the end of Interval I in a batch macroemulsion polymerization is predicted to be proportional to the aqueous phase radical flux to the power of 0.4, and to the initial surfactant concentration to the power of 0.6. The Smith Ewart model predicts particle numbers accurately for styrene and other water-insoluble monomers. Deviations from the SE theory occur when there are substantial amounts of radical desorption, aqueous phase termination, or when the calculation of absorbance efficiency is in error. Deviations with respect to order from the SE theory increase as the monomer water solubility increases.

2. Homogeneous Nucleation

   Although the SE micellar nucleation theory explains data for certain systems, it fails for others. This has led some authors to propose a different mechanism for nucleation. In the homogeneous nucleation theory, aqueous phase radicals polymerize to form oligomers. These latter continue to grow until they reach a critical chain length, the size of a primary particle, and then precipitate. Throughout the growth process, the oligomers may also flocculate or coagulate. This theory is typically employed for relatively water-soluble monomers. Slight variations of this theory have also been postulated.

   Prior to 1952, little evidence for homogeneous nucleation existed [Baxendale et al., 1946b,a] . In 1952, [Priest, 1952] studied the polymerization of vinyl acetate and presented a qualitative theory for homogeneous nucleation. He concluded from experimental work that aqueous phase nucleation is important in systems with monomers that have a relatively high water solubility. Primary particle formation occurs throughout the course of the reaction. During later periods of the reaction, large monomer-swollen polymer particles act as sinks for these primary particles, encouraging coagulation.

   In 1968, [Roe, 1968] developed the SE limiting case equations for particle number from the homogeneous nucleation theory. He showed that the SE equation for particle nucleation is not unique to micellar nucleation, but results from the SE assumptions. By assuming that (i) the nucleation stops upon depletion of micelles, (ii) the volumetric growth rate is constant, and (iii) the radical absorption is strictly a function of radical generation, he showed that the SE dependency on radical flux and surfactant concentration could be generated from homogeneous nucleation theory.

   [Fitch and Tsai, 1971] developed a quantitative theory for homogeneous nucleation. By using the collision theory for radical capture, [Fitch, 1973] has shown that the rate of radical capture is a function of radical production, particle number, particle

size, and diffusion distance. Primary particles may coagulate with each other because of their small size and lower surface charge. As particles coagulate, the surface to volume ratio decreases, which causes an increase in surface potential. When particles become sufficiently large, coagulation ceases due to insufficient kinetic energy to overcome the biparticle surface repulsion. Fitch and Tsai have provided experimental support for this theory by polymerizing MMA with different initiators.

[Ugelstad and Hansen, 1976] proposed that free radicals in the aqueous phase propagate with dissolved monomer. Primary particles form by precipitation when a critical chain length is reached. During growth from a monomer radical to a primary particle, each oligomer can (i) terminate with other radicals, (ii) precipitate if its length exceeds the critical chain length, or (iii) be captured by particle.

A fundamental extension to the homogeneous nucleation theory was proposed [Lichti et al., 1983, Feeney et al., 1984]. Their theory is based on the positive skewness of the particle size distribution (PSD) as a function of volume during Interval II. This implies that the rate of nucleation during Interval I increases with time until it eventually drops off at the end of nucleation. Lichti and Feeney claim that micellar nucleation or one step homogeneous nucleation incorrectly predict either decreasing or constant nucleation rates.

This theory has been given the name coagulative nucleation. According to Lichti and Feeney's mechanism, precipitated 'precursor particles' undergo coagulation to form 'true' or 'mature' latex particles. A precursor particle is unstable and said to be formed in either a micelle or the aqueous phase. Due to their small size and hydrophilic nature, the precursors have low swelling capacity and high radical desorption rates. Consequently, the propagation rate is low and these precursors tend to coagulate with other precursors or mature latex particles. These conclusions then rule out micellar nucleation as a possible mechanism for precursor formation.

[Maxwell et al., 1991] suggested that the values to be used for the critical chain length are much smaller than originally thought. They also suggested that oligomeric radical capture is independent of particle size and limited by the rate of propagation of the radical in the aqueous phase. However, this theory does not consider variations in other parameters with particle size.

3. Droplet Nucleation

Nucleation of monomer droplets has typically been neglected in emulsion polymerization. The large diameter (1-10 μ m) and small number (10^{13} versus 10^{21} micelles) of droplets in macroemulsions usually makes their consideration of no importance. Regardless of this, all droplets do get nucleated, because of their large size. These droplets show up in TEM photographs as abnormally large particles in very low concentrations. In 1973, [Ugelstad et al., 1973a] showed how submicron styrene monomer drops can be made stable enough to become numerically significant in nucleation when a co-stabilizer is used to enhance the stability of the smaller droplets. [Chamberlain et al., 1982] have presented experimental evidence that the efficiency of radical capture by droplets is much lower than that for micelles or particles. [Ugelstad et al., 1979, 1985] have shown how nucleation of monomer droplets can lead to latexes with large monodisperse particles. However, if insufficient shear or

co-stabilizer is used, the potential for production of bimodal PSDs exists [Ugelstad et al., 1973b, Hansen et al., 1976]. This could be desirable in certain instances.

The distinguishing feature of droplet nucleation as opposed to micellar or homogeneous nucleation is the nature of the particle at 'birth'. Droplets, which are nucleated into particles, begin as nearly 100% monomer. Micellar or homogeneous nucleated particles start out with much lower monomer concentrations and eventually swell to around 60% (for MMA) in the presence of monomer droplets. This fundamental difference may lead to large differences between mini-emulsion and macro-emulsion polymerizations in radical desorption and/or intraparticle termination during Intervals I and II.

4. Competition for Radicals

   As pointed out above, particle nucleation includes all three mechanisms - micellar, homogeneous, and droplet, since these mechanisms may compete and coexist in the same system. Often one will dominate. Therefore, any general model of emulsion polymerization should include all three mechanisms. [Hansen and Ugelstad, 1979] have presented probabilities for each of these mechanisms in the presence of all three. The competition for oligomeric radicals also includes particles that have been created with macroemulsions, since both micellar and homogeneous nucleation result in a large shift in the surface area from micelles to particles as the particles are created and grow.

Interval II - Particle Growth

SE Interval II begins at the cessation of nucleation, or in light of the nucleation theory just reviewed, when the particle number becomes relatively constant. Most theories developed for this interval assume a constant particle number and use the quasi-steady-state approximation (QSSA) for average number of radicals per particle. The kinetics and mechanisms of Interval II have been some of the most studied aspects of macro-emulsion polymerization. SE Interval II ends when the monomer droplets disappear and the monomer concentration in the particles begins to decrease.

The rate of polymerization during Interval II is usually considered constant for two reasons. The monomer concentration within the particle, as defined by equilibrium thermodynamics, is approximately constant in the presence of excess monomer. Mass transfer is assumed to be fast and particle size has little effect on this concentration. Secondly, emulsion polymerization kinetics tend to give a constant radical concentration within the particles during Interval II. Therefore, the rate of polymerization is approximately constant until the end of Interval II, where $[\mathrm{M}]_p$, $\bar{n}$, and k_p begin to change. These two assumptions have been substantiated by experimental observations and are considered reasonable. The challenge for Interval II is to determine the average number of radicals per particle. Particle monomer concentration can be determined as a function of particle radius by an equilibrium relationship equation [Morton et al., 1954] that considers both surface energy and mixing energy. Propagation rate coefficients have been widely studied and are readily available [Beuermann and Buback, 2002]. The particle number concentration is assumed constant.

Smith and Ewart developed three limiting cases for Interval II. Each of these cases can be generated through a balance of N_{pi} (the number of particles containing i radicals),

where the number of particles is considered constant (no nucleation). For Case 1, Smith and Ewart assume $N_{p0} >> N_{p1} >> N_{p2} >> \ldots$. For this case, $\bar{n}$ will be significantly less than 0.5. This case occurs when significant monomeric radical desorption occurs, and is more common with monomers of significant water solubility.

Case 2 assumes instantaneous termination of the existing radical with an entering radical. In this case, each particle will contain either zero or one radical, and $\bar{n}$ becomes 0.5. Styrene generally follows Case 2 kinetics. Smith and Ewart Case 3 assumes that both desorption from particles and aqueous phase termination may be neglected, and so $\bar{n} >> 1.0$. This occurs with large particles, and in the limit results in bulk kinetics.

Coagulation of latex particles during Interval II is often neglected. If surfactant is available in great enough proportion, the particles will remain stable throughout the reaction.

Interval III - Gel and Glass Effects

Interval III begins when all monomer droplets have vanished and/or the aqueous phase becomes unsaturated. Since each droplet in a macro-emulsion actually absorbs radicals, they cannot disappear but rather shrink to a point where they have no excess monomer. The monomer in the aqueous phase decreases corresponding to the decrease in the particles. The conversion at which Interval III begins varies for different monomers and systems, but is typically around 40 to 50%. However, it may not be as distinguishable in miniemulsions due to early initiation of the gel effect.

As the monomer within the particles is consumed by polymerization, the viscosity rises within the particles and the diffusion rate of the polymeric radicals decreases. This causes a reduction in the rate of termination, which corresponds to a dramatic increase in the radical concentration. A higher radical number within the particle results in an 'auto acceleration' of the rate of polymerization. Common practice is to model this auto acceleration or gel effect by decreasing the termination rate constant by several orders of magnitude as a function of percent monomer in the particle. A free volume approach has been used by [Sundberg et al., 1981]. [Buback et al., 1988] suggest a completely empirical approach from precise experimental data. Empirical correlations used in modeling the gel effect in bulk or solution polymerization have also been modified for use in emulsion processes [Barnette and Schork, 1987, Friis and Hamielec, 1973, Rawlings and Ray, 1988a,b].

The problem when applying correlations derived from other systems to emulsion polymerization is twofold. First, normal macro-emulsion particles are said to be created with 30 to 40% monomer in them and so the unbiased (zero conversion) termination rate is unknown. Secondly, the diffusional limitations in particles might be quite different from those observed in bulk or suspension polymerizations. For these reasons, an empirical approach is suggested.

If the reaction temperature is below the polymer glass transition temperature and the amount of monomer in the particle decreases far enough, the glass effect may become important. The polymerization rate virtually goes to zero because the particle becomes so internally viscous, essentially glasslike, that the diffusion of monomer to the radicals is limited. The glass transition point varies for different polymers. This effect has also been studied by [Sundberg et al., 1981, Ballard et al., 1986, Soh and Sundberg, 1982a,b].

2.1.2 The mechanism of mini-emulsion polymerization

In the previous discussion of macro-emulsion polymerization, all three forms of particle nucleation were discussed. In macro-emulsion polymerization, micellar and homogenous nucleation dominate. This is because the large sizes of the monomer droplets, and their consequent low interfacial area, make them ineffective in competing for water-borne free radicals. Droplet nucleation undoubtedly takes place in macro-emulsion polymerization, but it is generally considered to be insignificant. If the monomer droplet size can be reduced to below 0.5 μm, two phenomena will occur. First, the droplets will be able to compete successfully for water-borne free radicals with any remaining micelles. Secondly, the huge increase in interfacial area caused by the reduction in droplet size will result in a huge increase in interfacial area. This new interface will require a monolayer of surfactant to remain stable. The surfactant necessary to support this large interfacial area will come from the break-up of surfactant micelles. In a properly formulated mini-emulsion, all micelles will be sacrificed to support the droplet interfacial area. Therefore, not only do the small droplets compete effectively for micelles, their presence causes the destruction of the micelles, leaving droplet nucleation as the dominant particle nucleation process.

Mini-emulsions are produced by the combination of a high shear to break up the emulsion into submicron monomer droplets, and a surfactant/co-stabilizer system to retard monomer diffusion from the submicron monomer droplets. Both are necessary to effect predominant droplet nucleation (nucleation in which a preponderance of the particles originate from droplets rather than from micelles or from homogeneous nucleation). High shear is provided by a sonicator or a mechanical homogenizer. The surfactant is necessary to retard droplet coalescence caused by Brownian motion, settling or Stokes law creaming or settling. The co-stabilizer prevents Ostwald ripening. When a liquid emulsion is subjected to high shear, small droplets will result. There will still be a statistical distribution of droplet sizes. If the monomer is even slightly soluble in the continuous aqueous phase (and most are, as evidenced by the fact that Interval II of macro-emulsion polymerization takes place), the monomer will, over time, diffuse from the smaller monomer droplets into the larger ones. This results in a lower interfacial area (and interfacial energy), since the loss in interfacial area of the smaller droplets is larger than the gain in interfacial area of the larger ones. The reduction in interfacial energy is the driving force for degradation of the small droplets.

If Ostwald ripening is allowed to continue unchecked, creaming of the monomer will occur as the droplet sizes become large enough for Stokes law creaming to occur. This will occur in a matter of seconds to minutes. If the system is initiated, bulk polymerization of the monomer layer will occur. If the emulsion is stirred, an emulsion of large monomer droplets (of the order of those of a macro-emulsion) will result, and if the stirred emulsion is initiated, macro-emulsion polymerization will take place. A co-stabilizer functions to prevent Ostwald ripening by retarding monomer diffusion from the smaller droplets to the larger. Co-stabilizers should be highly insoluble in the aqueous phase (so that they will not diffuse out of the droplets), and highly soluble in the monomer droplets. Under these conditions, diffusion of the monomer out of the smaller droplets results in an increase in the concentration of the co-stabilizer in those particles (since, by definition, co-stabilizers are too insoluble in the aqueous phase to leave the droplet). The increase in free energy associated with the concentration of the co-stabilizer balances the decease from reduced interfacial area caused by Ostwald ripening, and, at some point, ripening stops. Since

all co-stabilizers are somewhat water-soluble, Ostwald ripening will proceed, but on a timescale of months, which is unimportant since the timescale of polymerization is minutes to hours.

In their original discovery of mini-emulsion polymerization, [Ugelstad et al., 1973a] used either CA or HDto retard monomer diffusion from submicron monomer droplets. Both CA and HD, referred to here as co-stabilizers, are volatile organic components and are therefore not entirely desirable in the final product.

Monomer droplet stability can be understood in terms of free energy. The partial molar free energy of adding a second component to a droplet is composed of two terms, the partial molar free energy of mixing and the interfacial partial molar free energy. The partial molar free energy of mixing ([Flory, 1953] expression) can be combined with the interfacial partial molar free energy to give

$$\frac{\Delta\bar{G}_i}{RT} = ln\varphi_i = (1 + m_{ij})\varphi_j + \chi_{ij}\varphi_j^2 + \frac{2\bar{V}_i\gamma}{RTr} \tag{2.1}$$

[Ugelstad et al., 1980] have applied this equation to various monomers and surfactants. It is clear from this equation that the free energy increases as the phase diameter decreases. The smaller the monomer droplet, the less stable it is. Therefore, a driving force exists for the monomer to diffuse from a small droplet to a larger one. Over time, non-monodisperse systems of droplets of pure monomer will decrease in number as the smaller droplets swell the larger ones and then disappear. Jannson [Jansson et al., 1983] has shown that this occurs in unagitated systems, and that the timescale for diffusional instability can be of the order of seconds.

Prior to 1962, droplets below 1 mm were considered too unstable to participate in the nucleation process. In 1962, [Higuchi and J.Misra, 1962] proposed that the addition of a water insoluble compound to the monomer will enhance the stability of small droplets by prohibiting diffusion. In 1973, [Ugelstad et al., 1973a] showed how submicron styrene droplets could be made stable enough to participate in the nucleation processes by adding small amounts of cetyl alcohol. Later, [Ugelstad, 1978] used Eq. (2.1) to explain these experimental observations.

It can be shown for two phases in equilibrium that the partial molar free energies must be equal. In an emulsion (or mini-emulsion), there are three phases: monomer droplets, the aqueous phase and polymer particles. Since monomer is soluble in all these phases, the equilibrium condition requires that the three phases have equal partial molar free energies. In the presence of monomer droplets, emulsion polymer particles contain 30-80% monomer in them. Therefore, they are said to be 'swollen' with monomer. [Ugelstad, 1978] and [Azad and Fitch, 1980] have shown that the addition of a third water-insoluble component to a swollen polymer particle can increase the monomer to polymer ratio. They have shown that an optimum chain size for the additive exists since the solubility of the additive increases as the chain size decreases. They found that the optimum hydrocarbon stabilizer is hexadecane. Others have found that if a fatty alcohol is used as the stabilizer, the minimum chain length required is 12 carbon atoms [El-Aasser et al., 1984].

[Fitch, 1980] have shown how this theory may be used to devise a method to prepare large monodisperse particles of predetermined size. By using the appropriate amount of cosurfactant, polymer particles can be swollen with monomer to the desired size. Polymerization in conditions that prevent additional nucleation results in large monodisperse polymer particles of size 1-100 μm. This method has been criticized by other groups as

being in error due to measurement selectivity.

If Ostwald ripening is retarded by using a co-stabilizer, predominant droplet nucleation can be achieved. This is the basis of mini-emulsion polymerization. One of the first comprehesive studies of mini-emulsion polymerization was done on styrene by [Choi et al., 1985].

2.1.3 Differences between macro-emulsion polymerization and mini-emulsion polymerization

Below a threshold of surfactant amount, which also depends on temperature, monomer concentration and the chemistry of the emulsifier, no microemulsion, but kinetically stabilized macro-emulsions are formed. Therefore, large monomer droplets (1-10μm in diameter), which are stabilized by surfactant, and empty or monomer-swollen surfactant micelles coexist in the initial state. For polymerization, one starts from large monomer droplets and surfactant micelles in the water phase. The watersoluble initiator forms oligoradicals from slightly watersoluble monomer units. These oligoradicals then enter the micelles and start to form particles. During polymerization, monomer diffuses through the water phase to the micelles in order to sustain polymer particle growth. Particles with a diameter of usually more than 100 nm are formed. Due to the increase of the interfacial area, the surface tension of a latex increases with polymerization. In the literature, the term emulsion polymerization is used for this process. [Hunkeler et al., 1994] For clarity, we defined it as a macro-emulsion polymerization as compared to micro- and mini-emulsion polymerization.

The differences between macro-emulsion polymerization and mini-emulsion polymerizations are obvious. In macro-emulsion polymerization, the latex particle does not correspond to the primary emulsion droplet, and the size is established by kinetic processes where kinetic parameters, such as temperature or the amount of initiator, play a predominant role. These factors remain unseen in mini-emulsion polymerization where the latexes are essentially a polymerized copy of the original droplets, the size of which is essentially given by dispersion process and droplet stability, but not by polymerization parameters.

In terms of the stability of the emulsion and in terms of the size of the resulting particles, mini-emulsions are in between macro-emulsions and micro-emulsions.

2.2 Mathematical modeling of macro-emulsion polymerization and mini-emulsion polymerization

2.2.1 Mathematical modeling of macro-emulsion polymerization

It has been long recognized that emulsion polymerization is a complex heterogeneous process involving transport of monomers and other species and free radicals between aqueous and organic phases. Compared to other heterogeneous polymerizations, like suspension or precipitation, emulsion polymerization is likely the most complicated system. The rate of polymerization in the organic phase is not only controlled by monomer partitioning but also affected by other phonomena like partilcle nucleation, and radical absorption. Particle stability is affected by emulsifier type, amount of emulsifier and ionic strength of the dispersion media. All these factors make modeling of this system very difficult. Other

difficulties encountered in modeling emulsion polymerization include numerical methods of solving sets of nonlinear ordinary differential (or integro-differential) equations coupled with algebraic equations and the lack of information on certain model parameters.[Gao and Penlidis, 2002] Though emulsion polymerization has been commercialized for more than half a century, some important aspects like particle nucleation, coagulation, etc. are still not well understood. To simulate this complicated process, [Gilbert, 1995] proposed the 0-1 model and identified the kinetics for styrene polymerization. This model was then used by [Coen et al., 1998] to model coagulation and secondary nucleation. Using the same model, [Sood, 2004] used capillary hydrodynamic fractionation (CHDF) and calorimetry to study the influence of the monomer addition protocol, emulsifier, and initiator charges on the evolution of the particle size distribution (PSD) of a seeded styrene system.

[Immanuel et al., 2002] used the pseudo-homopolymerization model, initially proposed by [Storti et al., 1989], to study the PSD for vinyl acetate and butyl acrylate polymerizaion and in a later work to study particularly the effect of surfactant type and coagulation on the PSD using CHDF and densimetry. This model was also used by [Ginsburge et al., 2003] to model and identify styrene/butyl acrylate copolymerization.

The difficulties in controlling the PSD also arise from the fact that the PSD is represented by partial differential equations that can be solved by different approximation methods (discretization methods, method of moments). [Ramkrishna, 2000] gave a good presentation of the population balance equations and the mathematical methods that can be used to solve them. [Immanuel and III, 2003b] presented an efficient solution technique for population balance equations that is not based on approximating the population balance equations. [Edouard et al., 2005] proposed the combination of mathematical models with existing on-line sensors to obtain a continuous estimation of the PSD by constructing nonlinear estimators and obtained an estimation of the whole PSD.

Finally, applying techniques of estimation and control to these models requires theoretical validation. [Semino and Ray, 1995a,b] proposed a theoretical study of the controllability of the PSD of continuous-emulsion polymerization reactors. The theoretical controllability of the system was demonstrated using a linearized process model and validated by simulation to the nonlinear model. The authors showed that the PSD is controllable using the manipulating variables: surfactant, initiator and inhibitor concentrations, and assuming monomer conversion and total number of particles in the reactor to be measured. However, the authors outline that the process is easier to be controlled using the surfactant flow rate that acts directly on the concentration of micelles. An experimental study of the evolution of the PSD in continuous reactors was done by [Ohmura et al., 1998]

Because of these difficulties, only few papers in the literature have treated the control of the whole PSD. [Crwoley et al., 2000] used the 0-1 model to obtain a bimodal target distribution of styrene polymerization. The authors compared both the surfactant feed rate and free concentration as control variables that were calculated by an optimization algorithm. To control the PSD, [Zeaiter et al., 2002] used the 0-1 model for styrene polymerization. The authors applied an optimal control strategy that calculates on-line the desired monomer flow rate required to obtain the desired PSD. [Immanuel and III, 2002] proposed an open-loop control strategy to control the PSD for vinyl acetate and butyl acrylate polymerization. The generated algorithm was based on the optimization of profiles of the feed rate of monomer and surfactant to obtain a target PSD. Later on, [Immanuel and III, 2003a] controlled the PSD using a multiobjective optimization

algorithm by both open-loop and feedback algorithms. [III et al., 2003] developed a hybrid model-based approach to control the PSD of styrene polymerization. The algorithm uses the partial least-squares model to optimize the feed rates of surfactant and initiator.

2.2.2 Mathematical modeling of mini-emulsion polymerization

Various mathematical treatments of specific mechanisms within the mini-emulsion polymerization reaction abound. This section will be limited to those papers that attempted to model the overall mini-emulsion polymerization reaction. Perhaps the earliest serious attempt to model this system was that by [Chamberlain et al., 1982]. Balances of the number of droplets, number of polymer particles and monomer conversion were constructed for batch mini-emulsion polymerization. Droplets and particles were considered to be monodisperse. Comparison of the model with experimental data led to the conclusion that free radical entry into monomer droplets is substantially less than for ordinary macro-emulsion particles. [Chern et al., 1986] published a model of approximately the same complexity for continuous stirred tank mini-emulsion polymerization with an oil-soluble initiator. [Delgado et al., 1986a,b, Asua et al., 1990, Rodriguez et al., 1989] published a series of papers focusing on the modeling of mini-emulsion copolymerization,particularly in relation to monomer transport. They described monomer transport in terms of a mass transfer coefficient and a driving force derived from an equilibrium concentration calculated from equating the partial molar free energies. This same group [Rodriguez et al., 1991] modeled seeded mini-emulsion polymerization (containing both polymeric seed particles and mini-emulsion droplets) with oil-soluble initiator. Monomer transfer by collision of droplets with particles was found to be important. [Fontenot and Schork, 1992a,b] published a very detailed model of batch macro- and mini-emulsion polymerization, indicating the differences between the two mechanisms, and including both micellar and droplet nucleation mechanisms. Significant droplet coalescence was predicted. The model was in good agreement with data. [Samer and Schork, 1997] published a mathematical model of continuous stirred tank (CSTR) and plug flow (PFR) mini-emulsion polymerization reactors. They were able to explain why the rate of polymerization for mini-emulsion polymerization in a CSTR is substantially higher than for macro-emulsion polymerization in the same reactor. All of the models discussed have been particle number models, containing no information about droplet size distribution or particle size distribution. None of them have attempted to model the formation of droplets during the miniemulsification stage. [Ma et al., 2002, 2003a,b,c] have completed detailed modeling of nitroxide mediated radical polymerization in mini-emulsion. They found that issues of distribution of the control agent between the aqueous and organic phases can be critical to maintain livingness.

In macro-emulsion polymerization, the monomer droplets due to their large size (10^3nm-10^4nm) and consequently small total surface area do not compete favourably with other loci of particle nucleation and are not considered to contribute significantly to particle nucleation. They serve primarily as reservoirs that supply monomer to the growing particles that are formed predominantly as nucleation in monomer-swollen micelles and aqueous phase. In mini-emulsion polymerization, the monomer droplets due to their small size (50-500nm) become the predominant loci of particle nucleation and subsequent polymerization. In this size range, the total surface area of the droplets is such that the surfactant amount typically used is adsorbed predominantly on the droplets resulting in

its unavailability to form micelles. The stability to these systems is usually achieved by using an anionic, e.g. sodium dodecyl sulphate and a co-stabilizer that is only soluble in the oil phase. The only difference between mini-emulsion polymerization and macro-emulsion polymerization recipes is the presence of co-stabilizer. Co-stabilizers should be water-insoluble and of low molecular weight. The small size of the droplets is the result of homogenizing the monomer-water mixture to high shear that breaks the droplets into nanosizes and these droplets are stabilized against coalescence and diffusional degradation for long time by appropriate surfactant/co-stabilizer combination. Coalescence may be precluded by the addition of an appropriate surfactant. Diffusional degradation or Ostwald ripening can be eliminated by the addition of a small amount of co-stabilizer. A model which is able to simulate both macro- and mini- emulsion homopolymerization must be rigorous yet computationally efficient. Assumptions made in simulation of macro-emulsion polymerizations are often not valid for mini-emulsion simulations. Consequently, the model which is developed herein includes mechanisms and assumptions that hold for the entire mini/macro range. Some of these mechanisms are often ignored in macro-emulsion polymerization models. These include limited monomeric diffusion, droplet nucleation, and dynamic balances on aqueous-phase and particle-phase radicals. According to these reasons, almost no one (to the author's knowledge, just [Fontenot and Schork, 1992a,b]) has yet presented a model which has the flexibility to simulate the full range of emulsion polymerizations from macro to micro and actually does it.

However, Most of the models developed for the macro-emulsion polymerization and mini-emulsion polymerization were focused on the particle size distribution and/or molecular weight distribution. To the best of our knowledge, no previous model research on the inside composition of the particles has been published. In this work, based on the comparison between macro-and mini-emulsion polymerization, a model on macro-emulsion polymerization, which could predict the radical chain size distribution for a given class of particle sizes, was established. It would give us a clear illustration of the process of polymerization in the particles. This model can also provide the particle size distribution. Furthermore, a model of mini-emulsion polymerization, which can provides the particle size distribtution and the change of droplets size, was established by comparison.

Bibliography

A. E. Alexander and D. H. Napper. Emulsion polymerization. *Prog. Polym. Sci.*, 3: 145–197, 1971.

M. Antonietti and K. Landfester. Polyreactions in miniemulsions. *Prog. Polym. Sci.*, 27: 689–757, 2002.

J. M. Asua, editor. *Principles and Applications. In Polymeric Dispersions.* Kluwer Academic, Dordrecht, 1997.

J. M. Asua. Miniemulsion polymerization. *Prog. Polym. Sci.*, 27:1283–1346, 2002.

J. M. Asua. Emulsion polymerization: from fundamental mechanisms to process developments. *J. Polym. Sci. Part. A: Polym. Chem.*, 42:1025–1041, 2004.

J. M. Asua, V. S. Rodriguez, C. A. Silebi, and M. S. El-Aasser. Miniemulsion copolymerization of styrene-methyl methacrylate: Effect of transport phenomena. *Makromol. Chem. M. Symp.*, 35–36:59–86, 1990.

A. R. M. Azad and R. M. Fitch, editors. *Polymer Colloids II.* Plenum, New York, 1980.

M. J. Ballard, R. G. Gilbert, D. H. Napper, P. J. Pomery, P. W. O'sullivan, and J. H. O'Donnell. Propagation rate coefficients from electron spin resonance studies of the emulsion polymerization of methyl methacrylate. *Macromolecules*, 19:1303–1308, 1986.

D. T. Barnette and F. J. Schork. Continuous miniemulsion polymerization. *Chem. Eng. Sci.*, 83:25–30, 1987.

K. E. J. Barrett, editor. *Dispersion Polymerization in Organic Media.* Wiley, London, 1975.

B. W. Barry. Self-bodying action of the mixed emulsifier sodium dodecyl sulfate/cetyl alcohol. *J. Colloid Interface Sci.*, 28:82–91, 1968.

J. H. Baxendale, S. Bywater, and M. G. Evans. The mechanism and kinetics of the initiation of polymerisation by systems containing hydrogen peroxide. *Trans. Faraday Soc.*, 42:675–684, 1946a.

J. H. Baxendale, M. G. Evans, and J. K. Kilham. The kinetics of polymerisation reactions in aqueous solution. *Trans. Faraday Soc.*, 42:668–675, 1946b.

S. Beuermann and M. Buback. Rate coefficients of free-radical polymerization deduced from pulsed laser experiments. *Prog. Polym. Sci.*, 27:191–254, 2002.

D. C. Blackley, editor. *Emulsion Polymerization.* Academic, New York, 1982.

M. Buback, L. H. Garcia-Rubio, R. G. Gilbert, D. H. Napper, J. Gulliot, A. E. Hamielec, D. Hill, K. F. O'driscoll, O. F. Olaj, J. Shen, D. Solomon, G. Moad, M. Stickler, M. Tirrell, and M. A. Winnick. Consistent values of rate parameters in free radical polymerization systems. *J. Polym. Sci. Pol. Phys.*, 26:293–297, 1988.

J. E. Carless and G. W. Hallworth. Viscosity of emulsifying agents at oil-water interfaces. *J. Colloid Interface Sci*, 26:75–88, 1968.

B. J. Chamberlain, D. H. Napper, and R. G. Gilbert. Polymerization within styrene emulsion droplets. *J. Chem. Soc. Farad. T. I.*, 78:591–606, 1982.

C. M. Chern, L. Gothjelpsen, and F. J. Schork. Computer simulation of continuous miniemulsion polymerization. *Polym. Proc. Eng.*, 4:1–30, 1986.

C. S. Chern and T. J. Chen. Effect of ostwald ripening on styrene miniemulsion stabilized by reactive cosurfactants. *Colloids Surface A*, 138:65–74, 1998.

Y. T. Choi, M. S. El-Aasser, E. D. Sudol, and J. W. Vanderhoff. Polymerization of styrene miniemulsions. *J. Polym. Sci. Pol. Chem.*, 23:2973–2987, 1985.

Y. J. Chou, M. S. El-Aasser, and J. W. Vanderhoff. Mechanism of emulsification of styrene using hexadecyltrimethyl ammonium bromide-cetyl. *J. Dispersion Sci. Technol.*, 1:129–150, 1980.

E. M. Coen, R. G. Gilbert, B. R. Morrison, H. Leube, and S. Peach. Modeling particle size distribution and secondary particle formatin in emulsion polymerization. *Polymer*, 39:7099–7112, 1998.

T. Crwoley, E. S. Meadows, E. Kostoulas, and F. J. Doyle III. Control of particle size distribution described by a population balance model of semibatch emulsion polymerization. *J. Process Control*, 10:419–432, 2000.

A. Saenz de Buruaga, I. Capek, J. C. de la Cal, and J. M. Asua. Kinetics of the photoinitiated inverse microemulsion polymerization of 2-methacryloyl oxyethyl trimethyl ammonium chloride. *J. Polym. Sci. Part. A: Polym. Chem.*, 36:737–748, 1998.

J. Delgado, M. S. El-Aasser, C. A. Silebi, and J. W. Vanderhoff. Minimization of axial dispersion in hydrodynamic chromatography (HDC). *Polym. Mat. Sci. Eng.*, 54:444, 1986a.

J. Delgado, M. S. El-Aasser, and J. W. Vanderhoff. Miniemulsion copolymerization of vinyl acetate and butyl acrylate. I. Differences between the miniemulsion copolymerization and the emulsion copolymerization processes. *J. Polym. Sci. Pol. Chem.*, 24: 861–874, 1986b.

D. P. Durbin, M. S. El-Aasser, G. W. Poehlein, and J. W. Vanderhoff. Influence of monomer preemulsification on formation of particles from monomer drops in emulsion polymerization. *J. Appl. Polym. Sci.*, 24:703–707, 1979.

D. Edouard, N. Sheibat-Othman, and H. Hammouri. Observer design for particle size distribution in emulsion polymerization. *AIChE J.*, 51:3167–3185, 2005.

M. S El-Aasser, C. D Lack, Y. T. Choi, T. I. Min, J. W. Vanderhoff, and F. M. Fowkes. Interfacial aspects of miniemulsions and miniemulsion polymers. *Colloids Surface*, 12: 79–97, 1984.

P. J. Feeney, D. H. Napper, and R. G. Gilbert. Coagulative nucleation and particle size distributions in emulsion polymerization. *Macromolecules*, 17:2520–2529, 1984.

R. M. Fitch. The homogeneous nucleation of polymer colloids. *Brit. Polym. J.*, 5:467–483, 1973.

R. M. Fitch, editor. *Polymer Colloids II.* Plenum, New York, 1980.

R. M. Fitch and C. H. Tsai, editors. *Polymer Colloids.* Plenum, New York, 1971.

P. J. Flory, editor. *Principles of Polymer Chemistry.* Cornell Univ Press, Ithaca, New York, 1953.

K. Fontenot and F. J. Schork. Simulation of mini/macro emulsion polymerizations. I: Development of the model. *Polym. React. Eng.*, 1:75–109, 1992a.

K. Fontenot and F. J. Schork. Simulation of mini/macro emulsion polymerizations. II: Sensitivities and experimental comparison. *Polym. React. Eng.*, 1:289–342, 1992b.

S. Friberg and L. Rydhag. System water-p-xylene-l-aminooctane-octanoic acid. II. Stability of emulsions in different regions. *Kolloid Z. Polym.*, 244:233–239, 1971.

N. Friis and A. E. Hamielec. Kinetics of styrene emulsion polymerization. *J. Polym. Sci.: Pol. Chem.*, 11:3321–3325, 1973.

J. Gao and A. Penlidis. Mathematical modeling and computer simulator/database for emulsion polymerizations. *Prog. Polym. Sci.*, 27:403–535, 2002.

J. L. Garden. Mechanism of emulsion polymerisation. *Brit. Polym. J.*, 2:1–12, 1970.

R. G. Gilbert, editor. *Emulsion polymerisation: a mechanistic approach.* Academic Press, San Diego, 1995.

E. Ginsburge, F. Pla, and C. Fonteix. Modelng and simulation of batch and semi-batch emulsion copolymerization of styrene and butyl acrylate. *Chem. Eng. Sci.*, 58:4493–4514, 2003.

G. W. Hallworth and J. E. Carless. Stabilization of oil-in-water emulsions by alkyl sulfates. Influence of the nature of the oil on stability. *J. Pharm. Pharmacol.*, 24:71–83, 1972.

G. W. Hallworth and J. E. Carless. Stabilization of oil-in-water emulsions by alkyl sulfates. *J. Pharm. Pharmacol.*, 25:85–95, 1973.

F. K. Hansen and J. Ugelstad. Particle nucleation in emulsion polymerization. III. Nucleation in systems with anionic emulsifier investigated by seeded and unseeded polymerization. *J. Polym. Sci.*, 17:3047–3067, 1979.

F. K. Hansen, E. B. Ofstad, and J. Ugelstad, editors. *Theory and Practice of Emulsion Technology.* Academic, New York, 1976.

W. D. Harkins. A general theory of the mechanism of emulsion polymerization. *J. Am. Chem. Soc.*, 69:1428–1444, 1947.

W. I. Higuchi and J.Misra. Physical degradation of emulsions via the molecular diffusion route and the possible prevention thereof. *J. Pharm. Sci.*, 51:459–466, 1962.

D. Hunkeler, F. Candau, C. Pichot, A. E. Hamielec, T. Y. Xie, J. Barton, V. Vaskova, J. Guillot, M. V. Dimonie, and K. H. Reichert. Heterophase polymerizations: A physical and kinetic comparison and categorization. *Adv. Polym. Sci.*, 112:115–133, 1994.

F. J. Doyle III, C. A. Harrison, and T. J. Crowley. Hybrid model-based approach to batch-to-batch control of particle size distribution in emulsion polymerization. *Comput. Chem. Eng.*, 27:1153–1163, 2003.

Ch. D. Immanuel and F. J. Doyle III. Open-loop control of particle size distribution in semi-batch emulsion copolymerization using a genetic algorithm. *Chem. Eng. Sci.*, 57, 2002.

Ch. D. Immanuel and F. J. Doyle III. Hierarchial multiobjective strategy for particle-size distribution control. *AIChE J.*, 49:2383–2399, 2003a.

Ch. D. Immanuel and F. J. Doyle III. Computationally efficient solution of population balance models incorporating nucleation growth and coagulation: Application to emulsion polymerization. *Chem. Eng. Sci.*, 58:3681–3698, 2003b.

Ch. D. Immanuel, C. F. Cordeiro, S. S. Sundaram, E. S. Meadows, T. J. Crowley, and F. J. Doyle III. Modeling of particle size distribution in emulsion co-polymerization: comparison with experimental data and parametric sensitivity studies. *Comput. Chem. Eng.*, 26:1133–1152, 2002.

Ch. D. Immanuel, T. J. Crowley, E. S. Meadows, C. F. Cordeiro, and F. J. Doyle III. Evolution of multimodal particle size distribution in vinly acetate/butyl acrylate emulsion copolymerization. *J. Polym. Sci. Part. A: Polym. Chem.*, 41:2332–2249, 2003.

L. H. Jansson, M. C. Wellons, and G. W. Poehlein. High swelling of latex particles without the utilization of swelling agents. *J. Polym. Sci. Pol. Lett.*, 21:937–943, 1983.

G. Lichti, R. G. Gilbert, and D. H. Napper. The mechanisms of latex particle formation and growth in the emulsion polymerization of styrene using the surfactant sodium dodecyl sulfate. *J. Polym. Sci. Pol. Chem.*, 21:269–291, 1983.

P. A. Lovell and M. S. El-Aasser, editors. *Emulsion Polymerization and Emulsion Polymers*. Wiley, Chichester, England, 1997.

J. W. Ma, M. F. Cunningham, K. B. McAuley, B. Keoshkerian, and M. K. Georges. Interfacial mass transfer in nitroxide-mediated miniemulsion polymerization. *Macromol. Theor. Simul.*, 11:953–960, 2002.

J. W. Ma, M. F. Cunningham, K. B. McAuley, B. Keoshkerian, and M. K. Georges. Model studies of nitroxide-mediated styrene miniemulsion polymerization - opportunities for process improvement. *Macromol. Theor. Simul.*, 12:72–85, 2003a.

J. W. Ma, M. F. Cunningham, K. B. McAuley, B. Keoshkerian, and M. K. Georges. Nitroxide-mediated radical polymerization of styrene in miniemulsion: model studies of alkoxyamine-initiated systems. *Chem. Eng. Sci.*, 58:1163–1176, 2003b.

J. W. Ma, J. A. Smith, M. F. Cunningham, K. B. McAuley, B. Keoshkerian, and M. K. Georges. Nitroxide mediated living radical polymerization of styrene in miniemulsion-modelling persulfate-initiated systems. *Chem. Eng. Sci.*, 58:1170–1190, 2003c.

I. A. Maxwell, B. R. Morrison, D. H. Napper, and R. G. Gilbert. Entry of free radicals into latex particles in emulsion polymerization. *Macromolecules*, 24:1629–1640, 1991.

M. Morton, S. Kaizermann, and M. W. Altier. Swelling of latex particles. *J. Colloid Interf. Sci.*, 9:300–312, 1954.

N. Ohmura, K. Kataoka, S. Watanabe, and M. Okubo. Controlling particle size by self-sustained oscillations in continuous emulsion polymerization of vinyl acetate. *Chem. Eng. Sci.*, 53, 1998.

I. Piirma, editor. *Emulsion Polymerization*. Academic, New York, 1982.

G. W. Poehlein. Emulsion polymerization. *ACS. Sym. Ser.*, 285:131–150, 1985.

G. W. Poehlein and D. J. Dougherty. Continuous emulsion polymerization. *Rubber chemistry and technology*, 50:601–639, 1977.

W. J. Priest. Partice growth in the aqueous polymerization of vinyl acetate. *J. Phys. Chem.*, 56:1077–1082, 1952.

L. M. Prince. A theory of aqueous emulsions: II. Mechanism of film curvature at the oil/water interface. *J. Colloid Interface Sci.*, 29:216–221, 1969.

D. Ramkrishna, editor. *Population Balances: Theory and Applications to Particulate Systems in Engineering*. Academic, San Diego, 2000.

J. B. Rawlings and W. H. Ray. The modeling of batch and continuous emulsion polymerization reactors. Part I: Model formulation and sensitivity to parameters. *Polym. Eng. Sci.*, 28:237–256, 1988a.

J. B. Rawlings and W. H. Ray. The modeling of batch and continuous emulsion polymerization reactors. Part II: Comparison with experimental data from continuous stirred tank reactors. *Polym. Eng. Sci.*, 28:257–274, 1988b.

V. S. Rodriguez, J. Delgado, C. A. Silebi, and M. S. El-Aasser. Interparticle monomer transport in miniemulsions. *Ind. Eng. Chem. Res.*, 28:65–74, 1989.

V. S. Rodriguez, J. M. Asua, M. S. El-Aasser, and C. A. Silebi. Mathematical modeling of seeded miniemulsion copolymerization for oil-soluble initiator. *J. Polym. Sci. Pol. Physics.*, 29:483–500, 1991.

C. P. Roe. Surface chemistry aspects of emulsion polymerization. *Ind. Eng. Chem.*, 60(9): 20–33, 1968.

J. M. Saenz and J. M. Asua. Dispersion polymerization in polar solvents. *J. Polym. Sci. Part. A: Polym. Chem.*, 33:1511–1521, 1995.

J. M. Saenz and J. M. Asua. Kinetics of the dispersion copolymerization of styrene and butyl acrylate. *Macromolecules*, 31:5215–5222, 1998.

C. J. Samer and F. J. Schork. Dynamic modeling of continuous miniemulsion polymerization reactors. *Polym. React. Eng.*, 5:85–124, 1997.

J. H. Schulman and E. G. Cockbain. Molecular interactions at oil-water interfaces. I. Molecular complex formation and stability. *Trans. Faraday Soc.*, 36:651–661, 1940.

D. Semino and W. H. Ray. Control of systems described by population balance equations-I. Controllability analysis. *Chem. Eng. Sci.*, 50:1805–1824, 1995a.

D. Semino and W. H. Ray. Control of systems described by population balance equations-II. Emulsion polymerization with constrained control action. *Chem. Eng. Sci.*, 50: 1825–1839, 1995b.

A. L. Smith, editor. *Theory and Practice of Emulsion Technology*. Academic Press, New York, 1976.

W. V. Smith and R. H. Ewart. Kinetics of emulsion polymerization. *J. Chem. Physics*, 16:592–600, 1948.

S. K. Soh and D. C. Sundberg. Diffusion-controlled vinyl polymerization. I. The gel effect. *J. Polym. Sci. Pol. Chem.*, 20:1299–1313, 1982a.

S. K. Soh and D. C. Sundberg. Diffusion-controlled vinyl polymerization. III. Free volume parameters and diffusion-controlled propagation. *J. Polym. Sci. Pol. Chem.*, 20:1331–1344, 1982b.

A. Sood. Particles size distribution control in emulsion polymerization. *J. Appl. Polym. Sci.*, 92:2884–2902, 2004.

G. Storti, S. Carra, and M. Morbidelli. Kinetics of multi monomer emulsion polymerization: The pseudo-homopolymerization approach. *J. Appl. Polym. Sci.*, 37:2443–2467, 1989.

D. C. Sundberg, J. Y. Hsieh, S. K. Soh, and R. F. Baldus. Diffusion-controlled kinetics in the emulsion polymerization of styrene and methyl methacrylate. *ACS. Sym. Ser.*, 165:327–343, 1981.

J. Ugelstad. Swelling capacity of aqueous dispersions of oligomer and polymer substances and mixtures thereof. *Makromol. Chem.*, 179:815–817, 1978.

J. Ugelstad and F. K. Hansen. Kinetics and mechanism of emulsion polymerization. *Rubber chemistry and technology*, 49:536–612, 1976.

J. Ugelstad, M. S. El-Aasser, and J. W. Vanderhoff. Emulsion polymerization: Initiation of polymerization in monomer droplets. *J. Polym. Sci. Pol. Lett*, 11:503–513, 1973a.

J. Ugelstad, H. Flagstad, F. K. Hansen, and T. Ellingsen. Studies on the emulsion polymerization of vinyl chloride by seed polymerization. *J. Polym. Sci.*, 42:473–485, 1973b.

J. Ugelstad, F. K. Hansen, and S. Lange. Emulsion polymerization of styrene with sodium hexadecyl sulphate/hexadecanol mixtures as emulsifiers. Initiation in monomer droplets. *Makromol. Chem.*, 175:507–521, 1974.

J. Ugelstad, K. H. Kaggerud, F. K. Hansen, and A. Berge. Absorption of low molecular weight compounds in aqueous dispersions of polymer-oligomer particles, 2. A two step swelling process of polymer particles giving an enormous increase in absorption capacity. *Makromol. Chem.*, 180:737–744, 1979.

J. Ugelstad, P. C. Mork, K. H. Kaggerud, T. Ellingsen, and A. Berge. Swelling of oligomer-polymer particles. New methods of preparation. *Adv. Colloid Interface Sci.*, 13:101–140, 1980.

J. Ugelstad, H. R. Mfutakamba, P. C. Mork, A. Ellingsenand Berge, R. Schmidt, L. Holm, A. Jorgedel, F. K. Hansen, and K. Nustad. Preparation and application of monodisperse polymer particles. *J. Polym. Sci. Pol. Sym*, 72:225–240, 1985.

D. Urban and K. Takamura, editors. *Polymer Dispersions and Their Industrial Applications*. Wiley-VCH, Weinheim, Germany, 2002.

H. Warson and C. A. Finch, editors. *Applications of Synthetic Resin Latices*. Wiley, Chichester, England, 2001.

J. Zeaiter, J. A. Romagnoli, G. W. Barton, V. G. Gomes, B. S. Hawkett, and R. G. Bilbert. Operation of semi-batch emulsion polymerization reactors: Moedling, validation and effect of operating conditions. *Chem. Eng. Sci.*, 2002.

Chapter 3

Modelling of Macro-emulsion Polymerization

In macro-emulsion polymerization, the main locus of polymerization lies within organic particles (in the size range of about 2nm to 1μm), which are dispersed in the aqueous phase. The particle-size distribution (PSD) is one of the most important characteristics of the emulsion as it determines most critical properties, including the rheological properties, adhesion, drying characteristics, solids content, film-forming properties, optical properties, and so on. Thus, many models have been developed for the PSD in macro-emulsion polymerization. But in emulsion polymerization, a certain particle acts as a nano bulk polymerization reactor, so there are also many polymers with different chain lengths (molecular weights) dispersed in the monomer solution (Figure 3.1). In the present work, a model on macro-emulsion polymerization has been established based on 0-1 model, which allows us to predict the radical chain size distribution for a given class of particle sizes.

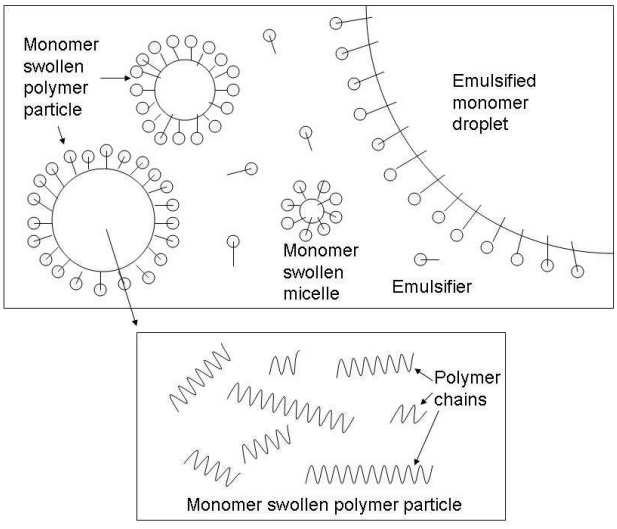

Figure 3.1: Composition in macro-emulsion polymerization

3.1 Notation

3.1.1 Nomenclature

A	surface area, m^3
a_s	surface area of particles covered by 1g surfactant molecule, $1.91\,10^6$ m^2/kg
D	sum of the component diameter, m
d	diameter of one unit component, m
$\overline{d}$	average diameter, m
f	radical efficiency, 0.5
f_h	a correction term that takes into account a possible lack of monomer in the droplets for homogeneous nucleation
f_m	a correction term that takes into account a possible lack of monomer in the droplets for micelle nucleation
I	initiator
[I]	concentration of initiator in aqueous phase, $kmol/m^3$
$[I]_{ini}$	initial concentration of initiator in aqueous phase, $kmol/m^3$
j_{crit}	minimum monomeric units
k	rate coefficient
M	monomer
$M^\bullet$	monomeric radical in the particles
$[M]_p$	concentration of monomer in particles, kg/m^3
$[M]_{pc}$	concentration of monomer in the new born particles which means the saturation concentration, $kmol/m^3$
$[M]_d$	moles of monomer in the droplets per volume of aqueous phase, $kmol/m^3$
MW_m	monomer molecular weight, 0.104 kg /kmol
m_m	mass of the monomer in the particles
N	number of component per volume unit of water
N_a	Avogadro's number, $6.02\,10^{26}$ $kmol^{-1}$
N_M	number of moles of monomers in the particles
N_p	number of moles of particles
n_M	number of moles of monomer for 1g of surfactent nesseccary for a new born particle
n_R	number of moles of monomer for 1 mole of radicals in the aqueous phase nesseccary for a new born particle
$\overline{n}$	average number of radicals per particle
P_i	Polymer chain with i monomeric units
r	radium of particles
$\mathcal{R}$	reactive rate
$R_w^\bullet$	radical in the aqueous phase
$R_0^\bullet$	initial radical in the particles
$R_i^\bullet$	radical with i monomeric units in the particles
$[R]_w$	concentration of monomer in aqueous phase, $kmol/m^3$
S	concentration of surfactant, kg/m^3
S_0	initial concentration of surfactant, kg/m^3
S_{cmc}	critical micellar concentration, $3.0kg/m^3$
S_e	limited concentration of the surfactant for nucleation, $0.514kg/m^3$
V	total volume, m^3

v	volume of one unit component, m^3
$\overline{v}$	average volume, m^3
$w_{i,j}$	percentage in moles of polymeric radical with i monomeric units in the particle of j monomeric units of whole polymers with 1 radical
ρ_{PSTY}	polymer density, $1.044\,10^3$ kg.m^{-3}
ρ_{STY}	momoner density, $0.878\,10^3$ kg. m^{-3}
ϕ_P	fraction by volume of polymers in the particles
ϕ_{Psat}	fraction by volume of polymers in the particles under saturation, 0.4
σ_j	percentage in moles of whole polymers with j monomeric units in the particle with 0 radical

Subscripts

cm	nucleation
cmc	critical micellar concentration
cmh	homogeneous nucleation
cmm	micelle nucleation
cp	capture of radicals in the aqueous phase by particles
d	droplet
dc	decomposition
i	number of monomeric units of polymer
ini	initial
j	number of monomeric units of whole polymers in a particle
m	monomer
min	minimum value
n	based on number
p	particle
pol	polymer
pr	propagation
trM	Chain transfer to monomer
v	based on volume
w	aqueous phase
1	1 radical
0	0 radical

3.1.2 Rate coefficient

$k_{cp} = 5.56\,10^{-14}\text{m}^3\text{kmol}^{-1}\text{s}^{-1}\text{m}^{-a}$ (in this system $a = 1$)
$k_{cm} = k_{cmm} = k_{cmh} = 7.85\,10^{-5}\text{m}^3\text{kmol}^{-1}\text{s}^{-1}$
$k_{dc} = 7.35\,10^{-6}$ s^{-1}
$k_{pr} = 3.54\,10^2$ m^{3}kmol^{-1}s^{-1}
$k_{trM} = 9.35\,10^{-3}$ m^{3}kmol^{-1}s-1

3.2 Modelling

3.2.1 Kinetic mechanism

A simple free radical kinetic mechanism is presented in this part.

Reactions in the aqueous phase

The polymerization process starts by the initiator decomposition (I) in the aqueous phase producing primary radicals ($I^\bullet$). The main reactions taking place in the aqueous phase are illustrated as followed.

- Initiation:

$$I \xrightarrow{f,k_{dc}} 2R_w^\bullet \tag{3.1}$$

- Nucleation: micelle nucleation

$$R_w^\bullet \xrightarrow{k_{cmm}} R_1^\bullet \tag{3.2}$$

homogeneous nucleation

$$R_w^\bullet \xrightarrow{k_{cmh}} R_1^\bullet \tag{3.3}$$

Reactions in the particles

A certain particle acts as a small bulk polymerization reactor. Propagation, chain transfer termination take place in it:

- Propagation:

$$\begin{cases} R_1^\bullet + M & \xrightarrow{k_{pr}} R_2^\bullet \\ R_i^\bullet + M & \xrightarrow{k_{pr}} R_{i+1}^\bullet \end{cases} \tag{3.4}$$

- Chain transfer to monomer:

$$R_i^\bullet + M \xrightarrow{k_{trM}} P_i + M^\bullet \tag{3.5}$$

- Capture of radicals in the aqueous phase by particles:

$$R_w^\bullet \xrightarrow{k_{cp}} R_1^\bullet \tag{3.6}$$

- Instantaneous termination: The entry of a radical into a particle which already contains a growing chain results in 'instantaneous' termination (to be more precise, termination on a timescale much less than the quantity of interest, such as polymerization rate, chain transfer rate). In this limit, intra-particle termination is so fast that is not rate determining.

$$R_i^\bullet + R_1^\bullet \xrightarrow{k_{pr}} P_{i+1} \tag{3.7}$$

We consider $R_1^\bullet$ and $M^\bullet$, both of which have one polymerization degree, have the same molecular weight in calculation, so there is no chain transfer for $R_1^\bullet$.

3.2.2 Kinetic reaction rate

Initiator decomposition

$$\mathcal{R}_{dc} = k_{dc}[\mathrm{I}] \tag{3.8}$$

Nucleation

- micelle nucleation

$$\mathcal{R}_{cmm} = k_{cm} \cdot f_m \cdot S_m \cdot [\mathrm{R}^\bullet]_w \tag{3.9}$$

in which

$$\begin{aligned} S_0 &= S_p + S_m + S_w + S_d \\ S_p &= \frac{A_p}{a_s} \end{aligned} \tag{3.10}$$

If $S_{cmc} + \frac{A_p}{a_s} < S_0$,

$$\begin{cases} S_m &= S_0 - S_{cmc} - \frac{A_p}{a_s} \\ S_w &= S_{cmc} \end{cases} \tag{3.11}$$

else

$$\begin{cases} S_m &= 0 \\ S_w &= \max(S_0 - \frac{A_p}{a_s}, 0) \end{cases} \tag{3.12}$$

Moreover, if $n_M \cdot S_m < [\mathrm{M}]_d$, $f_m = 1$ else $f_m = \dfrac{[\mathrm{M}]_d}{n_M \cdot S_M}$
with

$$n_M = a_s[\mathrm{M}]_{pc} \bullet \left[\frac{MW_m}{36\pi N_a \rho_{PSTY} \phi_{Psat}}\right]^{\frac{1}{3}} \tag{3.13}$$

- homogeneous nucleation

$$\mathcal{R}_{cmh} = k_{cm} \cdot f_h \cdot (S_w - S_e) \cdot [\mathrm{R}^\bullet]_w \tag{3.14}$$

in which if $n_R \cdot [\mathrm{R}^\bullet]_w < [\mathrm{M}]_d$, $f_h = 1$ else $f_h = \dfrac{[\mathrm{M}]_d}{n_R \cdot [\mathrm{R}^\bullet]_w}$
with

$$n_R = \frac{[\mathrm{M}]_{pc} MW_m}{\rho_{PSTY} \phi_{Psat}} \tag{3.15}$$

So

$$\mathcal{R}_{cm} = \mathcal{R}_{cmm} + \mathcal{R}_{cmh} = k_{cm} \cdot [f_m \cdot S_m + f_h \cdot (S_w - S_e)] \cdot [\mathrm{R}^\bullet]_w \tag{3.16}$$

The parameters used here are defined and caculated in Appendix 3.5.

Capture

$$\begin{aligned}\mathcal{R}_{cp,1} &= k_{cp}\overline{d}_{p,n,1}\cdot\frac{N_{p,1}\cdot[\mathrm{R}^{\bullet}]_w}{N_a}\\ \mathcal{R}_{cp,0} &= k_{cp}\overline{d}_{p,n,0}\cdot\frac{N_{p,0}\cdot[\mathrm{R}^{\bullet}]_w}{N_a}\\ \mathcal{R}_{cp} &= k_{cp}\overline{d}_{p,n}\cdot\frac{(N_{p,1}+N_{p,0})\cdot[\mathrm{R}^{\bullet}]_w}{N_a}\end{aligned} \tag{3.17}$$

Transfer to monomer (in particles)

$$\mathcal{R}_{trM} = k_{trM}[\mathrm{M}]_p\cdot\frac{N_{p,1}}{N_a} \tag{3.18}$$

Propagation in particles

$$\mathcal{R}_{pr} = k_{pr}[\mathrm{M}]_p\cdot\frac{N_{p,1}}{N_a} \tag{3.19}$$

3.2.3 Concept and kinetics of $w_{i,j}$ and σ_j

A model on macro-emulsion polymerization is established which allows us to predict radical chain size distribution in certain particles size and the total particles size distribution.

Assume that the number of monomeric units of whole polymers in a particle is j , and the number of monomeric units of the polymeric radical is i.
$w_{i,j}$ is the percentage in moles of polymeric radical with i monomeric units in the particle of j monomeric units of whole polymers with 1 radical.
σ_j is the percentage in moles of whole polymers with j monomeric units in the particle with 0 radical.
and $i \leq j$.

$$\begin{aligned}&\sum_{j=1}^{\infty}\sum_{i=1}^{j} w_{i,j} = 1\\ &\sigma_1 = 0\\ &\sum_{j=2}^{\infty}\sigma_j = 1\\ &N_p = N_{p,1} + N_{p,0}\\ &\overline{n} = \frac{N_{p,1}}{N_p}\\ &\mu_(m,n) = \sum_{j=1}^{\infty}\sum_{i=1}^{j} i^m j^n w_{i,j}\\ &\nu_k = \sum_{j=2}^{\infty} j^k\sigma_j\end{aligned} \tag{3.20}$$

As elaborated in appendix 3.5, before the droplets are exhausted with respect to monomer,

$$r_{p,j} = \left(\frac{3}{4}j\cdot\frac{MW_m}{\rho_{PSTY}\phi_{Psat}N_a}/\pi\right)^{1/3} \tag{3.21}$$

after droplets are exhausted with respect to monomer,

$$r_{p,j} = \left(\frac{3}{4} j \cdot \frac{MW_m}{\rho_{PSTY}\phi_P N_a}/\pi\right)^{1/3} \tag{3.22}$$

$$d_{p,j} = 2\, r_{p,j} \tag{3.23}$$

Nucleation

For styrene

$$j_{crit} = 1 \tag{3.24}$$

if $j = j_{crit}$
when $s_w \leq s_e$, $\mathcal{R}_{cmh} = 0$

$$\mathcal{R}_{cm} = \mathcal{R}_{cmm} = k_{cm} \cdot [f_m \cdot S_m] \cdot [\mathrm{R}^\bullet]_w \tag{3.25}$$

when$s_w \geq s_e$

$$\mathcal{R}_{cm} = \mathcal{R}_{cmm} + \mathcal{R}_{cmh} = k_{cm} \cdot [f_m \cdot S_m + f_h \cdot (S_w - S_e)] \cdot [\mathrm{R}^\bullet]_w \tag{3.26}$$

Propagation in particles

$$\mathcal{R}_{pr,i,j} = k_p[\mathrm{M}]_p \cdot \frac{N_{p,1}}{N_a} \cdot w_{i,j} = \mathcal{R}_{pr} \cdot w_{i,j} \tag{3.27}$$

Transfer to monomer

$$\mathcal{R}_{trM,i,j} = k_{trM}[\mathrm{M}]_p \cdot \frac{N_{p,1}}{N_a} \cdot w_{i,j} = R_{trM} \cdot w_{i,j} \tag{3.28}$$

Capture of radical

$$\begin{aligned} \mathcal{R}_{cp,i,j,1} &= k_{cp} d_{p,j} \cdot \frac{N_{p,1}[R^\bullet]_w}{N_a} \cdot w_{i,j} = \mathcal{R}_{cp} \cdot \frac{d_{p,j}}{\overline{d}_{p,n}} \cdot \overline{n} \cdot w_{i,j} \\ \mathcal{R}_{cp,j,0} &= k_{cp} d_{p,j} \cdot \frac{N_{p,0}[R^\bullet]_w}{N_a} \cdot \sigma_j = \mathcal{R}_{cp} \cdot \frac{d_{p,j}}{\overline{d}_{p,n}} \cdot (1 - \overline{n}) \cdot \sigma_j \end{aligned} \tag{3.29}$$

3.2.4 Population balance equation

A population balance is a balance on a defined set of dispersed entities, which accounts for the net accumulation of such entities in a given system as a result of all phenomena that add or remove entities from the set. Comprehensive discussion on the population balance framework can be found elsewhere [Randolph and Larsen, 1998]. In order to write the population balance equations, we must choose a set of variables, the phase coordinates, whose values if known as a function of time, will suffice to describe the dynamics of the development of the dispersed entities of the system. The population balance accounts for all the important ways in which the value of each phase coordinate changes with time. These ways can be subdivided into three types:
(1) Evolution: It is the event by which a phase coordinate associated with a dispersed

entity changes with time,
(2) Birth or Death: These are the events by which the number of dispersed entities changes either by birth of new entities or death of existing entities,
(3) Accumulation: It is the net balance of both evolution and birth/death events on the number of dispersed entities with a given value of phase coordinates.
The terms of the three types are collected together to give the population balance equations:

$$\text{Accumulation} = \text{Evolution} + \text{Birth} - \text{Death}$$

which is given by the following hyperbolic differential equation:

$$\frac{\partial \zeta(\eta,t)}{\partial t} + \frac{\partial \zeta(\eta,t)\, d\eta/dt}{\partial \eta} = \mathcal{R}_{generation}(\eta,t) \tag{3.30}$$

where $\zeta(\eta,t)$ is the population density function, $\mathcal{R}_{generation}$ is the rate of generation of new members in the population, and $d\eta/dt$ accounts for variation in the property η with time.

In the aqueous phase

$$\begin{aligned} \frac{d[\mathrm{I}]}{dt} &= -k_d[\mathrm{I}] \\ \frac{d[\mathrm{R}^{\bullet}_w]}{dt} &= 2k_d f[\mathrm{I}] - \mathcal{R}_{cm} - \mathcal{R}_{cp} \end{aligned} \tag{3.31}$$

Number of particles

- particles having 1 radical
  for $j = j_{crit}$

$$\begin{aligned} \frac{dN_{p,1}w_{1,j}}{dt} &= \mathcal{R}_{cm} - \mathcal{R}_{pr,1,j} - \mathcal{R}_{cp,1,j,1} \\ &= \mathcal{R}_{cm} - \mathcal{R}_{pr}\cdot w_{1,j} - \mathcal{R}_{cp}\cdot\frac{d_{p,j}}{\overline{d}_{p,n}}\cdot\overline{n}\cdot w_{1,j} \end{aligned} \tag{3.32}$$

  for $j = j_{crit}+1$

$$\begin{aligned} w_{1,j} &= 0 \\ \frac{dN_{p,1}w_{i,j}}{dt} &= \mathcal{R}_{pr,i-1,j-1} - \mathcal{R}_{pr,i,j} - \mathcal{R}_{cp,i,j,1} - \mathcal{R}_{trM,i,j} \\ &= \mathcal{R}_{pr}\cdot w_{i-1,j-1} - \mathcal{R}_{pr}\cdot w_{i,j} - \mathcal{R}_{cp}\cdot\frac{d_{p,j}}{\overline{d}_{p,n}}\cdot\overline{n}\cdot w_{i,j} - \mathcal{R}_{trM}\cdot w_{i,j} \\ &\quad (i\in[2,j]) \end{aligned} \tag{3.33}$$

for $j > j_{crit} + 1$

$$\begin{aligned}
\frac{dN_{p,1}w_{1,j}}{dt} &= \sum_{i=2}^{j-1} \mathcal{R}_{trM,i,j-1} - \mathcal{R}_{pr,1,j} - \mathcal{R}_{cp,1,j,1} + \mathcal{R}_{cp,j-1,0} \\
&= \mathcal{R}_{trM} \cdot \sum_{i=2}^{j-1} w_{i,j-1} - \mathcal{R}_{pr} \cdot w_{1,j} - \mathcal{R}_{cp} \cdot \frac{d_{p,j}}{\overline{d}_{p,n}} \cdot \overline{n} \cdot w_{1,j} + \mathcal{R}_{cp} \cdot \frac{d_{p,j-1}}{\overline{d}_{p,n}} \cdot (1-\overline{n}) \cdot \sigma_{j-1} \\
\frac{dN_{p,1}w_{i,j}}{dt} &= \mathcal{R}_{pr,i-1,j-1} - \mathcal{R}_{pr,i,j} - \mathcal{R}_{cp,i,j,1} - \mathcal{R}_{trM,i,j} \\
&= \mathcal{R}_{pr} \cdot w_{i-1,j-1} - \mathcal{R}_{pr} \cdot w_{i,j} - \mathcal{R}_{cp} \cdot \frac{d_{p,j}}{\overline{d}_{p,n}} \cdot \overline{n} \cdot w_{i,j} - \mathcal{R}_{trM} \cdot w_{i,j} \\
&(i \in [2,j])
\end{aligned} \tag{3.34}$$

- particles having 0 radical for $j > j_{crit}$

$$\begin{aligned}
\frac{dN_{p,0}\sigma_j}{dt} &= \sum_{i=1}^{j-1} \mathcal{R}_{cp,i,j-1,1} - \mathcal{R}_{cp,j,0} \\
&= \mathcal{R}_{cp} \cdot \frac{d_{p,j-1}}{\overline{d}_{p,n}} \cdot \overline{n} \cdot \sum_{i=1}^{j-1} w_{i,j-1} - \mathcal{R}_{cp} \cdot \frac{d_{p,j}}{\overline{d}_{p,n}} \cdot (1-\overline{n}) \cdot \sigma_j
\end{aligned} \tag{3.35}$$

By solving the previous differential equations together with the differential mass balances equations of the species in the aqueous phase, the distribution of the radical chain sizes for a given class of particle sizes can be predicted.

3.2.5 Initial condition

At $t = 0$

$$\begin{aligned}
[\mathrm{I}] &= [\mathrm{I}]_{ini} \\
[\mathrm{R}^{\bullet}]_w &= 0 \\
N_{p,1} &= 0 \\
N_{p,0} &= 0 \\
w_{1,1} &= 1 \\
w_{i,j} &= 0, \quad \forall (i,j) \neq (1,1) \\
\sigma_2 &= 1 \\
\sigma_i &= 0, \quad \forall j \neq 2
\end{aligned} \tag{3.36}$$

3.2.6 Total number of particles (N_p), number of particles containing a growing chain ($N_{p,1}$) and number of particles containing no growing chain ($N_{p,0}$)

By this model, the total number of particles (N_p), the number of particles containing a growing chain ($N_{p,1}$) and the number of particles containing no growing chain ($N_{p,0}$) can also be predicted.

Number of particles containing a growing chain, $N_{p,1}$ (Sum on $w_{i,j}$)

When we make an integration of $w_{i,j}$ on i and j, the number of particles containing a growing chain($N_{p,1}$) can be obtained.

- sum on i

$$\begin{aligned}
\frac{dN_{p,1}w_{1,1}}{dt} &= \mathcal{R}_{cm} - \mathcal{R}_{pr}\cdot w_{1,1} - \mathcal{R}_{cp}\cdot\frac{d_{p,1}}{\overline{d}_{p,n}}\cdot\overline{n}\cdot w_{1,1}\\
\sum_{i=1}^{2}\frac{dN_{p,1}w_{i,2}}{dt} &= \frac{dN_{p,1}w_{2,2}}{dt}\\
&= \mathcal{R}_{pr}\cdot w_{1,1} - \mathcal{R}_{pr}\cdot w_{2,2} - \mathcal{R}_{cp}\cdot\frac{d_{p,2}}{\overline{d}_{p,n}}\cdot\overline{n}\cdot w_{2,2} - \mathcal{R}_{trM}\cdot w_{2,2}\\
&(i\in[2,j])
\end{aligned} \tag{3.37}$$

for $j > 2$

$$\begin{aligned}
\sum_{i=1}^{j}\frac{dN_{p,1}w_{i,j}}{dt} &= \frac{d}{dt}\sum_{i=1}^{j}N_{p,1}w_{i,j}\\
&= \mathcal{R}_{trM}\cdot\sum_{i=2}^{j-1}w_{i,j-1} - \mathcal{R}_{pr}\cdot w_{1,j} - \mathcal{R}_{cp}\cdot\frac{d_{p,j}}{\overline{d}_{p,n}}\cdot\overline{n}\cdot w_{1,j}\\
&\quad+\mathcal{R}_{cp}\cdot\frac{d_{p,j-1}}{\overline{d}_{p,n}}\cdot(1-\overline{n})\cdot\sigma_{j-1} + \sum_{i=2}^{j}\mathcal{R}_{pr}\cdot w_{i-1,j-1} - \sum_{i=2}^{j}\mathcal{R}_{p}\cdot w_{i,j}\\
&\quad-\sum_{i=2}^{j}\mathcal{R}_{cp}\cdot\frac{d_{p,j}}{\overline{d}_{p,n}}\cdot\overline{n}\cdot w_{i,j} - \sum_{i=2}^{j}\mathcal{R}_{trM}\cdot w_{i,j}
\end{aligned} \tag{3.38}$$

- sum on i and j

$$\begin{aligned}
\sum_{j=1}^{\infty}\frac{d}{dt}\sum_{i=1}^{j}N_{p,1}w_{i,j} = {}& \mathcal{R}_{cm} - \mathcal{R}_{pr}\cdot w_{1,1} - \mathcal{R}_{cp}\cdot\frac{d_{p,1}}{\overline{d}_{p,n}}\cdot\overline{n}\cdot w_{1,1} + \mathcal{R}_{pr}\cdot w_{1,1} - \mathcal{R}_{pr}\cdot w_{2,2}\\
&-\mathcal{R}_{cp}\frac{d_{p,2}}{\overline{d}_{p,n}}\overline{n}\cdot w_{2,2} - \mathcal{R}_{trM}\cdot w_{2,2} + \sum_{j=3}^{\infty}\mathcal{R}_{trM}\cdot\sum_{i=2}^{j-1}w_{i,j-1}\\
&-\sum_{j=3}^{\infty}\mathcal{R}_{pr}\cdot w_{1,j} - \sum_{j=3}^{\infty}\mathcal{R}_{cp}\cdot\frac{d_{p,j}}{\overline{d}_{p,n}}\cdot\overline{n}\cdot w_{1,j} + \sum_{j=3}^{\infty}\mathcal{R}_{cp}\cdot\frac{d_{p,j-1}}{\overline{d}_{p,n}}\\
&\cdot(1-\overline{n})\cdot\sigma_{j-1} + \sum_{j=3}^{\infty}\sum_{i=2}^{j}\mathcal{R}_{pr}\cdot w_{i-1,j-1} - \sum_{j=3}^{\infty}\sum_{i=2}^{j}\mathcal{R}_{pr}\cdot w_{i,j}\\
&-\sum_{j=3}^{\infty}\sum_{i=2}^{j}\mathcal{R}_{cp}\cdot\frac{d_{p,j}}{\overline{d}_{p,n}}\cdot\overline{n}\cdot w_{i,j} - \sum_{j=3}^{\infty}\sum_{i=2}^{j}\mathcal{R}_{trM}\cdot w_{i,j}
\end{aligned} \tag{3.39}$$

$$\begin{aligned} \Rightarrow \frac{dN_{p,1}}{dt} &= \mathcal{R}_{cm} - \mathcal{R}_{pr} - \mathcal{R}_{cp,1} - \mathcal{R}_{trM} + \mathcal{R}_{trM} + \mathcal{R}_{p} + \mathcal{R}_{cp,0} \\ &= \mathcal{R}_{cm} - \mathcal{R}_{cp,1} + \mathcal{R}_{cp,0} \end{aligned} \tag{3.40}$$

which means that the number of particles containing a growing chain is added by nucleation and capture of radicals in the aqueous phase by particles containing no growing chain, but reduced by capture of radicals in the aqueous phase by particles containing a growing chain.

Number of particles containing no growing chain, $N_{p,0}$ (Sum on σ_j)

$$\begin{aligned} \frac{dN_{p,0}}{dt} &= \sum_{j=2}^{\infty} \frac{dN_{p,0}\sigma_j}{dt} \\ &= \mathcal{R}_{cp} \cdot \sum_{j=2}^{\infty} \frac{d_{p,j-1}}{\overline{d}_{p,n}} \cdot \overline{n} \cdot \sum_{i=1}^{j-1} w_{i,j-1} - \mathcal{R}_{cp} \cdot \sum_{j=2}^{\infty} \frac{d_{p,j}}{\overline{d}_{p,n}} \cdot (1-\overline{n}) \cdot \sigma_j \\ &= \mathcal{R}_{cp,1} - \mathcal{R}_{cp,0} \end{aligned} \tag{3.41}$$

which means that the number of particles containing a growing chain is added by capture of radicals in the aqueous phase by particles containing a growing chain, but reduced by capture of radicals in the aqueous phase by particles containing no growing chain.

Total number of particles N_p

$$\begin{aligned} N_p &= N_{p,0} + N_{p,1} = (\mathcal{R}_{cm} - \mathcal{R}_{cp,1} + \mathcal{R}_{cp,0}) + (\mathcal{R}_{cp,1} - \mathcal{R}_{cp,0}) \\ &= \mathcal{R}_{cm} \end{aligned} \tag{3.42}$$

which means that the total number of particles just depends on the rate of nucleation.

3.3 Validation

The system selected for validation includes styrene (monomer), sodium dodecyl sulfate (emulsifier). and potassium persulfate (initiator). The experimental data of [Massebeuf, 1997], who graduated from our lab is chosen for the purpose of validating the simulation. All of the experiments are run at 60°C.

For simpleness, the desorption of monomeric radicals in the particles into the aqueous phase is not involved in the simulation.

Figures 3.2 and 3.3 compare the experimental and simulated conversions. The effect of initial concentration of surfactant and that of initiator are checked. The polymerization rate decreases with the decreasing of concentration of surfactant or that of initiator. In general, a good agreement is observed between model and experiments.

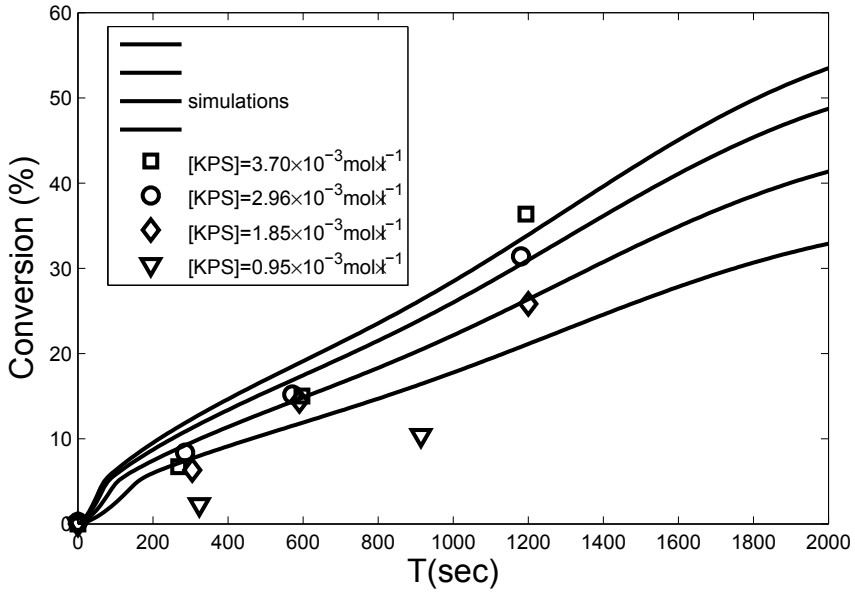

Figure 3.2: Comparison of the evolution of experimental and simulated conversions versus time for the initial concentrations of surfactant above the cmc and an initial concentration of initiator $[KPS]_0 = 3.70\,10^{-3}\text{mol.l}^{-1}$

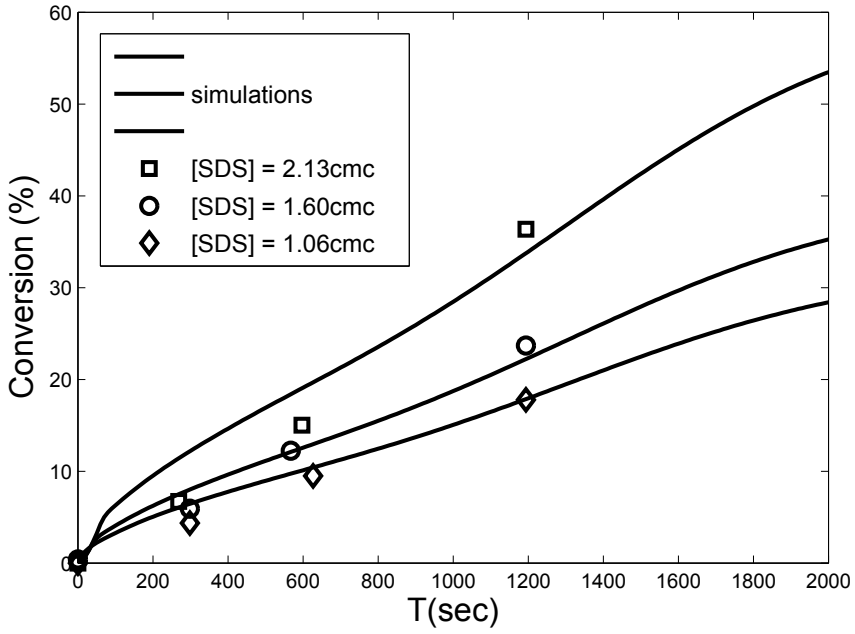

Figure 3.3: Comparison of the evolution of experimental and simulated conversions versus time for an initial concentration of initiator and an initial concentration of surfactant $[SDS]_0 = 2.13cmc$

3.4 Results and Discussion

The model can also predict the total particles size distribution and the radical chain size distribution for a given class of particle sizes. The initial condition of concentrations of surfactant $[SDS] = 2.13cmc$ and concentration of initiator $[KPS]_0 = 3.70\,10^{-3}\text{mol.l}^{-1}$ are chosen. As the result of the simulation, after 1240sec, the droplets in the system are exhausted.

3.4.1 Particle size distribution

Figures 3.4 and 3.5 illustrate the change of PSD's with time. At the beginning of the polymerization, although the radical entry into micelles is slower than that into particles by several orders of magnitude (the ratio between the entry rate coefficient of micelles and that of particles is 0.08 [Sood and Awasthi, 2004]), but the number of micelles is much larger than that of particles, so both the number of the particles and the particle size increase. As the time increases, the number of the particles is large enough to compete with micelles to capture the radicals, and the radical entry into micelles is slower than that into particles, thus most radicals are captured by particles, so the number of the particles is almost unchanged, and the particle size grows because of the propagation in the particles.

Figure 3.6 represents the averege number of radicals in the particles. Because the model established is based on the 0-1 model, and desorption of radicals in the particle into the aqueous phase is not considered in, the averege number of radicals in the particles is nearly 0.5.

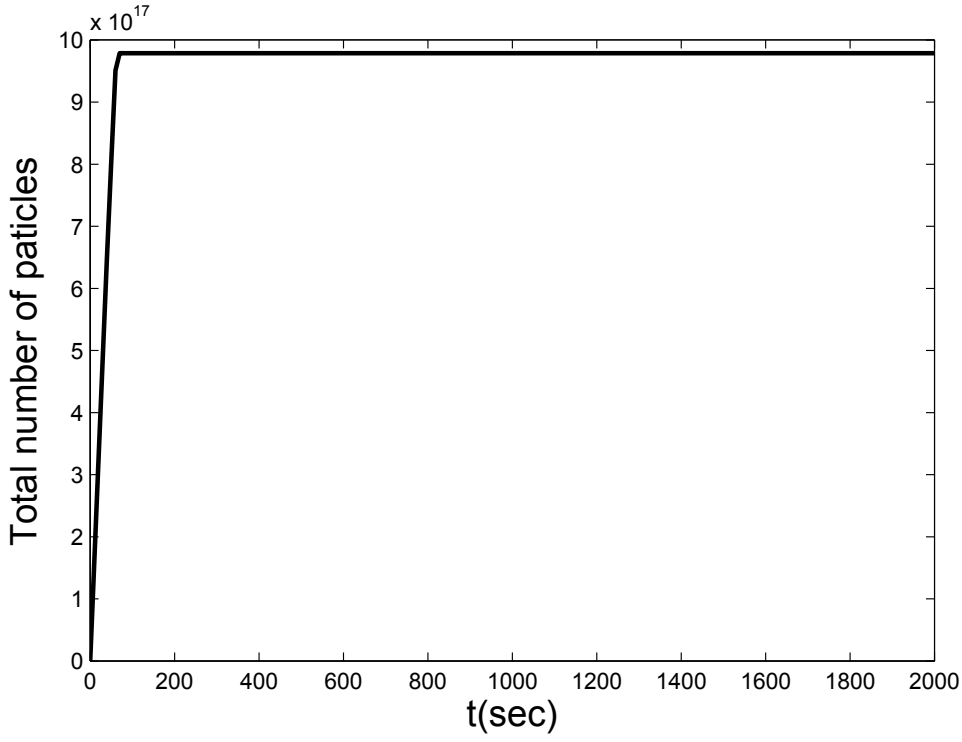

Figure 3.4: Evolution of number of particles with time

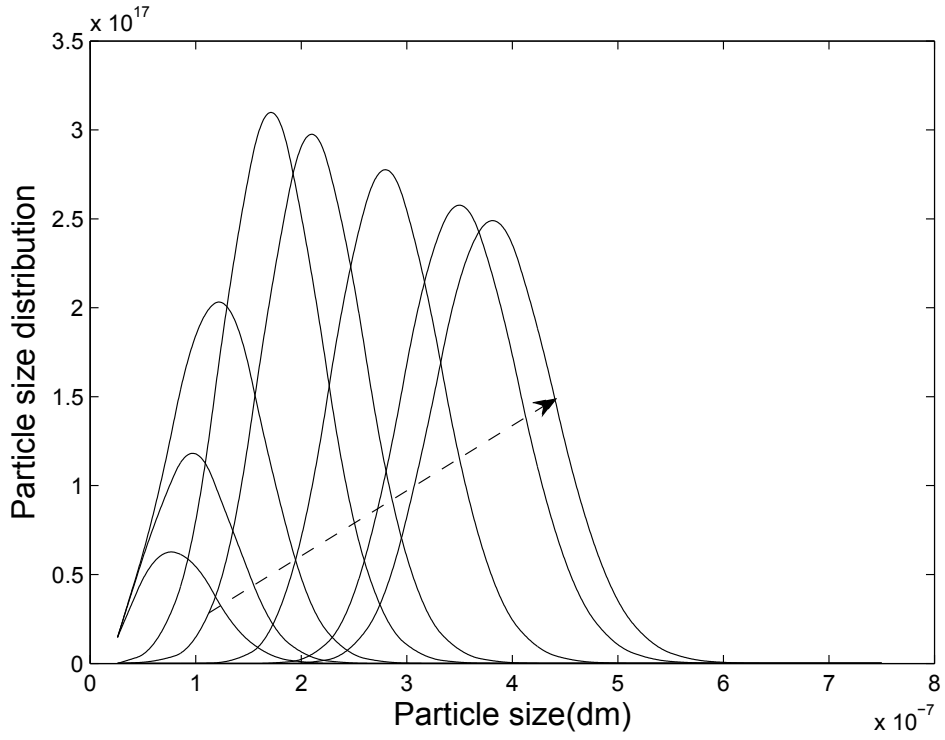

Figure 3.5: Particle size distribution (time increasinge with the direction of the arrow, t = 10sec, 20sec, 40sec, 110sec, 210sec, 510sec, 1010sec and 1310sec)

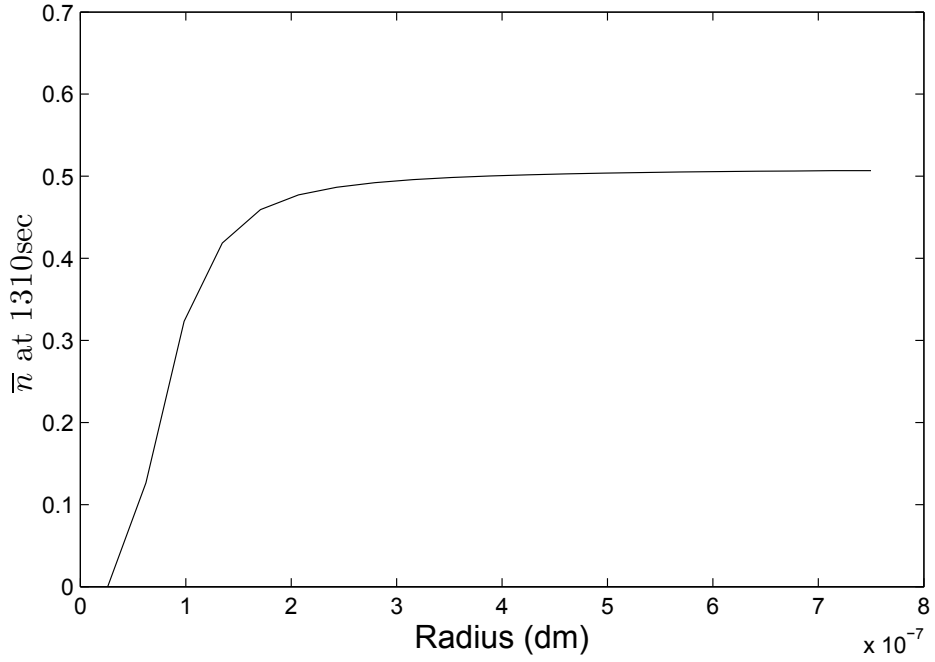

Figure 3.6: Average number of radicals in the particles at t = 1310sec

3.4.2 Radical size distribution in the particles

Figure 3.7 gives the radical chain size distribution in the particle with the particle radius of 9.8nm, 31.6nm, 46.4nm and 64.1nm at 10sec, when the polymerization just starts. Figure 3.8 gives the radical chain size distribution in the particle with the particle radius of 9.8nm, 31.6nm, 46.4nm and 64.1nm at 510sec, when the total number of particles is stable. Figure 3.9 gives the radical chain size distribution in the particle with the particle radius of 9.8nm, 31.6nm, 46.4nm and 64.1nm at 1310sec, when the droplets in the system are exhausted. In our present model, the transfer of polymeric radical to the monomers in the particles is taken into account, however the desorption of monomeric radicals in the particles into the aqueous phase is not considered. The former will increase the number of the radicals of small size, but the latter will decrease the number of the radicals of small size. This causes the number of the radicals of small size to be larger than the reality. In other words, whatever the stage of polymerization, and whatever the size of particles, the radical chain sizes are centered in the oligomeric radicals. To obtain a more precise radical chain size distribution, a model involving both transfer of polymeric radical to the monomers in the particles and desorption of monomeric radicals in the particles into the aqueous phase should be developed.

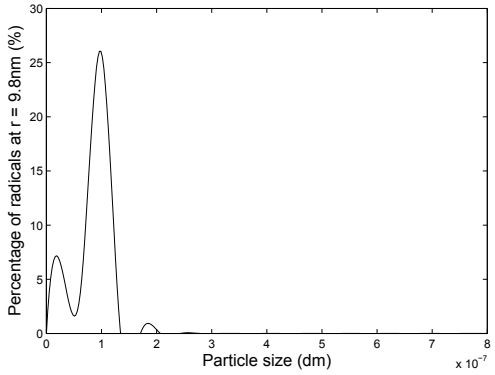

(a) r = 9.8nm, t = 10sec

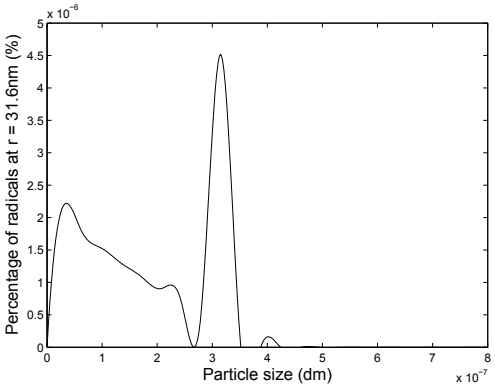

(b) $r = 31.6$nm, $t = 10$sec

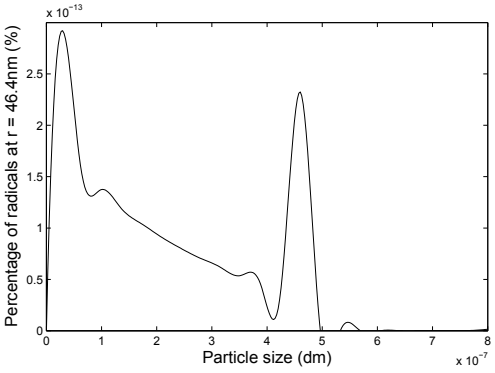

(c) $r = 46.4$nm, $t = 10$sec

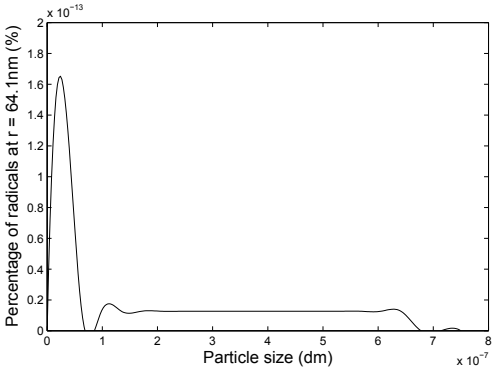

(d) $r = 64.1$nm, $t = 10$sec

Figure 3.7: Radical size distribution in the particles of certain size at $t = 10$ sec

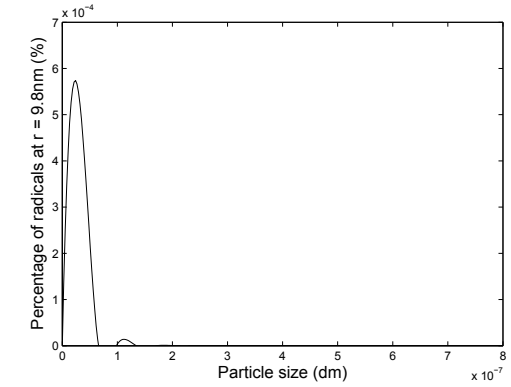

(a) r = 9.8nm, t = 510sec

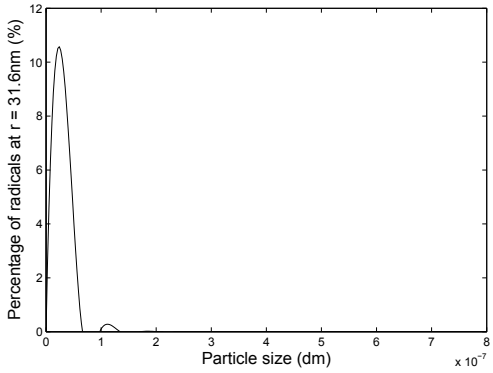

(b) $r = 31.6$nm, $t = 510$sec

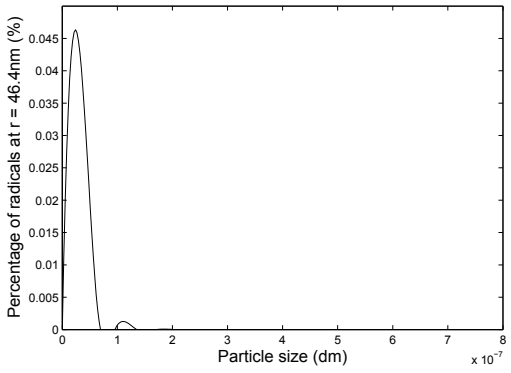

(c) $r = 46.4$nm, $t = 510$sec

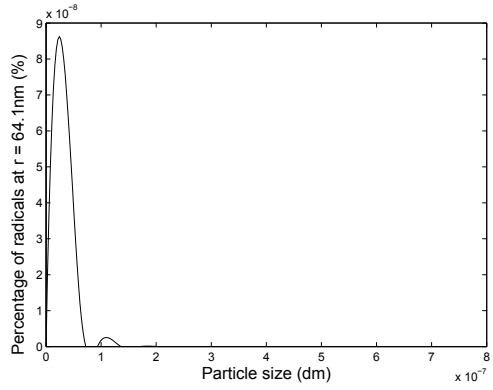

(d) $r = 64.1$nm, $t = 510$sec

Figure 3.8: Radical size distribution in the particles of certain size at $t = 510$ sec

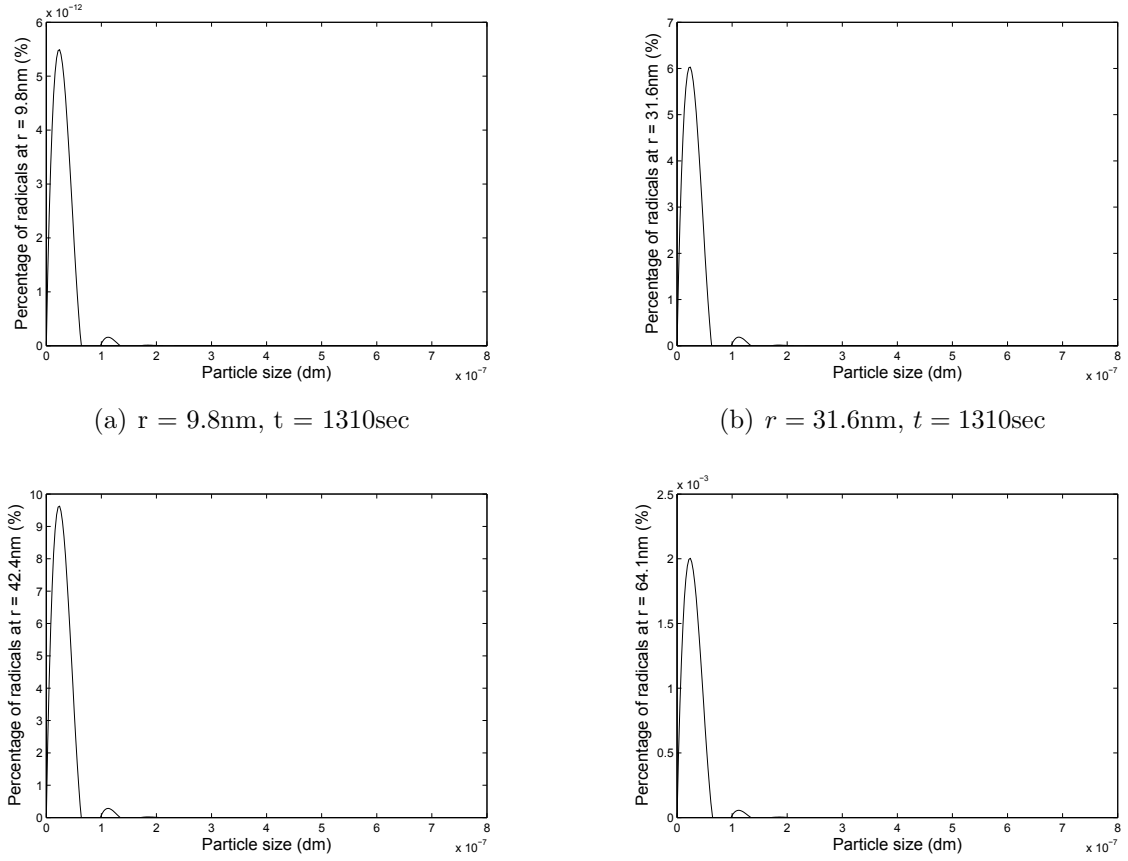

(a) r = 9.8nm, t = 1310sec

(b) $r = 31.6$nm, $t = 1310$sec

(c) $r = 42.4$nm, $t = 1310$sec

(d) $r = 64.1$nm, $t = 1310$sec

Figure 3.9: Radical size distribution in the particles of certain size at $t = 1310$sec

3.4.3 In the aqueous phase

Figure 3.10 and 3.11 shows the concentration of radicals and initiator in the aqueous phase. The initiator decreases linearly with the time. With respect to the radicals in the aqueous phase $R_w^\bullet$, the initiator decomposition reaction produces the radicals, while the nucleation and capture of the radicals by particle reactions consume them (eq.3.43). The reaction rate of the former one is much faster than that of the latter ones, the total reaction rate is controlled by the step with the lower reaction rate, and the step with faster reaction rate will produce a sufficient amount of radicals to support the latter steps. As the radical entry into micelles is slower than that into particles by several orders of magnitude (the ratio between the entry rate coefficient of micelles and that of particles is 0.08 [Sood and Awasthi, 2004]), at the beginning of polymerization, the concentration of radicals in the aqueous phase increases with the increase of the amount of particles. After some time, the amount of the particles does not change any more, the capture of radicals by the particles will be dominant with respect to nucleation, and some time is necessary to reach the chemical equilibrium state. After that, the concentration of radicals in the aqueous phase will be constant.

$$\begin{aligned} \mathrm{I} \xrightarrow{f,k_d} \mathrm{R}_w^\bullet \quad & \xrightarrow{k_{cm}} \mathrm{R}_1^\bullet \\ & \xrightarrow{k_{cp}} \mathrm{R}_1^\bullet \end{aligned} \tag{3.43}$$

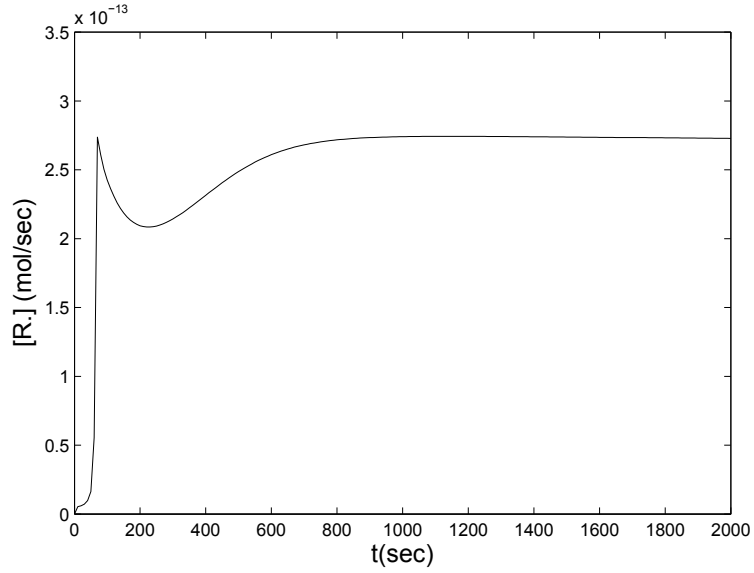

Figure 3.10: Concentration of radicals in the aqueous phase

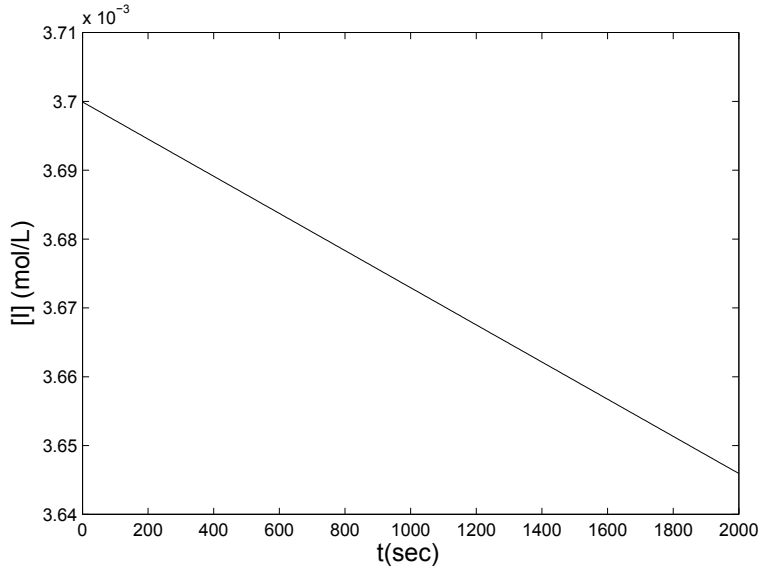

Figure 3.11: Concentration of initiator in the aqueous phase

3.5 Appendix A – Caculation of n_M and n_R

3.5.1 Caculation of n_R

The minimum polymeric radical in the particle has only one unit, thus

$$v_{pol,min} = \frac{1\, MW_m}{\rho_{PSTY}} \tag{3.44}$$

before droplets have disappeared

$$\begin{aligned} \phi_{Psat} &= \frac{v_{pol}}{v_{pol}+v_m} \\ v_{pol}(1-\phi_{Psat}) &= \phi_{Psat} v_m \\ v_{m,min} &= \frac{MW_m}{\rho_{PSTY}} \cdot \frac{1-\phi_{Psat}}{\phi_{Psat}} \end{aligned} \tag{3.45}$$

$$n_R = \frac{v_{m,min}\rho_{PSTY}}{MW_m} = \frac{\rho_{STY}}{\rho_{PSTY}} \cdot \frac{1-\phi_{Psat}}{\phi_{Psat}} = \frac{[\mathrm{M}]_{pc} MW_m}{\rho_{PSTY}\phi_{Psat}} \tag{3.46}$$

$$\rho_{STY}(1-\phi_{Psat}) = [\mathrm{M}]_{pc} MW_m \tag{3.47}$$

3.5.2 Caculation of n_M

$$\begin{aligned} v_{pol,1} &= \frac{MW_m}{\rho_{PSTY} N_a} \\ v_{m,1} &= \frac{n_R MW_m}{\rho_{STY} N_a} \end{aligned} \tag{3.48}$$

$$\begin{aligned} v_p &= \frac{\pi d_p^3}{6} = \frac{MW_m}{N_a \rho_{PSTY}} + \frac{n_R MW_m}{\rho_{STY} N_a} \\ &= \frac{MW_m}{N_a}\left[\frac{1}{\rho_{PSTY}} + \frac{1}{\rho_{PSTY}} \frac{1-\phi_{Psat}}{\phi_{Psat}}\right] \\ &= \frac{MW_m}{\rho_{PSTY}\phi_{Psat} N_a} \end{aligned} \tag{3.49}$$

$$A_p = \pi d^2 = \pi \left(\frac{6MW_m}{\pi \rho_{PSTY}\phi_{Psat} N_a}\right)^{2/3} \tag{3.50}$$

$$\begin{aligned} n_M &= \frac{n_R}{N_a}\left(\frac{A_p}{a_s}\right)^{-1} \\ &= \frac{[M]_{pc} MW_m a_s}{\rho_{PSTY}\phi_{Psat} N_a \pi}\left(\frac{6MW_m}{\pi \rho_{PSTY}\phi_{Psat} N_a}\right)^{-2/3} \\ &= a_s [\mathrm{M}]_{pc} \cdot \left[\frac{MW_m}{36\pi N_a \rho_{PSTY}\phi_{Psat}}\right]^{\frac{1}{3}} \end{aligned} \tag{3.51}$$

3.6 Appendix B – Caculation of $v_{p,j}$ and $r_{p,j}$

Volume of the polymers having j units

$$v_{pol,j} = \frac{j}{N_a}\frac{MW_m}{\rho_{PSTY}} \tag{3.52}$$

3.6.1 Before droplets disappeared

$$v_{p,j} = \frac{v_{pol,j}}{\phi_{Psat}} \tag{3.53}$$

so

$$\begin{aligned} v_{p,j} &= \frac{4}{3}\pi r_{p,j}^3 = \frac{MW_m j}{\rho_{PSTY}\phi_{Psat}N_a} \\ r_{p,j} &= \left(\frac{3}{4}\frac{MW_m j}{\pi\rho_{PSTY}\phi_{Psat}N_a}\right)^{1/3} \\ d_{p,j} &= 2\cdot r_{p,j} = \left(\frac{2\cdot MW_m j}{\pi\rho_{PSTY}\phi_{Psat}N_a}\right)^{1/3} \end{aligned} \tag{3.54}$$

3.6.2 After droplets disappeared

$$[M]_p = \frac{N_m}{V_{tot}} \tag{3.55}$$

$$\begin{aligned} m_{m,j} &= [M]_p MW_m v_{p,j} \\ v_{m,j} &= [M]_p \frac{MW_m}{\rho_{STY}} v_{p,j} \end{aligned} \tag{3.56}$$

$$\begin{aligned} v_{p,j} &= \frac{j}{Na}\frac{MW_m}{\rho_{PSTY}} + [M]_p\frac{MW_m}{\rho_{STY}}v_{p,j} \\ &= \frac{4}{3}\pi r_{p,j}^3 = \frac{\frac{j}{N_a}\frac{MW_m}{\rho_{PSTY}}}{1-[M]_p\frac{MW_m}{\rho_{STY}}} = \frac{j}{\phi_P N_a}\frac{MW_m}{\rho_{PSTY}} \end{aligned} \tag{3.57}$$

$$\begin{aligned} r_{p,j} &= \left(\frac{3}{4}\frac{MW_m j}{\pi\rho_{PSTY}\phi_P N_a}\right)^{1/3} \\ d_{p,j} &= 2\cdot r_{p,j} = \left(\frac{6\cdot MW_m j}{\pi\rho_{PSTY}\phi_P N_a}\right)^{1/3} \end{aligned} \tag{3.58}$$

in which

$$\phi_P = 1 - [M]_p\frac{MW_m}{\rho_{STY}} \tag{3.59}$$

3.6.3 Number average diameter of particles and volume average diameter of particles

Defining $v_{p,j} = \pi\alpha\cdot j$, so $d_{p,j} = (6\alpha j)^{1/3}$

- Before droplets have disappeared,

  $\alpha = \dfrac{MW_m}{\pi\rho_{PSTY}\phi_{Psat}N_a}$

- After droplets have disappeared,

  $\alpha = \dfrac{MW_m}{\pi\rho_{PSTY}\phi_P N_a}$

Volume average diameter of particles

$$\begin{aligned} V_p &= \sum_{j=1}^{\infty} v_{p,j} \cdot N_j = \sum_{j=1}^{\infty} v_{p,j} \cdot \left(N_{p,1} \cdot \sum_{i=1}^{j} w_{i,j} + N_{p,0} \cdot \sigma_j \right) \\ &= N_p \cdot \left[\overline{n} \sum_{j=1}^{\infty} \sum_{i=1}^{j} w_{i,j} \cdot v_{p,j} + (1-\overline{n}) \cdot \sum_{j=1}^{\infty} \sigma_j \cdot v_{p,j} \right] \\ \overline{v} &= \frac{V_p}{N_p} = \overline{n} \sum_{j=1}^{\infty} \sum_{i=1}^{j} w_{i,j} \cdot v_{p,j} + (1-\overline{n}) \cdot \sum_{j=1}^{\infty} \sigma_j \cdot v_{p,j} \\ &= \pi\alpha \cdot \left[\overline{n} \sum_{j=1}^{\infty} \sum_{i=1}^{j} w_{i,j} \cdot j + (1-\overline{n}) \cdot \sum_{j=1}^{\infty} \sigma_j \cdot j \right] \end{aligned} \tag{3.60}$$

so

$$\overline{d}_{p,v} = \left(\frac{6\overline{V}}{\pi} \right)^{1/3} = \left(6\alpha \cdot \left[\overline{n} \sum_{j=1}^{\infty} \sum_{i=1}^{j} w_{i,j} \cdot j + (1-\overline{n}) \cdot \sum_{j=1}^{\infty} \sigma_j \cdot j \right] \right)^{1/3} \tag{3.61}$$

Number average diameter of particles

$$\begin{aligned} D_{p,1} &= \sum_{j=1}^{\infty} d_{p,j} \cdot \left(N_{p,1} \cdot \sum_{i=1}^{j} w_{i,j} \right) = N_p \cdot \overline{n} \sum_{j=1}^{\infty} \sum_{i=1}^{j} w_{i,j} \cdot d_{p,j} \\ D_{p,0} &= \sum_{j=1}^{\infty} d_{p,j} N_{p,0} \cdot \sigma_j = N_p \cdot (1-\overline{n}) \cdot \sum_{j=1}^{\infty} \sigma_j \cdot d_{p,j} \\ D_p &= \sum_{j=1}^{\infty} d_p \cdot N_j = \sum_{j=1}^{\infty} d_{p,j} \cdot \left(N_{p,1} \cdot \sum_{i=1}^{j} w_{i,j} + N_{p,0} \cdot \sigma_j \right) = (6\alpha)^{1/3} \cdot \overline{n} \sum_{j=1}^{\infty} \sum_{i=1}^{j} w_{i,j} \cdot j^{1/3} \\ &= N_p \cdot \left[\overline{n} \sum_{j=1}^{\infty} \sum_{i=1}^{j} w_{i,j} \cdot d_{p,j} + (1-\overline{n}) \cdot \sum_{j=1}^{\infty} \sigma_j \cdot d_{p,j} \right] \\ \overline{d}_{p,n,1} &= \frac{D_{p,1}}{N_{p,1}} = \sum_{j=1}^{\infty} \sum_{i=1}^{j} w_{i,j} \cdot d_{p,j} = (6\alpha)^{1/3} \cdot \overline{n} \sum_{j=1}^{\infty} \sum_{i=1}^{j} w_{i,j} \cdot j^{1/3} \\ \overline{d}_{p,n,0} &= \frac{D_{p,0}}{N_{p,0}} = \sum_{j=1}^{\infty} \sigma_j \cdot d_{p,j} = (6\alpha)^{1/3} \cdot (1-\overline{n}) \cdot \sum_{j=1}^{\infty} \sigma_j \cdot j^{1/3} \\ \overline{d}_{p,n} &= \frac{D_p}{N_p} = \overline{n} \sum_{j=1}^{\infty} \sum_{i=1}^{j} w_{i,j} \cdot d_{p,j} + (1-\overline{n}) \cdot \sum_{j=1}^{\infty} \sigma_j \cdot d_{p,j} \\ &= (6\alpha)^{1/3} \cdot \left[\overline{n} \sum_{j=1}^{\infty} \sum_{i=1}^{j} w_{i,j} \cdot j^{1/3} + (1-\overline{n}) \cdot \sum_{j=1}^{\infty} \sigma_j \cdot j^{1/3} \right] \end{aligned} \tag{3.62}$$

Bibliography

S. Massebeuf, editor. *Optimisation Multicritere de Procedes Discontinus d'Homopolymerisation et de Copolymerisation en Emulsion.* Ph.D. thesis, l'Institut National Polytechnique de Lorraine, 1997.

A. D. Randolph and M. A. Larsen, editors. *Theory of Particulate Processes.* Academic, San Diego, 1998.

A. Sood and S. K. Awasthi. Population balance model for miniemulsion polymerization.1. Model development. *Macromol. Theory Simul.*, 13:603–614, 2004.

Chapter 4

Modelling of Mini-emulsion Polymerization

In macro-emulsion polymerization, micellar and homogenous nucleation dominate. This is because the large sizes of the monomer droplets, which are considered as the reservoir of the monomer, and their consequent low interfacial area, make them ineffective in competing for water-born free radicals. Droplet nucleation undoubtedly takes place in macro-emulsion polymerization, but it is generally considered to be insignificant. In a properly formulated mini-emulsion, all micelles will be sacrificed to support the droplet interfacial area. Therefore, not only do the small droplets compete effectively for micelles, their presence causes the destruction of the micelles, leaving droplet nucleation as the dominant particle nucleation process. To construct a model, the most important difference between macro- and mini- emulsion polymerization refers to the method used to determine the number of the nuclei places. In macro-emulsion polymerization, when the materials and the composition are selected, the size of micelles, swollen micelles and droplets are determined, and based on the balance of surfactants and monomers, the number of micelles and droplets can be calculated [Edouard et al., 2005]. However, in mini-emulsion polymerization, the droplet size distribution is affected by both the ratio between monomers and surfactant/co-stabilizer and physical and/or mechanical effects, high shear, sonicator or a mechanical homogenizer, etc. so the formation of droplets during the mini-emulsification stage is not modelled. By now, an initial droplet size distribution, defining the distribution in terms of analytical functions seems to be a convenient recourse [Sood and Awasthi, 2003]. In the present work, a model on mini-emulsion polymerization has been established which allows us to predict the particle size distribution and the change of the droplets sizes based on the balance of chemical potentials of the monomer in the reactor.

4.1 Notation

4.1.1 Nomenclature

A surface area, m^3
a_s surface area of particles covered by 1g surfactant molecule
D sum of the component diameter, m
d diameter of one unit component, m

$\bar{d}$	average diameter, m
d_m	mean size variable
Δd	gap between adjacent droplets
f	radical efficiency
F	fraction of the droplets with diameter d
I	initiator
$[I]$	concentration of initior in aqueous phase, kmol/m^3
$[I]_{ini}$	initial concentration of initior in aqueous phase, kmol/m^3
j_{crit}	minimum monomeric units
k	rate coefficient
m	mass
m_{mc}	ratio of the equivalent number of the molecular segment
M	monomer
MW_m	monomer molecular weight, $0.104\,10^3$kg /kmol
$M^\bullet$	monomeric radical in the particles
$[M]_{p,i,j}$	concentration of monomer in particles containing j units polymers formed from class i, kmol/m^3
$[M]^{aq}_{sat}$	saturation concentration of monomer in the aqueous phase, kmol/m^3
$\overline{[M]}_{p,1}$	average concentration of monomer in particles having 1 radical, kmol/m^3
N	number of component per volume unit of water
N_a	Avogadro's number
$\overline{n}$	average number of radicals per particle
P	probability density function
R	volume ratio between polymers and co-stabilizers in the particle
P_j	Polymer chain with j monomeric units
$R^\bullet_0$	initial radical in the particles
$R^\bullet_j$	radical with j monomeric units in the particles
$R^\bullet_w$	radical in the aqueous phase
$[R]_w$	concentration of monomer in aqueous phase, kmol/m^3
$\mathcal{R}$	reactive rate
S	concentration of surfactant, kmol/m^3
S_e	limited concentration of the surfactant for nucleation, kg/m^3
V	total volume, m^3
v	volume of one unit component, m^3
$\bar{v}$	average volume, m^3
$w_{i,j}$	percentage in moles of particles with 1 radical from ith class droplet (based on the volume of co-stabilizer), in jth element (total monomeric units of the polymers in the particle)
α	$4\gamma V_m/RT$
ρ_m	monomer density, $8.78\,10^2$kg/m^3
μ	chemical potential
σ	standard deviation
$\sigma_{i,j}$	percentage in moles of particles with 0 radical from ith class droplet (based on the volume of co-stabilizer), in jth element (total monomeric units of the polymers in the particle)
ϕ	volume fraction
χ	Flory-Huggin's interaction parameter

Subscripts

c	co-stabilizer
cm	nucleation
cmd	droplet nucleation
cmh	homogeneous nucleation
cp	capture of radicals in the aqueous phase by particles
d	droplet
dc	decomposition
ini	initial
m	monomer
$m \rightarrow p$	monomers transfered to particles
n	based on number
p	particle
pr	propagation
trM	Chain transfer to monomer
v	based on volume
w	aqueous phase
1	1 radical
0	0 radical

4.2 Initial droplet size distribution (DSD)

The droplet size distribution in mini-emulsion polymerization has not yet been measured. This distribution is determined by pre-emulsification and emulsification steps.

4.2.1 Pre-specified DSD

In the absence of knowledge of the full droplet size distribution, defining the distribution in terms of analytical functions seems to be a convenient recourse. The normal and Gaussian distribution is by far the most commonly used, and it arised when a large number of purely random factors are responsible for the distribution. In this work, the pre-specified DSD is represented by log-normal distribution, defined by a pre-specified mean and standard deviation. The probability density function, $P(d)$, of the normal distribution is expressed as:

$$P(d) = \frac{1}{\sqrt{(2\pi)\sigma}} \cdot \exp\left[-\left(\frac{d - d_m}{2\sigma^2}\right)^2\right] \tag{4.1}$$

where d is the size variable, d_m the mean, and σ the standard deviation. The fraction of the droplets between sizes d_1 and d_2 is given by $\int P(d)dd$, integrated from d_1 to d_2.

The fraction of the droplets with diameter d is

$$F(i) = \frac{P\left(d_{d,i,ini} - \frac{\Delta d}{2}\right) + P\left(d_{d,i,ini} + \frac{\Delta d}{2}\right)}{2}\Delta d \tag{4.2}$$

thus, the initial total number of droplet is

$$N_{d,tot,ini} = \frac{V_{m,ini} - [\mathrm{M}]^{aq}_{sat} \cdot V}{\frac{1}{6}\pi \cdot \sum_{i=1}^{\infty} F(i) d^3_{d,i,ini}} \tag{4.3}$$

initial number of droplet with size d

$$N_{d,i,ini} = N_{d,tot,ini} \cdot F(i) \tag{4.4}$$

4.2.2 Stability of the Droplet Size distribution

Miller found that the measured average size of the distribution, monitored over time, did not change when hexadecane (HD) was used as a co-stabilizer, whereas with cetyl alcohol (CA) as a co-stabilizer, the average size increased up to 1.5 h and leveled off after that. With an increase in the amount of CA, the rearrangement behavior was retarded, and the final average size decreased.

A theoretical analysis reconciling the aforementioned experimental observations in terms of a suitable theoretical framework was conducted by [Sood and Awasthi, 2003]. The instability may arise as a result of coalescence, which results from an insufficient barrier (e.g., electrostatic and viscoelastic) against contact or from molecular diffusion (popularly known as Ostwald ripening). Sodium dodecyl sulfate, an anionic surfactant, provides an electrostatic barrier against contact. In such cases, coalescence is normally called coagulation. The co-stabilizer, HD or CA (relatively low molecular weight, less water-soluble compounds), retards the molecular diffusion of the monomer.

Two droplets of different sizes can change their size without coming into contact, through molecular diffusion, the smaller droplet decreasing in size and larger droplet increasing in size. This can be retarded and stopped by the addition of a low molecular weight, less water-soluble component. In mini-emulsion polymerization, this role is played by the co-stablizer.

The process of molecular diffusion, in general, is governed by the difference between the chemical potential of the diffusing substance (a monomer in our case) in the two phases. The chemical potential of the monomer (μ) in a monomer droplet of diameter d, with the volume fraction of the costablizer (ϕ_c), is given as follows

$$\mu = \ln(1 - \phi_c) + (1 - m_{mc})\,\phi_c + \chi_{mc}\phi_c^2 + \frac{4\gamma V_m}{dRT} \tag{4.5}$$

where m_{mc} is the ratio of the equivalent number of the molecular segment, χ the interaction parameter, V_m the molar volume of the monomer, γ the interfacial tension, R universal gas constant, and T the temperature. This equation is based on the Flory-Huggins lattice theory of polymer solutions [Flory, 1953], the extension of [Morton et al., 1954]. involving the addition of an interfacial energy term for spherical phases, and the further extension of [Ugelstad and Hansen, 1976] for phases not involving a polymer as one of their components. The first three terms in this equation represent the partial molar free energy of mixing, with the first two terms representing the enthalpy of mixing, and are used to consider the nonideality of the system; the larger χ is, the greater the nonideality is. The fourth term represents the partial molar free energy of swelling. Defing $\alpha = 4\gamma V_m/RT$ and knowing

that $\ln(1-\phi_c) \approx -\phi_c$ for small values of ϕ_c, we can reduce the previous equation as follows:

$$\mu = -m_c\phi_c + \chi_{mc}\phi_c^2 + \alpha/d \tag{4.6}$$

From this equation (with some manipulation), it follows that the difference ($\Delta\mu$) between the chemical potentials of the two droplets of diameters d_1 and d_2 and co-stabilizer volume fractions $\phi_{c,1}$ and $\phi_{c,2}$ is given by

$$\Delta\mu = \alpha\left(1/d_1 - 1/d_2\right) - \left(\phi_{c,1} - \phi_{c,2}\right)\left[m - \chi\left(\phi_{c,1} + \phi_{c,2}\right)\right] \tag{4.7}$$

In the absence of the co-stabilizer ($\phi_{c,1} = \phi_{c,2} = 0$), only the first term in this equation, arising from the contribution to the free energy from swelling, accounts for $\Delta\mu$ of the two droplets. $\Delta\mu$, in this case, can never decrease, as the mass transfer through the molecular diffusion of the monomer from small droplets (having higher μ values) to large droplets (having lower μ values) will further increase this difference. As can be seen from the equation, this irreversible change in the droplet sizes can be retarded when a co-stabilizer is present. In its presence, the mass transfer of the monomer from the smaller droplets to the larger droplets changes their composition. As can be seen from the equation, this can result in the equalization of their chemical potentials, as the second term arising from the mixing of the two components compensates for the first term due to the swelling.

It can be realized that only the amounts of monomer in various phases change during the solution of the thermodynamic framework. The following changes in the representation of the various variables in the thermodynamic framework are made. The chemical potential of monomer in a droplet is expressed in terms of the three variables: the monomer volume fraction, the co-stabilizer volume fraction and the droplet diameter. The chemical potential of the monomer in the droplet is represented in terms of one variable, the monomer volume fraction, by realizing that the volume fractions of the components add to 1 and the volume of co-stabilizer in a droplet does not change with time (due to its insolubility) and is same as the initial volume. Thus, the equation of the chemical potential for ith class of droplet with the volume of co-stabilizer $v_{c,i}$, expressed in terms of the volume of the co-stabilizer, becomes

$$\begin{aligned}
\phi_{c,ini} &= \frac{V_{c,ini}}{V_{c,ini} + V_{m,ini}} \\
\phi_{m,ini} &= \frac{V_{m,ini}}{V_{c,ini} + V_{m,ini}} \\
v_{c,i,ini} &= \phi_{c,ini} \cdot 1/6\pi d_{d,i,ini}^3 \\
\mu_{d,i} &= \ln\left(1-\phi_{c,i}\right) + \left(1-m_{mc}\right)\phi_{c,i} + \chi_{mc}\phi_{c,i}^2 + \alpha/d_{d,i}
\end{aligned} \tag{4.8}$$

The chemical potential of the monomer in the aqueous phase is given by

$$\mu_w = \ln\phi_{m,w} + \left(1-m_{mw}\right)\left(1-\phi_{m,w}\right) + \chi_{mw}\left(1-\phi_{m,w}\right)^2 \tag{4.9}$$

where $V_{c,ini}$ and $V_{m,ini}$ are the initial amount of co-stabilizer and that of monomer in volume, and $v_{c,i,ini}$ is the volume of co-stabilizer of ith class of droplet obtained by log-normal distribution.

There are $2i+2$ variables in these $i = 1$ equations, the i $\phi_{c,i}$, i d, $\phi_{m,w}$ and μ. The volume of co-stabilizer in a droplet does not change with time (due to its insolubility, zero solubility in the aqueous phase being implied), and equal to the initial amount. Therefore

$$\phi_{c,i}d_{d,i}^3 = \phi_{c,ini}d_{d,i,ini}^3 \tag{4.10}$$

and the total amount of the monomer will also remain the same, which provides the last equation.

$$N_{d,i} = N_{d,i,ini} \tag{4.11}$$

$$\sum_{i=1}^{\infty} \frac{1}{6}\pi d_{d,i}^3 \left(1 - \phi_{c,i}\right) N_{d,i} + \phi_{m,w} \cdot V_w = V_{m,ini} \tag{4.12}$$

4.3 Droplet size distribution (DSD) and particle size distribution (PSD) during polymerization

To simplify the model, it is assumed that the monomer transport is thermodynamically governed. This may not be strictly true during the later stages of the polymerization as a result of the reduction in the transfer area between the droplets and the aqueous phase. It can be realized that only the amounts of monomer in various phases change during the solution of the thermodynamic framework. The following changes in the representation of the various variables in the thermodynamic framework are made. The chemical potential of monomer in a droplet is expressed with respect to the three following variables, the monomer volume fraction, the co-stabilizer volume fraction and the droplet diameter. The chemical potential of the monomer in the droplet is represented with respect to one variable, the monomer volume fraction.
Droplet

$$\begin{aligned} \phi_{c,d,i} &= \frac{v_{c,i,ini}}{\pi/6 d_{d,i}^3} \\ \mu_{d,i} &= \ln\left(1 - \phi_{c,d,i}\right) + \left(1 - m_{mc}\right)\phi_{c,d,i} + \chi_{mc}\phi_{c,d,i}^2 + \alpha/d_{d,i} \end{aligned} \tag{4.13}$$

Aqueous phase

$$\mu_w = \ln \phi_{m,w} + \left(1 - m_{mw}\right)\left(1 - \phi_{m,w}\right) + \chi_{mw}\left(1 - \phi_{m,w}\right)^2 \tag{4.14}$$

The chemical potential of monomer in a particle is expressed with respect to four variables, the volume fractions of the three components and the diameter of the particle. It can be expressed with respect to two variables, the volume fraction of monomer in the particle and the ratio of the volume of the polymer in the particle to that of the co-stabilizer. The amount of co-stabilizer in the particle is considered to be the same as the amount of co-stabilizer in the droplet from which that particle was nucleated. The chemical potential of monomer in a particle results:
Particle

$$\begin{aligned} \phi_{c,p,i,j} &= \frac{v_{c,i,ini}}{\pi/6 d_{p,i,j}^3} \\ R_{i,j} &= \frac{\phi_{p,p,i,j}}{\phi_{c,p,i,j}} = \frac{m_{p,i,j}/\rho_p}{v_{c,i,ini}} \Rightarrow \phi_{p,p,i,j} = \phi_{c,p,i,j} \cdot R_{i,j} \\ m_{p,i,j} &= MW_{mu} \cdot j \\ \mu_{p,i,j} &= \ln\left(1 - \phi_{c,p,i,j} - R_{i,j}\phi_{c,p,i,j}\right) + \left(1 - m_{mc}\right)\phi_{c,p,i,j} + \left(1 - m_{mp}\right)\phi_{c,p,i,j}R_{i,j} \\ &\quad + \chi_{mc}\phi_{c,p,i,j}^2 + \chi_{mp}\left(R_{i,j}\phi_{c,p,i,j}\right)^2 + \phi_{c,p,i,j}^2 R_{i,j}\left(\chi_{mc} + \chi_{mp} - \chi_{mp}m_{mc}\right) + \alpha/d_{p,i,j} \end{aligned} \tag{4.15}$$

Thus, each phase is represented by one variable, the volume fraction of monomer in that phase, so that, for a system consisting of n phases, there will be n variables. In order

to define this system completely, we need n equations. The equality of chemical potentials of monomer in all the phases provide $n-1$ equations. The last equation is provided by the mass balance of monomer: the initial mass of monomer is equal to the sum of mass of monomer in the droplets, aqueous phase and the particles and that converted to polymer.

$$\begin{aligned} m_{m,ini} = \quad & m_{m,d} + m_{m,p} + m_{m,w} + m_{m\to p,p} \\ & \sum_{i=1}^{\infty} \pi/6 d_{d,i}^3 \left(1-\phi_{c,d,i}\right) N_{d,i}\rho_m + \sum_{i=1}^{\infty}\sum_{j=1}^{\infty} \pi/6 d_{p,i,j}^3 \left(1-\phi_{c,p,i,j} - R_{i,j}\phi_{c,p,i,j}\right) N_{p,i,j}\rho_m \\ & +\phi_{m,w}\cdot V_w + \sum_{i=1}^{\infty}\sum_{j=1}^{\infty} j \cdot MW_m N_{p,i,j} \\ N_{d,i} = \quad & N_{d,i,ini} - \sum_{j=1}^{\infty} N_{p,i,j} \\ N_{p,i,j} = \quad & N_{p,i,j,1} + N_{p,i,j,0} = N_{p,1}\cdot w_{i,j} + N_{p,0}\cdot \sigma_{i,j} \end{aligned} \tag{4.16}$$

where N_d and N_p are the number in moles of droplets and that of particles.

4.4 Modelling

4.4.1 Kinetic mechanism

A simple free radical kinetic mechanism is presented in this part.

Reactions in the aqueous phase

As in macro-emulsion polymerization, the polymerization process in mini-emulsion polymerization starts by the initiator decomposition:

- Initiation:

$$\mathrm{I} \xrightarrow{f,k_{dc}} 2\mathrm{R}_w^{\bullet} \tag{4.17}$$

- Nucleation: The most important difference between macro- and mini- emulsion polymerization refers to the nuclei place. In mini-emulsion polymerization, instead of micelle nucleation, droplets are the main place to nucleate in.

  droplet nucleation

$$\mathrm{R}_w^{\bullet} \xrightarrow{k_{cmd}} \mathrm{R}_1^{\bullet} \tag{4.18}$$

  homogeneous nucleation

$$\mathrm{R}_w^{\bullet} \xrightarrow{k_{cmh}} \mathrm{R}_1^{\bullet} \tag{4.19}$$

Reactions in the particles

The reactions in the particles in mini-emulsion polymerization are almost the same as in macro-emulsion polymerization, excetp that the concentration of monomer in the particles is different depending on the size of the droplet and the quantity of the co-stabilizer in it.

- Propagation:

$$\begin{cases} \mathrm{R}_1^\bullet + \mathrm{M} & \xrightarrow{k_{pr}} \mathrm{R}_2^\bullet \\ \mathrm{R}_j^\bullet + \mathrm{M} & \xrightarrow{k_{pr}} \mathrm{R}_{j+1}^\bullet \end{cases} \tag{4.20}$$

- Chain transfer to monomer:

$$\mathrm{R}_j^\bullet + \mathrm{M} \xrightarrow{k_{trM}} \mathrm{P}_j + \mathrm{M}^\bullet\,(\mathrm{R}_1^\bullet) \tag{4.21}$$

- Capture of radicals in the aqueous phase by particles:

$$\mathrm{R}_w^\bullet \xrightarrow{k_{cp}} \mathrm{R}_1^\bullet \tag{4.22}$$

- Instantaneous termination:

$$\mathrm{R}_j^\bullet + \mathrm{R}_1^\bullet \xrightarrow{k_{pr}} \mathrm{P}_{i+1} \tag{4.23}$$

  We consider that $\mathrm{R}_1^\bullet$ and $\mathrm{M}^\bullet$, both of which have one polymerization degree, have the same molecular weight in the calculation, so that there is no chain transfer for $\mathrm{R}_1^\bullet$.

4.4.2 Kinetic reaction rate

Initiator decomposition

$$\mathcal{R}_{dc} = k_{dc}[\mathrm{I}] \tag{4.24}$$

Nucleation

- droplet nucleation

$$\mathcal{R}_{cmd} = k_{cm} \cdot S_d \cdot [\mathrm{R}^\bullet]_w \tag{4.25}$$

with

$$\begin{aligned} S_0 &= S_p + S_w + S_d \\ S_{d,i} &= \frac{A_{d,i}}{a_s} \\ S_d &= \frac{A_d}{a_s} \\ A_{d,i} &= N_{d,i}\pi d_{d,i}^2 \\ A_d &= \int_0^\infty \pi N_d(d) d^2 dd = \sum_{i=1}^{\infty} N_{d,i} d_{d,i}^2 \end{aligned} \tag{4.26}$$

- homogeneous nucleation

$$\mathcal{R}_{cmh} = k_{cm} \cdot (S_w - S_e) \cdot [\mathrm{R}^\bullet]_w \tag{4.27}$$

Thus

$$\mathcal{R}_{cm} = \mathcal{R}_{cmd} + \mathcal{R}_{cmh} = k_{cm} \cdot [S_d + (S_w - S_e)] \cdot [\mathrm{R}^\bullet]_w \tag{4.28}$$

Capture

$$\begin{aligned}\mathcal{R}_{cp,1} &= k_{cp}\overline{d}_{p,n,1}\cdot\frac{N_{p,1}\cdot[\mathrm{R}^{\bullet}]_w}{N_a}\\ \mathcal{R}_{cp,0} &= k_{cp}\overline{d}_{p,n,0}\cdot\frac{N_{p,0}\cdot[\mathrm{R}^{\bullet}]_w}{N_a}\\ \mathcal{R}_{cp} &= k_{cp}\cdot\frac{\overline{d}_{p,n}\cdot(N_{p,1}+N_{p,0})\cdot[\mathrm{R}^{\bullet}]_w}{N_a}\end{aligned} \tag{4.29}$$

Transfer to monomer (in particles)

$$\mathcal{R}_{trM} = k_{trM}\overline{[\mathrm{M}]}_{p,1}\cdot\frac{N_{p,1}}{N_a} \tag{4.30}$$

Propagation in particles

$$\mathcal{R}_{pr} = k_{pr}\overline{[\mathrm{M}]}_{p,1}\cdot\frac{N_{p,1}}{N_a} \tag{4.31}$$

4.4.3 Concept and kinetics of $w_{i,j}$ and $\sigma_{i,j}$

Comparing with macro-emulsion polymerization, the composition in mini-emulsion polymerization is much more complex because of the existence of co-stabilizer, which is insoluble in the aqueous phase. In mini-emulsion polymerization, the droplet sizes have a distribution, which is considered to be constant in macro-emulsion polymerization, and the concentrations of monomer in the particles are different depending on the size of the droplet and the quantity of the co-stabilizer in it. Due to these complex phenomena, in this study, to simplify, we just established a model which can just predict the total droplet size distribution, compared with the model of macro-emulsion polymerization, which can predict the radical chain size distribution of polymers for a given class of particle sizes.

The volume of a particle is composed of three parts: the volume of monomer in the particle, the volume of the polymer in the particle and that of the co-stabilizer. The amount of polymer in a particle is obtained by following the change of the mass of polymer formed in the particle due to polymerization. The volume of monomer in the particle is followed by the balance of the chemical potential of monomer in various phases. The amount of co-stabilizer in the particle is considered to be the same as the amount of co-stabilizer in the droplet from which that particle is nucleated. Thus, the amount of the co-stabilizer in the particles is unchanged during the polymerization process. We define:

• $w_{i,j}$ as the percentage of moles of particles with 1 radical from ith class droplet (based on the volume of co-stabilizer), in jth element (total monomeric units of the polymers in the particle)

• $\sigma_{i,j}$ as the percentage of moles of particles with 0 radical from ith class droplet (based on the volume of co-stabilizer), in jth element (total monomeric units of the polymers in the particle)

$$\begin{aligned}
&\sum_{j=1}^{\infty}\sum_{i=1}^{\infty} w_{i,j} = 1 \\
&\sigma_{i,1} = 0 \\
&\sum_{j=1}^{\infty}\sum_{i=1}^{\infty} \sigma_{i,j} = 1 \\
&N_p = N_{p,1} + N_{p,0} \\
&\overline{n} = \frac{N_{p,1}}{N_p}
\end{aligned} \tag{4.32}$$

Nucleation

for styrene

$$j_{crit} = 1 \tag{4.33}$$

when $i = 1$

$$\begin{aligned}
\mathcal{R}_{cmd} &= 0 \\
\mathcal{R}_{cm} &= \mathcal{R}_{cmh}
\end{aligned} \tag{4.34}$$

if $s_w \leq s_e$, $\mathcal{R}_{cmh} = 0$

$$\mathcal{R}_{cm,1} = \mathcal{R}_{cmd} = 0 \tag{4.35}$$

if $s_w \geq s_e$

$$\mathcal{R}_{cm,1} = \mathcal{R}_{cmh} = k_{cm} \cdot (S_w - S_e) \cdot [\mathrm{R}^{\bullet}]_w \tag{4.36}$$

when $i > 1$

$$\mathcal{R}_{cm,i} = \mathcal{R}_{cmd,i} = k_{cm} \cdot S_{d_i} \cdot [\mathrm{R}^{\bullet}]_w \tag{4.37}$$

Propagation in particles

$$\mathcal{R}_{pr,i,j} = k_{pr}[\mathrm{M}]_{p,i,j} \cdot \frac{N_{p,1}}{N_a} \cdot w_{i,j} = \mathcal{R}_{pr} \cdot w_{i,j} \frac{[\mathrm{M}]_{p,i,j}}{\overline{[\mathrm{M}]}_{p,1}} \tag{4.38}$$

Transfer to monomer

$$\mathcal{R}_{trM,i,j} = k_{trM}[\mathrm{M}]_{p,i,j} \cdot \frac{N_{p,1}}{N_a} \cdot w_{i,j} = R_{trM} \cdot w_{i,j} \frac{[\mathrm{M}]_{p,i,j}}{\overline{[\mathrm{M}]}_{p,1}} \tag{4.39}$$

Capture of radical

$$\begin{aligned}
\mathcal{R}_{cp,i,j,1} &= k_{cp} d_{p,i,j} \cdot \frac{N_{p,1}[R^{\bullet}]_w}{N_a} \cdot w_{i,j} = \mathcal{R}_{cp} \cdot \frac{d_{p,i,j}}{\overline{d}_{p,n}} \cdot \overline{n} \cdot w_{i,j} \\
\mathcal{R}_{cp,i,j,0} &= k_{cp} d_{p,i,j} \cdot \frac{N_{p,0}[R^{\bullet}]_w}{N_a} \cdot \sigma_{i,j} = \mathcal{R}_{cp} \cdot \frac{d_{p,i,j}}{\overline{d}_{p,n}} \cdot (1 - \overline{n}) \cdot \sigma_{i,j}
\end{aligned} \tag{4.40}$$

4.4.4 Population balance equation

The population balance equation

$$\text{Accumulation} = \text{Evolution} + \text{Birth} - \text{Death}$$

gives the following differential equation:

in the aqueous phase

$$\begin{aligned} \frac{d[\mathrm{I}]}{dt} &= -k_{dc}[\mathrm{I}] \\ \frac{d[\mathrm{R}^{\bullet}]_w}{dt} &= 2k_{dc}f[\mathrm{I}] - \mathcal{R}_{cm} - \mathcal{R}_{cp} \end{aligned} \tag{4.41}$$

Number of particles

- particles having 1 radical

  for $j = j_{crit} = 1$

$$\begin{aligned} \frac{dN_{p,1}w_{1,j}}{dt} &= \mathcal{R}_{cm,j} - \mathcal{R}_{pr,1,j} - \mathcal{R}_{cp,1,j,1} \\ &= \mathcal{R}_{cmh} - \mathcal{R}_{pr} \cdot w_{1,j} \frac{[\mathrm{M}]_{p,1,j}}{\overline{[\mathrm{M}]}_{p,1}} - \mathcal{R}_{cp} \cdot \frac{d_{p,1,j}}{\overline{d}_{p,n}} \cdot \overline{n} \cdot w_{1,j} \\ \frac{dN_{p,1}w_{i,j}}{dt} &= \mathcal{R}_{cm,i} - \mathcal{R}_{prr,i,j} - \mathcal{R}_{cp,i,j,1} \\ &= \mathcal{R}_{cmd,i} - \mathcal{R}_{pr} \cdot w_{i,j} \frac{[\mathrm{M}]_{p,i,j}}{\overline{[\mathrm{M}]}_{p,j}} - \mathcal{R}_{cp} \cdot \frac{d_{p,i,j}}{\overline{d}_{p,n}} \cdot \overline{n} \cdot w_{i,j} \end{aligned} \tag{4.42}$$

  for $j = j_{crit} + 1$

$$\begin{aligned} \frac{dN_{p,1}w_{i,j}}{dt} &= \mathcal{R}_{pr,i,j-1} - \mathcal{R}_{pr,i,j} - \mathcal{R}_{cp,i,j,1} - \mathcal{R}_{trM,i,j} \\ &= \mathcal{R}_{pr} \cdot w_{i,j-1} \frac{[\mathrm{M}]_{p,i,j-1}}{\overline{[\mathrm{M}]}_{p,1}} - \mathcal{R}_{pr} \cdot w_{i,j} \frac{[\mathrm{M}]_{p,i,j}}{\overline{[\mathrm{M}]}_{p,1}} - \mathcal{R}_{cp} \cdot \frac{d_{p,i,j}}{\overline{d}_{p,n}} \cdot \overline{n} \cdot w_{i,j} \\ &-\mathcal{R}_{trM} \cdot w_{i,j} \frac{[\mathrm{M}]_{p,i,j}}{\overline{[\mathrm{M}]}_{p,1}}, (i \in [1,n]) \end{aligned} \tag{4.43}$$

  for $j > j_{crit} + 1$

$$\begin{aligned} \frac{dN_{p,1}w_{i,j}}{dt} &= \mathcal{R}_{prr,i,j-1} + \mathcal{R}_{trM,i,j-1} - \mathcal{R}_{prr,i,j} + \mathcal{R}_{cp,i,j-1,0} - \mathcal{R}_{cp,i,j,1} - \mathcal{R}_{trM,i,j} \\ &= \mathcal{R}_{pr} \cdot w_{i,j-1} \frac{[\mathrm{M}]_{p,i,j-1}}{\overline{[\mathrm{M}]}_{p,1}} + \mathcal{R}_{trM} \cdot w_{i,j} \frac{[\mathrm{M}]_{p,i,j-1}}{\overline{[\mathrm{M}]}_{p,1}} - \mathcal{R}_{pr} \cdot w_{i,j} \frac{[\mathrm{M}]_{p,i,j}}{\overline{[\mathrm{M}]}_{p,1}} \\ &+\mathcal{R}_{cp} \cdot \frac{d_{p,i,j-1}}{\overline{d}_{p,n}} \cdot (1 - \overline{n}) \cdot \sigma_{i,j-1} - \mathcal{R}_{cp} \cdot \frac{d_{p,i,j}}{\overline{d}_{p,n}} \cdot \overline{n} \cdot w_{i,j} \\ &-\mathcal{R}_{trM} \cdot w_{i,j} \frac{[\mathrm{M}]_{p,i,j}}{\overline{[\mathrm{M}]}_{p,1}}, (i \in [1,n]) \end{aligned} \tag{4.44}$$

- particles having 0 radical

  for $j = j_{crit}$

$$\sigma_{i,j} = 0 \tag{4.45}$$

for $j > j_{crit}$

$$\begin{aligned} \frac{dN_{p,0}\sigma_{i,j}}{dt} &= \mathcal{R}_{cp,i,j-1,1} - \mathcal{R}_{cp,i,j,0} \\ &= \mathcal{R}_{cp} \cdot \frac{d_{p,i,j-1}}{\overline{d}_{p,n}} \cdot \overline{n} \cdot w_{i,j-1} - \mathcal{R}_{cp} \cdot \frac{d_{p,i,j}}{\overline{d}_{p,n}} \cdot (1-\overline{n}) \cdot \sigma_{i,j} \end{aligned} \tag{4.46}$$

4.4.5 Initial condition

At $t = 0$

$$\begin{aligned} [\mathrm{I}] &= [\mathrm{I}]_{ini} \\ [\mathrm{R}^{\bullet}]_w &= 0 \\ N_{p,1} &= 0 \\ N_{p,0} &= 0 \\ w_{1,1} &= 1 \\ w_{i,j} &= 0, \forall (i,j) \neq (1,1) \\ \sigma_{1,2} &= 1 \\ \sigma_{i,j} &= 0, \forall (i,j) \neq (1,2_) \end{aligned} \tag{4.47}$$

4.4.6 Total number of particles (N_p), number of particles containing a growing chain ($N_{p,1}$) and number of particles containing no growing chain ($N_{p,0}$)

Number of particles containing a growing chain $N_{p,1}$ (Sum on $w_{i,j}$)

When we make an integration of $w_{i,j}$ on i and j. The number of particles containing a growing chain($N_{p,1}$) can be obtained.

- sum on i

  for $j = j_{crt} = 1$

$$\begin{aligned} \sum_{i=1}^{\infty} \frac{dN_{p,1}w_{i,1}}{dt} &= \frac{d}{dt}\sum_{i=1}^{\infty} N_{p,1}w_{i,1} = \frac{d}{dt}\left(\sum_{i=1}^{\infty}\mathcal{R}_{cm,i} - \sum_{i=1}^{\infty}\mathcal{R}_{pr,i,1} - \sum_{i=1}^{\infty}\mathcal{R}_{cp,i,1,1}\right) \\ &= \mathcal{R}_{cm} - \frac{\mathcal{R}_{pr}}{[\mathrm{M}]_{p,1}}\sum_{i=1}^{\infty}(w_{i,1}[\mathrm{M}]_{p,i,1}) - \mathcal{R}_{cp} \cdot \frac{\overline{n}}{\overline{d}_{p,n}} \cdot \sum_{i=1}^{n}(d_{p,i,1} \cdot w_{i,1}) \end{aligned} \tag{4.48}$$

for $j = j_{crt} + 1 = 2$

$$\begin{aligned}
\sum_{i=1}^{\infty} \frac{dN_{p,1}w_{i,2}}{dt} &= \frac{d}{dt}\sum_{i=1}^{\infty} N_{p,1}w_{i,2} \\
&= \frac{d}{dt}\left(\sum_{i=1}^{\infty}\mathcal{R}_{pr,i,1}\sum_{i=1}^{\infty}\mathcal{R}_{pr,i,2} - \sum_{i=1}^{\infty}\mathcal{R}_{cp,i,2,1} - \sum_{i=1}^{\infty}\mathcal{R}_{trM,i,2}\right) \\
&= \frac{\mathcal{R}_{pr}}{\overline{[\mathrm{M}]}_{p,1}}\cdot\sum_{i=1}^{\infty} w_{i,1}[\mathrm{M}]_{p,i,1} - \frac{\mathcal{R}_{pr}}{\overline{[\mathrm{M}]}_{p,1}}\cdot\sum_{i=1}^{\infty} w_{i,2}[\mathrm{M}]_{p,i,2} \\
&\quad -\frac{\mathcal{R}_{cp}\cdot\overline{n}}{\overline{d}_{p,n}}\sum_{i=1}^{\infty}\cdot d_{p,i,2}\cdot w_{i,2} - \frac{\mathcal{R}_{trM}}{\overline{[\mathrm{M}]}_{p,1}}\cdot\sum_{i=1}^{\infty} w_{i,2}[\mathrm{M}]_{p,i,2}
\end{aligned} \tag{4.49}$$

for $j > j_{crt} + 1$

$$\begin{aligned}
\sum_{i=1}^{\infty} \frac{dN_{p,1}w_{i,j}}{dt} &= \frac{d}{dt}\sum_{i=1}^{\infty} N_{p,1}w_{i,j} \\
&= \frac{d}{dt}\left(\sum_{i=1}^{\infty}\mathcal{R}_{pr,i,j-1} + \sum_{i=1}^{\infty}\mathcal{R}_{trM,i,j-1} - \sum_{i=1}^{\infty}\mathcal{R}_{pr,i,j} + \sum_{i=1}^{\infty}\mathcal{R}_{cp,i,j-1,0} - \right. \\
&\quad \left. \sum_{i=1}^{\infty}\mathcal{R}_{cp,i,j,1} - \sum_{i=1}^{\infty}\mathcal{R}_{trM,i,j}\right) \\
&= \frac{\mathcal{R}_{pr}}{\overline{[\mathrm{M}]}_{p,1}}\Big(\sum_{i=1}^{\infty}(w_{i,j-1}[\mathrm{M}]_{p,i,j-1}) - \sum_{i=1}^{\infty}(w_{i,j}[\mathrm{M}]_{p,i,j})\Big) \\
&\quad +\frac{\mathcal{R}_{cp}}{\overline{d}_{p,n}}\sum_{i=1}^{\infty}(d_{p,i,j-1}\cdot\sigma_{i,j-1}(1-\bar{n}) - d_{p,i,j}\cdot w_{i,j}\bar{n}) \\
&\quad +\frac{\mathcal{R}_{trM}}{\overline{[\mathrm{M}]}_{p,1}}\Big(\sum_{i=1}^{\infty}(w_{i,j-1}[\mathrm{M}]_{p,i,j-1}) - \sum_{i=1}^{\infty}(w_{i,j}[\mathrm{M}]_{p,i,j})\Big)
\end{aligned} \tag{4.50}$$

- sum on j

$$\begin{aligned}
\sum_{j=1}^{\infty} \frac{dN_{p,1}w_{i,j}}{dt} &= \frac{dN_{p,1}w_{i,1}}{dt} + \frac{dN_{p,1}w_{i,2}}{dt} + \cdots + \frac{dN_{p,1}w_{1,j-1}}{dt} + \frac{dN_{p,1}w_{1,j}}{dt} \\
&= \mathcal{R}_{cm,i} - \mathcal{R}_{p,i,1} - \mathcal{R}_{cp,i,1} + \mathcal{R}_{p,i,1} - \mathcal{R}_{i,2} - \mathcal{R}_{cp,i,2,1} - \mathcal{R}_{trM,i,2} + \cdots \\
&\quad +\mathcal{R}_{pr,i,j-2} + \mathcal{R}_{trM,i,j-2} - \mathcal{R}_{pr,i,j-1} + \mathcal{R}_{cp,i,j-2,0} - \mathcal{R}_{cp,i,j-1,1} - \mathcal{R}_{trM,i,j-1} \\
&\quad +\mathcal{R}_{pr,i,j-1} + \mathcal{R}_{trM,i,j-1} - \mathcal{R}_{pr,i,j} + \mathcal{R}_{cp,i,j-1,0} - \mathcal{R}_{cp,i,j,1} - \mathcal{R}_{trM,i,j} \\
&= \mathcal{R}_{cm,i} - \sum_{j=1}^{\infty}\mathcal{R}_{cp,i,j,1} + \sum_{j=2}^{\infty}\mathcal{R}_{cp,i,j,0} \\
&= \mathcal{R}_{cm,i} + \frac{\mathcal{R}_{cp}}{\overline{d}_{p,n}}\sum_{j=1}^{\infty}(d_{p,i,j}\cdot\sigma_{i,j}(1-\bar{n}) - d_{p,i,j}\cdot w_{i,j}\bar{n})
\end{aligned} \tag{4.51}$$

- sum on i and j

$$\sum_{i=1}^{\infty}\frac{d}{dt}\sum_{j=1}^{\infty}N_{p,1}w_{i,j} = \sum_{i=1}^{\infty}\mathcal{R}_{cm,i}-\sum_{i=1}^{\infty}\sum_{j=1}^{\infty}\mathcal{R}_{cp,i,j,1}+\sum_{i=1}^{\infty}\sum_{j=2}^{\infty}\mathcal{R}_{cp,i,j,0} \tag{4.52}$$

$$\Rightarrow \frac{dN_{p,1}}{dt} = \mathcal{R}_{cm}-\mathcal{R}_{cp,1}+\mathcal{R}_{cp,0} \tag{4.53}$$

which means that the number of particles containing a growing chain is added by nucleation and capture of radicals in the aqueous phase by particles containing no growing chain, but reduced by capture of radicals in the aqueous phase by particles containing a growing chain.

Number of particles containing no growing chain, $N_{p,0}$ (Sum on $\sigma_{i,j}$)

- sum on i

$$\begin{aligned}\sum_{i=1}^{\infty}\frac{dN_{p,0}\sigma_{i,j}}{dt} &= \sum_{i=1}^{\infty}\mathcal{R}_{cp,i,j-1,1}-\sum_{i=1}^{\infty}\mathcal{R}_{cp,i,j,0}\\ &= \frac{\mathcal{R}_{cp}}{\overline{d}_{p,n}}\sum_{i=1}^{\infty}\left(d_{p,i,j-1}\cdot w_{i,j-1}\bar{n}-d_{p,i,j}\cdot\sigma_{i,j}(1-\bar{n})\right)\end{aligned} \tag{4.54}$$

- sum on j

$$\begin{aligned}\sum_{j=2}^{\infty}\frac{dN_{p,0}\sigma_{i,j}}{dt} &= \sum_{j=2}^{\infty}\mathcal{R}_{cp,i,j-1,1}-\sum_{j=2}^{\infty}\mathcal{R}_{cp,i,j,0}\\ &= \frac{\mathcal{R}_{cp}}{\overline{d}_{p,n}}\sum_{j=2}^{\infty}\left(d_{p,i,j-1}\cdot w_{i,j-1}\bar{n}-d_{p,i,j}\cdot\sigma_{i,j}(1-\bar{n})\right)\end{aligned} \tag{4.55}$$

- sum on i and j

$$\sum_{i=1}^{\infty}\frac{d}{dt}\sum_{j=2}^{\infty}N_{p,0}\sigma_{i,j} = \mathcal{R}_{cp,1}-\mathcal{R}_{cp,0} \tag{4.56}$$

which means that the number of particles containing a growing chain is added by capture of radicals in the aqueous phase by particles containing a growing chain, but reduced by capture of radicals in the aqueous phase by particles containing no growing chain.

Total number of particles N_p

$$\begin{aligned}N_p &= N_{p,0}+N_{p,1} = (\mathcal{R}_{cm}-\mathcal{R}_{cp,1}+\mathcal{R}_{cp,0})+(\mathcal{R}_{cp,1}-\mathcal{R}_{cp,0})\\ &= \mathcal{R}_{cm}\end{aligned} \tag{4.57}$$

which means that the total number of particles just depends on the rate of nucleation.

4.5 Results and Discussion

In this work, the polymerization system consists of styrene (monomer), water, sodium dodecyl sulfate (surfactant), hexadecanol (co-stabilizer), potassium persulfate (initiator) and sodium bicarbonate (buffer). The means of creating the droplet size distribution is a microfluidizer. The reactions are conducted in a dilatometer at a constant temperature of 70°C.

Also, the desorption of radicals in the particles into the aqueous phase is not involved in the model established now.

4.5.1 No transport of mononer between particles or between droplets

At the beginning, we supposed that the mononers were restrained by co-stabilizer, and could not be transported in various phases, the log-normal distribution was used to determine the initial droplet size distribution. During the polymerization, the concentration of monomers in the particles was determined by the initial droplet size and the particle size. Figure 4.1 shows the initial droplet size distribution defined by a mean diameter of 100nm and by a standard deviation of 20nm. and Figure 4.2 illustrates the variation of PSDs with time. The particle size distribution deviates from the log-normal distribution with a small tail at the left, and the distribution becomes broader than that of droplet size distribution. Before 1000 sec, with the reactive time increased, the average particle size becomes larger and larger, and after 1000 sec, the change is little.

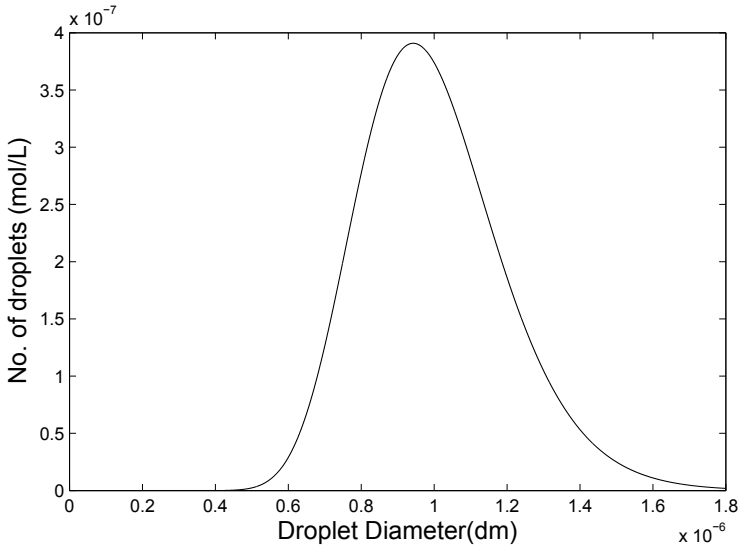

Figure 4.1: Initial droplet size distribution predicted by log-normal distribution

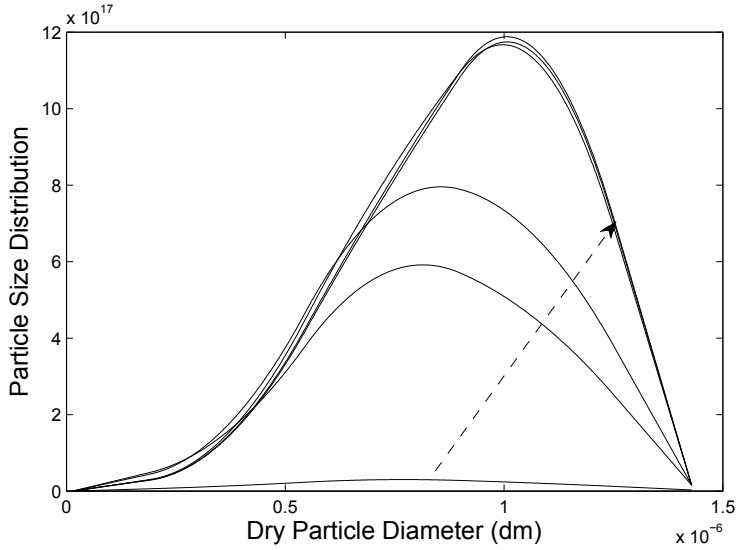

Figure 4.2: Particle size distribution (time increasing with the direction of the arrow, t = 1sec, 50sec, 100sec, 500sec, 1000sec and 1500sec)

Figure 4.3 represents the evolution of the total number of particles with time. The radical entry into droplets is slower than that into particles by several orders of magnitude ([Sood and Awasthi, 2004]), so that in a short time, the number of particles is large enough to prevent the radical entry into droplets, and the number of the particles is nearly constant. In this model, the maximum particle size that we defined is 150 nm, however a part of the particles will grow into larger ones, which is not represented in the model results, thus there is a small decrease trend after 400sec.

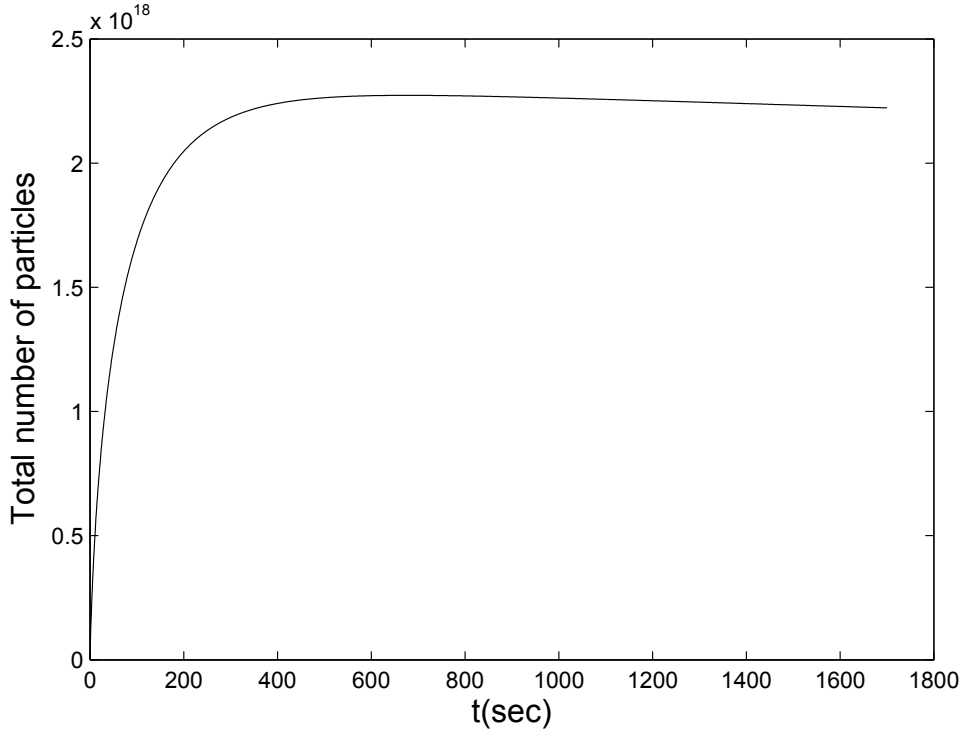

Figure 4.3: Evolution of number of particles with time

Figures 4.4 and 4.5 show the concentration of radicals and initiator in the aqueous phase. The initiator decreases linearly with time. The concentration of radicals in the aqueous phase is constant when the concentration of particles is constant.

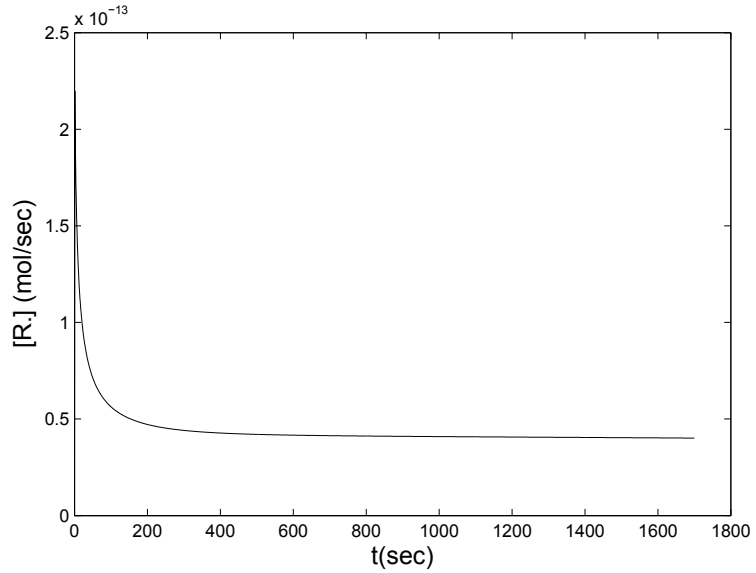

Figure 4.4: Concentration of radicals in the aqueous phase

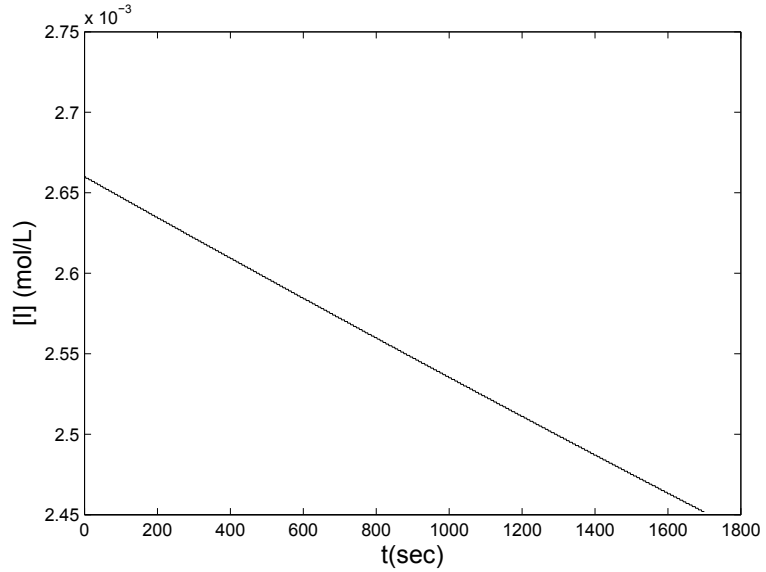

Figure 4.5: Concentration of initiator in the aqueous phase

4.5.2 Stability of the droplet size with the co-stabilizer

One kinetic feature that mini-emulsion polymerization shares with the macro-emulsion polymerization is that monomer transport is thermodynamically governed [Rodriguez et al., 1989, 1991]. In mini-emulsion polymerization, the diffusion of monomers from smaller droplets to larger ones is prevented by co-stabilizer. The final droplet sizes from the pre-distribution obtained from the log-normal distribution with a mean diameter of 100nm and a standard deviation of 20nm are given in Table 4.1 As required by molecular

diffusion (or Ostwald ripening), the smaller droplets decrease in size, the larger droplets increase in size and the average diameter remains nearly the same.

Table 4.1: Results of Equilibrium Swelling Thermodynamics

Fraction of droplets	Initial diameter (nm)	Final diameter (nm)
0.03	50	48
0.24	75	74
0.46	100	100
0.24	125	127
0.03	150	153
average diameter	100	100

4.5.3 Thermodynamically governed monomer transport during polymerization

As explained in section 4.3, in the presence of co-stabilizer, the monomers would be re-distributed during the polymerization. It means that the particle size, the droplet size would change along the time.

Validation

The model predictions are compared with the experimental data taken from literature [Choi et al., 1985].

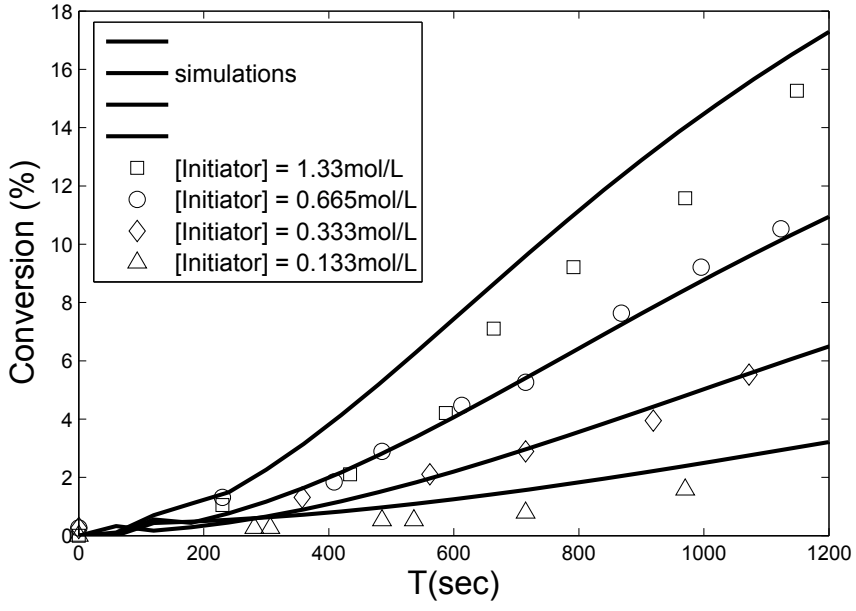

Figure 4.6: Comparison of the evolution of experimental and simulated conversions versus time for the initial concentrations of initiator

Figure 4.6 compares the experimental and simulated conversions. The effect of initial concentration of initiator is checked. The polymerization rate decreases with the decreasing of concentration of initiator. In general, a good agreement is observed between model and experiments.

Particle size distribution

The evolution of the particle size distribution with time for an initiator concentration equal to $1.33\,10^{-3}$mol.l^{-1} is given in Figure 4.7. Initially, the growth rate is very high due to higher monomer volume fraction in the particles, this lasts about 100sec. After that, the rate of growth decreases neatly due to the decrease of concentration of monomer in the particles. As the growth rate of total number of particles just depends on the rate of nucleation, with the time increase, the number of droplets decreases, and meanwhile, the newly formed particles will compete with the droplets to capture the radicals, inducing a decrease of the rate of nucleation. Thus, the growth rate of total number of particles decreases with the time. It can also been seen that the number of particles with the dry diameter near 80nm increases faster than that of particles with other dry diameters.

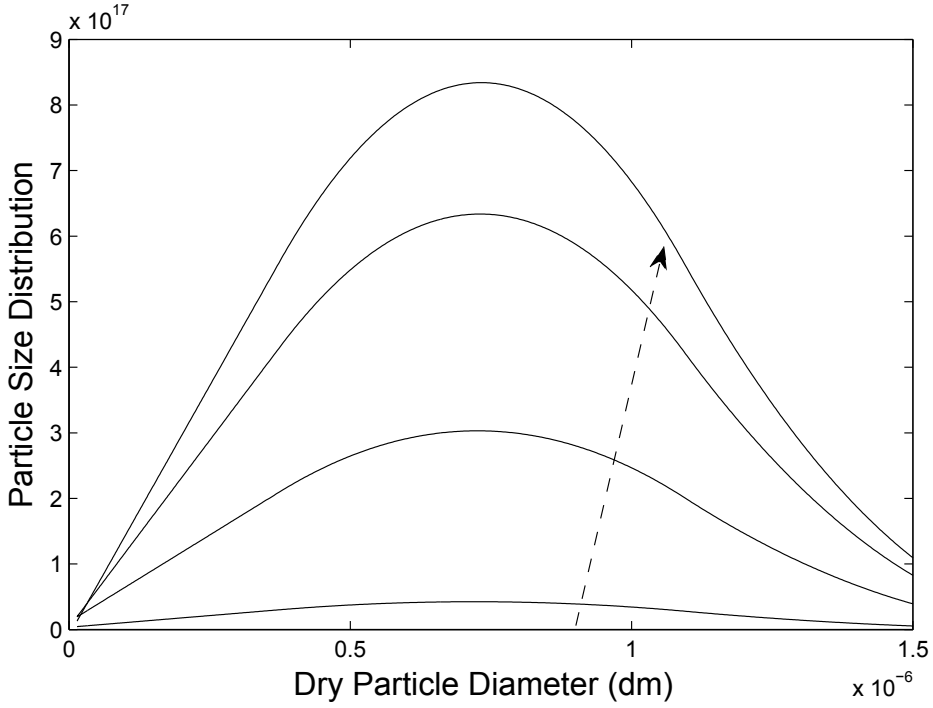

Figure 4.7: Particle size distribution (time increasinge with the direction of the arrow, t = 1sec, 50sec, 100sec, 500sec, 1000sec and 1500sec)

Variations of the droplet sizes

The changes of the droplet sizes of five different droplet classes with time are given in Figure 4.8. The initial droplet sizes are given in Table 4.1, i.e. at $t = 0$s, the droplet sizes of the five different droplet classes are 48, 74, 100, 127, 153nm. It should be noted that, in the model validation, based on the data to be validated, a monodisperse droplet size distribution had been assumed. As the polymerization time increases, the differences of

sizes of the droplets of the different droplet classes tend to be small, which means that the droplet size distribution becomes narrow. Thus, more monomer will be transferred from the larger droplets to the particles than from smaller ones. This also shows that our model is general enough to incorporate a full droplet size distribution.

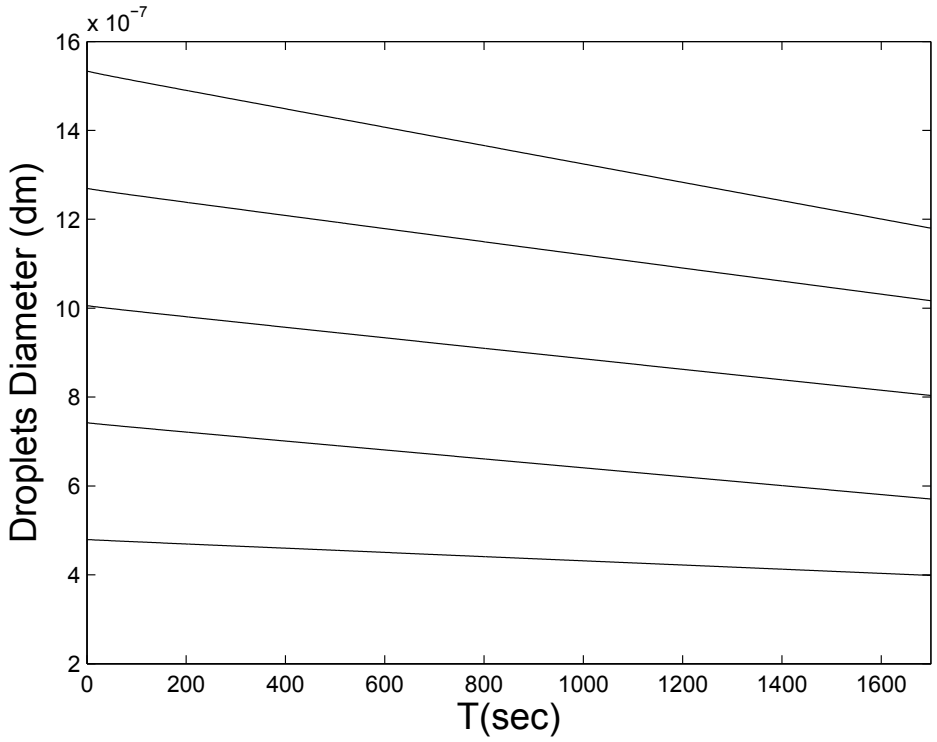

Figure 4.8: Variations of the droplet sizes of five different droplet classes, the initial droplets size are given in Table 4.1. At $t = 0$s, the droplet sizes of the five different droplet classes are 48, 74, 100, 127, 153nm.

In the aqueous phase

Figures 4.9 and 4.10 show the concentrations of radicals and initiator in the aqueous phase. The general tendency is similar to that of macro-emulsion polymerization (section 3.4.3). The initiator decreases linearly with the time, while for the radicals in the aqueous phase $R_w^\bullet$, at the beginning of polymerization, it increases with the increasing of the amount of particles. When the amount of the particles does not change, the capture of radicals by the particles becomes dominant with respect to nucleation, and some time is needed to reach the chemical equilibrium state. In the same way as in section 4.5.1, the maximum particle size considered in the model is 150 nm. After that, a part of the particles will grow into larger ones, not considered in the model results, thus there will be a slow decrease of amount of particles. This causes the slow decrease of the concentration of radicals in the aqueous phase.

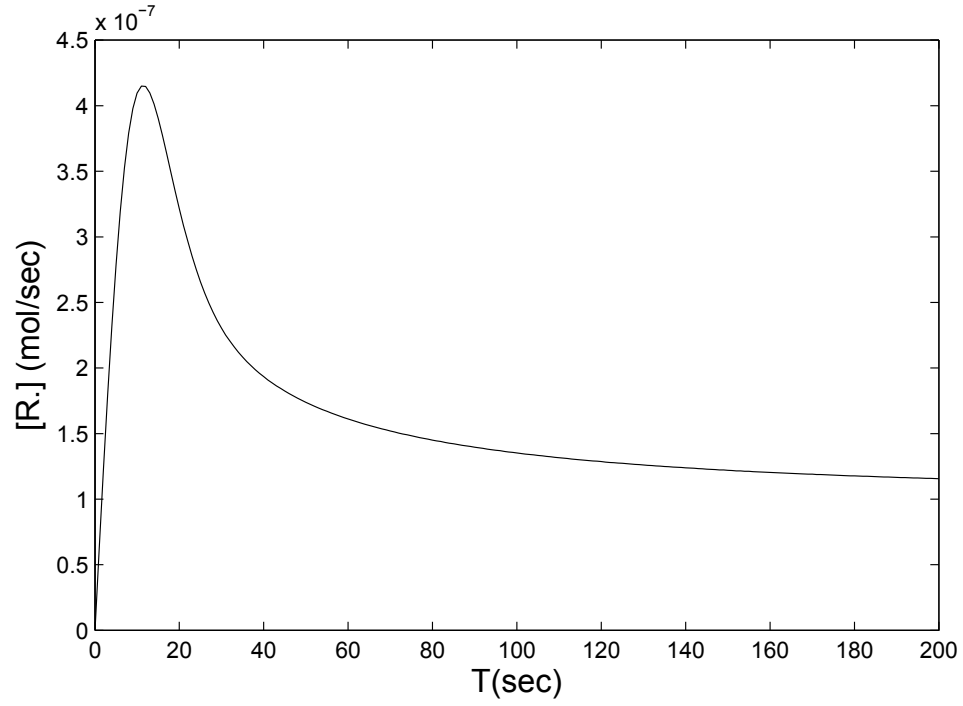

Figure 4.9: Concentration of radicals in the aqueous phase

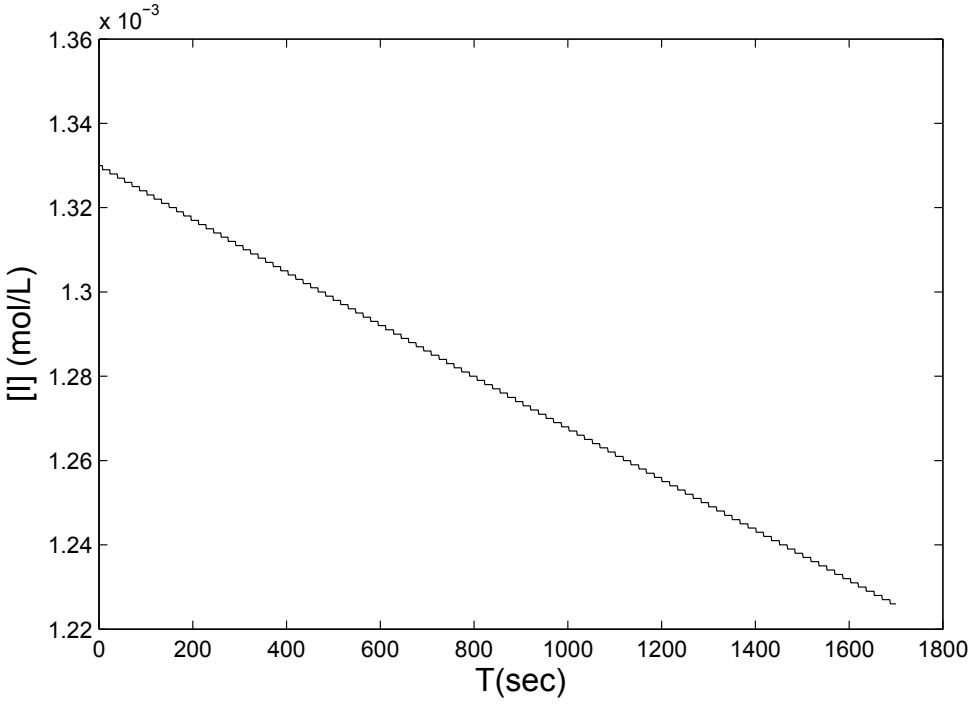

Figure 4.10: Concentration of initiator in the aqueous phase

4.6 Appendix C

4.6.1 Moles of concentration of monomer in particles

$$
\begin{aligned}
[\mathrm{M}]_{p,i,j} &= \frac{M_{m,p,i,j}}{v_{p,i,j}} = \frac{m_{m,p,i,j}/MW_m}{v_{p,i,j}} = \frac{v_{m,p,i,j}/(\rho_m MW_m)}{v_{p,i,j}} \\
&= \frac{v_{p,i,j}\cdot(1-\phi_{c,p,i,j}-R_{i,j}\phi_{c,p,i,j})/(\rho_m MW_m)}{v_{p,i,j}} = \frac{1-\phi_{c,p,i,j}-R_{i,j}\phi_{c,p,i,j}}{\rho_m MW_m)} \\
\overline{[\mathrm{M}]}_{p,1} &= \frac{\sum_{i=1}^{\infty}\sum_{j=1}^{\infty}[\mathrm{M}]_{p,i,j}N_{p,i,j,1}}{N_{p,1}} = \frac{1}{\rho_m MW_m}\sum_{i=1}^{\infty}\sum_{j=1}^{\infty} w_{i,j}\cdot(1-\phi_{c,p,i,j}-R_{i,j}\phi_{c,p,i,j}) \\
\overline{[\mathrm{M}]}_{p,0} &= \frac{\sum_{i=1}^{\infty}\sum_{j=2}^{\infty}[\mathrm{M}]_{p,i,j}N_{p,i,j,1}}{N_{p,1}} = \frac{1}{\rho_m MW_m}\sum_{i=1}^{\infty}\sum_{j=2}^{\infty} \sigma_{i,j}\cdot(1-\phi_{c,p,i,j}-R_{i,j}\phi_{c,p,i,j})
\end{aligned}
\tag{4.58}
$$

4.6.2 Number average diameter of particles and volume average diameter of particles

$$
\begin{aligned}
v_{p,i,j} &= \frac{v_{c,i,ini}}{\phi_{c,p,i,j}} = \frac{\pi}{6}d_{p,i,j}^3 \\
d_{p,i,j} &= \left(\frac{6v_{c,i,ini}}{\pi\phi_{c,p,i,j}}\right)^{1/3}
\end{aligned}
\tag{4.59}
$$

Volume average diameter of particles

$$
\begin{aligned}
V_{tot,p,1} &= \sum_{i=1}^{\infty}\sum_{j=1}^{\infty} v_{i,j}\cdot N_{p,i,j,1} = N_{p,1}\sum_{i=1}^{\infty}\sum_{j=1}^{\infty} v_{p,i,j}w_{i,j} \\
V_{tot,p,0} &= \sum_{i=1}^{\infty}\sum_{j=2}^{\infty} v_{i,j}\cdot N_{p,i,j,0} = N_{p,0}\sum_{i=1}^{\infty}\sum_{j=2}^{\infty} v_{p,i,j}\sigma_{i,j} \\
V_{tot,p} &= V_{tot,p,1}+V_{tot,p,0} = \sum_{i=1}^{\infty}\sum_{j=1}^{\infty} v_{i,j}\cdot(N_{p,i,j,1}+N_{p,i,j,0}) \\
&= N_{p,1}\sum_{i=1}^{\infty}\sum_{j=1}^{\infty} v_{p,i,j}w_{i,j} + N_{p,0}\sum_{i=1}^{\infty}\sum_{j=2}^{\infty} v_{p,i,j}\sigma_{i,j} \\
\overline{v}_{v,p,1} &= V_{tot,p,1}/N_{p,1} = \sum_{i=1}^{\infty}\sum_{j=1}^{\infty} v_{p,i,j}w_{i,j} \\
\overline{v}_{v,p,0} &= V_{tot,p,0}/N_{p,0} = \sum_{i=1}^{\infty}\sum_{j=2}^{\infty} v_{p,i,j}\sigma_{i,j}
\end{aligned}
\tag{4.60}
$$

Number average diameter of particles

$$
\begin{aligned}
D_{p,tot,1} &= \sum_{i=1}^{\infty}\sum_{j=1}^{\infty} d_{p,i,j} N_{p,i,j,1} \\
D_{p,tot,0} &= \sum_{i=1}^{\infty}\sum_{j=2}^{\infty} d_{p,i,j} N_{p,i,j,0} \\
D_{p,tot} &= D_{p,tot,1} + D_{p,tot,0} = \sum_{i=1}^{\infty}\sum_{j=1}^{\infty} d_{p,i,j} N_{p,i,j,1} + \sum_{i=1}^{\infty}\sum_{j=2}^{\infty} d_{p,i,j} N_{p,i,j,0} \\
\overline{d}_{p,n,1} &= D_{p,tot,1}/N_{p,1} = \sum_{i=1}^{\infty}\sum_{j=1}^{\infty} d_{p,i,j} w_{i,j} \\
\overline{d}_{p,n,0} &= D_{p,tot,0}/N_{p,0} = \sum_{i=1}^{\infty}\sum_{i=1}^{\infty} d_{p,i,j} \sigma_{i,j} \\
\overline{d}_{p,n} &= D_{p,tot}/N_p = \bar{n} \sum_{i=1}^{\infty}\sum_{j=1}^{\infty} d_{p,i,j} w_{i,j} + (1-\bar{n}) \sum_{i=1}^{\infty}\sum_{i=1}^{\infty} d_{p,i,j} \sigma_{i,j}
\end{aligned}
\tag{4.61}
$$

Bibliography

Y. T. Choi, M. S. El-Aasser, E. D. Sudol, and J. W. Vanderhoff. Polymerization of styrene miniemulsions. *J. Polym. Sci. Pol. Chem.*, 23:2973–2987, 1985.

D. Edouard, N. Sheibat-Othman, and H. Hammouri. Observer design for particle size distribution in emulsion polymerization. *AIChE J.*, 51:3167–3185, 2005.

P. J. Flory, editor. *Principles of Polymer Chemistry*. Cornell Univ Press, Ithaca, New York, 1953.

M. Morton, S. Kaizermann, and M. W. Altier. Swelling of latex particles. *J. Colloid Interf. Sci.*, 9:300–312, 1954.

V. S. Rodriguez, J. Delgado, C. A. Silebi, and M. S. El-Aasser. Interparticle monomer transport in miniemulsions. *Ind. Eng. Chem. Res.*, 28:65–74, 1989.

V. S. Rodriguez, J. M. Asua, M. S. El-Aasser, and C. A. Silebi. Mathematical modeling of seeded miniemulsion copolymerization for oil-soluble initiator. *J. Polym. Sci. Pol. Physics.*, 29:483–500, 1991.

A. Sood and S. K. Awasthi. Initial droplet size distribution in miniemulsion polymerization. *J. Appl. Polym. Sci.*, 88:3058–3065, 2003.

A. Sood and S. K. Awasthi. Population balance model for miniemulsion polymerization.1. Model development. *Macromol. Theory Simul.*, 13:603–614, 2004.

J. Ugelstad and F. K. Hansen. Kinetics and mechanism of emulsion polymerization. *Rubber chemistry and technology*, 49:536–612, 1976.

Chapter 5

Conclusion on Modelling of Emulsion Polymerization

The main differences between macro- and mini- emulsion polymerization are related to the nucleation mechanism. In macro-emulsion polymerization, micelle nucleation is the dominant particle nucleation process, and the monomer droplets are considered as the reservoir of the monomer, but in mini-emulsion polymerization, droplet nucleation is the dominant one. To construct a model, the most important difference between macro- and mini- emulsion polymerization refers to the methods used to determine the number of the nuclei places. In macro-emulsion polymerization, when the materials and the composition are selected, the size of micelles, swollen micelles and droplets are determined, and based on the balance of surfactants and monomers, the number of micelles and droplets can be calculated. However, in mini-emulsion polymerization, the droplet size distribution is affected by the ratio between monomers and surfactant/co-stabilizer and physical and/or mechanical effects, high shear, sonicator or a mechanical homogenizer, etc., which renders it much more difficult to calculate.

A model about macro-emulsion polymerization has been established based on 0-1 model, which allows us to predict the radical chain size distribution for a given class of particle sizes and the particle size distribution. By comparison, a model on mini-emulsion polymerization has been established based on the balance of chemical potentials of the monomer in the reactor, which allows us to predict the particle size distribution and the change of the droplets sizes. In general, a good agreement is observed between models and data from the literature. For macro-emulsion polymerization, the model shows that, at the beginning, both the number of the particles and the particle size increase, and as the time increases,the number of the particles is almost unchanged, but the particle size grows. As the desorption of monomeric radicals in the particles was ignored in the model, the radical chain sizes are centered in the oligomeric radicals. To obtain a more precise radical chain size distribution, a model involving both transfer of polymeric radical to the monomers in the particles and desorption of monomeric radicals in the particles into the aqueous phase should be developed. For the mini-emulsion polymerization, the amounts of monomer in various phases (droplets, particles and aqueous phase) are decided by the balance of chemical potentials of the monomer in these phases. This determines the droplet sizes and the particle sizes. Initially, the growth rate of particle size is very high and, later, it decreases neatly due to decreasing monomer concentration in the particles. During the polymerization process, more monomer will transfer from the larger droplets

to the particles than from smaller ones.

Chapter 6

Introduction on Grafted Polypropylene by Reactive Extrusion

Polyolefins (POs) have become and have remained the most used thermoplastics in the world since their discovery in the 1950s, recognized by the Nobel Prize for Chemistry awarded jointly to Professor Karl Ziegler and Professor Giulio Natta in 1963. A broad range of chemically stable and environmentally safe materials with very useful thermal and mechanical properties can be obtained going from homopolyethylene to isotactic homopolypropylene and the related copolymers.

The inertness of polyolefins has been one of their important features in many applications, but at the same time a drawback for applications for which surface wettability or interaction with polar products is required.

The successful grafting of maleic anhydride (MAH) and its derivatives to the paraffin backbone of the macromolecules constituting a polyolefin achieved in the 1970-1980s. [Kaufman and Falcetta, 1977, Gaylord and Mishra, 1983, Gloor et al., 1994, Ruggeri et al., 1983] opened the way to modified polyolefins characterized by an acceptable affinity with polar organic molecules, metal and minerals, thus acting also as an efficient compatibilizer for a large number of blends [Feldman, 2005, Koning et al., 1998, Liu and Baker, 1992, Xanthos and Dagli, 1991], composites [Vasile, 2000] and nanocomposites [Alexandre and Dubois, 2000, Ray and Okamoto, 2003, Ciardelli et al., 2008]. After the above pioneering work regarding the grafting of polar functional groups on various polyolefins backbone, extended investigations were performed both in academy and industry. The main objectives were the understanding of the mechanism, the control of the process and relations between the modified structure and the additional properties. The process, as originally performed, is very sustainable, being carried out in mechanical mixers and extruders without solvent. However, to reach the low viscosity necessary for homogeneously diffused chemical modification, high temperature was used (well over the polyolefin melting point) and a peroxide as free-radical generator to activate the grafting reaction was added. The thermal and mechanical stress and the presence of free-radicals made the process very difficult to control as far as the grafting main reaction is concerned, while at the same time they produce variable extent side reactions with particular reference to degradation and chain extension cross-linking/branching of polyolefin macromolecules.

At the start, using the aforementioned grafting of polar groups, the process was widely used without further improvement and fundamental understanding. The technique was considered mature until a deeper understanding at the molecular level became evident

for quality control, environmental safety, and performance improvement. Since that time, a large number of researchers worldwide have been involved in the investigation and development of the subject reaction bringing useful information and opening new routes to controlled structures in terms of functionalization degree and final molecular architecture.

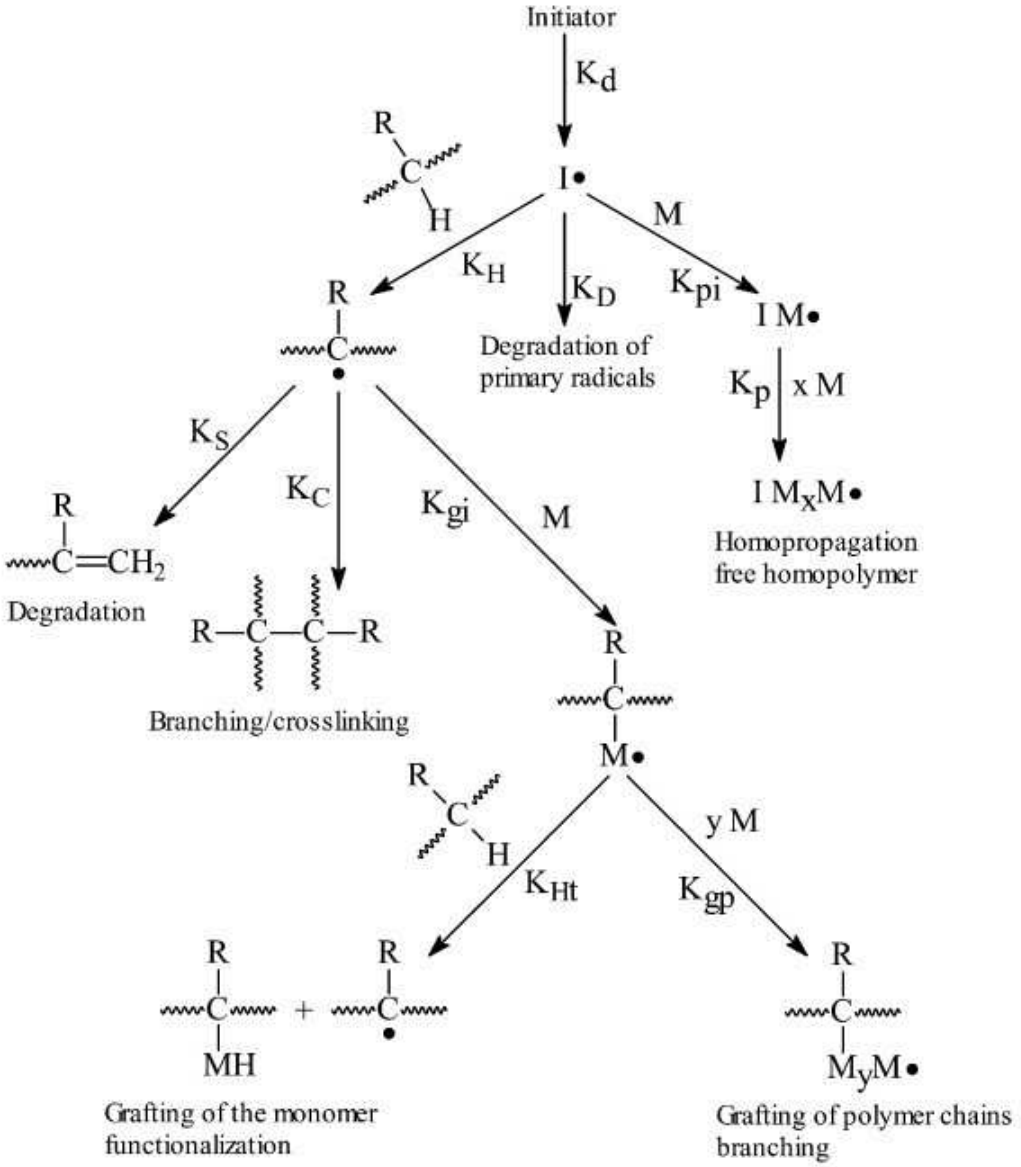

Figure 6.1: General scheme of radical post-modification of a polyolefin

A scheme [Al-Malaika, 1996] of the post-polymerization radical functionalization reaction (Scheme 6.1) provides the grafting of a functional monomer(M) onto the backbone of a polyolefin by the generation of the macroradical, and its successive conversion into a non-radical inserted polar group by a combination of grafting and transfer reactions. The use of radicals at generally high temperature (necessary to carry out the reaction in the fluid polymer melt) renders the process nonselective and with limited specificity. From the mechanistic point of view, the most important side reactions are determined by the

reactivity and stability of the different formed radicals. The primary radical (formed by decomposition of the initiator, (Kd) can generate a macroradical by hydrogen abstraction from the backbone of the polyolefin (KH), can start the free homopolymerization of the functionalizing agent (Kpi) and/or degradation (KD). The macroradical generated by KH can give a functionalized macroradical by a grafting reaction of the polar monomer (Kgi); it can also produce branched/cross-linked and/or degraded macromolecules by coupling (KC) and scission reactions (KS). The functionalized macroradical can generate the functionalized product by hydrogen transfer reaction (KHt) and propagate the monomer graft homopolymerization reaction (Kgp). The balance between the functionalized product and undesired species is strongly dependent on different key parameters all referring to the reagents structure and experimental conditions: type of the monomer and initiator, the chemical composition of the polyolefin macromolecules in terms of monomeric units, sequence and tacticity, type of equipment, time and temperature [Russell, 2002].

Polypropylene PP is one of the three largest plastics considered to belong to the commodity plastic materials due to its relative low mechanical performance, high tensile strength, stiffness and chemical resistance [Moore and A.Larson, 1996]. On the other hand, the price of this material is comparatively low about 1 Eur/kg. This is a huge economic benefit and that is why PP is widely used in many fields. However, some of its properties still need to be improved, such as relatively low melt strength, heat resistance and chemical resistance. The functionnalization of polypropylene (PP) through grafting unsaturated monomers such as maleic anhydride (MAH), acrylic acid and its derivatives, in the presence of organic peroxide as an initiator, has received much attention over the past decades. The modified PP has been used extensively for compatibilization of immiscible polypropylene-polyamide and polypropylene-polyester blends, as well as to improve the interfacial adhesion of PP with glass and carbon fibers, and even as a processing aid for degradable plastic [Paul and Newman, 1978, Gaylord, 1989]. Fuctionalized PP has been prepared successfully by using solution [Minoura et al., 1969], melt [Ruggeri et al., 1983, Gaylord and Mehta, 1982, Gaylord et al., 1983] and solid state routes [Rengarajan et al., 1990, Singh, 1992]. Among them, the melt process has widely been used in the industry owing to its economic and operational advantages. However, the grafting degree of MAH onto PP is low. During the past few decades, to find a way of improving the grafting degree of MAH, many studies have focused on the grafting mechanism. [Minoura et al., 1969, Gaylord et al., 1983, Al-Malaika, 1996, Russell and Kelusky, 1988, De Roover et al., 1995, Heinen et al., 1996, Moad, 1999, Russell, 2002].

The structure of the polyolefin in terms of type of monomers and comonomers, distribution of sequences, presence and amount of branching (short and long), presence and content of double bonds or aryl units from aromatic olefins affects the hydrogen abstraction occurrence (KH) from the macromolecular chain and strongly affects the stability of the formed macroradicals. It is well known that tertiary macroradicals are thermodynamically favored and tertiary hydrogen atoms are three or four times more reactive than secondary hydrogen atoms at 160°C [Russell, 2002]; this is confirmed by the fact that the grafting level is generally higher for ethylene-propylene(EPM) than for linear polyethylenes (LLDPE or HDPE) [Ciardelli et al., 2004] under the same experimental conditions. As the temperature rises, abstraction from the various types of C-H bond becomes less discriminated kinetically and the process less selective. At high temperature, degradation (KS) is favored by extensive branching, while linearity and double bonds favor cross-linking (KC); these last reactions modify the macromolecular structure and

molecular weight, thus affecting the mechanical/physical properties of the parent material. Polypropylene macroradicals undergo easy breakdown by β-scission reactions [Gaylord and Mehta, 1982] and macroradicals derived from linear polyethylene or polyolefin containing a low amount of double bonds can easily react together [Bremner and Rudin, 1993] by radical-radical combination; both of these reactions compete with grafting but in some cases can be successfully exploited for the synthesis of polymers with controlled rheological properties [Tzoganakis et al., 1988, Berzin et al., 2000]. The β-scission reaction is a monomolecular reaction (KS), while chain extension and cross-linking occur by macroradicals coupling (KC). This requires the presence in the reaction medium of higher amounts of macroradicals favoring this latter reaction, while the former is not affected. Selectivity is also observed with preferential conversion of aliphatic blocks versus styrene blocks [Ciardelli et al., 2000]. On the basic of a detailed study on the molecular structure of MAH grafted PP and the results of the literature [De Roover et al., 1995, Heinen et al., 1996, Al-Malaika, 1996], Shi. and Hu et al. presented the concept of nanoreactors of organically modified montmorillonite [Shi et al., 2006a,b, 2007]. Preconfinement of DCP in the nanometer-scale galleries of an o-MMT allowed concentrating MAH molecules on its outer surface and slowing down the release of primary radicals to the grafting reaction volume. Consequently, the selectivity of the grafting of MAH onto PP was significantly increased, and encapsulation effect of active species preconfined in organically modified montmorillonite was considered the primary reason. In this work, organically modified montmorillonite(o-MMT) was used as nanoreactor. Not only the preconfinement effect of the MMT and the relationship between MMT and MAH were considered, and the rule of the grafting was also studied.

To prepare high melt strength polypropylene (HMSPP), scientists have explored many methods. Cross-linking of polyolefin is simple, appropriate and commonly used for applications. Peroxide cross-linking, radiation cross-linking and silane cross-linking are the three main cross-linking methods employed industrially [Dalai and Chen, 2002, Smedberg et al., 2003, Fiaz and Gilbert, 1998]. Unfortunately, peroxide cross-linking induces serious degradation of PP chains, even serious cross-linking, and radiation cross-linking is limited by the materials thickness and the process needs an inert atmosphere, which results in high cost and complicated manufacturing technology [An et al., 2008].

Silane grafting and cross-linking of PP is a recently developed alternative approach to preparing HMSPP [An et al., 2008, Demjen et al., 1999, Huang and Liu, 1998, Zhou et al., 2009, Beltran and Mijangos, 2000, Jain et al., 2006]. The way of making cross-linkable PP through silane grafting followed by water cross-linking has various advantages, such as easy processing, low cost and capital investment, and favourable properties in the processed materials.

To get silane cross-linked polypropylene, the key step is the grafting of silane on polypropylene. However, the process is very complicated. The radical grafting of a monomer on PP in the presence of a peroxide initiator is often accompanied by the degradation of the PP backbone and the polymerization of the monomer, which results in fewer chances for the grafting of silanes. The relationships among them are very complicated. When it is produced in the industrial process, the aim is to maximize the ratio of the silane grafted on PP, to minimize the degradation of the PP backbone and the polymerization of the silane, which is a multiobjective decision problem for the industrialists. Thus, the purpose is to choose the best balance among all the defined and conflicting objectives. To reach this aim, a multicriteria optimization of the process is necessary.

Bibliography

S. Al-Malaika, editor. *Reactive modifiers for polymers*. Blackie Academic and Professional Chapman and Hall, London, 1996.

M. Alexandre and P. Dubois. Polymer-layered silicate nanocomposites: preparation, properties and uses of a new class of materials. *Mater. Sci. Eng.*, 28:1–63, 2000.

Y. J. An, Z. J. Zhang, and W. G. Bi. Characterization of high melt strength polypropylene synthesized via silane grafteing initiated by in situ heat induction reaction. *J. Appl. Polym. Sci.*, 110:3727–3732, 2008.

M. Beltran and C. Mijangos. Silane grafting and moisture cross - linking of polypropylene. *Polym. Eng. Sci.*, 40:1534–1541, 2000.

F. Berzin, B. Vergnes, P. Dufoss¨¨, and L. Delamare. Delamare L. Modeling of peroxide initiated controlled degradation of polypropylene in a twin screw extruder. *Polym. Eng. Sci.*, 40:344–356, 2000.

T. Bremner and A. Rudin. Peroxide modification of linear low - density polyethylene: a comparison of dialkyl peroxides. *J. Appl. Polym. Sci.*, 49:785–798, 1993.

F. Ciardelli, M. Aglietto, E. Passaglia, and F. Picchioni. Controlled functionalization of olefin/styrene copolymers through free radical processes. *Polym. Adv. Technol.*, 11: 371–376, 2000.

F. Ciardelli, M. Aglietto, M. B. Coltelli, E. Passaglia, G. Ruggeri, and S. Coiai. Functionalization of polyolefins in the melt. *NATO. Sci. Ser. II: Math. Phys. Chem.*, 175: 47–71, 2004.

F. Ciardelli, S. Coiai, E. Passaglia, A. Pucci, and G. Ruggeri. Nanocomposites based polyolefins and functional thermoplastic materials. *Polym. Int.*, 57:805–836, 2008.

S. Dalai and W. X. Chen. Radiation effects on LDPE/EVA blends. *J. Appl. Polym. Sci.*, 86:1296–1302, 2002.

B. De Roover, M. Sciavons, V. Carlier, J. Devaux, R. Legras, and A. Momtaz. Molecular characterization of maleic anhydride-functionalized polypropylene. *J. Polym. Sci. Part A: Polym. Chem.*, 33:829–842, 1995.

Z. Demjen, B. Pukanszky, and J. Nagy. Possible coupling reactions of functional silanes and polypropylene. *Polymer*, 40:1763–1773, 1999.

D. Feldman. Polyblend compatibilization. *J. Macromol. Sci. Part A: Pure Appl. Chem.*, 42:587–605, 2005.

M. Fiaz and M. Gilbert. Silane cross-linking of plasticized poly(vinyl chloride). *Adv. Polym. Technol.*, 17:37, 1998.

N. G. Gaylord. Use Surfactants to Blend Polymers. *Chem. tech.*, 19:435, 1989.

N. G. Gaylord and M. Mehta. Role of homopolymerization in the peroxide-catalyzed reaction of maleic anhydride and polyethylene in the absence of solvent. *J. Polym. Sci. Polym. Lett. Ed.*, 20:481–486, 1982.

N. G. Gaylord and M. K. Mishra. Nondegradative reaction of maleic anhydride and molten polypropylene in the presence of peroxides. *J. Polym. Sci. Polym. Lett. Ed.*, 21:23–30, 1983.

N. G. Gaylord, M. Mehta, and V. Kumar. Graft copolymerization of maleic anhydride onto polyethylene. *Polym. Sci. Technol.*, 21:171–182, 1983.

P. E. Gloor, Y. Tang, A. E. Kostanska, and A. E. Hamielec. Chemical modification of polyolefins by free radical mechanisms: a modeling and experimental study of simultaneous random scission, branching and crosslinking. *Polymer*, 35:1012–1030, 1994.

W. Heinen, C.H. Rosenmolle, C.B. Wenzel, H.J.M. de Groot, J. Lurtenburg, and M.van Duin. 13C NMR study of the grafting of maleic anhydride onto polyethene, polypropene, and ethene-propene copolymers. *Macromolecules*, 29:1151–1157, 1996.

H. Huang and N. C. Liu. Nondegradative melt functionalization of polypropylene with glycidyl methacrylate. *J. Appl. Polym. Sci.*, 67:1957–1963, 1998.

S. Jain, J. G. P. Goossens, and M. van Duin. Synthesis, characteriztion and properties of (vinyl triethoxy silane-grafted pp)/silica nanocomposites. *Macromol. Symp.*, 233: 225–234, 2006.

H. S. Kaufman and J. J. Falcetta, editors. *Introduction to polymer science and technology: an SPE Text-book.* Wiley, New York, 1977.

C. Koning, M. Van Duin, C. Pagnoulle, and R. Jerome. Strategies for compatibilization of polymer blends. *Prog. Polym. Sci.*, 23:707–757, 1998.

N. C. Liu and W. E. Baker. Reactive polymers for blend compatibilization. *Adv. Polym. Technol.*, 11:149–262, 1992.

Y. Minoura, M. Ueda, S. Mizunuma, and M. Oba. The reaction of polypropylene with maleic anhydride. *J. Appl. Polym. Sci.*, 13:1625–1640, 1969.

G. Moad. The synthesis of polyolefin graft copolymers by reactive extrusion. *Prog. Polym. Sci.*, 24:1527–1528, 1999.

Jr. E. P. Moore and G. A.Larson, editors. *Polypropylene Handbook.* Hanser, Munich, 1996.

J. R. Paul and S. Newman, editors. *Polymer blends.* Academic Press, New York, 1978.

S. Sinha Ray and M. Okamoto. Polymer/layered silicate nanocomposites: a review from preparation to processing. *Prog. Polym. Sci.*, 28:1539–1641, 2003.

R. Rengarajan, V. R. Parameswaran, S. Lee, M. Vicic, and P. L. Rinaldi. Nmr analysis of polypropylene-maleic anhydride copolymer. *J. Polym. Sci. Polym. Lett. Ed.*, 31:1703, 1990.

G. Ruggeri, M. Aglietto, A. Petragnani, and F. Ciardelli. Some aspects of polypropylene functionalization by free radical reactions. *Chem. Eng. Sci.*, 19:863–866, 1983.

K. E. Russell. Free radical graft polymerization and copolymerization at higher temperature. *Prog. Polym. Sci.*, 27:1007–1038, 2002.

K. E. Russell and E.C. Kelusky. Grafting of maleic anhydride to n-eicosane. *J. Polym. Sci. Part A: Polym. Chem.*, 26:2273–2280, 1988.

D. Shi, G.-H. HU, and R. K. Y. Li. Concept of nano-reactor for the control of the selectivity of the free radical grafting of maleic anhydride onto polypropylene in the melt. *Chem. Eng. Sci.*, 61:3780–3784, 2006a.

D. Shi, Y. Zhu, Z. Ke, J. Yin, W. Jiang, and G.-H. Hu. Nano-reactors for controlling the selectivity of the free radical grafting of maleic anhydride onto polypropylene in the melt. *polym. Eng. Sci.*, 46:1143–1156, 2006b.

D. Shi, W. Yu, R. K. Y. Li, Z. Ke, and J. Yin. An investigation on the dispersion of montmorillonite (MMT) primary particles in PP matrix. *Chem. Eng. Sci.*, 43:3250–3257, 2007.

R. P. Singh. Surface grafting onto polypropylene-a survey of recent developments. *Prog. Polym. Sci.*, 17:251–281, 1992.

A. Smedberg, T. Hjertberg, and B. Gustafsson. Effect of molecular structure and topology on network formation in peroxide cross-linked polyethylene. *Polymer*, 44:3395–3405, 2003.

C. Tzoganakis, J. Vlachopoulos, and A. E. Hamielec. Production of controlled - rheology polypropylene resins by peroxide promoted degradation during extrusion. *Polym. Eng. Sci.*, 28:170–180, 1988.

C. Vasile, editor. *Handbook of polyolefins. 2nd ed.* Marcel Dekker, New York, 2000.

M. Xanthos and S. S. Dagli. Compatibilization of polymer blends by reactive processing. *Polym. Eng. Sci.*, 31:926–935, 1991.

H. Zhou, M. Hu, and Y. Hu. Influence of coagents on the silane grafting and cross-linking of polypropylene. *Polym. Plast. Tech. Eng.*, 48:193–200, 2009.

Chapter 7

Organically Modified Montmorillonite as Nanoreactor to Improve the Grafting Degree of Maleic Anhydride onto Polypropylene

7.1 Experimental

7.1.1 Materials

The PP powder used in this work was kindly supplied by Sinopec Yangzi petrochemical Company Ltd., The peroxide, dicumyl peroxide (DCP, 98 %), and the monomer, MAH, were purchased from Sinopharm Chemical Reagent Co. Ltd. They were used without further purification. Organically modified MMT denoted as o-MMT (Nanomer I.44PA) was purchased from Amcol Inc, USA.

7.1.2 Confinement of peroxide in o-MMT

A given amount of the o-MMT was charged to 100 ml of acetone. The o-MMT / acetone mixture was homogenized under ultrasound for 1 h. In parallel, a prescribed amount of DCP was dissolved in 10ml of acetone. Thereafter, the solution of DCP in acetone was added slowly to the above-mentioned o-MMT / acetone mixture under continuous stirring. The mass ratio of the o-MMT and DCP was 1:1. The whole system was kept stirring for 3 h at room temperature before it was cast onto a polytetrafluoroethylene plate. The o-MMT confined DCP was denoted as DCP/o-MMT and was obtained after acetone was evaporated completely at room temperature. The DCP/o-MMT powder was then dried in a vacuum oven at 50°C for 24 h before use for subsequent free radical grafting reactions.

7.1.3 Melt free radical grafting of MAH onto PP

The grafting reaction was carried out in a Haake batch mixer (HBI system 90) equipped with a mixing chamber and two rotors inside at 190°C for 7 min. The rotation speed of

the mixer was 65 rpm. The materials (MAH, PP powder and (DCP/o-MMT) powder) were pre-mixed and then charged to mixer simultaneously. For comparison a purpose, the same grafting reaction was carried out in a conventional manner, i.e., DCP was not pre-confined in the o-MMT. The concentrations of DCP in each system were kept the same. After the grafting, PP-g-MAH products were dissolved in hot xylene and then precipitated in acetone. The precipitates were further washed twice with acetone to completely remove MAH residues. The purified PP-g-MAH products were dried in a vacuum oven at 80°C for 12 h for subsequent analyses.

7.1.4 Measurement of grafting degree

The grafting degree, defined as the weight percentage of MAH in PP-g-MAH, was measured by a chemical titration method [Shi et al., 2001]. A small amount (1g) of dried Residue 3 was dissolved in 100 ml of boiling xylene in a conical flask and a few drops of water were added to hydrolyze all anhydride functions. Afterwards, 10 ml of 0.05N potassium hydroxide solution in methanol was added into the flask . The formed solution was back titrated with 0.03N trichloroacetic solution in xylene using cresol red as the indicator. A blank test for PP was carried out by the same method. Grafting degree was calculated from the following equation.

$$G(\%wt) = \frac{(V_0 - V_1)\ N}{2\,W\,1000}\,M_W\,100\% \tag{7.1}$$

where, G (%wt) is the grafting degree of MAH on PP-g-MAH, V_0 (ml) the acid volume used in the blank test, V_1 (ml) the acid volume used in the test with the sample, N the acid concentration (mol/l) and W is the weight of the sample (g). The M_W of MAH is 98.

7.1.5 Measurement of the molecular weights of PP-g-MAH

The molecular weights of PP-g-MAH samples were measured using a high temperature GPC of GPC V2000 Waters. A differential refractometer detector coupled with a "chromatography data station" provided by Digital was used for recording and analyzing the signal. 1,2,4-Trichlorobenzene was used as the eluent. Samples were dissolved in 1,2,4-trichlorobenzene at 150°C and the PP-g-MAH concentrations were in the range of 2.5-3.5mg/ml. The injected volume was 200 μl and the eluent flow rate was 1.0 ml/min. The whole measuring system was maintained at 150°C.

7.1.6 Characterization of o-MMT dispersion

Characterization of o-MMT particle or platelet dispersion was carried out using transmission electron microscopy (TEM). For the TEM analysis, a JEOL model JEM-1230 (Jeol Japan Inc.) was used. As polypropylene is a soft polymer, the use of an ultramicrotome (RMC model MTXL) in cryogenic conditions was needed to cut samples for TEM analysis.

7.2 Results

Table 7.1 gathers the compositions of all the trials carried out in this work and selected characteristics of the PP-g-MAH. There were two types of experiments:
system 1: PP/DCP/MAH grafting system without o-MMT(No. 1-10),
system 2: PP/(DCP/o-MMT)/MAH grafting system(No. 11-20).

Table 7.1: Compositions of all the trials carried out in this work and selected characteristics of the PP-g-MAH

Trial ♯	PP(g):o-MMT/DCP(DCP)(g):MAH(g)	DG wt%	M_n(kg/mol)	M_w(kg/mol)
0	PP/o-MMT*=40:1	-	-	-
System 1.(PP/(DCP)/MAH)				
1	40: (0.25): 1	0.422	42.3	110.7
2	40: (0.50): 1	0.458	43.8	113.9
3	40: (1.00): 1	0.532	39.9	94.6
4	40: (1.50): 1	0.528	50.0	122.5
5	40: (1.00): 2	0.375	55.8	211.1
6	40: (1.00): 3	0.367	61.8	221.4
7	40: (1.00): 4	0.369	55.6	224.6
8	40: (0.50): 2	0.375	53.2	155.8
9	40: (0.50): 3	0.368	50.9	202.2
10	40: (0.50): 4	0.377	46.6	170.5
System 2. (PP/(o-MMT/DCP)/MAH)				
11	40: 0.50: 1	0.471	47.2	113.1
12	40: 1.00: 1	0.510	42.2	118.7
13	40: 2.00: 1	0.599	36.2	93.7
14	40: 3.00: 1	0.578	38.0	98.3
15	40: 2.00: 2	0.494	46.3	135.1
16	40: 2.00: 3	0.438	41.1	128.3
17	40: 2.00: 4	0.399	51.5	194.0
18	40: 1.00: 2	0.394	55.7	189.1
19	40: 1.00: 3	0.399	55.3	162.4
20	40: 1.00: 4	0.382	49.9	187.9
System 3. (PP/o-MMT*/DCP/MAH)				
26	40: 1: 1: 3	0.412	-	-

o-MMT* was not pre-treated by acetone and ultrasound

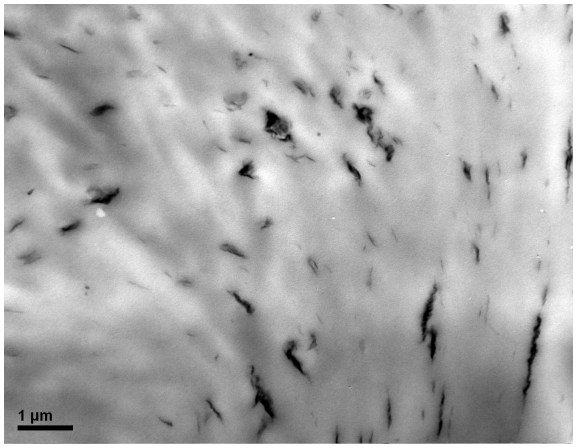

(a) trial 0 (PP/o-MMT=40: 1wt, o-MMT without pre-treatment)

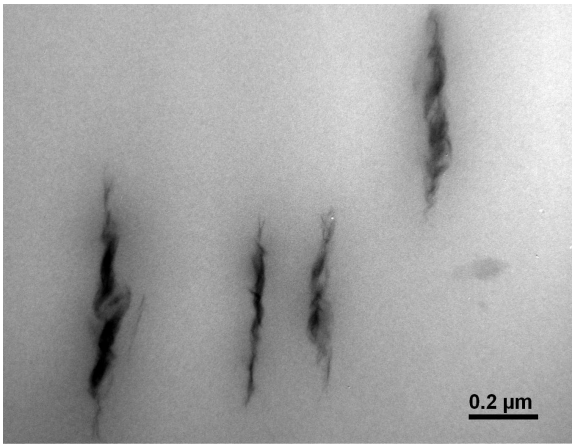

(b) trial 0 (PP/o-MMT=40: 1wt, o-MMT without pre-treatment)

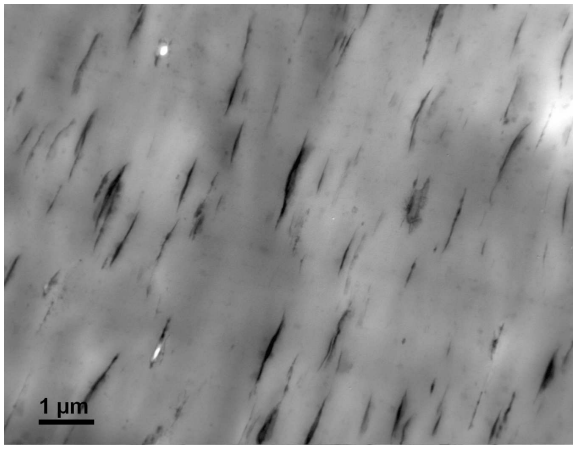

(c) trial 26 (PP/o-MMT/DCP/MAH=40: 1: 1: 3wt, o-MMT without pre-treatment)

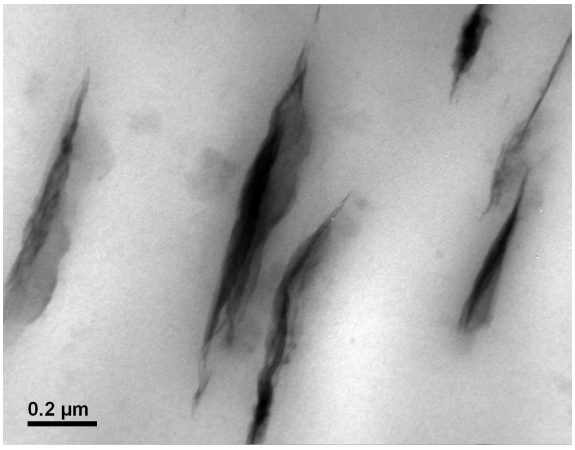

(d) trial 26 (PP/o-MMT/DCP/MAH=40: 1: 1: 3wt, o-MMT without pre-treatment)

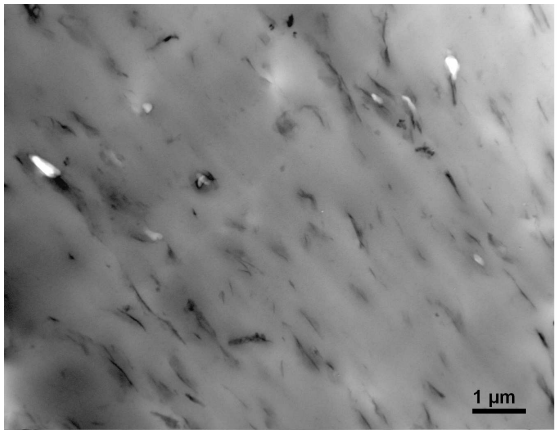

(e) trial 16 (PP/(o-MMT/DCP)/MAH=40:2:3wt, DCP pre-confined in o-MMT with the ratio 1:1wt)

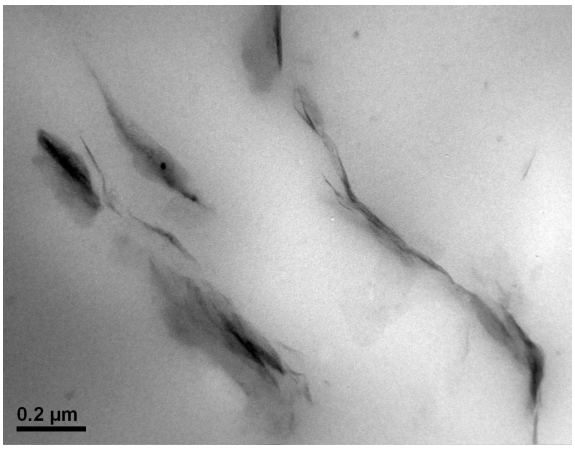

(f) trial 16 (PP/(o-MMT/DCP)/MAH=40:2:3wt, DCP pre-confined in o-MMT with the ratio 1:1wt)

Figure 7.1: TEM micrographs of PP/o-MMT of trial 0, 16, 26.

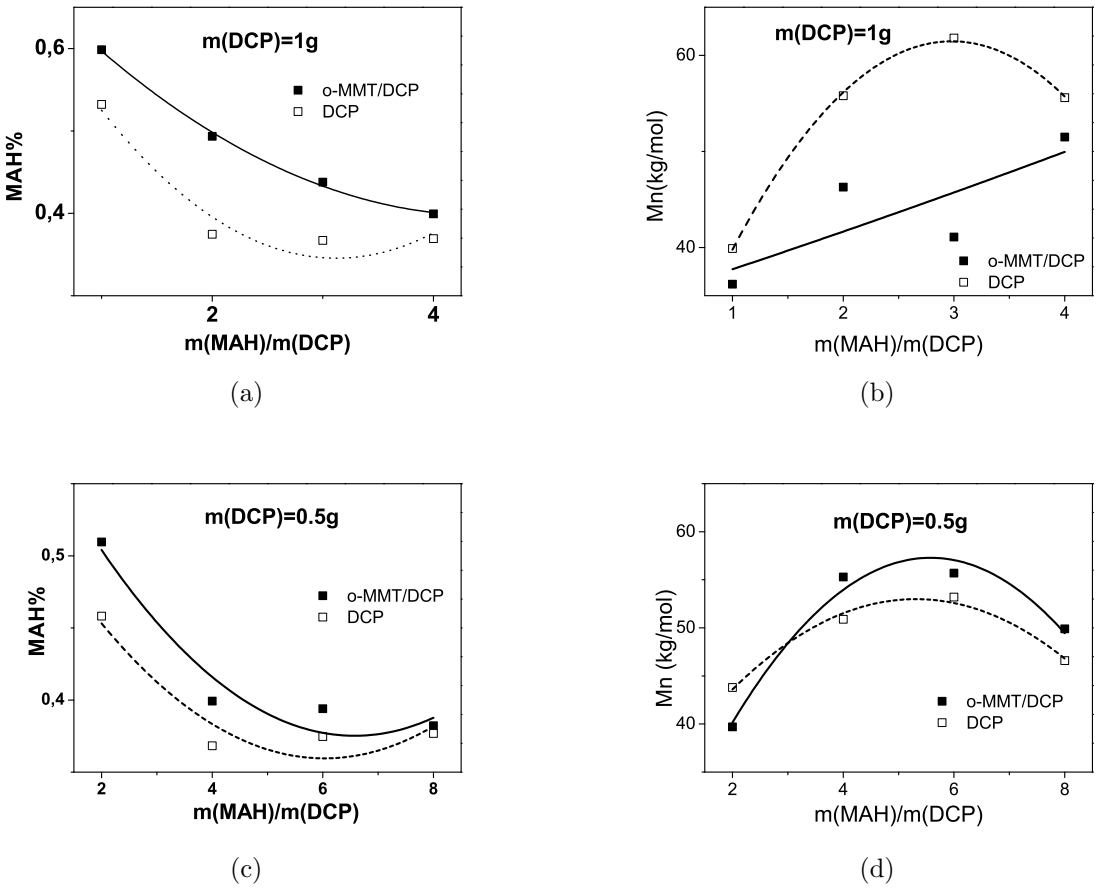

Figure 7.2: Comparison among the PP/DCP/MAH, PP/(DCP/o-MMT)/MAH grafting systems in terms of the evolution of the grafting degree and that of the molecular weight of the PP-g-MAH as a function of the MAH content for a given DCP content.

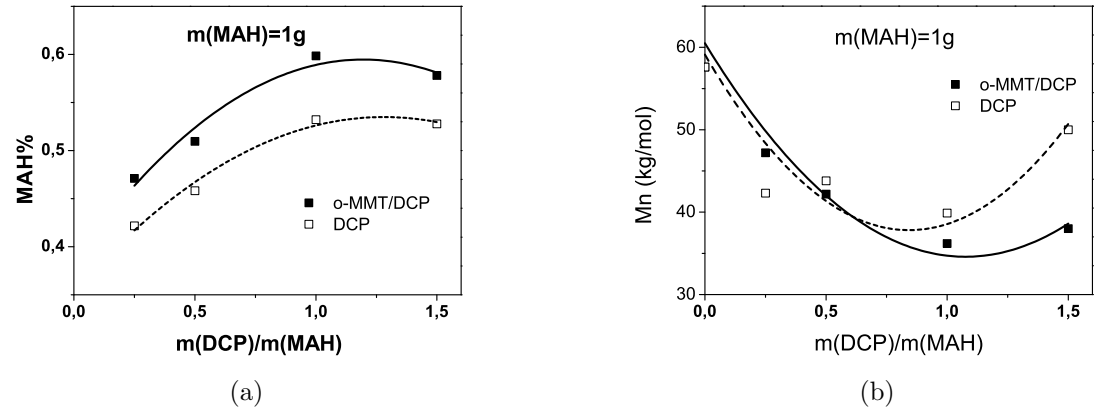

Figure 7.3: Comparison among the PP/DCP/MAH, PP/(DCP/o-MMT)/MAH grafting systems in terms of the evolution of the grafting degree and that of the molecular weight of the PP-g-MAH as a function of the DCP content for a given MAH content.

Figures 7.1(a), 7.1(b), 7.1(c), 7.1(d), 7.1(e), 7.1(f) show the dispersion of o-MMT particles or platelets in PP or PP and PP-g-MAH phase. Samples used in Figure 7.1(a) were the products of trial 0 composed by PP: o-MMT=40:1(wt), with no reactions but just blending in the Haake batch mixer and the o-MMT was not pre-treated of acetone and ultrasound. Samples used in Figure 7.1(b) were the products of trial 26 which have the same composition of trial 16 but with o-MMT not pre-treated of acetone and ultrasound, which means DCP was not pre-confined in o-MMT. Samples used in Figure 7.1(c) was the products of trial 16. No matter whether it was pre-treated, o-MMT can be dispersed homogeneously in the PP phase, and by pre-treatment of acetone and ultrasound, the width of the MMT galleries became larger which has been proved by [Shi et al., 2006] using Wide angle X ray diffraction(XAXD).

Figure 7.2 compares the evolution of the grafting degree of MAH and that of the number average molecular weight of the PP-g-MAH, M_n, as a function of the MAH content among the grafting systems. Figure 7.3 compares the evolution of the grafting degree of MAH and that of the number average molecular weight of the PP-g-MAH, M_n, as a function of the DCP content among the grafting systems. The grafting degree in the o-MMT nanoreactor grafting system were always higher than those in the classical one, but the number average molecular weight in the o-MMT nanoreactor grafting system were not higher than those in the classical one, which is not in agreement with the phenomenon reported by [Shi et al., 2006].

7.3 Discussion

The PP-g-MAH grafting reaction mechanisms were expatiated by [Shi et al., 2001] as follows:

the classical grafting system is expected to follow more or less the reaction scheme in Figure 7.4. According to this reaction mechanism, a primary free radical $RO^{\bullet}$ formed by the decomposition of a peroxide molecule may follow one of the following two different reaction pathways:

Pathway A: $RO^{\bullet}$ reacts with an unsaturated monomer MAH to form a saturated free radical $RM^{\bullet}$. The latter will not participate in any grafting reactions because it cannot further propagate but can only undergo termination by dismutation.

Pathway D: $RO^{\bullet}$ reacts with a hydrogen atom of the polymer (PP), and preferentially a tertiary one, to form the corresponding macroradical $PP^{\bullet}$. The latter may also follow one of the following two different reaction pathways:

Pathway E: fragmentation to two shorter segments by the so-called β -scission.

Pathway F: grafting

No matter what path it is followed, when more grafting happens, more termination of disproportionation will happen, which results in the reduction of the average molecular weight of the products. So the higher the grafting degree is, the smaller the average molecular weight of the products.

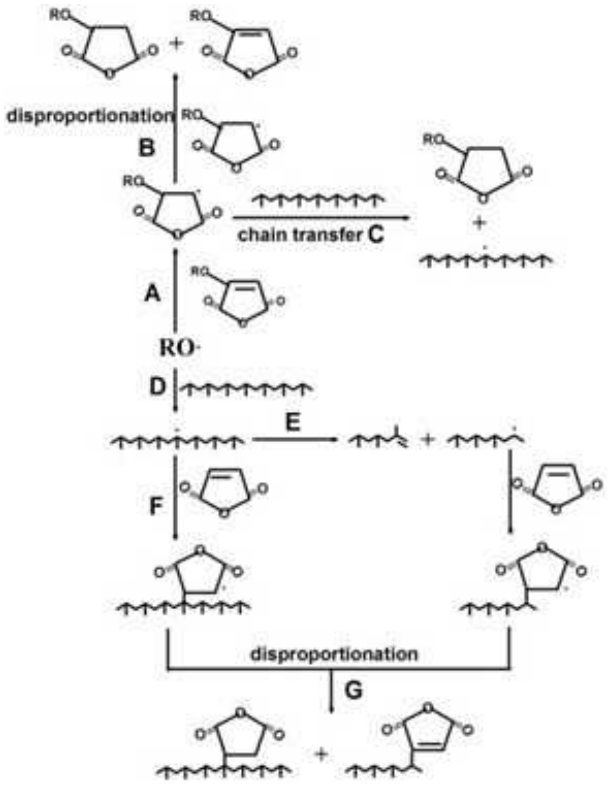

Figure 7.4: A simplified reaction scheme of the PP-g-MAH grafting system (from [Shi et al., 2006]).

Why was the performance of the o-MMT nanoreactor grafting system higher than that of the classical one? Firstly, as PP is immiscible with MAH, in the classical grafting systems, when the molecular of PP is high, its melt viscosity should be high too, which makes it difficult for the MAH monomers to diffuse into the PP chains. So MAH can meet and react with PP$^{\bullet}$ at long odds. But in the systems with o-MMT as nanoreactors, as the interactions between MAH and MMT surface are relatively strong (PP-g-MAH is often used as compatibilizer between PP and MMT in preparing PP/MMT nanocomposites [Kawasumi et al., 1997, Hasegawa et al., 2000b,a, Nam et al., 2001]), MAH will be enriched around o-MMT. Moreover, the dispersion of the o-MMT in the PP phase is homogeneous (Figure 7.1), when PP$^{\bullet}$ forms around the o-MMT, MAH will react immediately with it. For that reason, with the same initial contents of MAH and DCP, both the MAH grafting degree onto PP of trial 16 and that of trial 26 are higher than that of trial 6. Another obvious and important difference between the classical grafting system and that with the o-MMT nanoreactors is that in the first one, RO$^{\bullet}$ primary radicals are formed evenly over the entire reacting volume. Once formed, they are in direct and immediate contact with MAH and/or PP. In the last one, however, they are formed only inside the galleries of the o-MMT (Figure 7.5). They cannot react with the PP and/or MAH before they have diffused out of the o-MMT galleries. Since the decomposition of ROOR to RO$^{\bullet}$ is a reversible reaction, the rate with which RO$^{\bullet}$ primary radicals are generated in the PP/MAH/(DCP/o-MMT) grafting system is expected to be much lower than that in the PP/MAH/DCP system. In other words, the role the o-MMT plays here is to slow down the rate of release of RO$^{\bullet}$ from within the o-MMT galleries to the outside reaction volume occupied by the PP and MAH. It is similar to that of encapsulation of active species. As

such, the rate of primary radical formation is no more controlled by temperature alone but by both temperature and diffusion. Without pre-treatment of acetone and ultrasound, the width of the o-MMT galleries is smaller than that with pre-treatment, which is not wide enough for DCP to be dispersed in [Shi et al., 2006], so there is no encapsulation effect in trial 26, which is the main reason why MAH grafting degree onto PP of trial 26 is lower than that of trial 16.

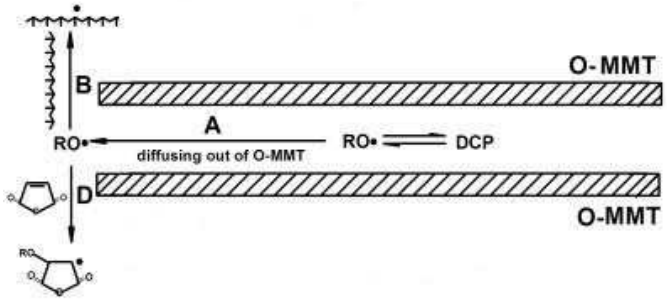

Figure 7.5: A simplified reaction scheme of DCP homolytic fragmentation and diffusion in o-MMT

In the PP/MAH/DCP system without o-MMT, with the constant initial DCP content, when the ratio between MAH and DCP is large enough, by increasing the content of MAH, pathway A in Figure 7.4 is favored and the number of radicals attacking the PP chain are decreased, so as for the PP chain scission, the grafting degree reduces. The same situation will occur in the PP/MAH/(DCP/o-MMT)system, in which MAH will be enriched around o-MMT. By increasing the content of MAH, o-MMT will be isolated with PP, which means that $RO^{\bullet}$ dispersed from the o-MMT cannot enter in contact with PP, most free radicals in the grafting system are under the form of $RM^{\bullet}$. In other words, most MAH molecules would be consumed up by $RO^{\bullet}$ before they can react with $PP^{\bullet}$ to form PP-g-MAH, and pathway A will be the main reaction. Thus in Figure 7.3, with the constant initial DCP, the grafting degree is reduced by increasing the content of MAH both in the system with o-MMT and without it.

When the initial MAH content is constant, with DCP content from small to large, when DCP content is small, pathway A in Figure 7.4 is favored, the grafting degree is low. With the increasing of the DCP content, the grafting degree increase. But when the DCP content is large enough, pathway A and B in Figure 7.4 can be neglected, and primary radicals formed from the decomposition of the DCP are primarily used to generate PP macroradicals (path D), but without enough MAH to graft on the PP macroradicals, PP macroradicals suffer to β-scission and termination. Thus, in Figure 7.3, the grafting degree firstly increases and then decreases with increase of the DCP content. Moreover, it seems that when the initial ratio between MAH and DCP equals to one, the grafting degree will be the largest.

7.4 Conclusions

The aim of this work was to apply the concept of nanoreactor to the reactive extrusion process of the free radical grafting of maleic anhydride onto polypropylene (PP) to increase

the MAH grafting degree on the PP, an important process in the polymer industry. Both the strong interactions between MAH and MMT surface and the encapsulation of active species effect improved the grafting degree. With excessive MAH, a cage will be formed to prevent the formation of $PP^{\bullet}$ and reduce the grafting degree. A certain ratio of MAH and DCP is necessary to get the optimized grafting degree.

Bibliography

N. Hasegawa, H. Okamoto, M. Kato, A. Tsukigase, and A. Usuki. Polyolefin-clay hybrids based on modified polyolefins and organophilic clay. *Macromol. Mater. Eng.*, 76:76–79, 2000a.

N. Hasegawa, H. Okamoto, M. Kato, and A. Usuki. Preparation and mechanical properties of polypropylene-clay hybrids based on modified polypropylene and organophilic clay. *J. Appl. Polym. Sci.*, 78:1918–1922, 2000b.

M. Kawasumi, N. Hasegawa, M. Kato, A. Uski, and A. Okada. Preparation and mechanical properties of polypropylene-clay hybrids. *Macromolecules*, 30:6333–6338, 1997.

P.H. Nam, P. Maiti, M. Okamoto, T. Kotaka, N. Hasegawa, and A. Usuki. A hierarchical structure and properties of intercalated polypropylene/clay nanocomposites. *Polymer*, 42:9633–9640, 2001.

D. Shi, J. Yang, Z. Yao, Y Wang, H. Huang, W. Jing, J. Yin, and G. Costa. Functionalization of isotactic polypropylene with maleic anhydride by reactive extrusion: mechanism of melt grafting. *Polymer*, 42:5549–5557, 2001.

D. Shi, G.-H. HU, and R. K. Y. Li. Concept of nano-reactor for the control of the selectivity of the free radical grafting of maleic anhydride onto polypropylene in the melt. *Chem. Eng. Sci.*, 61:3780–3784, 2006.

Chapter 8

Grafting of Silane onto Polypropylene by Reactive Extrusion

8.1 Modeling Strategy

8.1.1 Selection of operating conditions

The preliminary experiments as well as the knowledge already acquired on the reactive extrusion led us to choose three operating conditions (also called factors in the following paragraphs). These factors are those which a priori are most capable to influence significantly the properties of the reactive extrusion and which are easy to operate. It is necessary to choose the ranges of the various operating parameters. Thus, the feed rate, Q, was defined between 1kg/h to 10kg/h. The barrel temperature, T, was varied from 200 to 240°C. The screw rotation speed, N, was set between 100 and 500 rpm. These factors and their corresponding ranges are given in Table 8.1.

Table 8.1: Variation range of the different process factors

Factors	Minimum	Maximum
$Q(kg/h)$	1	10
$T(°C)$	200	240
$N(rpm)$	100	500

All these factors are real values (continuous variation between extremum), and must be normalized by reduction in the range $[-1, +1]$. For this, the minimum and the maximum of each operating conditions take the values -1 and $+1$, respectively.

8.1.2 Experimental design

In order to obtain a model with correct specification and well determined parameters, a series of experiments must be conducted. Given the fact that the expected responses do not vary in a linear manner with the selected variable and to enable the quantification of the prediction of the responses, a D-optimal plan was selected, where the response

could be modeled in a quadratic manner [Pukelsheim, 1993]. The D-optimal criterion is often used when a minimum number of experiments are needed. The optimal number of experiments to be conducted was obtained using an evolutionary algorithm previously developed in our laboratory [Bicking et al., 1994, Fonteix et al., 1995].

The rotatability method will be used to complete the experimental design in order to increase the number of degrees of freedom and to choose the needed experiments to validate the polynomial model. An experimental design is rotatable if the prediction error variance depends only on the distance between every experiment and the centre of the studied domain (symmetry of revolution). Measurements that quantify the degree of rotatability of a response surface design were introduced by [Khuri, 1988] and developed by [Rached et al., 2008].

The centre point of the experimental design is replicated four times in order to obtain the confidence interval of the calculated coefficients of the model and to observe the reproducibility ($Q = 5.5$kg/h, $T = 220$°C, $N = 300$rpm).

8.1.3 D-optimality criterion

The use of the D-optimality criterion implies the choice of a mathematical model to represent the responses versus the experimental factors. Moreover, a quadratic polynomial may be selected in order to take into account curvatures existing in the models. This type of criterion is often used when a minimum number of experiments is needed. The desired number of runs is extracted from the candidate design to give an experimental design which minimizes the standard error of the estimates of the coefficients of the chosen model.

When the result P_i of an experiment x_j can be predicted by $P_i = f^T(x_j)\theta$ where θ is a vector of coefficients, a set P of experiments can be modeled by $P = X\theta$, where X is the matrix of the row vectors $f^T(x_j)$ and x_j the vector of factors which defines the jth experiment. When the results of the experiments are obtained, the vector of coefficients can be calculated.

In this case, a confidence region is defined for the coefficients of the model with a signification level α such as [Walter and Pronzato, 1997])

$$(\theta - \hat{\theta})^T (X^T - X)(\theta - \hat{\theta}) \leq \frac{p}{q-p}(e^T e) F_\alpha(p, q-p) \tag{8.1}$$

where θ is the vector of unknown coefficients, $\hat{\theta}$ the vector of calculated coefficients, e the vector of residues, and X the model matrix. p and q denote respectively the number of coefficients of the model and the number of experiments. $F_\alpha(p, q-p)$ is the Fisher-Snedecor variable with a probability α ([Fisher, 1970, Snedecor and Cochran, 1989])

The confidence region corresponds to an ellipsoid centered on $\hat{\theta}$ and its volume is inversely proportional to the determinant of the information matrix ($X^T X$). The criterion of D-optimality leads to the location of the experimental points so that $\left|X^T X\right|$ is maximum and finally minimizes the volume of the confidence region of the coefficients. Multiplication of the dispersion matrix, $(X^T X)^{-1}$ by the experimental variance, σ_m^2, gives the variance-covariance matrix, $V(\hat{\theta})$, where diagonal and non-diagonal terms correspond to the variances and covariances of the estimators of the coefficients, respectively. In order to determine the error variance on the coefficients of the model, σ_r^2, the determinant of the

information matrix is used as dividing factor. Therefore, the maximization of $\left|(X^TX)\right|$ leads to the reduction of the error variance on the coefficients.

A 2D representation of the confidence region is shown in Figure 8.1. For a number of degrees of freedom (NDF) different from zero, there is a confidence region, $[\hat{\theta}_{min};\hat{\theta}_{max}]$, for the parameter $\hat{\theta}$ based on Eq. (8.1)

$$\hat{\theta}_i - \sigma_r^2\sqrt{p\cdot F_{0.05}(p,q-p)\cdot(X^TX)^{-1}_{ii}} \leq \theta_i \leq \hat{\theta}_i + \sigma_r^2\sqrt{p\cdot F_{0.05}(p,q-p)\cdot(X^TX)^{-1}_{ii}} \quad (8.2)$$

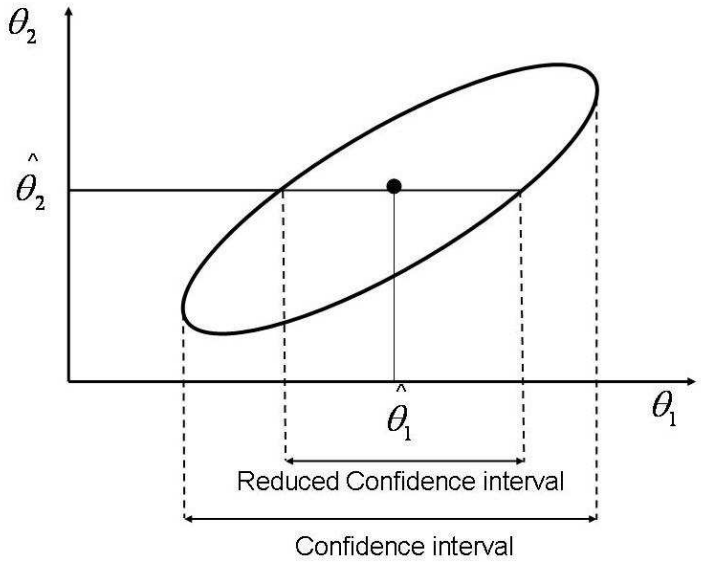

Figure 8.1: 2D representation of the confidence region and the reduced interval

It also gives information on the degree of correlation of the coefficients considered. A reduced confidence interval, $[\hat{\theta}^{red}_{min};\hat{\theta}^{red}_{max}]$, is also calculated considering all the coefficients at their optimal value except one

$$\hat{\theta}_i - \sigma_r^2\sqrt{\frac{p\cdot F_{0.05}(p,q-p)}{(X^TX)^{-1}_{ii}}} \leq \theta_i \leq \hat{\theta}_i + \sigma_r^2\sqrt{\frac{p\cdot F_{0.05}(p,q-p)}{(X^TX)^{-1}_{ii}}} \quad (8.3)$$

This interval is used to determine whether the parameter value is significantly different from zero. If 0 belongs the confidence interval, the corresponding coefficient is negligible.

8.1.4 Polynomial model description

Because of the complex reactions in the extruder, it is difficult to establish a model based on the reaction mechanism. A possibility is to consider the reactor as a black box and to develop empirical relationships between process variables and product properties. Polynomials allow to simulate, with any precision, any set of experimental values. The only restriction is to choose a high enough degree to obtain a satisfactory representation of the phenomenon and small enough to avoid a too high number of parameters. In order to determine a polynomial model, the first step is to begin by a first-degree model. However such a model does not permit to treat non-linear phenomena. For this reason, two kinds

of second-degree polynomial models have been chosen so as to be able to represent them in a satisfactory way.

In this study, the aim is to obtain the percentage of grafted silane, that of polymerized silane, complex viscosity $\eta_{0.063}$ of dry samples, and the tensile properties for different operating conditions, i.e. the feed rate, Q, the barrel temperature, T, and the screw rotation speed, N. Thus, inputs and outputs of the simulation model are defined.

Indeed, for three factors, the structures of the polynomial models are the following:

1. Model I

$$y = a_0 + a_1 Q + a_2 T + a_3 N + a_{11} Q^2 + a_{22} T^2 + a_{33} N^2 + a_{12} QT + a_{13} QN + a_{23} TN + \epsilon_i \quad (8.4)$$

2. Model II

$$y = a_0 + a_1 Q + a_2 T + a_3 N + a_{12} QT + a_{13} QN + a_{23} TN + a_{123} QTN + \epsilon_i \quad (8.5)$$

where y is the value of the criterion for experiment number i, Q, T and N represent, in the same order, the normalized values of the feed rate, Q, the barrel temperature, T, and the screw rotation speed, N. The a_is are the coefficients of the polynomial to be determined. ϵ is the unknown experimental error. In the present case, for model I, more than ten experiments need to be performed to get a significant statistical model. For model II, more than eight experiments need to be performed to get a significant statistical model. In this study, 13 experiments mentioned in the section about experimental design were chosen to obtain the coefficients of the model.

Figure 8.2 shows a schematic representation of this simulation package.

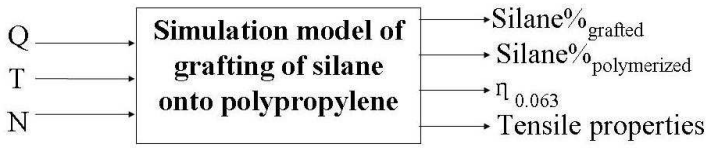

Figure 8.2: Schematic representation of inputs - outputs of the model

This leads to a system of equations represented in the following matrix form

$$\boldsymbol{P} = \boldsymbol{X}\,\boldsymbol{a} + \boldsymbol{\epsilon} \quad (8.6)$$

The model coefficients were calculated using a multilinear regression. A 95% ($\alpha = 5\%$) confidence interval is defined to estimate the uncertainty on the calculated coefficients.

8.1.5 Reduction of the model

The coefficients were estimated. However, the validation of the model is possible if the number of degrees of freedom is greater than zero, the number of degrees of freedom being equal to the number of experiments selected for estimation minus the number of coefficients of the model. In this research, as two different models are selected for simulation, the number of coefficients and the number of degrees of freedom are different (refer to section 8.4). A reduction of the model is thus necessary, i.e., certain coefficients are to be discarded. The confidence interval determined for each coefficient was used to reduce the

model. Any coefficient whose confidence interval contains zero is likely to be non significant from a statistical point of view, and this tendency is all the more important as the confidence interval is centered on zero. Let us define the ratio between the minimum and the maximum of the confidence region, Θ with $Max(|\hat{\Theta}^{app}_{min}|, |\hat{\Theta}^{app}_{max}|)/Min(|\hat{\Theta}^{app}_{min}|, |\hat{\Theta}^{app}_{max}|)$. If $\hat{\Theta}^{app}_{min} \cdot \hat{\Theta}^{app}_{max} < 0$ and Θ is close to 1, the corresponding coefficient must be discarded. The methodology used is summarized in Figure 8.3. When one loop is completed, the number of coefficients in the model is decreased by one unity. After elimination of the less significant coefficient, a new polynomial model is obtained, and the loop will stop until zero belongs to none of the confidence intervals, which will lead to the final model.

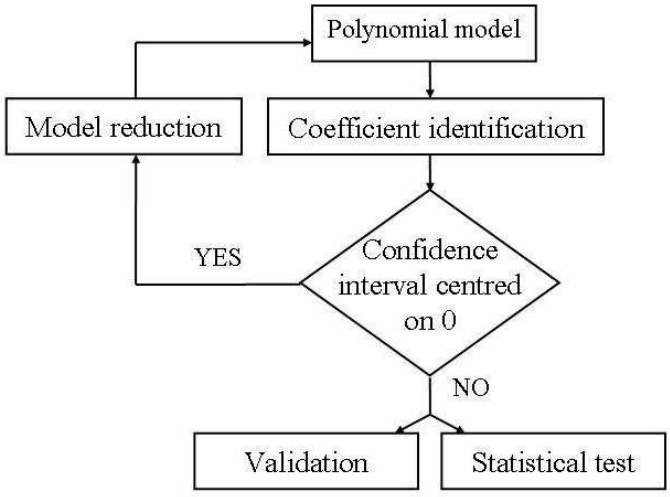

Figure 8.3: Steps of the polynomial modelling

8.2 Experimental

8.2.1 Materials

Polypropylene (PPH 760 and Accurel XP100), the silane ATM (Dow Corning Z-6530), co-agent ethylsorbate, the initiator (1,1,4,4-tetramethyl-1,4-butanediyl)bis(1,1-dimethylethyl) (LUPEROX 101), aox additive (Iragox 1010 and Irgafos 168) were kindly supplied by DOW Corning. Xylene was purchased from Sigma-Aldrich Corporation. All these commercial chemicals were used directly without further purification. Actone was standard laboratory reagent used as received.

8.2.2 Homopolymerization of ATM

A stainless reactor was used to polymerize ATM in xylene under the nitrogen using 2, 2'-azobis(2-methylbutyronitile) (AMBN) as the initiator. The composition of the polymerization system was: ATM/AMBN/xylene = 50ml/0.5g/100ml. The polymerization was carried out at 65°C.

8.2.3 Silane grafting

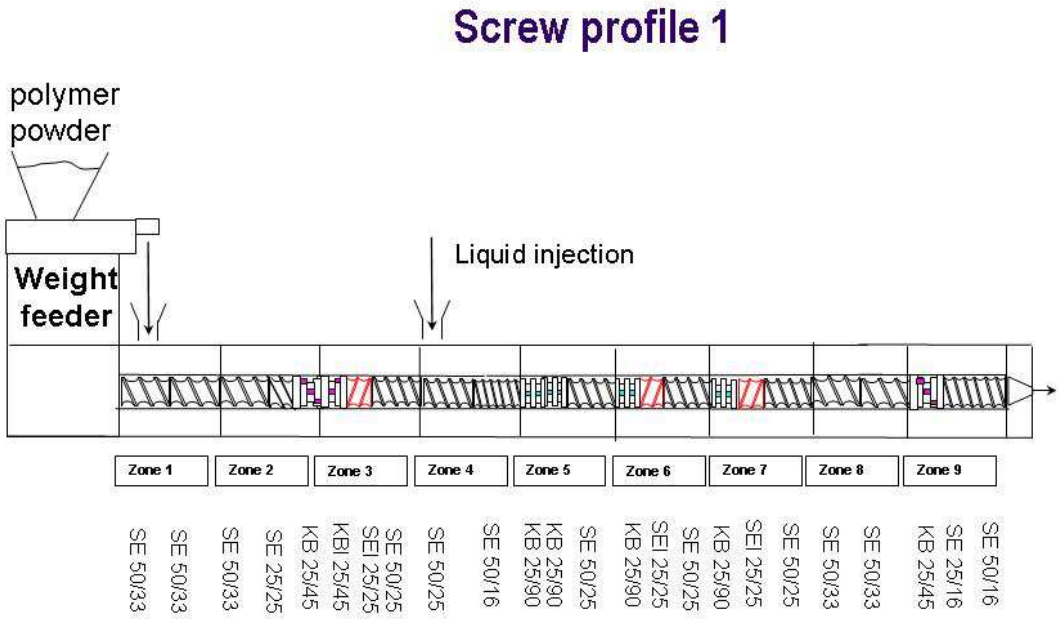

(a) Screw profile 1

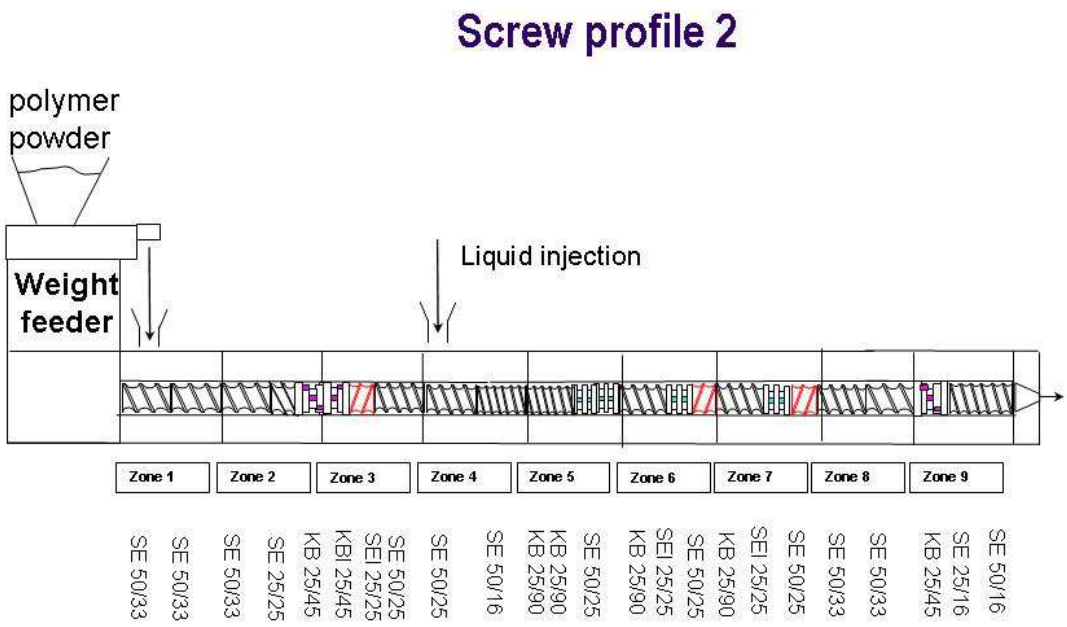

(b) Screw profile 2

Figure 8.4: Screw profiles 1 and 2

The silane grafting process was carried out in a twin-screw extruder. Two screw profiles were used for the free radical grafting of silane onto PP and they are shown in Figure 8.4. The PP was fed at the hopper, after PP was melted, the mixture of required amounts of ATM, coagent, peroxide and additive were added into the apparatus. The PP was fed at the hopper and the small molecules including the peroxide were injected to the

extruder at Zone 4. The only difference between those two screw profiles was that the second kneading zone of the first screw profile was closer to the injection port of the small molecules than the second one. The objective was to study the effect of local mixing between PP and small molecule reagents on the quality of the grafted product in terms of the percentages of grafted and homo-polymerized silanes as well as the degree of PP chain degradation as a result of free radical chemistry. For all runs, the composition of the grafting system was constant and is shown as Table 8.2.

Table 8.2: Composition of the grafting system

Type	Nature	Ingredients Ref.	Physical	Ratio (% weight)	Ratio (phr)
Polymer 1	PP	PPH760	Pellets	85.59	100.00
Polymer 2	Porus PP	Accurel XP100	Pellets	8.56	10.00
Additive	Aox	Iragox 1010	Powder	0.43	0.50
Additive	Aox	Irgafos 168	Powder	0.43	0.50
Silane	ATM	Dow Corning Z-6530	Liquid	3.00	3.50
Co-Agent	Sorbate	Ethylsorbate	Liquid	1.82	2.13
Additive	Peroxide	Luperox 101	Liquid	0.17	0.20

8.2.4 Determination of percentages of grafted and polymerized silane

Three kinds of samples were pressed to films with 70 μ m thick by melt compression in a hot press at 210°C for FTIR analysis using a Thermo-Nicolet Avatar 370. They were:

- original samples Coming out of the extruder without any further treatment
- dried samples From the original ones in the form of pellets of $\Phi 2mm \times 4mm$, and then drying in a vacuum oven at 120°C for 20 hours in order to remove the residues of ATM and coagent
- extracted samples From the original ones, dissolved in boiling xylene and then precipitated in acetone at room temperature to remove the unreacted monomers and possible ATM polymer.

The method of calculating the percentages of grafted and polymerized ATM was shown as appendix.

Figure 8.5 shows the evolution of the percentage of the loss in mass of each of two samples of DOW CORNING designated as R1 and R2 as a function of the drying time at 120°C. It is seen that for both samples, the loss in mass reaches a plateau after about 10 hours of drying. Moreover, the data are relatively reproducible (each sample is analyzed three times in an independent manner). For those reasons, in this work the drying time determining the percentages of non-reacted ATM and sorbate was chosen to be 20 hours.

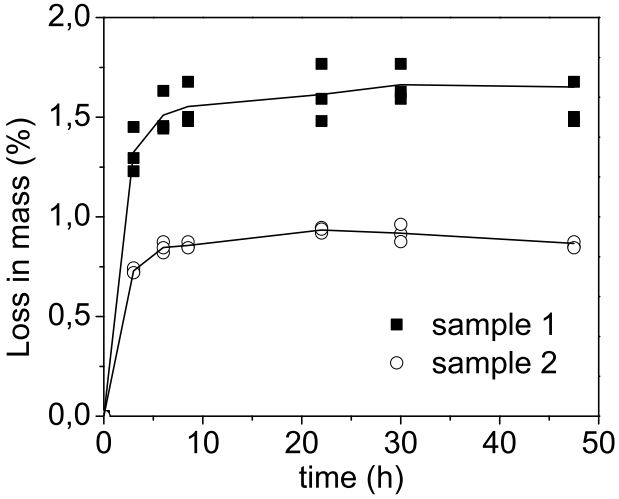

Figure 8.5: Evolution of the percentage of the loss in mass of PP-g-ATM original samples as a function of drying time in a vacuum oven at 120°C.

8.2.5 FTIR analysis

To obtain infrared spectra, a Thermo-Nicolet Avatar 370 FTIR spectrometer was used. Samples were pressed to films about 70μm thick by melt compression in a hot press at 210°C.

8.2.6 Molecular weight distribution

Molecular weight and distribution (MWD) measured using a Viscotek high-temperature gel permeation chromatography (GPC) with triple detectors. The polymer samples were dissolved in 1, 2, 4-trichlorobenzene (TCB) at a concentration of 0.1 wt.% and were measured at 135°C with a flow rate of 1 ml/min. The GPC was equipped with two TSK-GEL and one GMH-H(S)HT columns. The retention times were calibrated at 135°C against known monodisperse polystyrene (PS) standards.

8.2.7 Rheological properties

To study the degree of degradation of PP backbone, dynamic melt rheological measurements were carried out using a Rheometric Scientific RDA3 stress controlled rheometer with parallel plate geometry (diameter of 15mm and a gap of 1.0 mm). Small amplitude oscillatory shear was performed in the frequency range 0.01-100 rad/s at 180°C. A strain of 1% was used. It ensured that all samples were in the linear viscoelastic regime. The values of the complex viscosity, η^* of many samples do not reach its Newtonian-plateau at 0.063 s^{-1}, the lowest frequency value employed in this work. Nevertheless, they are the closest to those of the zero frequency complex viscosity η_0 which are related to the molecular weights of the samples.

8.2.8 Tensile strength

Specimen preparation
1. Original samples in the form of pellets of about $\Phi 2mm \times 4mm$ were dried in vacuum oven at 130°C for 24h, named dried samples.
2. Dried samples were melted in twin screw extruder at 190°C and then injected in the mold at 190°C to get specimens uncrosslinked, the type of the specimen is shown in Figure 8.6.
3. Uncrosslinked specimens were crosslinked in boiling 1% acetic acid aqueous solution for 24h to get specimens crosslinked.

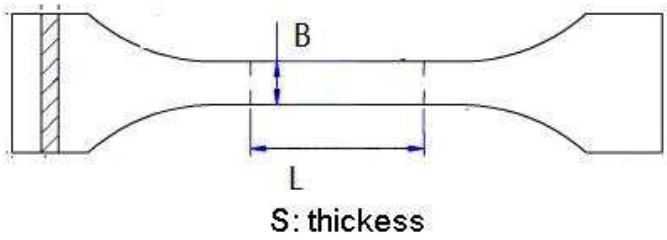

Figure 8.6: Form of the specimen, $L = 80$mm, $B = 10$mm, $S = 4$mm

Tensile strength was measured according to Zwick/Roell Z020 at 23 °C, with crosshead speed of 50mm/min. because of the limitation of the amount of the original samples, uncrosslinked samples were tested once and crosslinked samples were repeated twice.

8.3 Results and Discussion

8.3.1 Homopolymerization of ATM

After the polymerization, the polymerized system was a transparent solution and its viscosity became higher. Moreover, no precipitates were found. When it was poured in acetone, chloroform or THF, a new transparent solution was formed. When it was dried in vacuum oven at 60°C for 72h, xylene was evaporated and the remaining system was colourless and transparent gel. Surprisingly, it could not be dissolved in xylene or THF anymore. Apparently, chemical reactions occurr but the types of reactions remain unknown.

8.3.2 FTIR characterization

To ensure that ATM grafting occurres during the processing, FTIR spectroscopy was performed on original samples, dried samples and extractive samples. Figure 8.7. and Table 8.3 show the main peak assignments in ATM and polypropylene. There are strong characteristic absorption peaks that are assigned to the silane carbon bonds, Si-CH at 770 cm^{-1} and absorption peaks at 1191 and 1086 cm^{-1} characteristic of the methoxy groups Si-O-CH_3 [Ahmed et al., 2009]. It indicates that silane grafting reactions occur. No significant peak at 1060 cm^{-1}, which was assigned to the Si-O-Si bound[Jain et al.,

2006], illustrates that no cross-linking reaction happen. It is proved by the extraction process that there was no insoluble material during solution.

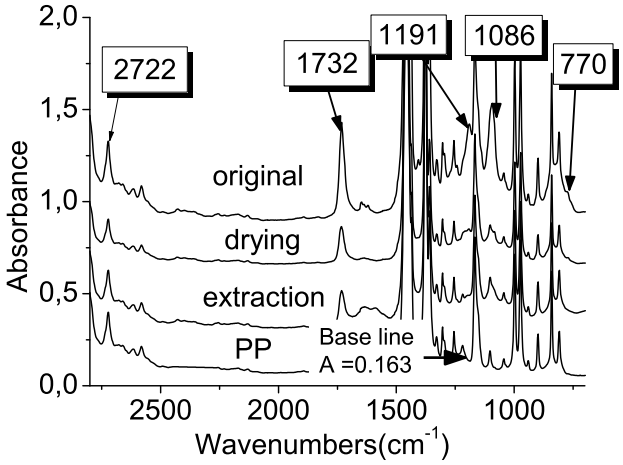

Figure 8.7: FT-IR spectra of the PP and sample 1

Table 8.3: Assignments of IR Spectra

Wavenumber (cm^{-1})	Group	Remark
770	Si-O-CH_3	Si-O-CH_3 (CH3 rocking)
1086	Si-O-C	O-C stretching vibration of reacted or unreacted silane
1191	Si-O-C	O-CH_3 rocking vibration
1732	-C=O	C=O stretching vibration
2722	-C-H	-C-H stretching vibration

The concentration of an entity can be calculated using the Beer-Lambert law:

$$A = \epsilon\, c\, l \tag{8.7}$$

in which A is the absorbance, ϵ the extinction coefficient, c the concentration of the entity and l is the path length.

The peak at 1191cm^{-1} is characteristic of silane and the one at 2720cm^{-1} is characteristic of PP. Therefore $A1191/A2720$ presents the ratio between the mass of silane and that of PP. Since the absorbance of the pure PP at 1191cm^{-1} is not zero, it should be substracted when determining the absorbance of PP-g-ATM product at this wave number. If it is assumed that there is no loss in small molecules during the reactive extrusion process and during the preparation of films by compression in a hot press at 210°C of the original samples, the values of A_{1191}/A_{2720} of all the original samples should be a constant. They should correspond to the maximum silane content in the PP, namely, 3.5g silane per 100g PP (see Table 8.2). Table 8.4 confirms that the A_{1191}/A_{2720} values of original

samples are almost the same, except Q10-5 and Q5.5-4-p2. The maximum A1191/A2720 of the original sample is 1.346 and is chosen to correspond to the maximum silane content in the PP. Figure 8.8 and Table 8.5 compare percentage of reacted ATM, which is the sum of the percentages of both grafted and polymerized ATM, calculated by the mathod of loss in mass and by that of FTIR. It is seen that most data points fall on both sides of the diagonal line and that they are very scattered. This indicates that at least one of the two methods is not good.

The loss in mass method developed in this work is simple and convenient. However, its accuracy could be jeopardized by the loss of non-reacted silane and sorbate molecules during the reactive extrusion process and during the storage of the original samples. As for the FTIR method, it may also have trouble with the loss of non-reacted silane and sorbate molecules during the preparation of films by compression in a hot press at 210°C of the original samples. Dried and extracted samples do not have this problem because free silane and sorbate are removed from the PP-g-ATM product. Therefore, it is believed that the results obtained from FTIR are more reproducible and reliable. This is further confirmed by repeated experiments (Table 8.6). The experimental errors are within 15%, which is acceptable.

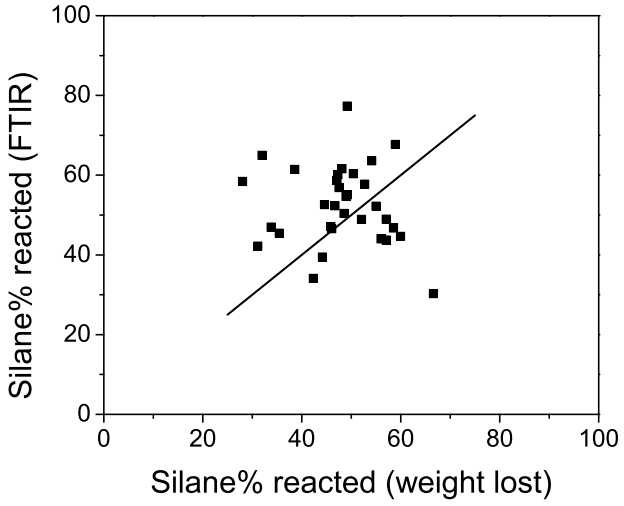

Figure 8.8: Comparison of the percentage of reacted ATM calculated by loss in mass and that by FTIR. The diagonal line corresponds to the percentage of reacted silane calculated by loss in mass with respect to the percentage of reacted silane calculated by FTIR.

Table 8.4: Ratios of absorbance between characteristic peaks and percentages of reacted silane

Sample	Original $\frac{A1191}{A2720}$	Dried $\frac{A1191}{A2720}$	Extracted $\frac{A1191}{A2720}$	Reacted $\frac{A1191}{A2720}$	Silane%* grafted	Silane%* polymerized	Silane%* reacted
Q10-1	1.228	0.823	0.800	0.023	44.74	2.33	47.07
Q10-2	1.102	0.748	0.525	0.223	16.91	22.57	39.48
Q10-3	1.131	0.695	0.475	0.220	11.85	22.26	34.12
Q10-4	1.143	0.790	0.570	0.220	21.47	22.26	43.73
Q10-5	0.780	0.657	0.505	0.152	14.89	15.38	30.27
Q10-6	1.034	0.793	0.564	0.229	20.86	23.18	44.03
Q10-7	1.037	0.799	0.523	0.276	16.71	27.93	44.64
Q5.5-1	1.208	0.878	0.731	0.147	37.76	14.88	52.64
Q5.5-2	1.332	0.967	0.554	0.413	19.85	41.80	61.64
Q5.5-3	1.281	0.902	0.658	0.244	30.37	24.69	55.07
Q5.5-4	1.161	0.920	0.612	0.308	25.72	31.17	56.89
Q1-1	1.228	0.986	0.496	0.490	13.98	49.62	63.60
Q1-2	1.141	0.820	0.575	0.245	21.97	24.79	46.76
Q1-3	1.227	1.027	0.652	0.375	29.76	37.96	67.72
Q1-4	1.183	0.954	0.582	0.372	22.68	37.66	60.34
Q1-5	1.181	0.928	0.607	0.321	25.21	32.52	57.73
Q1-6	1.280	0.952	0.755	0.197	40.19	19.98	60.16
Q1-7	1.169	0.874	0.613	0.261	25.82	26.40	52.22
Q1-8	1.273	0.875	0.544	0.331	18.83	33.50	52.33
Q5.5-t1-re	1.119	1.000	0.638	0.362	28.35	36.64	64.98
Q5.5-t2-re	1.346	0.965	0.778	0.187	42.52	18.93	61.44
Q5.5-t3-re	1.244	1.122	0.896	0.226	54.46	22.87	77.33
Q5.5-t4-re	1.167	0.938	0.758	0.180	40.49	18.22	58.71
Q5.5-1-p2	1.307	0.822	0.696	0.126	34.22	12.75	46.97
Q5.5-2-p2	1.321	0.807	0.582	0.225	22.68	22.77	45.45
Q5.5-3-p2	1.259	0.775	0.582	0.193	22.67	19.55	42.22
Q5.5-4-p2	0.841	0.841	0.532	0.309	17.62	31.27	48.89
Q5.5-5-p2	1.184	0.856	0.576	0.280	22.07	28.34	50.41
Q5.5-6-p2	1.156	0.818	0.546	0.272	19.04	27.53	46.56
Q5.5-7-p2	1.172	0.842	0.688	0.154	33.41	15.59	48.99
Q5.5-8-p2	1.234	0.935	0.731	0.204	37.76	20.65	58.41
Q5.5-9-p2	1.141	0.898	0.615	0.283	26.02	28.64	54.66

'p2'	Profile 2
Q5,5-t'i'-re	'i'th repeated sample with the same condition
*	Percentage of reacted silane calculated based on FTIR

Table 8.5: Percentage of the loss in mass determined by vacuum drying

Sample	Feed rate (kg/hr)	Temp (°C)	Screw speed (rpm)	Loss in mass (%)	Silane%# reacted	Silane%* reacted	Silane%* - Silane%#
Q10-1	10	200	100	2.61	45.85	47.07	1.22
Q10-2	10	200	300	2.69	44.19	39.48	-4.71
Q10-3	10	200	500	2.78	42.32	34.12	-8.21
Q10-4	10	220	100	2.07	57.05	43.73	-13.32
Q10-5	10	220	300	1.61	66.60	30.27	-36.33
Q10-6	10	240	100	2.12	56.02	44.03	-11.98
Q10-7	10	240	500	1.93	59.96	44.64	-15.32
Q5.5-1	5.5	200	300	2.67	44.61	52.64	8.03
Q5.5-2	5.5	220	100	2.50	48.13	61.64	13.51
Q5.5-3	5.5	220	300	2.45	49.17	55.07	5.90
Q5.5-4	5.5	220	500	2.53	47.51	56.89	9.38
Q1-1	1	200	100	2.21	54.15	63.60	9.45
Q1-2	1	200	300	2.00	58.51	46.76	-11.75
Q1-3	1	200	500	1.98	58.92	67.72	8.80
Q1-4	1	200	300	2.39	50.41	60.34	9.93
Q1-5	1	220	100	2.28	52.70	57.73	5.03
Q1-6	1	220	300	2.54	47.30	60.16	12.86
Q1-7	1	240	100	2.17	54.98	52.22	-2.76
Q1-8	1	240	500	2.57	46.68	52.33	5.65
Q5.5-t1-re	5.5	220	300	3.28	31.95	64.98	33.03
Q5.5-t2-re	5.5	220	300	2.96	38.59	61.44	22.85
Q5.5-t3-re	5.5	220	300	2.45	49.17	77.33	28.16
Q5.5-t4-re	5.5	220	300	2.55	47.10	58.71	11.61
Q5.5-1-p2	5.5	200	100	3.19	33.82	46.97	13.15
Q5.5-2-p2	5.5	200	300	3.11	35.48	45.45	9.97
Q5.5-3-p2	5.5	200	500	3.32	31.12	42.22	11.10
Q5.5-4-p2	5.5	220	100	2.31	52.07	48.89	-3.18
Q5.5-5-p2	5.5	220	300	2.48	48.55	50.41	1.86
Q5.5-6-p2	5.5	220	500	2.60	46.06	46.56	0.51
Q5.5-7-p2	5.5	240	100	2.07	57.05	48.99	-8.06
Q5.5-8-p2	5.5	240	300	3.47	28.01	58.41	30.40
Q5.5-9-p2	5.5	240	500	2.46	48.96	54.66	5.70

'p2'	Profile 2
Q5,5-t'i'-re	'i'th repeated sample with the same condition
#	Percentage of reacted silane calculated based on the weight lost
*	Percentage of reacted silane calculated based on FTIR

Table 8.6: Reproducibility of FTIR results

Sample	A1732/A2720	A1191/A2720	A1086/A2720	A1086/A1191
R1-1extr-1	0.613	0.568	0.590	1.038
R1-1extr-2	0.734	0.723	0.768	1.053
R2-1extr-1	0.506	0.514	0.553	1.077
R2-1extr-2	0.505	0.475	0.518	1.092
R2-2extr-2	0.637	0.607	0.623	1.027
Q10-3-1extr-1	0.615	0.639	0.615	1.003
Q10-3-1extr-2	0.693	0.660	0.693	1.038
Q10-3-2extr-2	0.636	0.645	0.636	1.020
Q1-3-1extr-1	0.774	0.652	0.690	1.059
Q1-3-1extr-2	0.892	0.790	0.837	1.061

-1extr:	extraction once
-2extr:	extraction twice
-1:	first sample
-2:	second sample

8.3.3 Percentages of grafted and polymerized silane as well as reacted silane

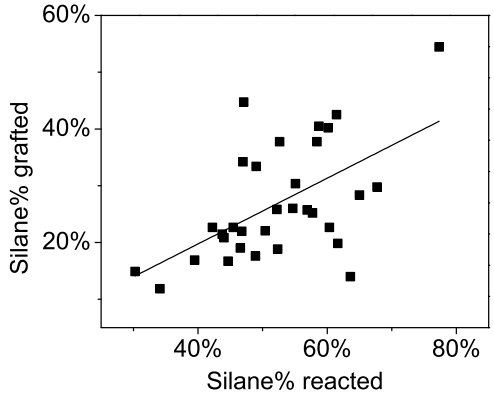

(a) Percentage of grafted silane versus that of reacted (grafted and polymerized) silane

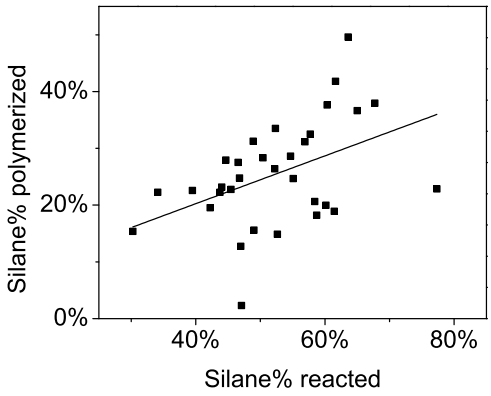

(b) Percentage of polymerized silane versus that of reacted silane

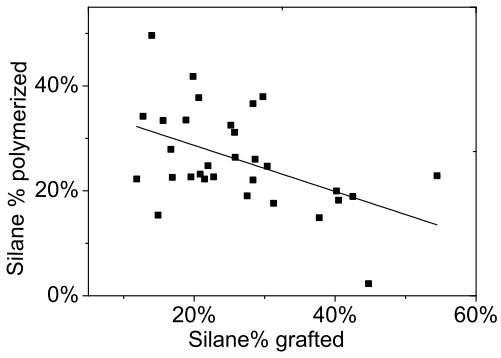

(c) Percentage of grafted silane versus that of polymerized silane

Figure 8.9: Relationships among the percentages of grafted, polymerized and reacted (grafted and polymerized) silane

Relationship among percentages of grafted, polymerized and reacted (grafted and polymerized) silane

Figure 8.9 shows the relationship among the percentages of grafted, polymerized and reacted silane.

Effect of screw speed

Figures 8.10 show the effect of screw speed on the percentages of grafted, polymerized and reacted silane.

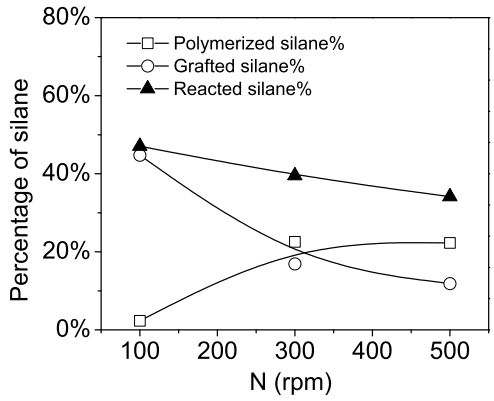

(a) $T = 200°C$, $Q = 10kg/h$; Q10-1, 2,3

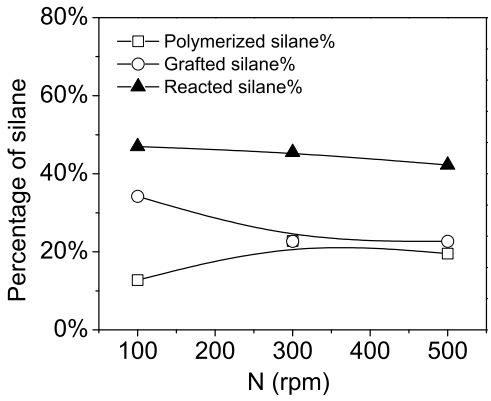

(b) $T = 200°C$, $Q = 5.5kg/h$; Q5.5-1-p2, Q5.5-2-p2, Q5.5-3-p2

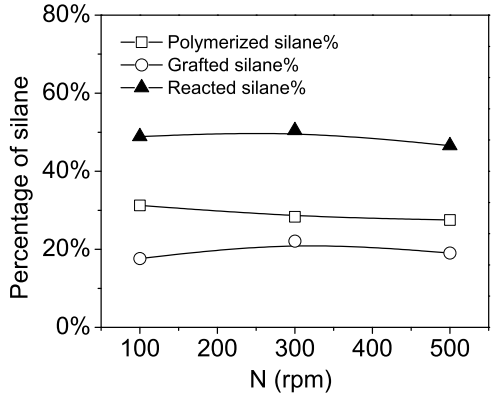

(c) $T = 220°C$, $Q = 5.5kg/h$; Q5.5-4-p2, Q5.5-5-p2, Q5.5-6-p2

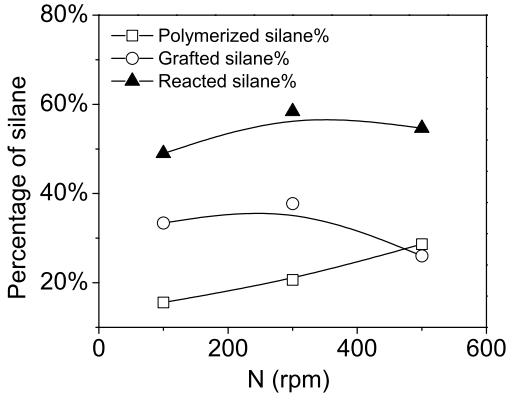

(d) $T = 240°C$, $Q = 5.5kg/h$; Q5.5-7-p2, Q5.5-8-p2, Q5.5-9-p2

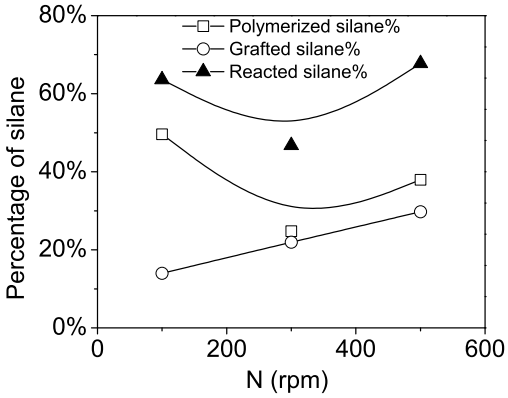

(e) $T = 200°C$, $Q = 1kg/h$; Q1-1, 2, 3

Figure 8.10: Effect of screw speed on the percentages of grafted, polymerized and reacted silane

Effect of barrel temperature

Figures 8.11 show the effect of barrel temperature on the percentages of grafted, polymerized and reacted silane.

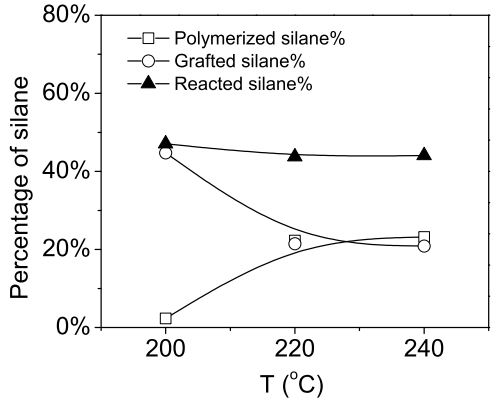

(a) $Q = 10$kg/h, $N = 100$rpm; Q10-1, 4, 6

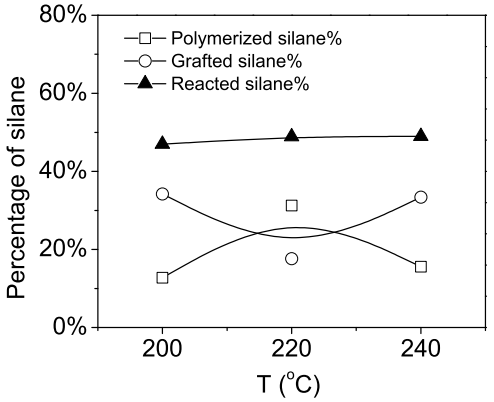

(b) $Q = 5.5$kg/h, $N = 100$rpm; Q5.5-1-p2, 4, 7

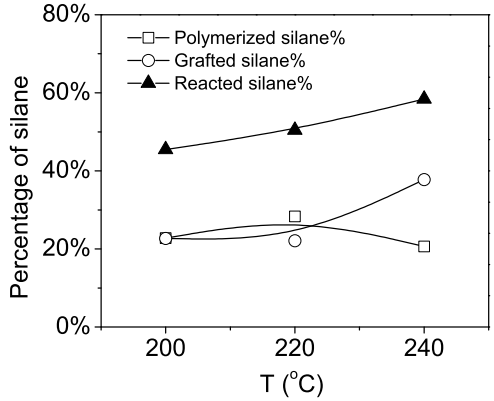

(c) $Q = 5.5$kg/h, $N = 300$rpm; Q5.5-2-p2, 5, 8

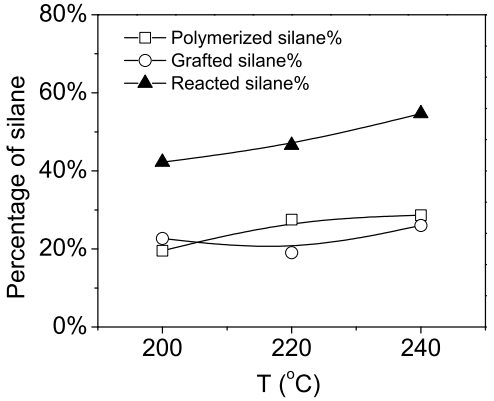

(d) $Q = 5.5$kg/h, $N = 500$rpm; Q5.5-3-p2, 6, 9

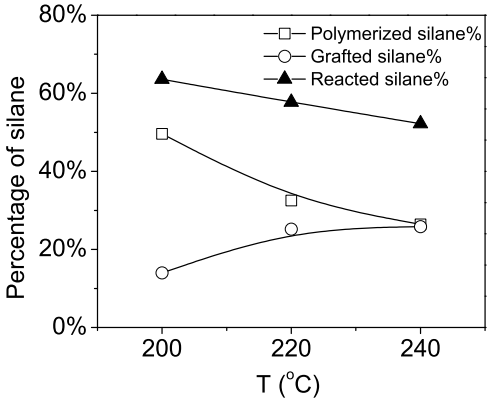

(e) $Q = 1$kg/h, $N = 100$rpm; Q1-1, 5,7

Figure 8.11: Effect of barrel temperature on the percentages of grafted, polymerized and reacted silane.

Effect of feed rate

Figures 8.12 show the effect of feed rate on the percentages of grafted, polymerized and reacted silane.

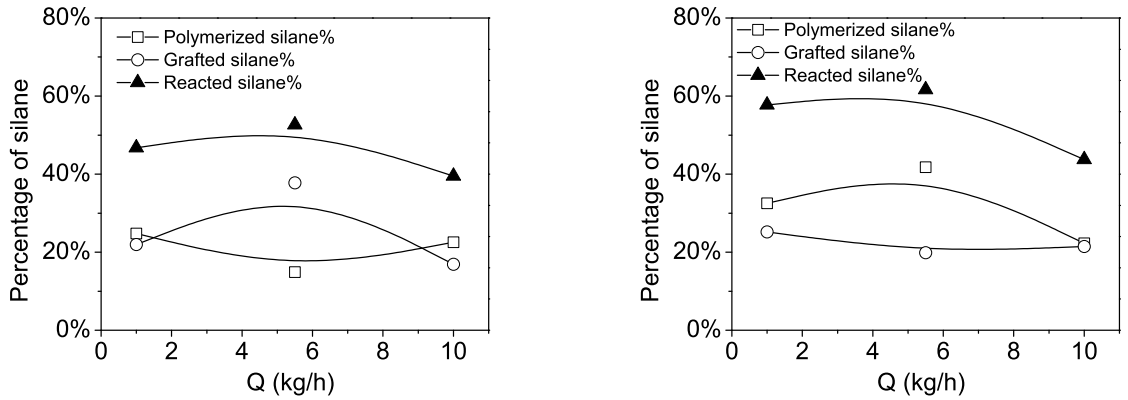

(a) $T = 200°C$, $N = 300$rpm; Q1-2, Q5.5-1, Q10-2 (b) $T = 220°C$, $N = 100$rpm; Q1-5, Q5.5-2, Q10-4

Figure 8.12: Effect of feed rate on the percentages of grafted, polymerized and reacted silane

It is not easy to make obvious conclusions based on these figures as an experimental design was used to design these experiments. Conclusions become obvious after a model is developed, as will be discussed later.

8.3.4 Effect of screw profile on the percentages of grafted and polymerized silane

Table 8.7 compares the two screw profiles in terms of the percentages of grafted and polymerized silane. It is seen that screw profile 1 systematically outperforms screw profile 2 in terms of the percentage of grafted silane except Q5.5-3 and Q5.5-8-p2. In other words, the percentages of grafted silane obtained with screw profile 1 are always higher than those with screw profile 2, indicating that screw profile 1 is more efficient for the grafting of silane. The same is true for the percentage of reacted (grafted and polymerized) silane, indicating that there is less un-reacted silane left in the PP-g-ATM product for screw profile 1. Furthermore, the percentages of polymerized silane obtained with screw profile 1 are always higher than those with screw profile 2. These results show that the quality of local mixing between the PP melt and the liquid reagents is a key to the grafting reaction. In order to ensure good local mixing, it is important that the location at which the liquid reagents are injected be as close as possible to the downstream mixing block. This is the most important conclusion of this work.

Table 8.7: Comparison of Profiles 1 and 2

Sample		$Q5.5-1$ $Q5.5-2-p2$	$Q5,5-2$ $Q5,5-4-p2$	$Q5,5-3$ $Q5,5-8-p2$	$Q5.5-4$ $Q5.5-6-p2$
Feed rate	kg/h	5.5	5.5	5.5	5.5
Temperature	°C	200	220	240	220
Screw speed	rpm	300	100	300	500
Profile 1	Grafted silane%	37.76	19.85	30.37	25.72
	Polymerized silane%	14.88	41.80	24.69	31.17
	Reacted silane%	52.64	61.64	55.07	56.89
Profile 2	Grafted silane%	22.68	17.62	37.76	19.04
	Polymerized silane%	22.77	31.27	20.65	27.53
	Reacted silane%	45.45	48.89	58.41	46.56
Difference between Profiles 1 and 2	Grafted silane%	15.08	2.23	−7.39	6.68
	Polymerized silane%	−7.89	10.53	4.04	3.64
	Reacted silane%	7.19	12.75	−3.34	10.33

8.3.5 Melt viscosity of PP-g-ATM

The values of the complex viscosity, η^* of many samples do not reach its Newtonian-plateau at 0.063 s^{-1}, the lowest frequency value employed in this work. Nevertheless, they are the closest to those of the zero frequency complex viscosity η^0 which are related to the molecular weights of the samples. Table 8.11 shows the values of η^* of PP-g-ATM at 0.063 s^{-1} and 180°C

Effect of screw speed

Figures 8.13, 8.14, 8.15, 8.16 show the effect of screw speed on η^* of PP-g-ATM.

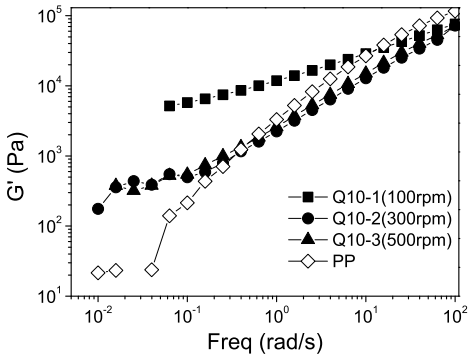

(a) G' of dried samples

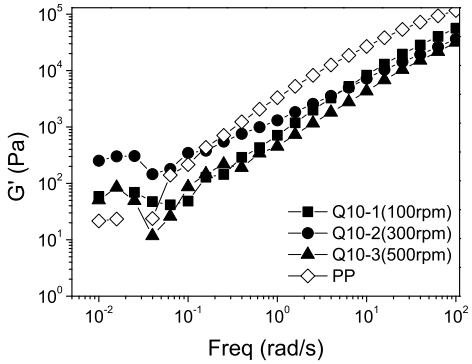

(b) G' of extracted samples

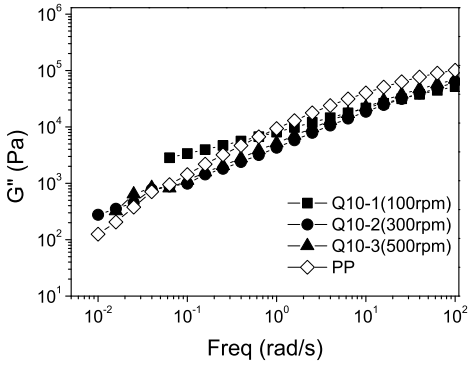

(c) G" of dried samples

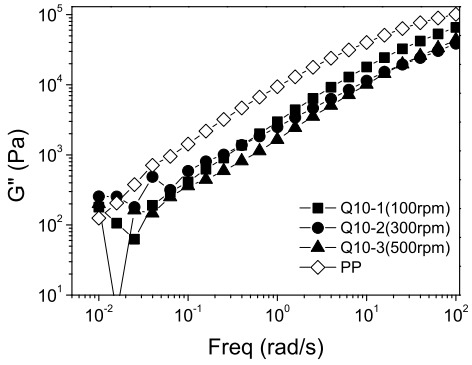

(d) G" of extracted samples

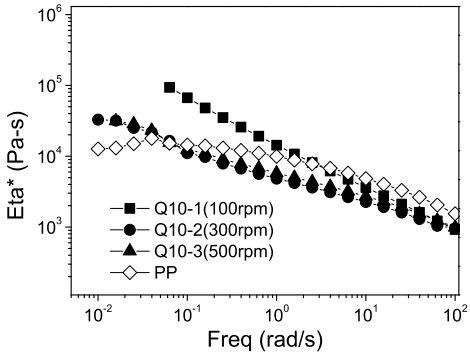

(e) η^* of dried samples

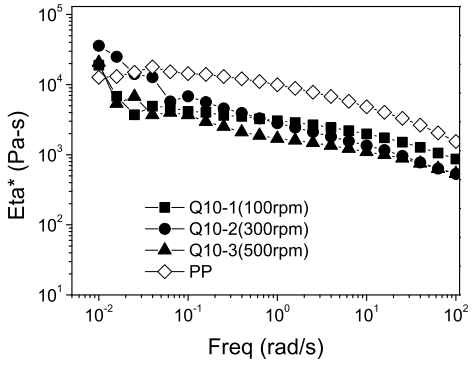

(f) η^* of extracted samples

Figure 8.13: Effect of the screw speed on the rheological properties of PP-g-ATM (T = 200°C, Q = 10kg/h, Q10-1, Q10-2, Q10-3)

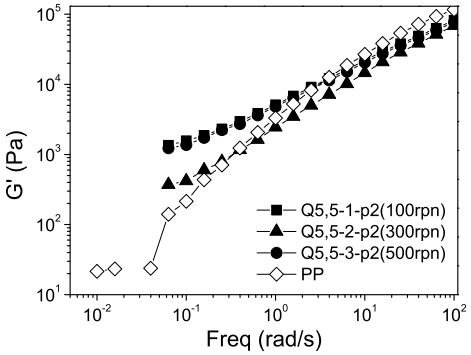

(a) G' of dried samples

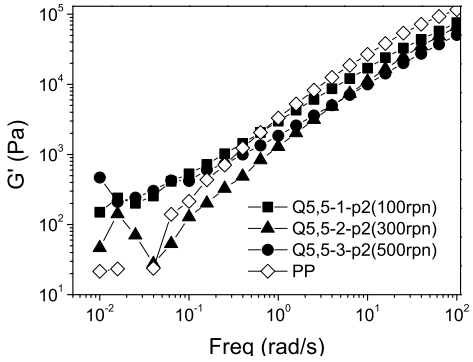

(b) G' of extracted samples

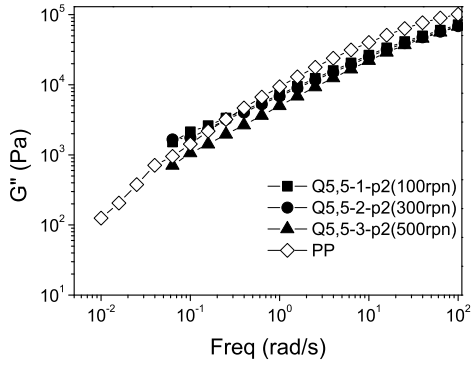

(c) G" of dried samples

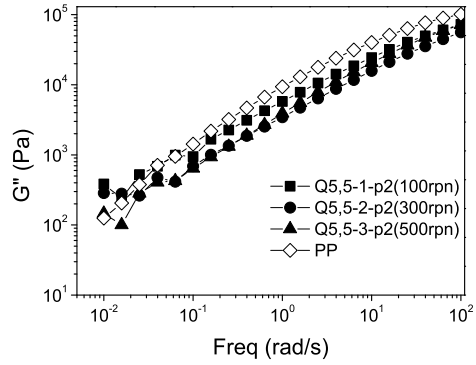

(d) G" of extracted samples

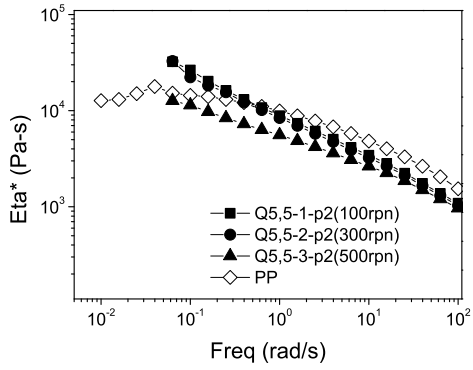

(e) η^* of dried samples

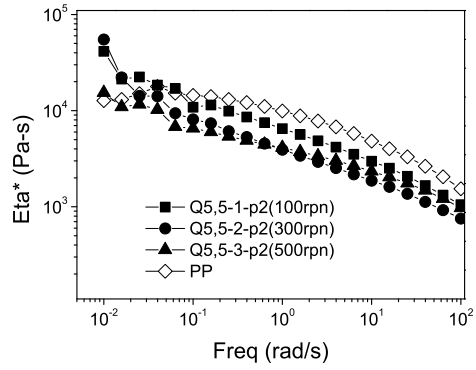

(f) η^* of extracted samples

Figure 8.14: Effect of the screw speed on the rheological properties of PP-g-ATM (T = 200°C, Q = 5.5kg/h, Q5.5-1-p2, Q5.5-2-p2, Q5.5-3-p2

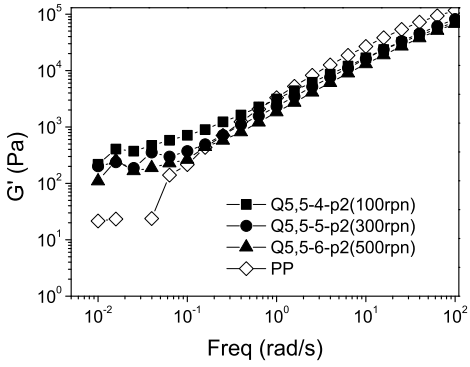

(a) G' of dried samples

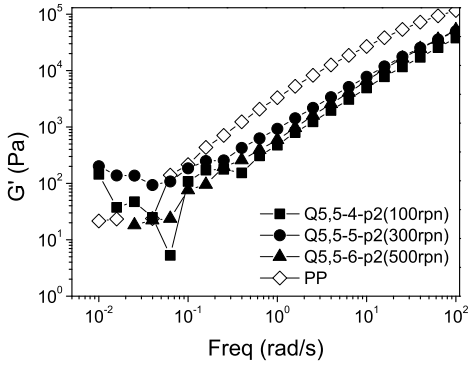

(b) G' of extracted samples

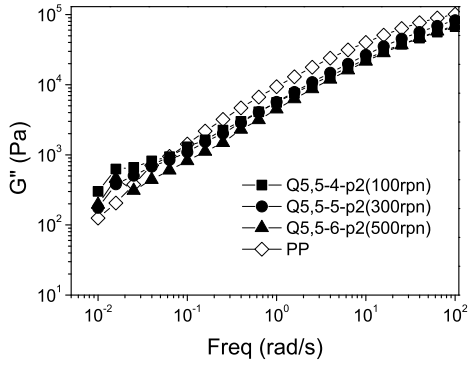

(c) G" of dried samples

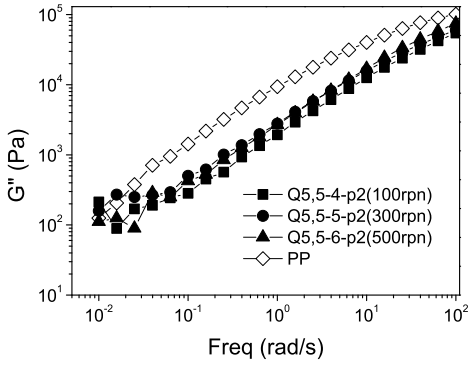

(d) G" of extracted samples

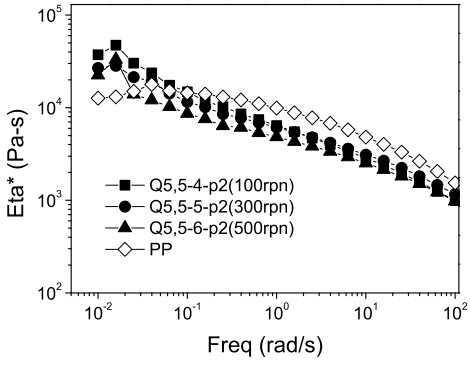

(e) η^* of dried samples

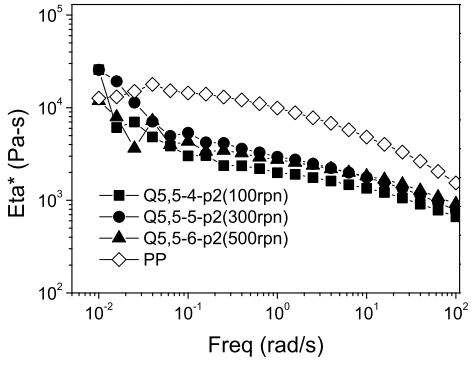

(f) η^* of extracted samples

Figure 8.15: Effect of the screw speed on the rheological properties of PP-g-ATM (T = 220°C, Q = 5.5kg/h, Q5.5-4-p2, Q5.5-5-p2, Q5.5-6-p2)

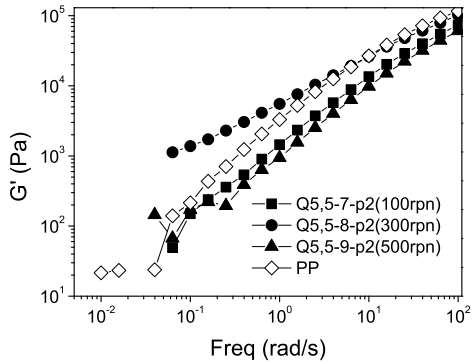

(a) G' of dried samples

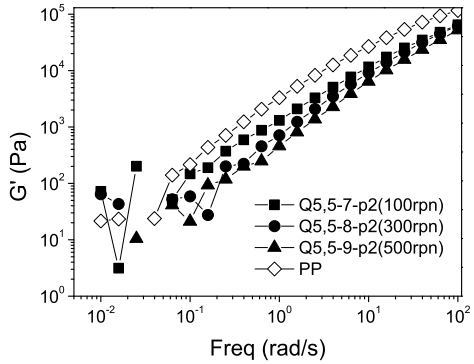

(b) G' of extracted samples

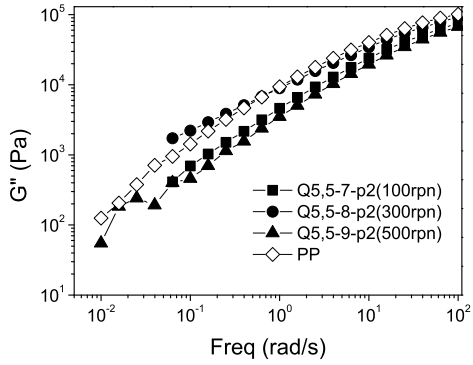

(c) G" of dried samples

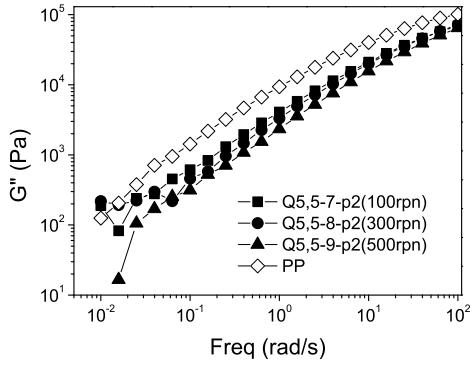

(d) G" of extracted samples

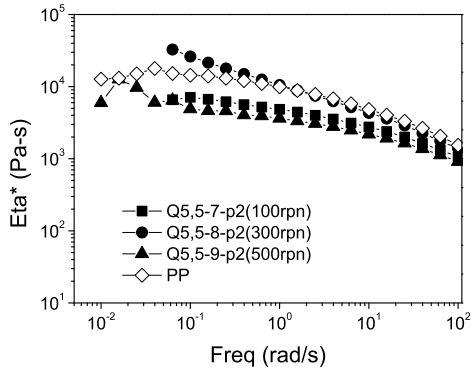

(e) η^* of dried samples

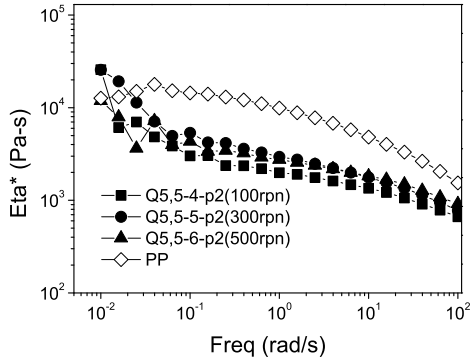

(f) η^* of extracted samples

Figure 8.16: Effect of the screw speed on the rheological properties of PP-g-ATM (T = 240°C, Q = 5.5kg/h, Q5.5-7-p2, Q5.5-8-p2, Q5.5-9-p2)

Effect of barrel temperature

Figures 8.17, 8.18, 8.19, 8.20, 8.21 show the effect of barrel temperature on η^* of PP-g-ATM

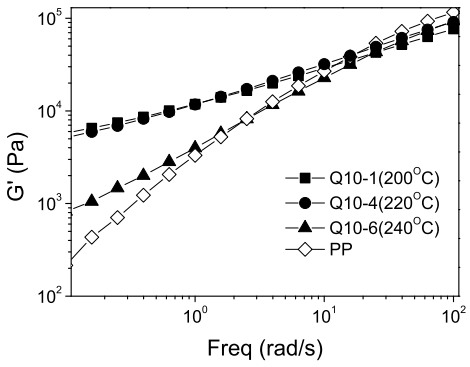

(a) G' of dried samples

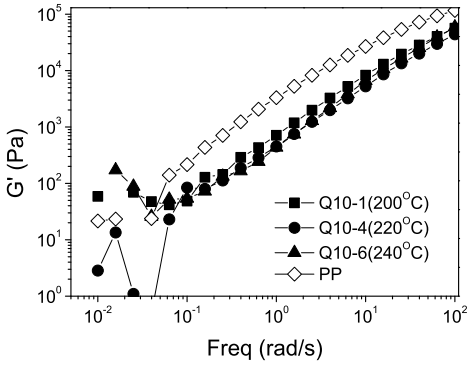

(b) G' of extracted samples

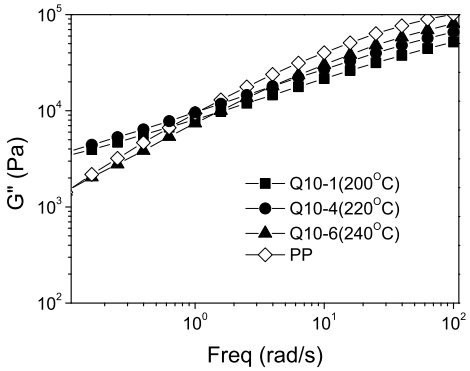

(c) G" of dried samples

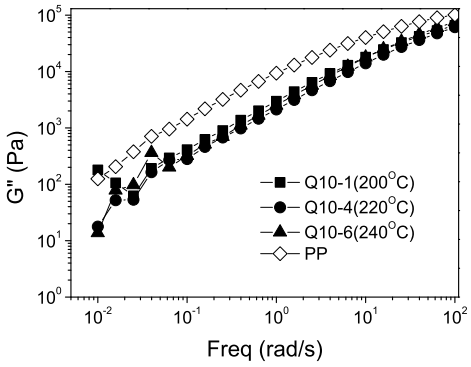

(d) G" of extracted samples

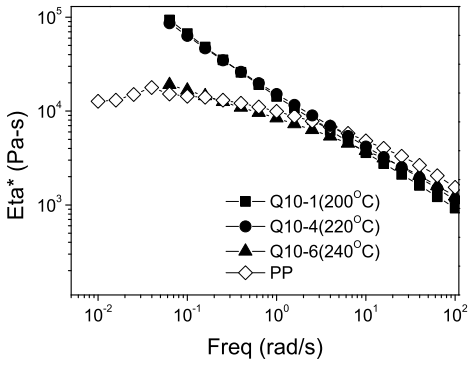

(e) η^* of dried samples

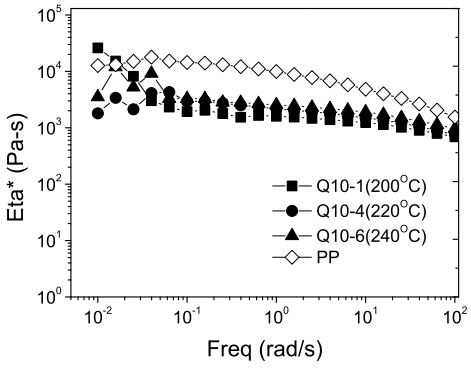

(f) η^* of extracted samples

Figure 8.17: Effect of the screw speed on the rheological properties of PP-g-ATM (N = 100rpm, Q = 10kg/h, Q10-1, Q10-4, Q10-6)

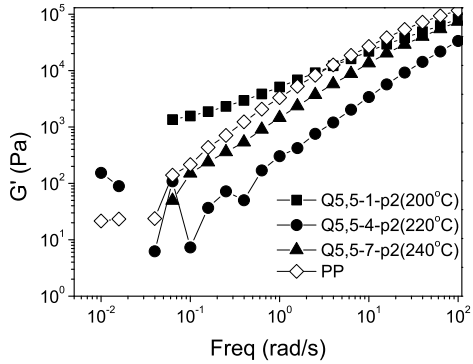

(a) G' of dried samples

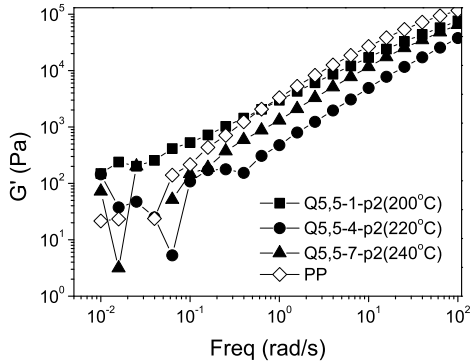

(b) G' of extracted samples

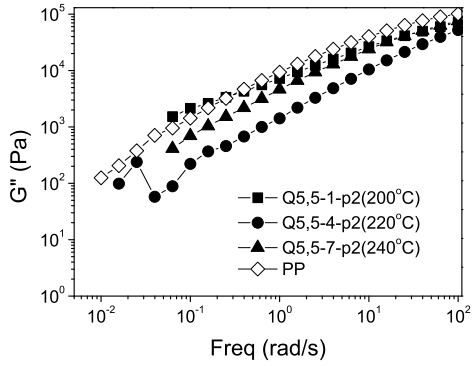

(c) G" of dried samples

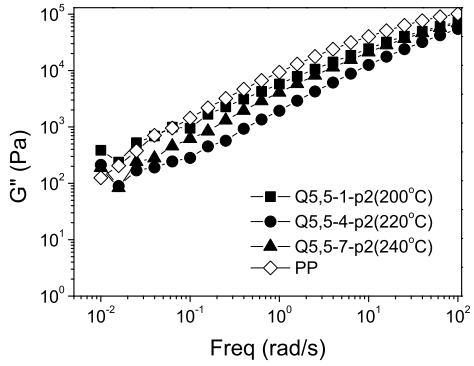

(d) G" of extracted samples

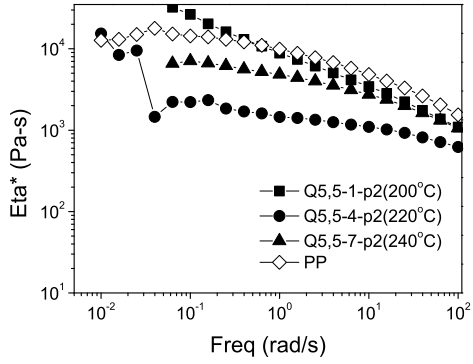

(e) η^* of dried samples

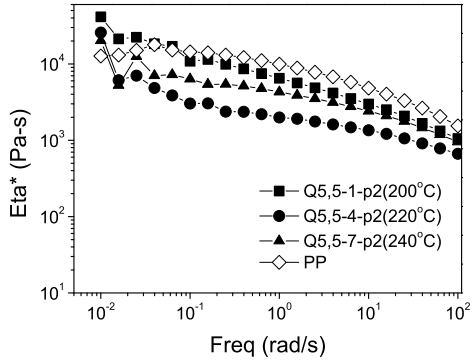

(f) η^* of extracted samples

Figure 8.18: Effect of the screw speed on the rheological properties of PP-g-ATM (N = 100rpm, Q = 5.5kg/h, Q5.5-1-p2, Q5.5-4-p2, Q5.5-7-p2)

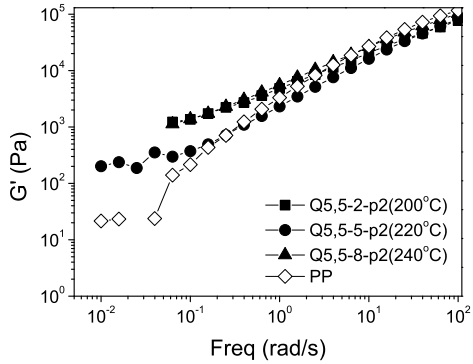

(a) G' of dried samples

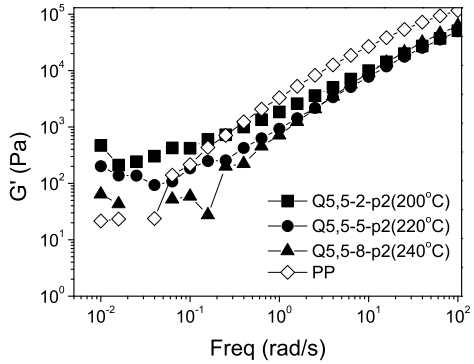

(b) G' of extracted samples

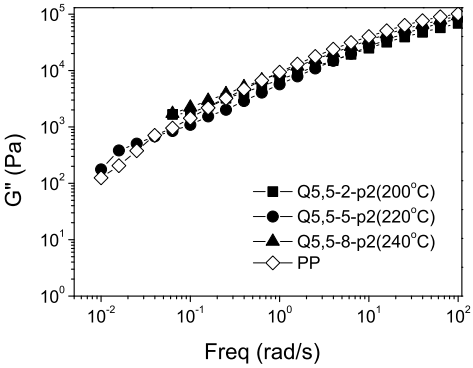

(c) G" of dried samples

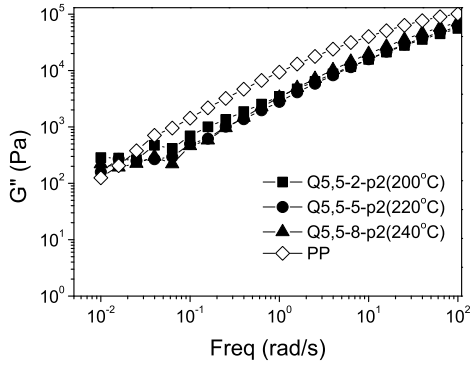

(d) G" of extracted samples

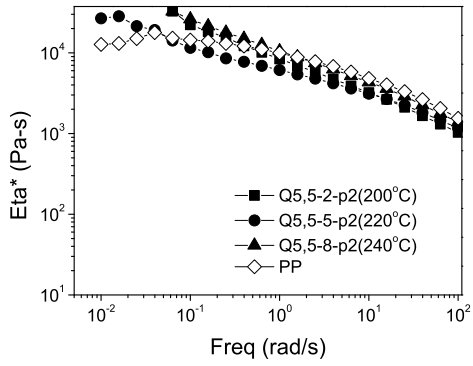

(e) η^* of dried samples

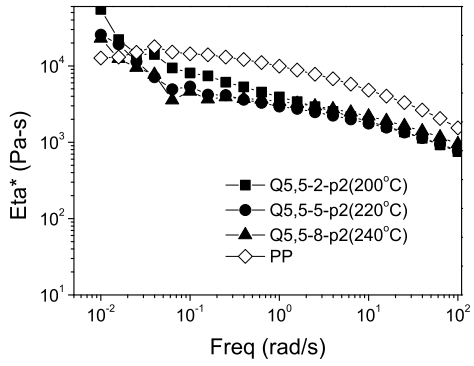

(f) η^* of extracted samples

Figure 8.19: Effect of the screw speed on the rheological properties of PP-g-ATM (N = 300rpm, Q = 5.5kg/h, Q5.5-2-p2, Q5.5-5-p2, Q5.5-8-p2)

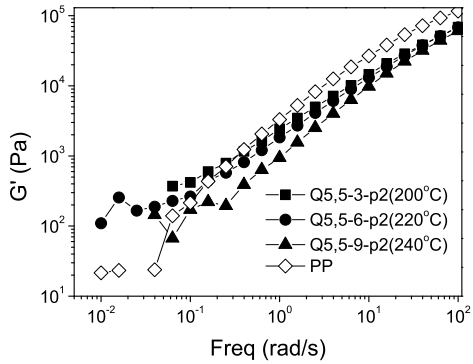

(a) G' of dried samples

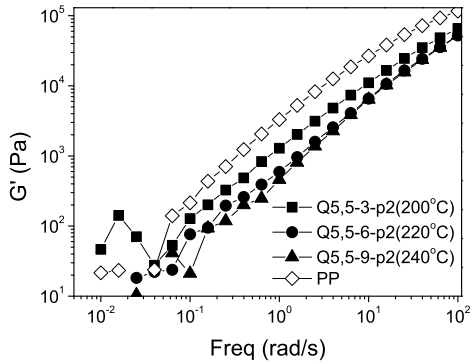

(b) G' of extracted samples

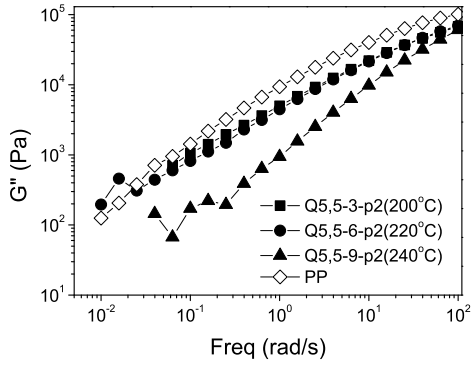

(c) G" of dried samples

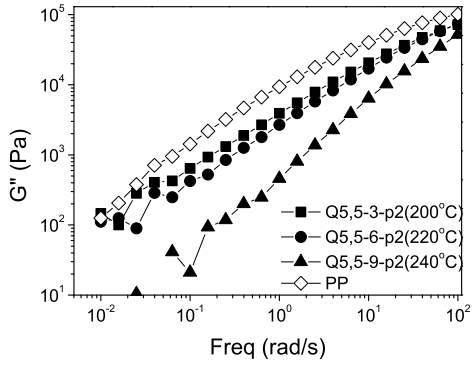

(d) G" of extracted samples

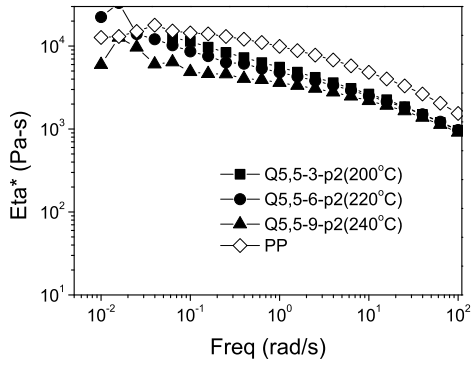

(e) η^* of dried samples

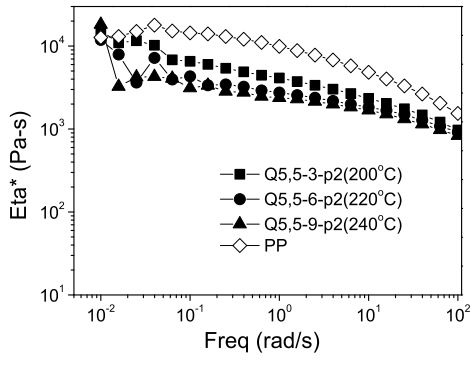

(f) η^* of extracted samples

Figure 8.20: Effect of the screw speed on the rheological properties of PP-g-ATM (N = 300rpm, Q = 5.5kg/h, Q5.5-3-p2, Q5.5-6-p2, Q5.5-9-p2)

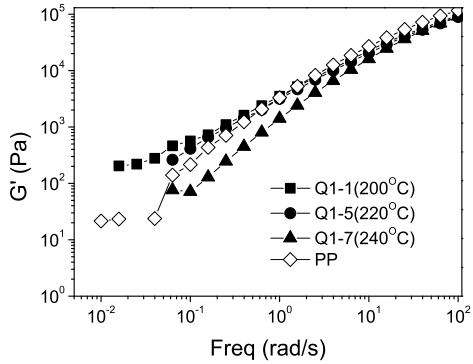

(a) G' of dried samples

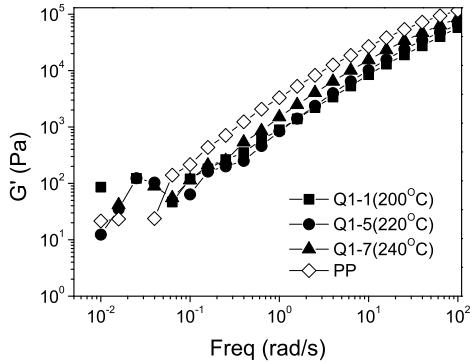

(b) G' of extracted samples

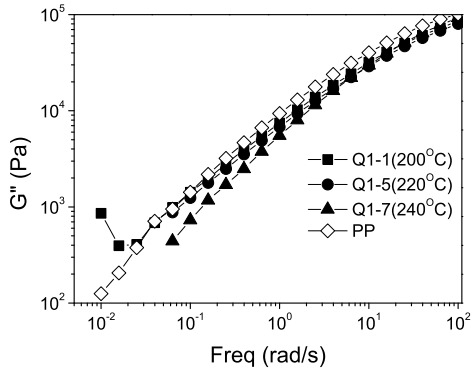

(c) G" of dried samples

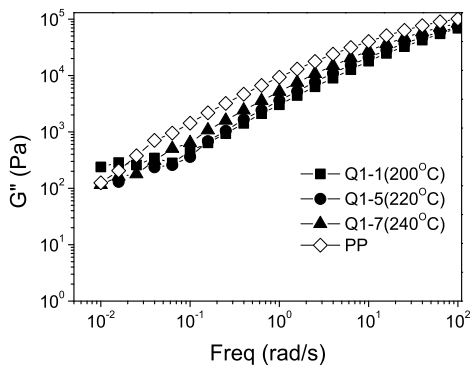

(d) G" of extracted samples

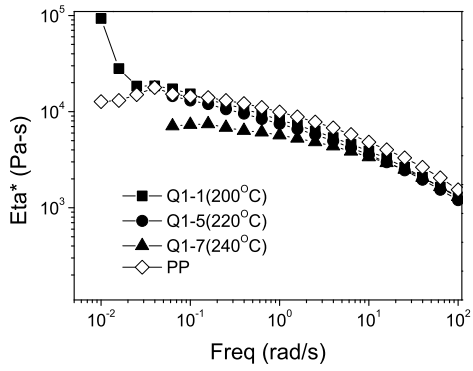

(e) η^* of dried samples

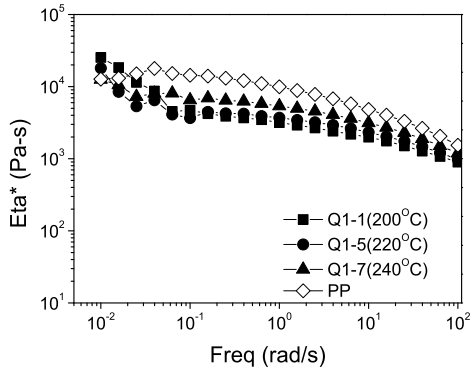

(f) η^* of extracted samples

Figure 8.21: Effect of the screw speed on the rheological properties of PP-g-ATM (N = 100rpm, Q = 1kg/h, Q1-1, Q1-5, Q1-7)

Effect of feed rate

Figures 8.22 show the effect of feed rate on η^* of PP-g-ATM

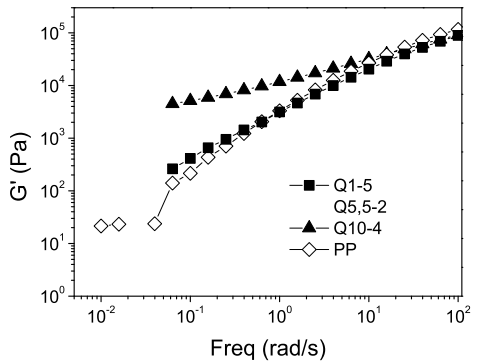

(a) G' of dried samples

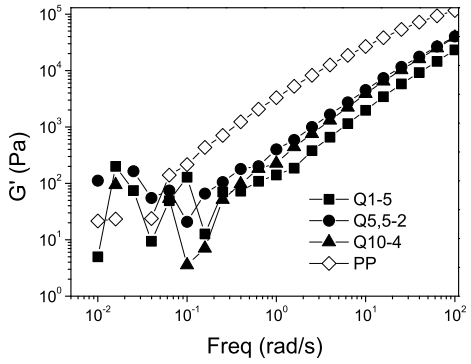

(b) G' of extracted samples

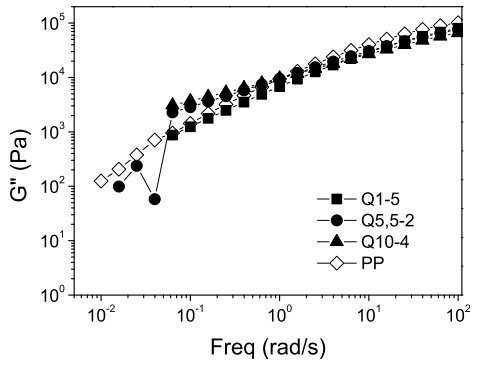

(c) G" of dried samples

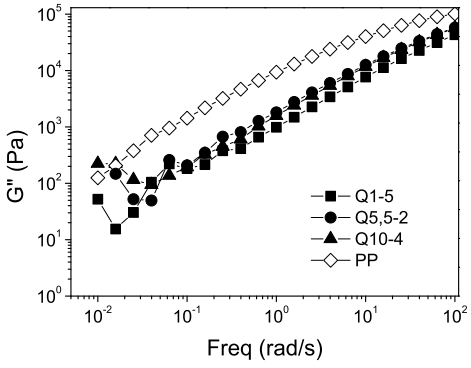

(d) G" of extracted samples

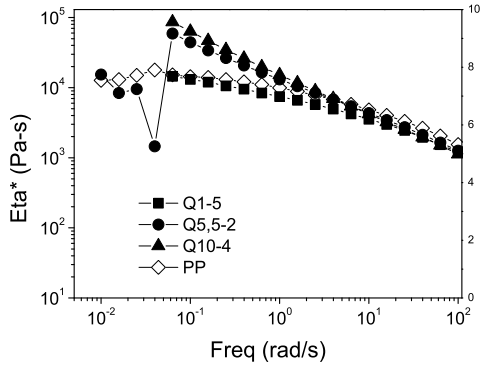

(e) η^* of dried samples

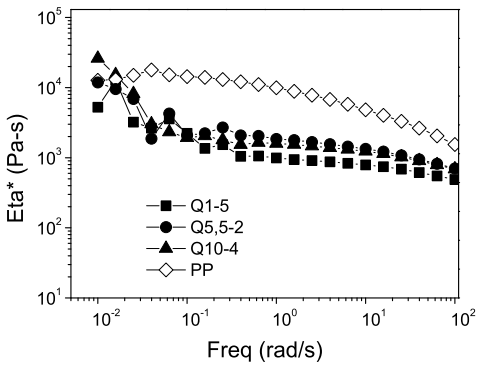

(f) η^* of extracted samples

Figure 8.22: Effect of the screw speed on the rheological properties of PP-g-ATM ($T = 220°C$, $N = 100$rpm, Q1-5, Q5.5-2, Q10-4)

The following remarks can be made based on Table 8.11 and the Figures 8.13, 8.14, 8.15, 8.16, 8.17, 8.18, 8.19, 8.20, 8.21, 8.22 :

- The process conditions allow tuning the close-to-zero-frequency viscosity of the PP-g-ATM by a factor of 10 ranging from $7.1\,10^4$ to $5.6\,10^5$ Pa.s.
- If sample Q1-6-dry is ignored, with the decrease of the feed rate, or the increase of

the barrel temperature and/or the screw speed, the viscosity will decrease, which indicates that the PP chain degradation will be severe. In other words, a long residence time, a high barrel temperature and/or strong mixing intensity will make the PP chain degradation severe.

- It appears that the feed rate and barrel temperature have greater effects than the screw speed.

8.3.6 Effect of Q and N for a given Q/N for screw profile 2

The ratio between feed rate and screw speed, Q/N, characterizes the overall degree of fill and intensity of mixing in a twin screw extruder. Table 8.8 shows the percentages of grafted, polymerized and reacted silane as well as the melt viscosity of the dried PP-g-ATM products for a ratio Q/N of 1.1/60 kg/screw turn and screw profile 2 which is more sensitive to processing parameters. For one silane and two silane grafting systems, a high feed rate and a high screw speed will decrease the percentage of grafted silane. The same is true for the percentage of reacted silane, within experimental errors. By contrast, the percentage of polymerized silane follows more or less the opposite trend.

Table 8.8: Effect of Q and N on the percentages of grafted, polymerized and reacted silane for a given Q/N of 1.1/60 kg/screw turn

Sample	Feed rate (kg/hr)	Temp (°C)	Screw speed (rpm)	Grafted silane%	Polymerized silane%	Reacted silane%	$\eta_{0.063}$(10^4Pa.s) Dry	extr
Q5.5-Q/N-1s	5.5	220	300	26.83	34.76	61.59	0.442	0.077
Q8-Q/N-1s	8	220	440	19.10	24.21	43.31	0.166	0.094
Q10-Q/N-1s	10	220	545	16.40	27.68	44.07	0.185	0.080
Q2-Q/N-2s	2	220	109	29.13	16.66	45.80	0.229	0.091
Q8-Q/N-2s	8	220	440	18.10	23.79	41.89	0.170	0.058
Q/N	Feed rate/screw speed = 1.1/60 kg/screw turn							
1s	One silane (ATM)							
2s	A mixture of two silanes (ATM + another silane)							

When Q/N is fixed, the overall degree of filling and the intensity of mixing are fixed, whatever Q and N. An increase in Q with a concomitant increase in N does not change the degree of fill or the intensity of mixing but shortens the residence time. As a result, the time available for polymerization of silane is shortened and the percentages of grafted and polymerized silane are reduced. This indicates that apart from local mixing between PP and monomers at the injection location, the residence time is also an important process parameter.

8.3.7 Effect of the nature of silane for screw profile 2

Table 8.9 compares the one silane (ATM) and two silane grafting systems in terms of the grafted and polymerized silane and the melt viscosity. It is noted the performance of these two grafting systems is very close. This is a very interesting result which is also expected.

Table 8.9: Comparison of the one silane and two silane grafting systems in terms of grafted, polymerized and reacted silane

Sample	Feed rate (kg/hr)	Temp (°C)	Screw speed (rpm)	Grafted silane%	Polymerized silane%	Reacted silane%	$\eta_{0.063}$(10^4Pa.s) Dry	extr
Q8-Q/N-1s	8	220	440	19.10	24.21	43.31	0.166	0.094
Q8-Q/N-2s	8	220	440	18.10	23.79	41.89	0.170	0.058
Q/N	Feed rate/screw speed = 1.1 kg/screw turn							
1s	One silane (ATM)							
2s	A mixture of two silanes (ATM + another silane)							

8.3.8 Molecular weight distribution of PP-g-ATM

Figure 8.23 shows a typical GPC curve for a sample that is either dried or extracted. For the dried sample, the molecular weight distribution (MWD) is not monodispersed. There is a small peak corresponding to larger molecular weights. It is assigned to homopolymerized silane. After the extraction this peak disappears. Table 8.10 shows the values of M_n and M_w of some of the PP-g-ATM samples.

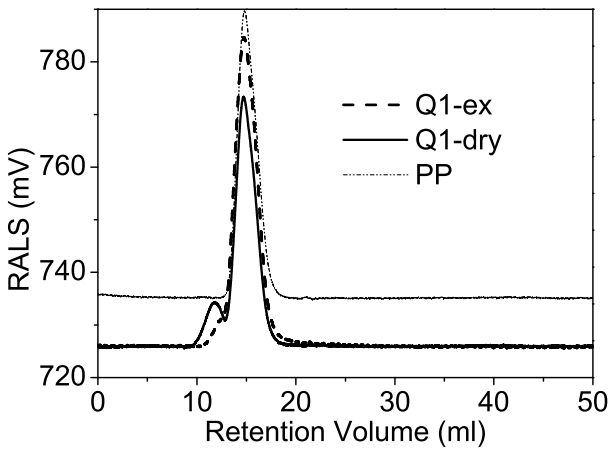

Figure 8.23: Typical GPC curves for dried and extracted PPg-g-ATM (Q1-1)

Table 8.10: Average molecular weights of PP-g-ATM

Sample	Feed rate (kg/h)	Temperature (°C)	Screw speed (rpm)	M_n	M_w	DPI	$\eta_{0.063}$ (10^4Pa.s)
Pure-PP	-	-	-	66833	291637	4.36	1.52
Q1-1-dry	1	200	100	66363	261193	3.94	1.73
Q1-1-ex	1	200	100	110749	304843	2.75	0.45
Q1-5-ex	1	220	100	72895	231217	3.17	0.41
Q1-6-ex	1	220	300	137159	507308	3.70	0.36
Q5,5-2-ex	5.5	220	100	116726	354841	3.04	0.21
Q5,5-3-dry	5.5	240	300	76756	286619	3.73	2.39
Q5,5-3-ex	5.5	220	300	120717	323381	2.68	0.41
Q5,5-4-dry	5.5	220	500	73188	268982	3.68	1.75
Q5,5-4-ex	5.5	220	500	81697	268121	3.28	0.18
Q10-1-ex	10	200	100	75893	257774	3.40	0.33
Q10-3-dry	10	200	500	58666	293697	5.01	1.54
Q10-3-ex	10	200	500	114764	292128	2.55	0.40
Q10-4-ex	10	220	100	77019	280128	3.64	0.29
Q10-5-ex	10	220	300	75376	271119	3.60	0.23
Q10-6-ex	10	240	100	83832	282522	3.37	0.33

'dry' Original samples dried in a vacuum oven
'extr' Samples after extraction

Figure 8.24 shows the relationship between the molecular weight of PP-g-ATM and its complex viscosity. Surprisingly, for both dried and extracted samples, the molecular weight decreases with increasing complex viscosity. This can be explained by the fact that there is always a fraction of the sample that is not fully soluble in the solvent used for the GPC measurement. In other words, GPC only measures the soluble fraction of the sample while the complex viscosity is a measure of the entire sample including both the soluble and insoluble fractions.

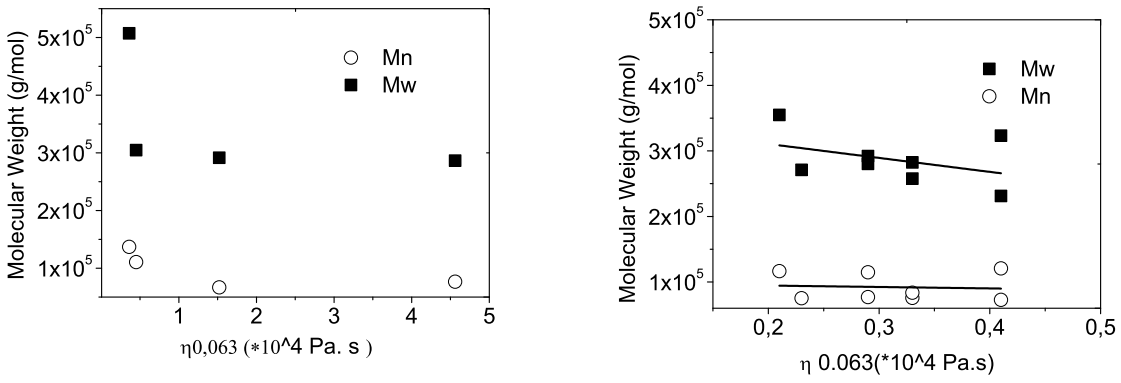

(a) Dried PP-g-ATM samples

(b) Extracted PP-g-ATM samples

Figure 8.24: Relationship between molecular weight and complex viscosity for PP-g-ATM

8.3.9 Tensile strength

Figure 8.25 shows the representative Stress-strain curves of Q5.5-1. The results are shown in Tables 8.11, 8.12. Compared to the pure PP, the silane-grafted samples shows higher tensile stress, with comparable modulus. On contrary, the elongation at yield stress and that at break drop after grafting reaction. A further decrease in this property can be found in the crosslinked sample. Not only the elongation at yield stress and that at break, but also tensile stress and modulus change upon crosslinking. An increase in tensile stress and modulus is observed due to the presence of crosslink net work.

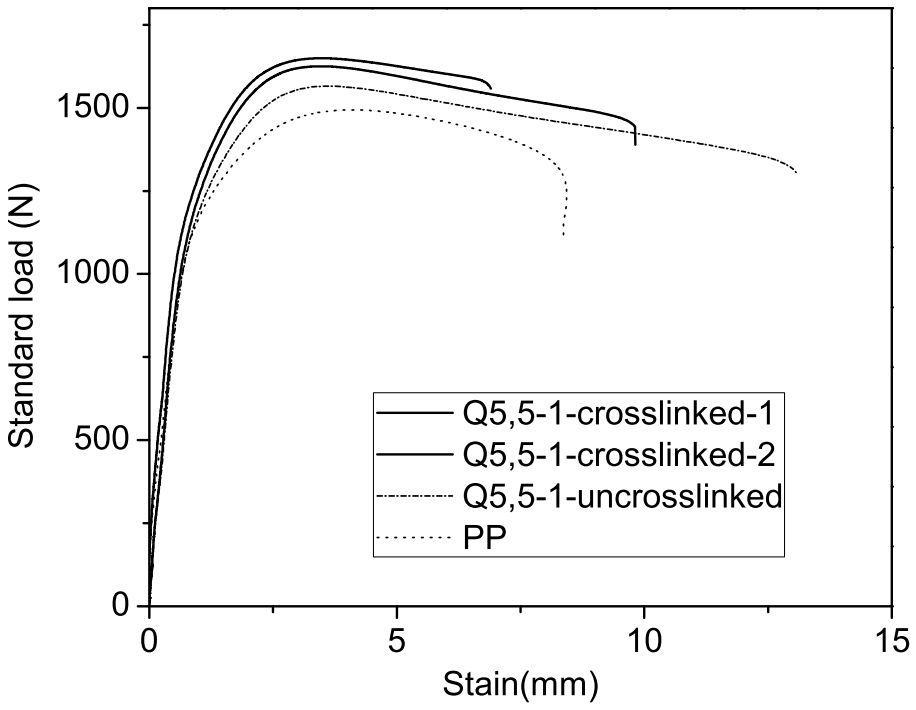

Figure 8.25: Stress-strain curves of PP and Q5.5-1

Table 8.11: Percentage of reacted silane and complex viscosity of PP-g-ATM

Sample	Feed rate (kg/h)	Temperature (°C)	Screw speed (rpm)	Silane%* grafted	Silane%* polymerized	Torque	$\eta_{0.063}$ (10^4Pa.s) dry	extr
PP	-	-	-	-	-	-	1.52	
Q10-1	10	200	100	2.33	44.74	>110	1.42	0.33
Q10-2	10	200	300	22.57	16.91	75	1.65	0.58
Q10-3	10	200	500	22.26	11.85	74	1.54	0.40
Q10-4	10	220	100	22.26	21.47	91	3.32	0.29
Q10-5	10	220	300	15.38	14.89	75	2.78	0.23
Q10-6	10	240	100	23.18	20.86	98	1.91	0.33
Q10-7	10	240	500	27.93	16.71	67	1.89	0.19
Q5.5-1	5.5	200	300	14.88	37.76	66	2.93	0.38
Q5.5-2	5.5	220	100	41.80	19.85	65	2.11	0.21
Q5.5-3	5.5	240	300	24.69	30.37	58	2.39	0.41
Q5.5-4	5.5	220	500	31.17	25.72	63	1.75	0.18
Q1-1	1	200	100	49.62	13.98	51	1.73	0.45
Q1-2	1	200	300	24.79	21.97	63	0.94	0.17
Q1-3	1	200	500	37.96	29.76	53	1.01	0.20
Q1-4	1	200	300	37.66	22.68	-	-	-
Q1-5	1	220	100	32.52	25.21	50	1.45	0.41
Q1-6	1	220	300	19.98	40.19	54	1.83	0.36
Q1-7	1	240	100	26.40	25.82	50	0.74	0.14
Q1-8	1	240	500	33.50	18.83	52	0.44	0.19
Q5.5-t1-re	5.5	220	300	36.64	28.35	60	3.66	-
Q5.5-t2-re	5.5	220	300	18.93	42.52	60	2.56	-
Q5.5-t3-re	5.5	220	300	22.87	54.46	61	1.42	-
Q5.5-t4-re	5.5	220	300	18.22	40.49	60	1.93	-
Q5.5-1-p2	5.5	200	100	12.75	34.22	-	3.23	1.70
Q5.5-2-p2	5.5	200	300	22.77	22.68	60	3.27	0.94
Q5.5-3-p2	5.5	200	500	19.55	22.67	-	1.27	0.68
Q5.5-4-p2	5.5	220	100	31.27	17.62	61	1.75	0.38
Q5.5-5-p2	5.5	220	300	28.34	22.07	-	1.42	0.49
Q5.5-6-p2	5.5	220	500	27.53	19.04	57	1.02	0.39
Q5.5-7-p2	5.5	240	100	15.59	33.41	-	1.03	0.72
Q5.5-8-p2	5.5	240	300	20.65	37.76	54	3.26	0.36
Q5.5-9-p2	5.5	240	500	28.64	26.02	-	0.64	0.41
Q5.5-Q/N-1s	5.5	220	300	34.76	26.83	-	0.44	0.077
Q8-Q/N-1s	8	220	440	24.21	19.10	-	0.17	0.094
Q10-Q/N-1s	10	220	545	27.68	16.40	-	0.19	0.080
Q2-Q/N-2s	2	220	109	16.66	29.13	-	0.23	0.091
Q8-Q/N-2s	8	220	440	23.79	18.10	-	0.17	0.058

'dry'	Original samples dried in a vacuum oven
'extr'	Samples after extraction
'p2'	Profile 2
Q5,5-t'n'-re	'n'th repeated sample with the same condition
Q/N	Feed rate/screw speed = 1.1 kg/screw turn
1s	One silane (ATM)
2s	A mixture of two silanes (ATM + another silane)

Table 8.12: Tensile strength properties of PP-g-ATM

Sample	Yield stress (MPa)		Elongation at yield stress (mm)		Stress at break (N)		Young's Modulus (kPa)		Elongation at break (%)	
	cr	un	cr	un	cr	un	cr	un	cr	un
PP	37.7		4.2		1050		1990		19.4	
Q10-1	45.6	39.7	2.9	3.3	1630	1210	2240	2080	17.5	22.5
Q10-2	45.6	41.3	2.7	2.9	1560	1280	3060	2230	18.6	13.9
Q10-3										
Q10-4	43.4	40.6	3.4	3.4	1570	1330	2340	2980	18.1	32.1
Q10-5	40.8	38.4	2.9	3.2	1480	1350	2580	1740	9.8	12.7
Q10-6	40.3	37.9	2.9	2.9	1330	1100	2120	2140	24.4	10.0
Q10-7	40.1	36.4	2.7	3.6	1460	1280	2810	2210	10.0	17.7
Q5.5-1	41.7	40.2	3.4	3.6	1470	1300	2460	1890	16.7	26.2
Q5.5-2	42.5	39.4	3.1	3.3	1490	1340	2380	1890	18.0	24.5
Q5.5-3	43.9	38.3	2.8	3.1	1570	1180	2550	2200	11.6	18.6
Q5.5-4	40.4	37.2	3.1	3.2	1360	1160	2130	2000	12.7	10.5
Q1-1	41.0	36.2	2.5	3.0	1450	1170	2090	2100	9.9	9.8
Q1-2	41.8	38.6	3.0	3.0	1400	1150	2490	2250	20.6	15.2
Q1-3	40.4	40.8	3.2	4.0	1530	1240	2110	1900	10.1	18.8
Q1-4										
Q1-5	44.5	39.4	3.3	3.9	1530	1300	2180	2060	23.4	20.5
Q1-6	40.3		3.0		1440		2030		14.0	
Q1-7	39.9	37.9	3.3	3.0	1470	1270	1880	2360	14.2	16.1
Q1-8										
Q5.5-t1-re	44.5	41.8	3.2	3.5	1500	1470	2540	2410	16.6	20.3
Q5.5-t2-re	44.4	45.5	3.2	2.9	1540	1590	2280	2670	16.5	79.2
Q5.5-t3-re	44.4	42.5	3.0	2.9	1570	1410	2510	2440	19.7	14.3
Q5.5-t4-re	42.9	44.1	3.3	2.8	1440	1490	2770	2480	22.1	19.9
Q5.5-1-p2	43.5	41.6	3.3	3.1	1580	1340	2500	2430	23.9	742.3
Q5.5-2-p2	45.2	42.9	2.9	3.0	1610	1510	2230	2190	15.8	9.9
Q5.5-3-p2	42.9	39.6	3.0	3.1	1550	1290	2170	2180	16.3	29.8
Q5.5-4-p2	45.6	43.9	2.7	2.7	1660	1520	2670	2880	15.6	14.3
Q5.5-5-p2	42.7	42.5	3.3	3.7	1520	1520	2340	2120	15.2	14.0
Q5.5-6-p2	43.0	42.7	3.7	3.0	1560	1570	2270	2320	16.3	712.4
Q5.5-7-p2	43.9	42.8	3.7	2.9	1390	1500	2110	2120	32.3	10.9
Q5.5-8-p2	40.5		2.7		1430		2330		12.6	
Q5.5-9-p2	43.0		3.7		1530		2230		16.5	
Q5.5-Q/N-1s	42.4	41.2	4.1	4.0	1480	1520	2200	2040	20.1	13.2
Q8-Q/N-1s	42.0	38.9	3.9	4.0	1560	1470	2360	2150	13.0	10.6
Q10-Q/N-1s	40.0	39.8	3.0	3.5	1540	1550	1980	2340	8.2	8.2
Q2-Q/N-2s	43.8	41.5	4.0	3.3	1540	1440	1910	2380	16.6	15.5
Q8-Q/N-2s	42.2	36.8	3.7	3.4	1530	1350	1940	1670	14.3	10.8

'dry'	Original samples dried in a vacuum oven
'extr'	Samples after extraction
'p2'	Profile 2
Q5,5-t'n'-re	'n'th repeated sample with the same condition
Q/N	Feed rate/screw speed = 1.1 kg/screw turn
1s	One silane (ATM)
2s	A mixture of two silanes (ATM + another silane)
cr	crosslinked
un	uncrosslinked

Figures 8.26, 8.27, 8.28, 8.29, 8.30 show the relationships between tensile properties percentage of grafted/reacted silane and complex viscosity. During silane grafting reaction, silane grafting reaction and PP chain scission reaction reaction happen at the same time, silane and crosslinking can improve the material tensile properties, but PP chain scission will affect it complicatedly. Thus, simple relationships between the tensile properties and percentage of grafted/reacted silane or that between the tensile properties and complex viscosity cannot be found.

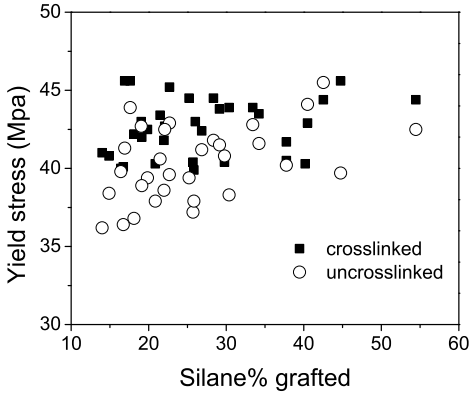

(a) Relationships between yield stress and percentage of grafted silane

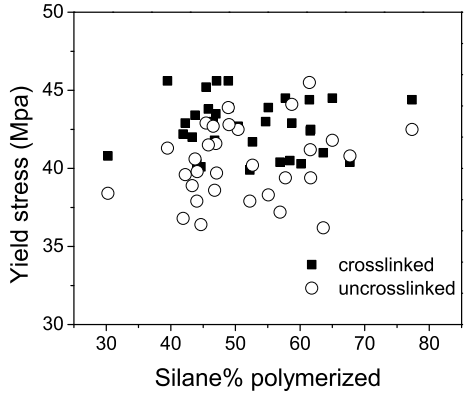

(b) Relationships between yield stress and percentage of polymerized silane

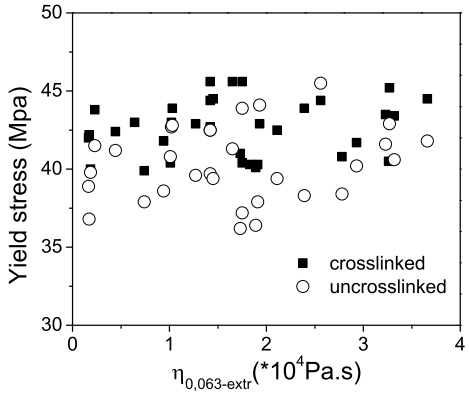

(c) Relationships between yield stress and complex viscosity

Figure 8.26: Relationships between yield stress and percentage of grafted/polymerized silane and complex viscosity

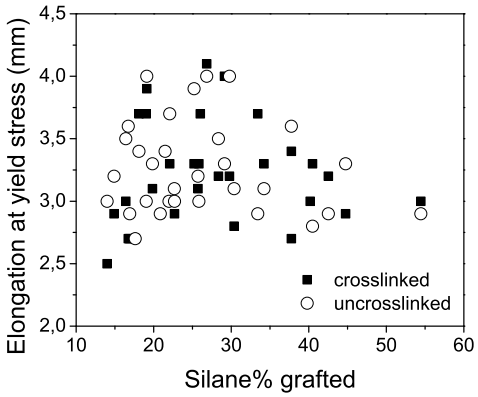

(a) Relationships between elongation at yield stress and percentage of grafted silane

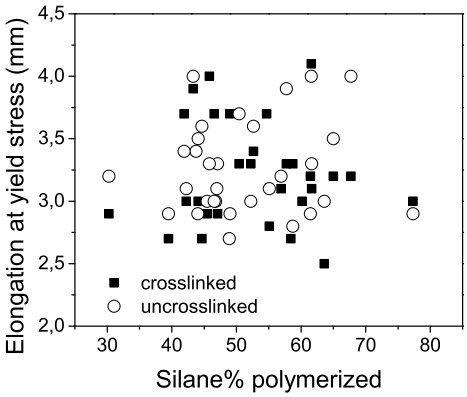

(b) Relationships between elongation at yield stress and percentage of polymerized silane

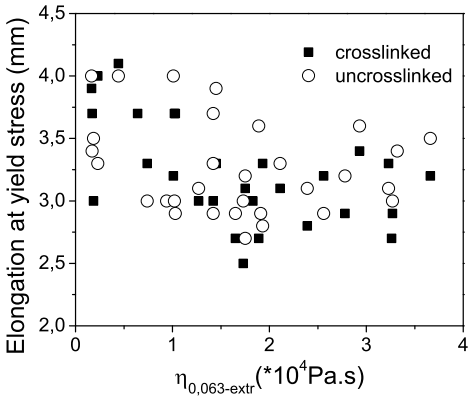

(c) Relationships between elongation at yield stress and complex viscosity

Figure 8.27: Relationships between elongation at yield stress and percentage of grafted/polymerized silane and complex viscosity

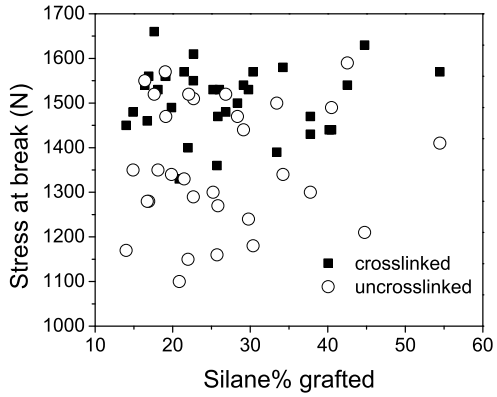

(a) Relationships between stress at break and percentage of grafted silane

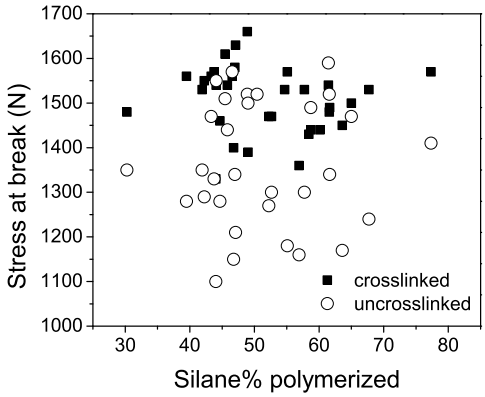

(b) Relationships between stress at break and percentage of polymerized silane

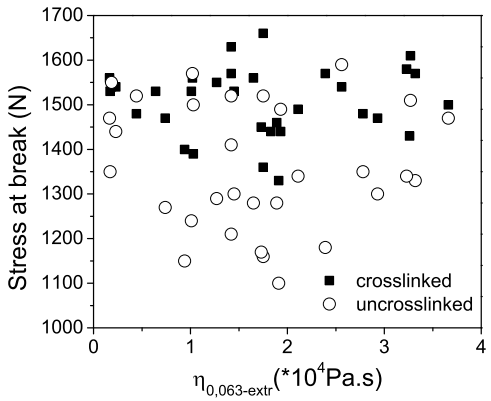

(c) Relationships between stress at break and complex viscosity

Figure 8.28: Relationships between stress at break and percentage of grafted/polymerized silane and complex viscosity

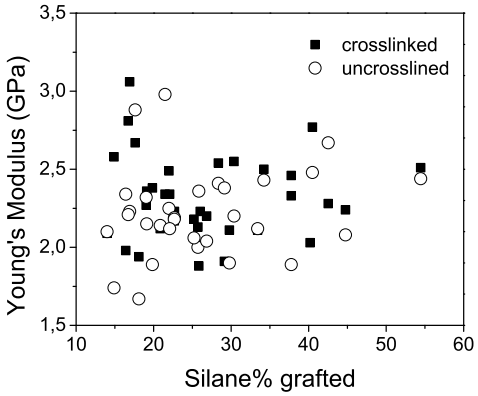

(a) Relationships between Young's modulus and percentage of grafted silane

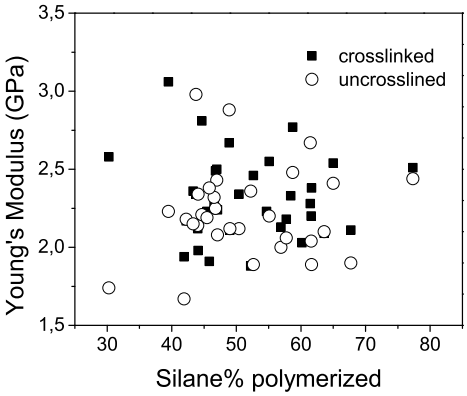

(b) Relationships between Young's modulus and percentage of polymerized silane

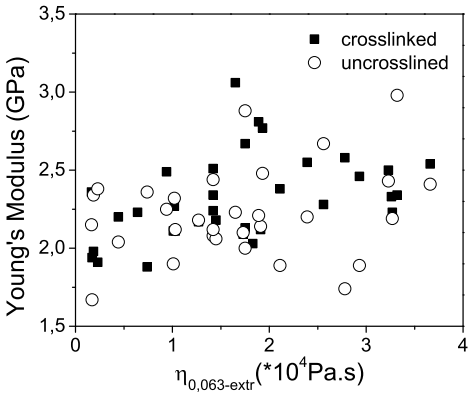

(c) Relationships between Young's modulus and complex viscosity

Figure 8.29: Relationships between Young's modulus and percentage of grafted/polymerized silane and complex viscosity

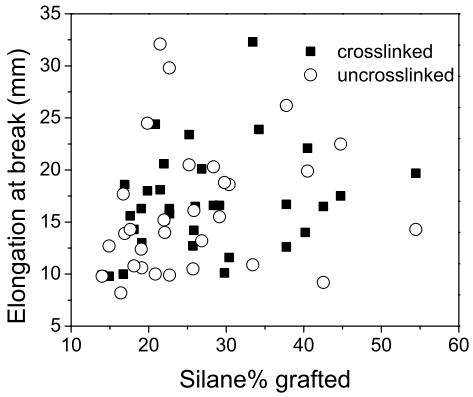

(a) Relationships between elongation at break and percentage of grafted silane

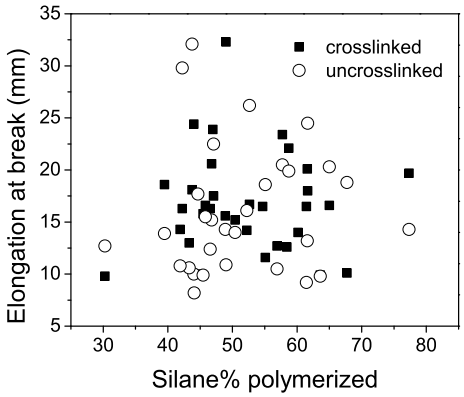

(b) Relationships between Yelongation at break and percentage of polymerized silane

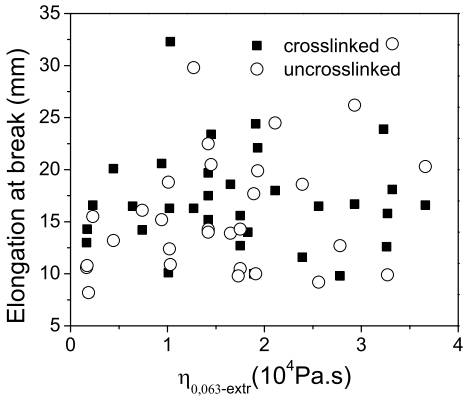

(c) Relationships between elongation at break and complex viscosity

Figure 8.30: Relationships between elongation at break and percentage of grafted/polymerized silane and complex viscosity

8.4 Modelling results

8.4.1 Model for percentage of grafted and polymerized silane

13 samples (NO. 13(Q1-1), 15(Q1-3), 19(Q1-7), 20(Q1-8), 2(Q10-1), 4(Q10-3), 7(Q10-6), 8(Q10-7), 18(Q1-6), 6(Q10-5), 9(Q5.5-1), 11(Q5.5-3), 10(Q5.5-2)) were chosen to establish the model I, and 6 samples (NO. 12(Q5.5-4), 17(Q1-5), 5(Q10-4), 3(Q10-2), 16(Q1-2), 14(Q1-4)) were used for validation.

13 samples (NO. 13(Q1-1), 15(Q1-3), 19(Q1-7), 20(Q1-8), 2(Q10-1), 4(Q10-3), 7(Q10-6), 8(Q10-7), 14(Q1-2), 3(Q10-2), 5(Q10-4), 11(Q5.5-3), 17(Q1-5)) were chosen to establish the model II, and 6 samples (NO. 12(Q5.5-4), 10(Q5.5-2), 9(Q5.5-1), 6(Q10-5), 16(Q1-6), 14(Q1-4)) were used for validation.

The results are shown followed.

Percentage of grafted silane

Table 8.13: Fisher-Snedecor test for percentage of grafted silane

Ratio	$F = \sigma_1^2/\sigma_2^2$	$(n_1; n_2)$	$1/F_{0.025}(n_2, n_1)$	$F_{0.025}(n_1, n_2)$	Validation
Model I					
Validation/Identification	1.390	(6 ; 5)	0.228	4.950	Yes
Validation/Replication	1.522	(6 ; 3)	0.210	8.941	Yes
Identification /Replication	1.094	(5 ; 3)	0.185	9.014	Yes
Model II					
Validation/Identification	2.783	(6 ; 7)	0.238	3.866	Yes
Validation/Replication	0.893	(6 ; 3)	0.210	8.941	Yes
Identification /Replication	0.321	(7 ; 3)	0.230	8.887	Yes

Table 8.14: Apparent confidence interval of the initial model coefficients with a risk of 5% for percentage of grafted silane

Coefficients	Values of $\hat{a}$	$\hat{a}_{min}$	$\hat{a}_{max}$	$\hat{a}_{min}^{red}$	$\hat{a}_{max}^{red}$	Θ	Significant
Model I							
a_0	0.2755	-0.5049	1.0559	-0.0131	0.5641	2.0915	Yes
a_1	-0.0195	-0.3486	0.3095	-0.3486	0.3095	1.1262	Yes
a_2	-0.0255	-0.3545	0.3035	-0.3545	0.3035	1.1680	Yes
a_3	0.0353	-0.4032	0.3326	-0.3822	0.3115	1.2124	Yes
a_{11}	-0.0001	-0.7805	0.7803	-0.3292	0.3289	1.0003	No
a_{22}	0.0651	-0.7153	0.8455	-0.2639	0.3942	1.1821	Yes
a_{33}	-0.1123	-0.8927	0.6681	-0.4592	0.2345	1.3363	Yes
a_{12}	-0.0249	-0.3928	0.3430	-0.3928	0.3430	1.1453	Yes
a_{13}	-0.0573	-0.4252	0.3106	-0.4252	0.3106	1.3689	Yes
a_{23}	0.0075	-0.3604	0.3753	-0.3604	0.3753	1.0414	No
Model II							
a_0	0.2247	0.1212	0.3282	0.1232	0.3262	2.7081	Yes
a_1	-0.0129	-0.1223	0.0965	-0.1186	0.0928	1.2668	Yes
a_2	-0.0038	-0.1145	0.1070	-0.1141	0.1066	1.0705	No
a_3	-0.0300	-0.1476	0.0876	-0.1458	0.0858	1.6847	Yes
a_{12}	-0.0174	-0.1353	0.1004	-0.1332	0.0983	1.3476	Yes
a_{13}	-0.0447	-0.1625	0.0731	-0.1604	0.0711	2.2212	Yes
a_{23}	0.0075	-0.1220	0.1369	-0.1220	0.1369	1.1224	No
a_{123}	0.0644	-0.0650	0.1938	-0.0650	0.1938	2.9799	Yes

According to Fisher-Snedecor test (Table 8.13), both models are validated, but from Student test (Figure 8.31), for the model II, most of the data points for the validation

and replication are out of the confidence interval, thus this model cannot be used to simulate. With regard to the model I, although the confidence interval is broader than that of model I, but only one replication data point is out confidence interval and it does not deviate much, we can consider that the model I is validated with the following equation with the coefficients shown in Tables 8.14 and 8.15.

$$y = a_0 + a_1Q + a_2T + a_3N + a_{22}T^2 + a_{33}N^2 + a_{12}QT + a_{13}QN \tag{8.8}$$

Table 8.15: Standard deviation and confidence interval of the polynomial model coefficients of both polynomial models with a risk of 5% for percentage of grafted silane

Coefficients	Values of $\hat{a}$	$\hat{a}_{min}$	$\hat{a}_{max}$	$\hat{a}^{red}_{min}$	$\hat{a}^{red}_{max}$
Model I: $y = a_0 + a_1Q + a_2T + a_3N + a_{22}T^2 + a_{33}N^2 + a_{12}QT + a_{13}QN$					
a_0	0.2755	-0.0850	0.6359	0.1151	0.4358
a_1	-0.0195	-0.2023	0.1633	-0.2023	0.1633
a_2	-0.0255	-0.2083	0.1573	-0.2083	0.1573
a_3	-0.0353	-0.2339	0.1633	-0.2280	0.1574
a_{22}	0.0651	-0.3657	0.4960	-0.1177	0.2479
a_{33}	-0.1124	-0.5008	0.2760	-0.3051	0.0803
a_{12}	-0.0249	-0.2293	0.1795	-0.2293	0.1795
a_{13}	-0.0573	-0.2617	0.1471	-0.2617	0.1471
Model II: $y = a_0 + a_1Q + a_3N + a_{12}QT + a_{13}QN + a_{123}QTN$					
a_0	0.225	0.1547	0.2953	0.1558	0.2942
a_1	-0.0129	-0.0874	0.0617	-0.0849	0.0591
a_3	-0.0299	-0.1101	0.0502	-0.1088	0.049
a_{12}	-0.0174	-0.0977	0.0628	-0.0963	0.0614
a_{13}	-0.0447	-0.125	0.0356	-0.1236	0.0342
a_{123}	0.0644	-0.0238	0.1526	-0.0238	0.1526

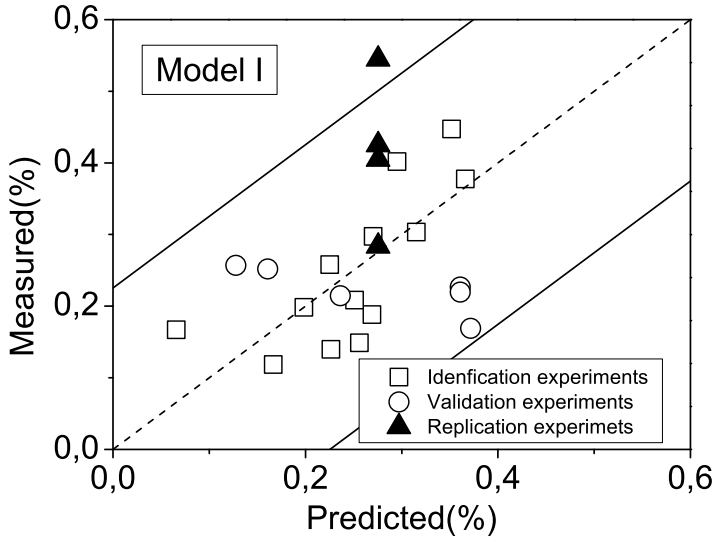

(a) model I

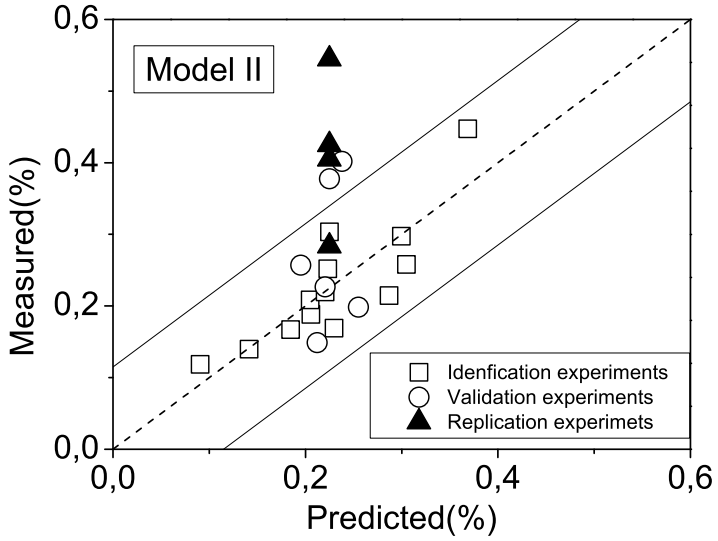

(b) model II

Figure 8.31: Comparison between experimental and calculated percentage of grafted silane

Percentage of polymerized silane

According to Fisher-Snedecor test (Table 8.16), both models are validated. According to Student test (Figure 8.32), the confidence intervals of the two models are similar and not broad. Each model presents a point outside the confidence interval but with a small deviation. However, for model I, a predicted value is smaller than zero, meaning that the percentage of polymerized silane is negative, which is illogical, thus model I should be discarded. Model II does not present the same problem and it can be considered that

model II is validated with equation (8.9)

$$y = a_0 + a_1 Q + a_3 N + a_{12} QT + a_{13} QN + a_{123} QTN \tag{8.9}$$

The coefficients of model (8.9) are given in Tables 8.17 and 8.18.

Table 8.16: Fisher-Snedecor test for percentage of polymerized silane

Ratio	$F = \sigma_1^2/\sigma_2^2$	$(n_1; n_2)$	$1/F_{0.025}(n_2, n_1)$	$F_{0.025}(n_1, n_2)$	Validation
Model I					
Validation/Identification	3.377	(6 ; 5)	0.228	4.95	Yes
Validation/Replication	2.441	(6 ; 3)	0.21	8.941	Yes
Identification /Replication	0.723	(5 ; 3)	0.185	9.014	Yes
Model II					
Validation/Identification	2.014	(6 ; 7)	0.238	3.866	Yes
Validation/Replication	1.448	(6 ; 3)	0.21	8.941	Yes
Identification /Replication	0.719	(7 ; 3)	0.23	8.887	Yes

Table 8.17: Apparent confidence interval of the initial model coefficients with a risk of 5% for percentage of polymerized silane

Coefficients	Values of $\hat{a}$	$\hat{a}_{min}$	$\hat{a}_{max}$	$\hat{a}_{min}^{red}$	$\hat{a}_{max}^{red}$	Θ	Significant
Model I							
a_0	0.2694	-0.2317	0.7705	0.0841	0.4547	3.3258	Yes
a_1	-0.0764	-0.2877	0.1349	-0.2877	0.1349	2.1324	Yes
a_2	0.0087	-0.2026	0.2199	-0.2026	0.2199	1.0854	No
a_3	0.0252	-0.2111	0.2614	-0.1976	0.2479	1.2383	Yes
a_{11}	-0.0926	-0.5937	0.4085	-0.3039	0.1187	1.4535	Yes
a_{22}	-0.0716	-0.5727	0.4295	-0.2828	0.1397	1.3332	Yes
a_{33}	0.1737	-0.3274	0.6748	-0.0490	0.3964	2.0615	Yes
a_{12}	0.0678	-0.1685	0.3040	-0.1685	0.3040	1.8043	Yes
a_{13}	0.0366	-0.1997	0.2728	-0.1997	0.2728	1.3661	Yes
a_{23}	0.0045	-0.2317	0.2407	-0.2317	0.2407	1.0386	No
Model II							
a_0	0.2725	0.1474	0.3977	0.1498	0.3953	2.6976	Yes
a_1	-0.0581	-0.1903	0.0741	-0.1859	0.0696	2.5676	Yes
a_2	0.0031	-0.1308	0.1370	-0.1303	0.1365	1.0476	No
a_3	0.0198	-0.1223	0.1620	-0.1201	0.1598	1.3245	Yes
a_{12}	0.0448	-0.0976	0.1872	-0.0951	0.1847	1.9178	Yes
a_{13}	0.0279	-0.1145	0.1703	-0.1121	0.1678	1.4868	Yes
a_{23}	0.0045	-0.1520	0.1609	-0.1520	0.1609	1.0589	No
a_{123}	-0.0424	-0.1989	0.1140	-0.1989	0.1140	1.7441	Yes

Table 8.18: Standard deviation and confidence interval of the polynomial model coefficients of both polynomial models with a risk of 5% for percentage of polymerized silane

Coefficients	Values of $\hat{a}$	$\hat{a}_{min}$	$\hat{a}_{max}$	$\hat{a}^{red}_{min}$	$\hat{a}^{red}_{max}$
Model I: $y = a_0 + a_1Q + a_3N + a_{11}Q^2 + a_{22}T^2 + a_{33}N^2 + a_{12}QT + a_{13}QN$					
a_0	0.26941	-0.01286	0.55168	0.16503	0.3738
a_1	-0.07638	-0.1954	0.04264	-0.1954	0.04264
a_3	0.02515	-0.10791	0.15821	-0.1003	0.1506
a_{11}	-0.09261	-0.37488	0.18966	-0.21163	0.0264
a_{22}	-0.07156	-0.35383	0.21071	-0.19058	0.04745
a_{33}	0.17374	-0.10853	0.45601	0.04828	0.29919
a_{12}	0.06775	-0.06531	0.20081	-0.06531	0.20081
a_{13}	0.03655	-0.09651	0.16961	-0.09651	0.16961
Model II: $y = a_0 + a_1Q + a_3N + a_{12}QT + a_{13}QN + a_{123}QTN$					
a_0	0.272	0.188	0.357	0.189	0.355
a_1	-0.058	-0.147	0.031	-0.144	0.028
a_3	0.02	-0.076	0.116	-0.075	0.114
a_{12}	0.045	-0.051	0.141	-0.05	0.139
a_{13}	0.028	-0.068	0.124	-0.067	0.122
a_{123}	-0.042	-0.148	0.063	-0.148	0.063

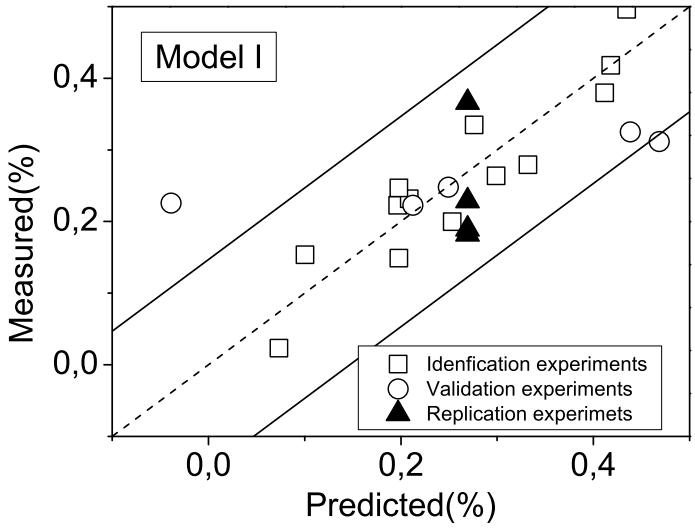

(a) model I

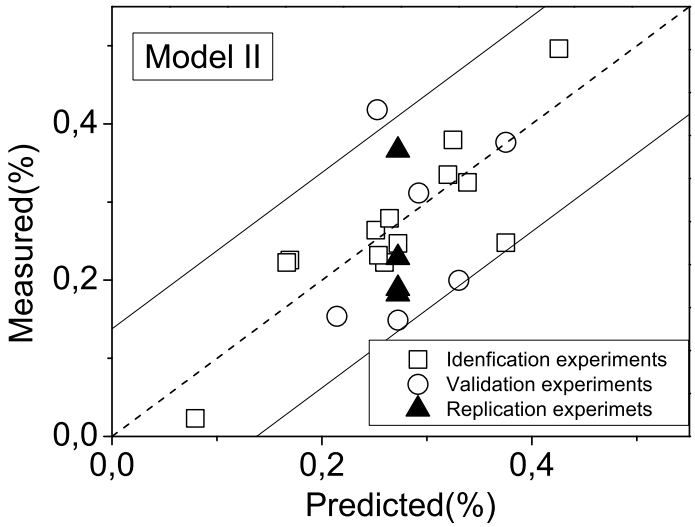

(b) model II

Figure 8.32: Comparison between experimental and calculated percentage of polymerized silane

8.4.2 Model for complex viscosity

13 samples (NO. 13(Q1-1), 15(Q1-3), 19(Q1-7), 20(Q1-8), 2(Q10-1), 4(Q10-3), 7(Q10-6), 8(Q10-7), 18(Q1-6), 6(Q10-5), 9(Q5.5-1), 11(Q5.5-3), 10(Q5.5-2)) were chosen to establish the model I, and 5 samples (NO. 12(Q5.5-4), 17(Q1-5), 5(Q10-4), 3(Q10-2), 16(Q1-2)) were used for validation.

13 samples (NO. 13(Q1-1), 15(Q1-3), 19(Q1-7), 20(Q1-8), 2(Q10-1), 4(Q10-3), 7(Q10-6), 8(Q10-7), 14(Q1-2), 3(Q10-2), 5(Q10-4), 11(Q5.5-3), 17(Q1-5)) were chosen to establish the model II, and 5 samples (NO. 12(Q5.5-4), 10(Q5.5-2), 9(Q5.5-1), 6(Q10-5), 16(Q1-6)) were used for validation.

The results are shown in the following.

Complex viscosity of dried samples

Table 8.19: Fisher-Snedecor test for complex viscosity of dried samples

Ratio	$F = \sigma_1^2/\sigma_2^2$	$(n_1; n_2)$	$1/F_{0.025}(n_2, n_1)$	$F_{0.025}(n_1, n_2)$	Validation
Model I					
Validation/Identification	27.751	(5 ; 4)	0.193	6.256	No
Validation/Replication	0.923	(5 ; 3)	0.185	9.014	Yes
Identification /Replication	0.033	(4 ; 3)	0.152	9.117	No
Model II					
Validation/Identification	1.826	(5 ; 9)	0.21	3.482	Yes
Validation/Replication	0.629	(5 ; 3)	0.185	9.014	Yes
Identification /Replication	0.344	(9 ; 3)	0.06	8.812	Yes

Table 8.20: Apparent confidence interval of the initial model coefficients with a risk of 5% for complex viscosity of dried samples

Coefficients	Values of $\hat{a}$	$\hat{a}_{min}$	$\hat{a}_{max}$	$\hat{a}_{min}^{red}$	$\hat{a}_{max}^{red}$	Θ	Significant
Model I							
a_0	2.8125	1.7548	3.8702	2.4214	3.2036	2.2055	Yes
a_1	0.3790	-0.0670	0.8250	-0.0670	0.8250	12.3174	Yes
a_2	-0.1260	-0.5720	0.3200	-0.5720	0.3200	1.7876	Yes
a_3	-0.1150	-0.6136	0.3836	-0.5851	0.3551	1.5996	Yes
a_{11}	-0.5075	-1.5652	0.5502	-0.9535	-0.0615	2.8447	Yes
a_{22}	-0.1525	-1.2102	0.9052	-0.5985	0.2935	1.3369	Yes
a_{33}	-0.8175	-1.8752	0.2402	-1.2876	-0.3474	7.8061	Yes
a_{12}	0.3000	-0.1986	0.7986	-0.1986	0.7986	4.0209	Yes
a_{13}	0.1400	-0.3586	0.6386	-0.3586	0.6386	1.7808	Yes
a_{23}	0.0350	-0.4636	0.5336	-0.4636	0.5336	1.1510	No
Model II							
a_0	1.5356	0.4426	2.6285	0.4635	2.6076	5.9384	Yes
a_1	0.5007	-0.6543	1.6558	-0.6152	1.6166	2.5305	Yes
a_2	0.0560	-1.1138	1.2257	-1.1095	1.2215	1.1005	No
a_3	-0.2619	-1.5037	0.9799	-1.4843	0.9605	1.5345	Yes
a_{12}	0.2691	-0.9749	1.5132	-0.9532	1.4915	1.5522	Yes
a_{13}	0.0251	-1.2189	1.2692	-1.1972	1.2475	1.0413	No
a_{23}	0.0350	-1.3317	1.4017	-1.3317	1.4017	1.0526	No
a_{123}	-0.0700	-1.4367	1.2967	-1.4367	1.2967	1.1080	No

According to Fisher-Snedecor test (Table 8.19), the ratio of Validation/Identification of the model I is larger than $F_{0.025;n_1;n_2}$. It means that the variance of valication is not equal to the variance of identification, so model I is not validated. By association with the Figure of Student test (Figure 8.33, Tables 8.20 and 8.21), we found that, by use of

the identification data, model I can be well established with a narrow confidence interval, but it cannot be used to predict because of almost all the data points for validation and replication are out of the confidence interval. This conclusion is agreed with that from Fisher-Snedecor test. According to Fisher-Snedecor test, the model II is validated, but with respect to Student test, 2 data points for validation and replication are out of the confidence interval and the one for replication deviates greatly, so neither of the models is validated.

Table 8.21: Standard deviation and confidence interval of the polynomial model coefficients of both polynomial models with a risk of 5% for complex viscosity of dried samples

Coefficients	Values of $\hat{a}$	$\hat{a}_{min}$	$\hat{a}_{max}$	$\hat{a}^{red}_{min}$	$\hat{a}^{red}_{max}$
Model I: $y = a_0 + a_1Q + a_2T + a_3N + a_{11}Q^2 + a_{22}T^2 + a_{33}N^2 + a_{12}QT + a_{13}QN$					
a_0	2.8125	2.027	3.598	2.522	3.103
a_1	0.379	0.0478	0.7102	0.0478	0.7102
a_2	-0.126	-0.4572	0.2052	-0.4572	0.2052
a_3	-0.115	-0.4853	0.2553	-0.4641	0.2341
a_{11}	-0.5075	-1.293	0.278	-0.8387	-0.1763
a_{22}	-0.1525	-0.938	0.633	-0.4837	0.1787
a_{33}	-0.8175	-1.603	-0.032	-1.1666	-0.4684
a_{12}	0.3	-0.0703	0.6703	-0.0703	0.6703
a_{13}	0.14	-0.2303	0.5103	-0.2303	0.5103
Model II: $y = a_0 + a_1Q + a_3N + a_{12}QT$					
a_0	1.5311	0.923	2.1393	0.9324	2.1298
a_1	0.4964	-0.1374	1.1302	-0.1268	1.1195
a_3	-0.2628	-0.9562	0.4306	-0.9454	0.4199
a_{12}	0.2683	-0.426	0.9626	-0.4144	0.9509

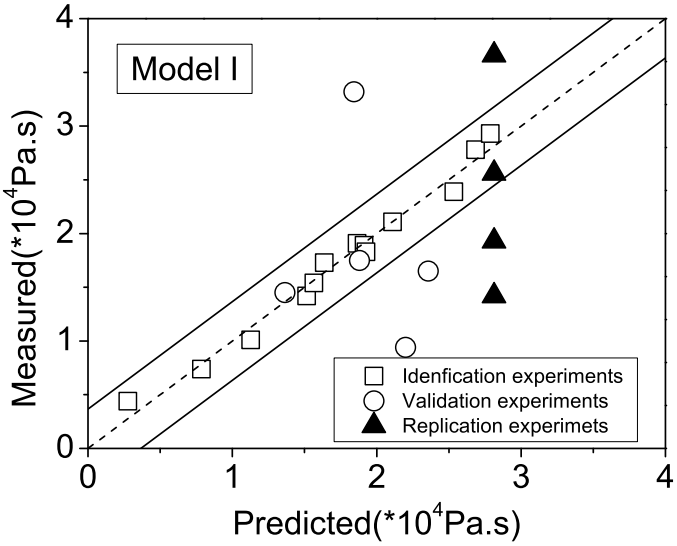

(a) model I

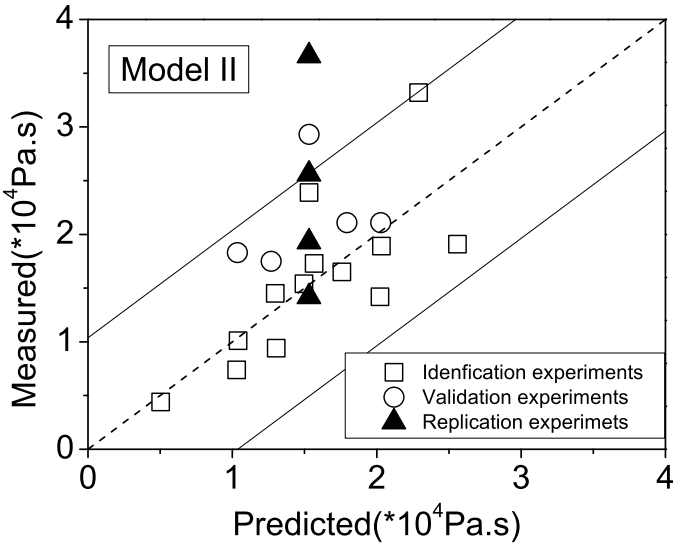

(b) model II

Figure 8.33: Comparison between experimental and calculated complex viscosity of dried samples

Complex viscosity of extracted samples

According to Fisher-Snedecor test (Table 8.22), both models are validated, and according to Student test (Figure 8.34), both models are validated, but for the model I, only one data is out of the confidence interval although it does not deviate far, and its confidence interval is broader than that of the model II, thus the model II is better and is chosen to simulate in this case with the following equation whose coefficients are shown in Tables 8.23 and 8.24.

$$y = a_0 + a_1 Q + a_2 T + a_3 N + a_{12} QT + a_{13} QN + a_{123} QTN \tag{8.10}$$

Table 8.22: Fisher-Snedecor test for complex viscosity of extracted samples

Ratio	$F = \sigma_1^2/\sigma_2^2$	$(n_1; n_2)$	$1/F_{0.025}(n_2, n_1)$	$F_{0.025}(n_1, n_2)$	Validaiton
Model I					
Validation/Identification	2.538	(5 ; 6)	0.202	4.387	Yes
Validation/Replication					
Identification /Replication					
Model II					
Validation/Identification	0.762	(5 ; 6)	0.202	4.387	Yes
Validation/Replication					
Identification /Replication					

Table 8.23: Apparent confidence interval of the initial model coefficients with a risk of 5% for complex viscosity of extracted samples

Coefficients	Values of $\hat{a}$	$\hat{a}_{min}$	$\hat{a}_{max}$	$\hat{a}_{min}^{red}$	$\hat{a}_{max}^{red}$	Θ	Significant
Model I							
a_0	0.2938	-0.4648	1.0523	0.0132	0.5743	2.2639	Yes
a_1	0.0140	-0.3058	0.3338	-0.3058	0.3338	1.0915	Yes
a_2	-0.0500	-0.3698	0.2698	-0.3698	0.2698	1.3706	Yes
a_3	-0.0338	-0.3914	0.3239	-0.3709	0.3034	1.2084	Yes
a_{11}	0.0012	-0.7573	0.7598	-0.3186	0.3211	1.0033	No
a_{22}	0.1013	-0.6573	0.8598	-0.2186	0.4211	1.3081	Yes
a_{33}	-0.1175	-0.8761	0.6411	-0.4546	0.2196	1.3666	Yes
a_{12}	0.0138	-0.3439	0.3714	-0.3439	0.3714	1.0800	No
a_{13}	0.0163	-0.3414	0.3739	-0.3414	0.3739	1.0952	Yes
a_{23}	0.0113	-0.3464	0.3689	-0.3464	0.3689	1.0650	No
Model II							
a_0	0.3051	0.1044	0.5059	0.1082	0.5021	4.8469	Yes
a_1	0.0491	-0.1631	0.2613	-0.1559	0.2541	1.6023	Yes
a_2	-0.0514	-0.2662	0.1635	-0.2654	0.1627	1.6281	Yes
a_3	-0.0360	-0.2641	0.1921	-0.2605	0.1886	1.3745	Yes
a_{12}	-0.0202	-0.2487	0.2083	-0.2447	0.2044	1.1937	Yes
a_{13}	0.0348	-0.1937	0.2633	-0.1897	0.2594	1.3596	Yes
a_{23}	0.0113	-0.2398	0.2623	-0.2398	0.2623	1.0938	No
a_{123}	-0.0638	-0.3148	0.1873	-0.3148	0.1873	1.6808	Yes

Table 8.24: Standard deviation and confidence interval of the polynomial model coefficients of both polynomial models with a risk of 5% for complex viscosity of extracted samples

Coefficients	Values of $\hat{a}$	$\hat{a}_{min}$	$\hat{a}_{max}$	$\hat{a}^{red}_{min}$	$\hat{a}^{red}_{max}$
Model I: $y = a_0 + a_1Q + a_2T + a_3N + a_{22}T^2 + a_{33}N^2 + a_{13}QN$					
a_0	0.2944	0.0051	0.5838	0.1658	0.4231
a_1	0.014	-0.1327	0.1607	-0.1327	0.1607
a_2	-0.05	-0.1967	0.0967	-0.1967	0.0967
a_3	-0.0336	-0.193	0.1258	-0.1883	0.121
a_{22}	0.1011	-0.2447	0.4469	-0.0456	0.2478
a_{33}	-0.1169	-0.4287	0.1948	-0.2716	0.0377
a_{13}	0.0163	-0.1478	0.1803	-0.1478	0.1803
Model II: $y = a_0 + a_1Q + a_2T + a_3N + a_{12}QT + a_{13}QN + a_{123}QTN$					
a_0	0.3051	0.1535	0.4567	0.1564	0.4538
a_1	0.0491	-0.1111	0.2093	-0.1057	0.2039
a_2	-0.0514	-0.2136	0.1109	-0.213	0.1103
a_3	-0.036	-0.2082	0.1363	-0.2055	0.1336
a_{12}	-0.0202	-0.1927	0.1524	-0.1897	0.1494
a_{13}	0.0348	-0.1377	0.2074	-0.1347	0.2044
a_{123}	-0.0638	-0.2533	0.1258	-0.2533	0.1258

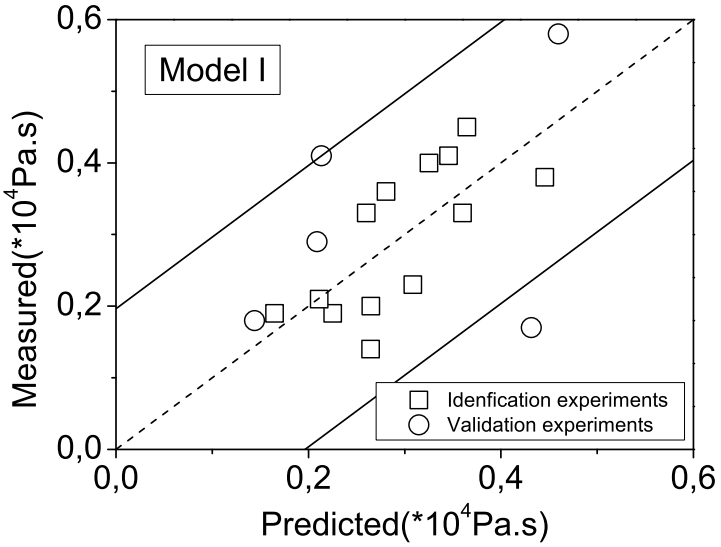

(a) model I

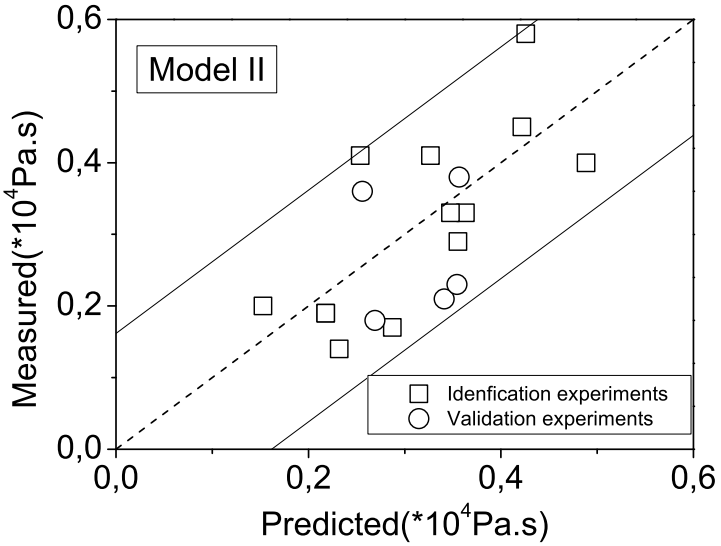

(b) model II

Figure 8.34: Comparison between experimental and calculated complex viscosity of dried samples

8.4.3 Model for torque

13 samples (NO. 13(Q1-1), 15(Q1-3), 19(Q1-7), 20(Q1-8), 2(Q10-1), 4(Q10-3), 7(Q10-6), 8(Q10-7), 18(Q1-6), 6(Q10-5), 9(Q5.5-1), 11(Q5.5-3), 10(Q5.5-2)) were chosen to establish the model I, and 5 samples (NO. 12(Q5.5-4), 17(Q1-5), 5(Q10-4), 3(Q10-2), 16(Q1-2)) were used for validation.

13 samples (NO. 13(Q1-1), 15(Q1-3), 19(Q1-7), 20(Q1-8), 2(Q10-1), 4(Q10-3), 7(Q10-6), 8(Q10-7), 14(Q1-2), 3(Q10-2), 5(Q10-4), 11(Q5.5-3), 17(Q1-5)) were chosen to establish the model II, and 5 samples (NO. 12(Q5.5-4), 10(Q5.5-2), 9(Q5.5-1), 6(Q10-5),

16(Q1-6)) were used for validation.

Table 8.25: Fisher-Snedecor test for torque

Ratio	$F = \sigma_1^2/\sigma_2^2$	$(n_1; n_2)$	$1/F_{0.025}(n_2, n_1)$	$F_{0.025}(n_1, n_2)$	Validation
Model I					
Validation/Identification	5.972	(5 ; 5)	0.198	5.05	No
Validation/Replication	2752.101	(5 ; 3)	0.185	9.014	No
Identification/Replication	460.82	(5 ; 3)	0.185	9.014	No
Model II					
Validation/Identification	0.665	(5 ; 8)	0.208	3.688	Yes
Validation/Replication	133.837	(5 ; 3)	0.185	9.014	No
Identification/Replication	201.137	(8 ; 3)	0.246	8.845	No

Table 8.26: Apparent confidence interval of the initial model coefficients with a risk of 5% for torque

Coefficients	Values of $\hat{a}$	$\hat{a}_{min}$	$\hat{a}_{max}$	$\hat{a}_{min}^{red}$	$\hat{a}_{max}^{red}$	Θ	Significant
Model I							
a_0	58.1250	-14.4295	130.6795	31.2943	84.9557	9.0564	Yes
a_1	15.5000	-15.0917	46.0917	-15.0917	46.0917	3.0541	Yes
a_2	-5.4000	-35.9917	25.1917	-35.9917	25.1917	1.4287	Yes
a_3	-7.8750	-42.0775	26.3275	-40.1215	24.3715	1.5982	Yes
a_{11}	10.8750	-61.6795	83.4295	-19.7167	41.4667	1.3526	Yes
a_{22}	16.3750	-56.1795	88.9295	-14.2167	46.9667	1.5830	Yes
a_{33}	-16.0000	-88.5545	56.5545	-48.2465	16.2465	1.5658	Yes
a_{12}	-2.1250	-36.3275	32.0775	-36.3275	32.0775	1.1325	No
a_{13}	-8.8750	-43.0775	25.3275	-43.0775	25.3275	1.7008	Yes
a_{23}	0.6250	-33.5775	34.8275	-33.5775	34.8275	1.0372	No
Model II							
a_0	67.3125	54.3082	80.3168	54.5561	80.0689	1.4789	Yes
a_1	14.9821	1.2389	28.7254	1.7049	28.2594	23.1867	Yes
a_2	-3.0625	-16.9804	10.8554	-16.9301	10.8051	1.5642	Yes
a_3	-6.9375	-21.7127	7.8377	-21.4820	7.6070	2.7703	Yes
a_{12}	0.0964	-14.7055	14.8984	-14.4481	14.6409	1.0131	No
a_{13}	-8.2036	-23.0055	6.5984	-22.7481	6.3409	3.4865	Yes
a_{23}	0.6250	-15.6363	16.8863	-15.6363	16.8863	1.0799	No
a_{123}	0.6250	-15.6363	16.8863	-15.6363	16.8863	1.0799	No

According to Fisher-Snedecor test (Table 8.25), because the four value of the repeated experiments are almost the same, Validation/Replication and Identification /Replication

are much larger than $F_{0.025}(n_1, n_2)$, which means that the differences between the simulation and the experiment are mainly due to the modelling error, rather than the experiments error or measurement error. From Student test (Figure 8.35), for the model I, 3 of the 5 data points for validation are out of the confidence interval, so the model I should be abandoned, and for the model II, all of the data points are in the confidence interval and it's narrow, so we can consider the model II is validated and the model is shown as followed with the coefficients in Tables 8.26 and 8.27.

$$y = a_0 + a_1 Q + a_2 T + a_3 N + a_{13} QN \tag{8.11}$$

Table 8.27: Standard deviation and confidence interval of the polynomial model coefficients of both polynomial models with a risk of 5% for torque

Coefficients	Values of $\hat{a}$	$\hat{a}_{min}$	$\hat{a}_{max}$	$\hat{a}^{red}_{min}$	$\hat{a}^{red}_{max}$
Model I: $y = a_0 + a_1 Q + a_2 T + a_3 N + a_{11} Q^2 + a_{22} T^2 + a_{33} N^2 + a_{13} QN$					
a_0	58.125	16.5178	99.7322	42.7387	73.5113
a_1	15.5	-2.0431	33.0431	-2.0431	33.0431
a_2	-5.4	-22.9431	12.1431	-22.9431	12.1431
a_3	-7.875	-27.4888	11.7388	-26.3671	10.6171
a_{11}	10.875	-30.7322	52.4822	-6.6681	28.4181
a_{22}	16.375	-25.2322	57.9822	-1.1681	33.9181
a_{33}	-16	-57.6072	25.6072	-34.4921	2.4921
a_{13}	-8.875	-28.4888	10.7388	-28.4888	10.7388
Model II: $y = a_0 + a_1 Q + a_2 T + a_3 N + a_{13} QN$					
a_0	67.3125	57.1262	75.0126	58.8676	75.7574
a_1	14.9655	6.0255	23.9055	6.1758	23.7553
a_2	-3.0625	-12.2764	6.1514	-12.2431	6.1181
a_3	-6.9375	-16.7189	2.8439	-16.5662	2.6912
a_{13}	-8.2069	-18.0002	1.5864	-17.8356	1.4218

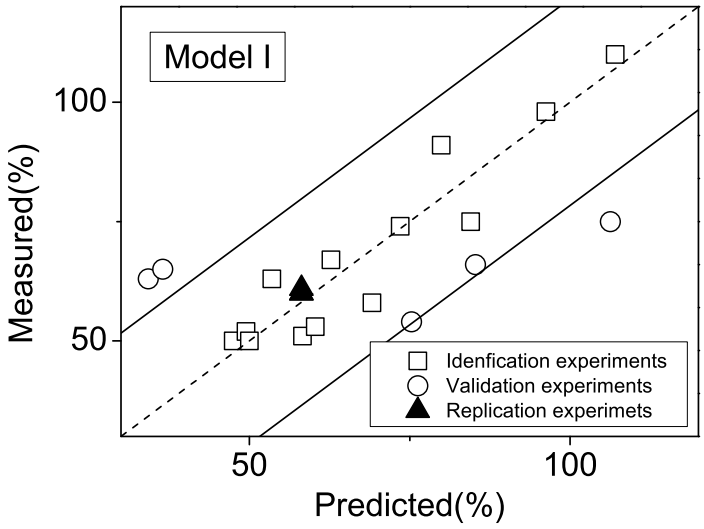

(a) model I

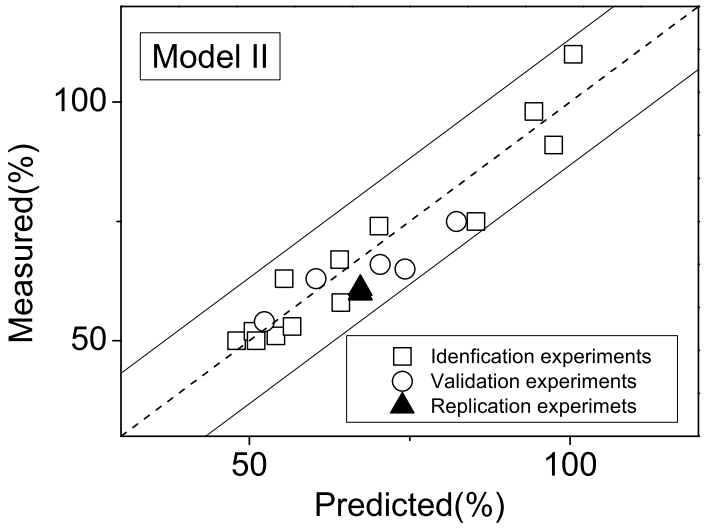

(b) model II

Figure 8.35: Comparison between experimental and calculated torque

8.4.4 Model for tensile strengthen

12 samples (NO. 13(Q1-1), 15(Q1-3), 19(Q1-7), 2(Q10-1), 7(Q10-6), 8(Q10-7), 6(Q10-5), 9(Q5.5-1), 11(Q5.5-3), 10(Q5.5-2), 12(Q5.5-4), 3(Q10-2)) were chosen to establish the model I for tensile strengthen of uncrosslinked specimens, and 3 samples (NO. 5(Q10-4), 17(Q1-5), 14(Q1-2)) were used for validation.

11 samples (NO. 13(Q1-1), 15(Q1-3), 19(Q1-7), 2(Q10-1), 7(Q10-6), 8(Q10-7), 14(Q1-2), 3(Q10-2), 5(Q10-4), 11(Q5.5-3), 17(Q1-5)) were chosen to establish the model II for tensile strengthen of uncrosslinked specimens, and 4 samples (NO. 12(Q5.5-4), 10(Q5.5-2), 9(Q5.5-1), 6(Q10-5)) were used for validation.

12 samples (NO. 13(Q1-1), 15(Q1-3), 19(Q1-7), 2(Q10-1), 7(Q10-6), 8(Q10-7), 18(Q1-6), 6(Q10-5), 9(Q5.5-1), 11(Q5.5-3), 10(Q5.5-2), 12(Q5.5-4)) were chosen to establish the model I for tensile strengthen of crosslinked specimens, and 4 samples (NO. 3(Q10-2), 5(Q10-4), 17(Q1-5), 14(Q1-2)) were used for validation.

11 samples (NO. 13(Q1-1), 15(Q1-3), 19(Q1-7), 2(Q10-1), 7(Q10-6), 8(Q10-7), 14(Q1-2), 3(Q10-2), 5(Q10-4), 11(Q5.5-3), 17(Q1-5)) were chosen to establish the model II for tensile strengthen of crosslinked specimens, and 5 samples (NO. 12(Q5.5-4), 10(Q5.5-2), 9(Q5.5-1), 6(Q10-5), 18(Q1-6)) were used for validation.

The results are shown in Tables 8.28, 8.29, 8.30, 8.31, 8.32, 8.33, 8.34, 8.35, 8.36, 8.37, 8.38, 8.39, 8.40, 8.41, 8.42, 8.43, 8.44, 8.45, 8.46, 8.47, 8.48, 8.49, 8.50, 8.51, 8.52, 8.53, 8.54, 8.55, 8.56, 8.57 and Figures 8.36, 8.37, 8.38, 8.39, 8.40, 8.41, 8.42, 8.43, 8.44, 8.45. Most Fisher-Snedecor test show that the models are not validated, even those which can obey the Fisher-Snedecor test, in Student test, either the confidence interval is too broad, which means the errors between the results resulting from the model and the experiment data are very large so that we can consider that all of the predicted results are unreliable, or the data points for validation and replication deviate far from the confidence interval, thus we can conclude that the two kinds of polynomial models we chose cannot be used to model the tensile strengthen.

Table 8.28: Fisher-Snedecor test for yield stress of uncrosslinked specimens

Ratio	$F = \sigma_1^2/\sigma_2^2$	$(n_1; n_2)$	$1/F_{0.025}(n_2, n_1)$	$F_{0.025}(n_1, n_2)$	Validation
Model I					
Validation/Identification	2.524	(3 ; 5)	0.111	5.41	Yes
Validation/Replication	1.056	(3 ; 3)	0.108	9.277	Yes
Identification /Replication	0.419	(5 ; 3)	0.185	9.014	Yes
Model II					
Validation/Identification	1.465	(4 ; 5)	0.16	5.192	Yes
Validation/Replication	0.657	(4 ; 3)	0.152	9.117	Yes
Identification /Replication	0.448	(5 ; 3)	0.185	9.014	Yes

Table 8.29: Apparent confidence interval of the initial model coefficients with a risk of 5% for yield stress of uncrosslinked specimens

Coefficients	Values of $\hat{a}$	$\hat{a}_{min}$	$\hat{a}_{max}$	$\hat{a}^{red}_{min}$	$\hat{a}^{red}_{max}$	Θ	Significant
Model I							
a_0	38.9619	28.7272	49.1967	34.4858	43.4381	1.7126	Yes
a_1	0.2114	-9.9400	10.3628	-5.2708	5.6936	1.0425	No
a_2	-0.8615	-9.7660	8.0430	-6.0301	4.3072	1.2142	Yes
a_3	0.1916	-6.0624	6.4455	-5.2906	5.6737	1.0632	No
a_{11}	-0.4741	-13.8144	12.8662	-5.9562	5.0081	1.0737	No
a_{22}	0.6759	-12.6049	13.9567	-4.8063	6.1581	1.1072	Yes
a_{33}	-0.7118	-13.4649	12.0413	-6.1940	4.7704	1.1182	Yes
a_{12}	-0.6643	-7.6884	6.3597	-6.5250	5.1964	1.2089	Yes
a_{13}	-0.6761	-11.6902	10.3381	-7.0063	5.6542	1.1308	Yes
a_{23}	-0.8489	-11.8631	10.1652	-7.1792	5.4813	1.1670	No
Model II							
a_0	39.1750	33.9363	44.4137	36.4343	41.9157	1.3087	Yes
a_1	0.2000	-5.8755	6.2755	-2.6745	3.0745	1.0681	No
a_2	-0.8750	-6.1137	4.3637	-3.9050	2.1550	1.4010	Yes
a_3	0.5750	-5.6267	6.7767	-2.6388	3.7888	1.2044	Yes
a_{12}	-1.0500	-7.1255	5.0255	-4.2638	2.1638	1.4179	Yes
a_{13}	-0.6000	-7.0065	5.8065	-3.8138	2.6138	1.2067	Yes
a_{23}	-0.8750	-7.4836	5.7336	-4.5859	2.8359	1.3052	Yes
a_{123}	-0.1500	-6.6932	6.3932	-3.8609	3.5609	1.0469	No

Table 8.30: Standard deviation and confidence interval of the polynomial model coefficients of both polynomial models with a risk of 5% for yield stress of uncrosslinked specimens

Coefficients	Values of $\hat{a}$	$\hat{a}_{min}$	$\hat{a}_{max}$	$\hat{a}^{red}_{min}$	$\hat{a}^{red}_{max}$
Model I: $y = a_0 + a_2T + a_{22}T^2 + a_{33}N^2 + a_{12}QT + a_{13}QN + a_{23}TN$					
a_0	39.0007	35.8708	42.1306	37.4971	40.5043
a_2	-0.7837	-2.9539	1.3865	-2.5198	0.9525
a_{22}	0.3998	-3.1424	3.942	-1.4417	2.2413
a_{33}	-0.9595	-4.4924	2.5733	-2.801	0.8819
a_{12}	-0.614	-2.7136	1.4857	-2.5826	1.3547
a_{13}	-0.8207	-3.3235	1.6821	-2.947	1.3057
a_{23}	-0.7043	-3.2071	1.7985	-2.8307	1.422
Model II: $y = a_0 + a_2T + a_3N + a_{12}QT + a_{13}QN + a_{23}TN$					
a_0	39.1331	37.3208	40.9453	37.6203	40.6458
a_2	-0.7622	-2.6274	1.103	-2.4345	0.9102
a_3	0.5132	-1.6172	2.6435	-1.2607	2.287
a_{12}	-1.0366	-3.0068	0.9336	-2.8104	0.7373
a_{13}	-0.7683	-2.7412	1.2046	-2.5421	1.0055
a_{23}	-0.7146	-3.0158	1.5865	-2.7629	1.3336

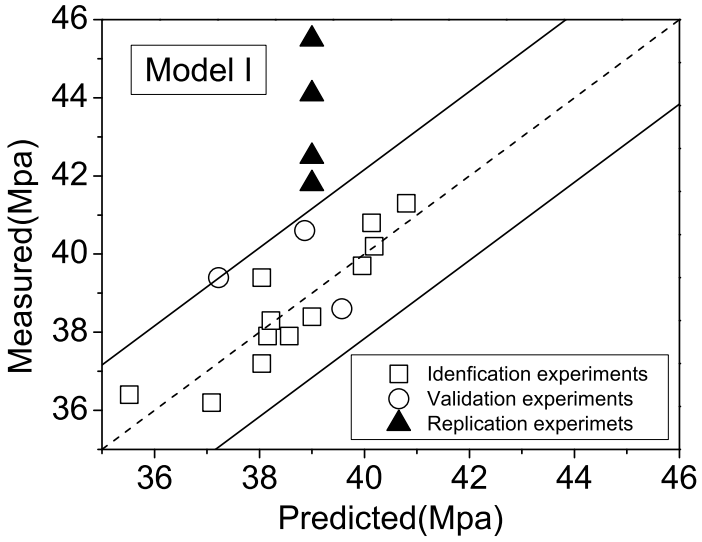

(a) model I

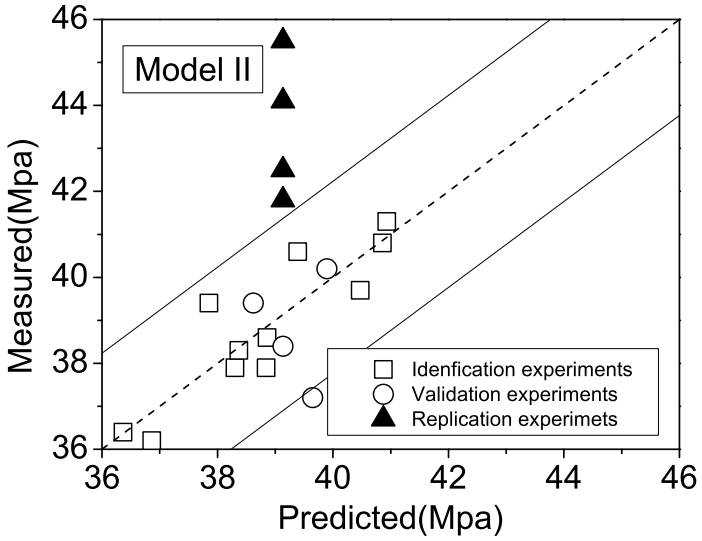

(b) model II

Figure 8.36: Comparison between experimental and calculated yield stress of uncrosslinked specimens

Table 8.31: Fisher-Snedecor test for yield stress of crosslinked specimens

Ratio	$F = \sigma_1^2/\sigma_2^2$	$(n_1; n_2)$	$1/F_{0.025}(n_2, n_1)$	$F_{0.025}(n_1, n_2)$	Validation
Model I					
Validation/Identification	9.157	(4 ; 3)	0.152	9.117	No
Validation/Replication	27.939	(4 ; 3)	0.152	9.117	No
Identification /Replication	3.051	(3 ; 3)	0.108	9.277	Yes
Model II					
Validation/Identification	3.103	(5 ; 4)	0.193	6.256	Yes
Validation/Replication	14.838	(5 ; 3)	0.185	9.014	Yes
Identification /Replication	4.781	(4 ; 3)	0.152	9.117	Yes

Table 8.32: Apparent confidence interval of the initial model coefficients with a risk of 5% for yield stress of crosslinked specimens

Coefficients	Values of $\hat{a}$	$\hat{a}_{min}$	$\hat{a}_{max}$	$\hat{a}_{min}^{red}$	$\hat{a}_{max}^{red}$	Θ	Significant
Model I							
a_0	41.9731	31.6695	52.2768	37.5846	46.3616	1.6507	Yes
a_1	-0.4400	-8.4121	7.5321	-5.5074	4.6274	1.1168	Yes
a_2	0.6294	-8.1614	9.4201	-4.4380	5.6968	1.1542	Yes
a_3	-0.3253	-7.4735	6.8229	-6.0712	5.4206	1.0954	No
a_{11}	-1.0044	-12.6257	10.6169	-6.0718	4.0630	1.1892	Yes
a_{22}	1.1938	-13.5258	15.9133	-4.1811	6.5686	1.1765	Yes
a_{33}	-0.7878	-13.1250	11.5494	-6.5337	4.9581	1.1364	Yes
a_{12}	-1.0294	-7.9856	5.9268	-6.7753	4.7165	1.3474	Yes
a_{13}	-1.9097	-11.9919	8.1726	-8.1160	4.2966	1.4673	Yes
a_{23}	2.0097	-8.0726	12.0919	-4.1966	8.2160	1.4979	Yes
Model II							
a_0	43.7271	36.5113	50.9430	39.9521	47.5022	1.3953	Yes
a_1	-0.7896	-9.1581	7.5788	-4.7490	3.1697	1.2084	Yes
a_2	0.1729	-7.0430	7.3887	-4.0007	4.3464	1.0491	No
a_3	1.2529	-7.2894	9.7951	-3.1738	5.6795	1.3437	Yes
a_{12}	-2.8354	-11.2038	5.5331	-7.2620	1.5913	2.0249	Yes
a_{13}	-1.4154	-10.2397	7.4090	-5.8420	3.0113	1.3821	Yes
a_{23}	1.8093	-7.2935	10.9121	-3.3022	6.9208	1.4961	Yes
a_{123}	-1.8218	-10.8344	7.1909	-6.9333	3.2897	1.5067	Yes

Table 8.33: Standard deviation and confidence interval of the polynomial model coefficients of both polynomial models with a risk of 5% for yield stress of crosslinked specimens

Coefficients	Values of $\hat{a}$	$\hat{a}_{min}$	$\hat{a}_{max}$	$\hat{a}^{red}_{min}$	$\hat{a}^{red}_{max}$
Model I: $y = a_0 + a_1Q + a_2T + a_{11}Q^2 + a_{22}T^2 + a_{33}N^2 + a_{12}QT + a_{13}QN + a_{23}TN$					
a_0	41.8099	35.9557	47.6641	39.0063	44.6135
a_1	-0.5504	-5.1531	4.0524	-3.7877	2.687
a_2	0.765	-4.2472	5.7773 -	2.4723	4.0024
a_{11}	-0.8641	-7.6554	5.9271	-4.1015	2.3732
a_{22}	1.4466	-6.8143	9.7076	-1.9871	4.8804
a_{33}	-0.8763	-8.2601	6.5075	-4.5472	2.7945
a_{12}	-1.165	-4.9744	2.6443	-4.8358	2.5058
a_{13}	-2.0327	-7.9196	3.8543	-5.9976	1.9323
a_{23}	2.1327	-3.7543	8.0196	-1.8323	6.0976
Model II: $y = a_0 + a_1Q + a_3N + a_{12}QT + a_{13}QN + a_{23}TN + a_{123}QTN$					
a_0	43.6398	39.2317	48.0479	40.9672	46.3124
a_1	-0.6372	-4.4858	3.2113	-3.4403	2.1658
a_3	1.1581	-4.2015	6.5176	-1.9759	4.292
a_{12}	-2.7276	-7.7225	2.2674	-5.8615	0.4064
a_{13}	-1.2555	-5.3436	2.8326	-4.3894	1.8784
a_{23}	1.6476	-2.6759	5.9711	-1.9712	5.2663
a_{123}	-1.7251	-7.4307	3.9804	-5.3439	1.8936

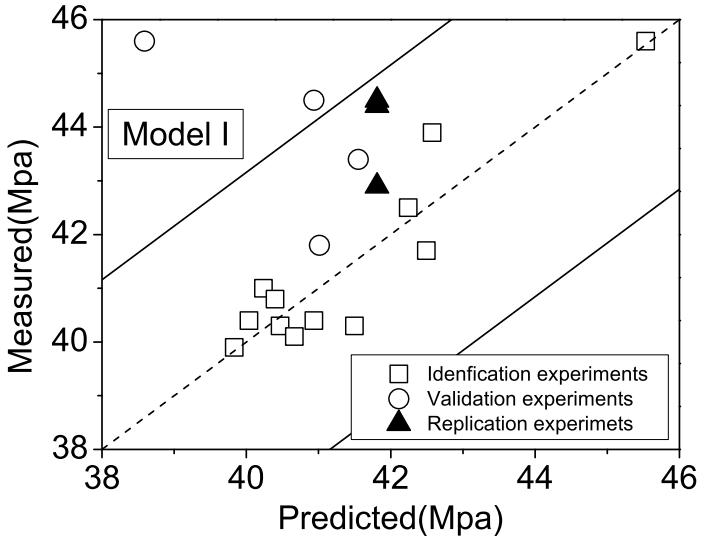

(a) model I

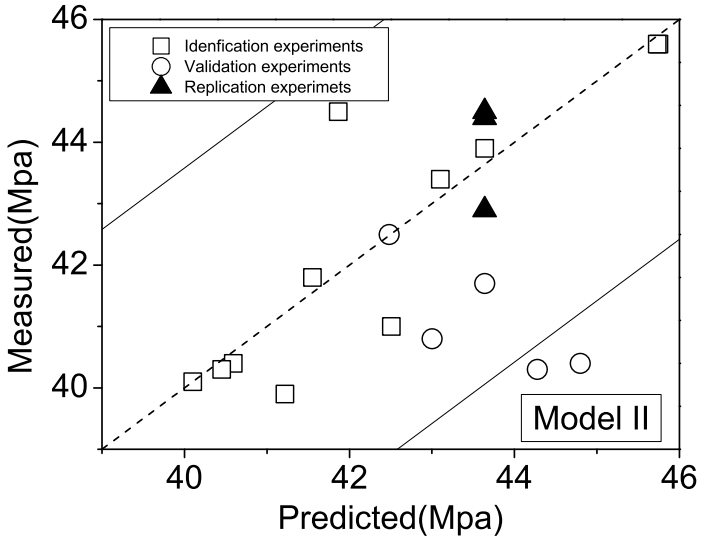

(b) model II

Figure 8.37: Comparison between experimental and calculated yield stress of crosslinked specimens

Table 8.34: Fisher-Snedecor test for elongation at yield stress of uncrosslinked specimens

Ratio	$F = \sigma_1^2/\sigma_2^2$	$(n_1; n_2)$	$1/F_{0.025}(n_2, n_1)$	$F_{0.025}(n_1, n_2)$	Validation
Model I					
Validation/Identification	5.4	(3 ; 6)	0.112	4.757	No
Validation/Replication	4.319	(3 ; 3)	0.108	9.277	Yes
Identification /Replication	0.8	(6 ; 3)	0.21	8.941	Yes
Model II					
Validation/Identification	0.376	(4 ; 6)	0.162	4.534	Yes
Validation/Replication	0.547	(4 ; 3)	0.152	9.117	Yes
Identification /Replication	1.456	(6 ; 3)	0.21	8.941	Yes

Table 8.35: Apparent confidence interval of the initial model coefficients with a risk of 5% for elongation at yield stress of uncrosslinked specimens

Coefficients	Values of $\hat{a}$	$\hat{a}_{min}$	$\hat{a}_{max}$	$\hat{a}_{min}^{red}$	$\hat{a}_{max}^{red}$	Θ	Significant
Model I							
a_0	3.2354	0.1378	6.3330	1.8807	4.5901	45.9680	Yes
a_1	-0.1295	-3.2019	2.9429	-1.7888	1.5297	1.0880	Yes
a_2	-0.0110	-2.7060	2.6840	-1.5753	1.5533	1.0082	No
a_3	0.2408	-1.6521	2.1336	-1.4185	1.9000	1.2915	Yes
a_{11}	-0.0924	-4.1300	3.9451	-1.7517	1.5668	1.0469	No
a_{22}	0.1670	-3.8525	4.1865	-1.4922	1.8262	1.0867	Yes
a_{33}	0.0457	-3.8141	3.9055	-1.6135	1.7049	1.0240	No
a_{12}	0.0427	-2.0832	2.1685	-1.7311	1.8164	1.0410	No
a_{13}	-0.1718	-3.5053	3.1617	-2.0877	1.7441	1.1087	Yes
a_{23}	0.0968	-3.2367	3.4303	-1.8191	2.0127	1.0598	Yes
Model II							
a_0	3.1364	1.1021	5.1708	2.0721	4.2007	4.6917	Yes
a_1	-0.0364	-2.3957	2.3228	-1.1527	1.0798	1.0314	No
a_2	-0.0364	-2.0708	1.9979	-1.2131	1.1402	1.0365	Yes
a_3	-0.0764	-2.4847	2.3319	-1.3244	1.1716	1.0656	Yes
a_{12}	0.2364	-2.1228	2.5957	-1.0116	1.4844	1.2227	Yes
a_{13}	-0.0236	-2.5114	2.4642	-1.2716	1.2244	1.0191	No
a_{23}	0.0079	-2.5585	2.5742	-1.4332	1.4489	1.0061	No
a_{123}	0.3921	-2.1488	2.9330	-1.0489	1.8332	1.3650	Yes

Table 8.36: Standard deviation and confidence interval of the polynomial model coefficients of both polynomial models with a risk of 5% for elongation at yield stress of uncrosslinked specimens

Coefficients	Values of $\hat{a}$	$\hat{a}_{min}$	$\hat{a}_{max}$	$\hat{a}^{red}_{min}$	$\hat{a}^{red}_{max}$
Model I: $y = a_0 + a_1Q + a_3N + a_{22}T^2 + a_{13}QN + a_{23}TN$					
a_0	3.2423	2.6160	3.8686	2.8885	3.5961
a_1	-0.1691	-0.6863	0.3480	-0.6025	0.2642
a_3	0.2556	-0.1922	0.7035	-0.1777	0.689
a_{22}	0.1303	-0.631	0.8915	-0.3031	0.5636
a_{13}	-0.1971	-0.7874	0.3933	-0.6974	0.3033
a_{23}	0.1221	-0.4683	0.7124	-0.3783	0.6224
Model II: $y = a_0 + a_2T + a_3N + a_{12}QT + a_{123}QTN$					
a_0	3.1212	2.3835	3.8588	2.6621	3.5802
a_2	-0.0532	-0.5673	0.4609	-0.5607	0.4543
a_3	-0.0941	-0.9836	0.7953	-0.6324	0.4442
a_{12}	0.2583	-0.5291	1.0458	-0.2800	0.7966
a_{123}	0.4104	-0.5364	1.3573	-0.2111	1.032

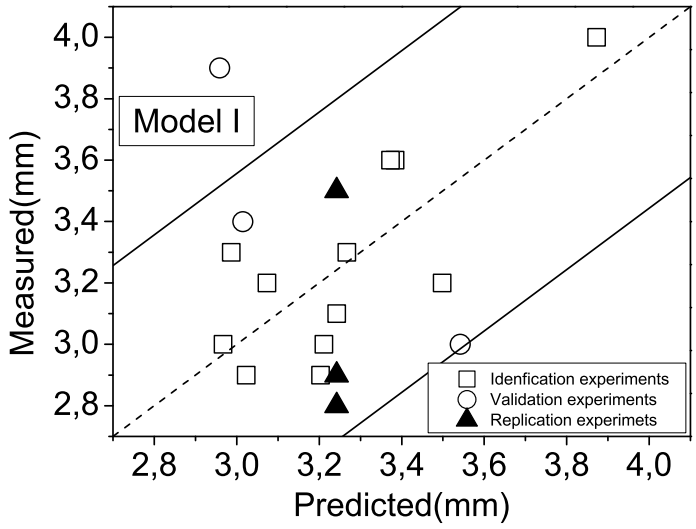

(a) model I

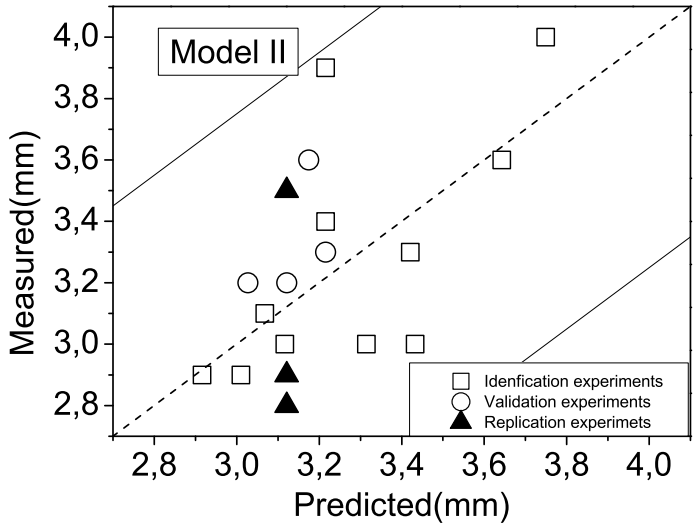

(b) model II

Figure 8.38: Comparison between experimental and calculated elongation at yield stress of uncrosslinked specimens

Table 8.37: Fisher-Snedecor test for elongation at yield stress of crosslinked specimens

Ratio	$F = \sigma_1^2/\sigma_2^2$	$(n_1; n_2)$	$1/F_{0.025}(n_2, n_1)$	$F_{0.025}(n_1, n_2)$	Validaiton
Model I					
Validation/Identification	6.849	(4 ; 5)	0.160	75.192	Yes
Validation/Replication	9.163	(4 ; 3)	0.152	9.117	No
Identification /Replication	1.338	(5 ; 3)	0.185	9.014	Yes
Model II					
Validation/Identification	2.902	(5 ; 6)	0.202	4.387	Yes
Validation/Replication	8.754	(5 ; 3)	0.185	9.014	Yes
Identification /Replication	3.016	(6 ; 3)	0.210	8.941	Yes

Table 8.38: Apparent confidence interval of the initial model coefficients with a risk of 5% for elongation at yield stress of crosslinked specimens

Coefficients	Values of $\hat{a}$	$\hat{a}_{min}$	$\hat{a}_{max}$	$\hat{a}_{min}^{red}$	$\hat{a}_{max}^{red}$	Θ	Significant
Model I							
a_0	3.0153	1.5473	4.4833	2.3901	3.6406	2.8976	Yes
a_1	-0.0275	-1.1633	1.1083	-0.7495	0.6945	1.0496	No
a_2	-0.0441	-1.2965	1.2084	-0.7660	0.6779	1.0729	Yes
a_3	0.1130	-0.9055	1.1314	-0.7057	0.9316	1.2495	Yes
a_{11}	-0.1434	-1.7992	1.5123	-0.8654	0.5785	1.1897	Yes
a_{22}	0.1844	-1.9128	2.2816	-0.5814	0.9502	1.1928	Yes
a_{33}	-0.0433	-1.8010	1.7145	-0.8619	0.7754	1.0505	No
a_{12}	-0.1684	-1.1595	0.8227	-0.9871	0.6502	1.4095	Yes
a_{13}	-0.0042	-1.4407	1.4323	-0.8885	0.8800	1.0059	No
a_{23}	-0.2208	-1.6573	1.2157	-1.1050	0.6635	1.3632	Yes
Model II							
a_0	2.8107	1.6734	3.9481	2.2157	3.4057	2.3593	Yes
a_1	-0.0190	-1.3381	1.3000	-0.6431	0.6050	1.0293	No
a_2	-0.0107	-1.1481	1.1266	-0.6685	0.6471	1.0190	No
a_3	-0.2440	-1.5905	1.1024	-0.9418	0.4537	1.4428	Yes
a_{12}	0.1024	-1.2166	1.4214	-0.5953	0.8001	1.1683	Yes
a_{13}	-0.0310	-1.4218	1.3599	-0.7287	0.6668	1.0455	No
a_{23}	-0.2036	-1.6383	1.2312	-1.0092	0.6021	1.3307	Yes
a_{123}	0.2952	-1.1253	1.7158	-0.5104	1.1009	1.5247	Yes

Table 8.39: Standard deviation and confidence interval of the polynomial model coefficients of both polynomial models with a risk of 5% for elongation at yield stress of crosslinked specimens

Coefficients	Values of $\hat{a}$	$\hat{a}_{min}$	$\hat{a}_{max}$	$\hat{a}^{red}_{min}$	$\hat{a}^{red}_{max}$
Model I: $y = a_0 + a_2T + a_3N + a_{11}Q^2 + a_{22}T^2 + a_{12}QT + a_{23}TN$					
a_0	3.0142	2.5476	3.4808	2.8102	3.2182
a_2	-0.0603	-0.3253	0.2047	-0.2959	0.1753
a_3	0.1066	-0.2087	0.4218	-0.1605	0.3737
a_{11}	-0.1516	-0.6844	0.3813	-0.3871	0.0840
a_{22}	0.1508	-0.3679	0.6695	-0.0991	0.4006
a_{12}	-0.1666	-0.4630	0.1298	-0.4337	0.1005
a_{23}	-0.2368	-0.5385	0.0650	-0.5253	0.0517
Model II: $y = a_0 + a_2T + a_3N + a_{12}QT + a_{123}QTN$					
a_0	2.8072	2.3952	3.2192	2.5475	3.0669
a_3	-0.2493	-0.7491	0.2504	-0.5539	0.0552
a_{12}	0.1108	-0.3324	0.5540	-0.1938	0.4153
a_{23}	-0.2167	-0.5683	0.1350	-0.5683	0.1350
a_{123}	0.3010	-0.2317	0.8336	-0.0507	0.6526

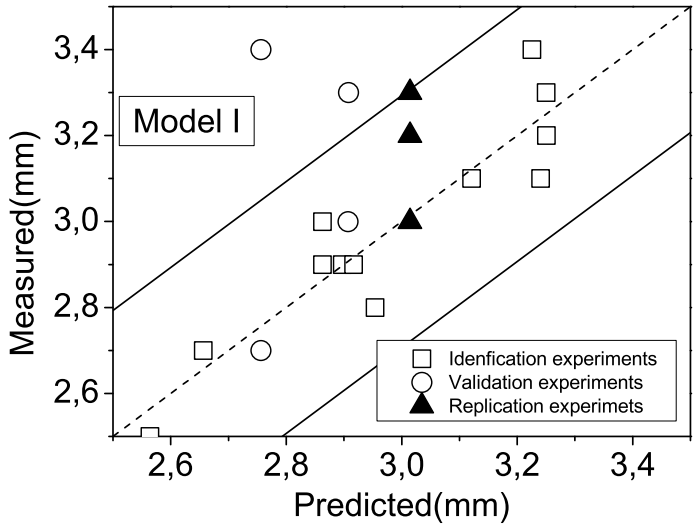

(a) model I

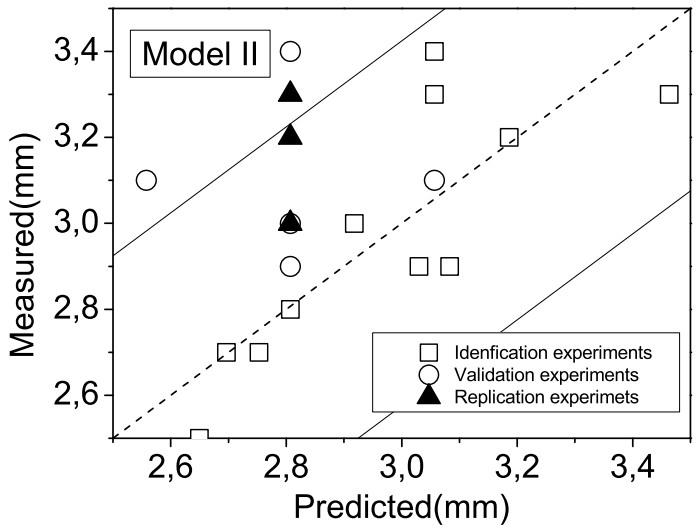

(b) model II

Figure 8.39: Comparison between experimental and calculated elongation at yield stress of crosslinked specimens

Table 8.40: Fisher-Snedecor test for stress at break of uncrosslinked specimens

Ratio	$F = \sigma_1^2/\sigma_2^2$	$(n_1; n_2)$	$1/F_{0.025}(n_2, n_1)$	$F_{0.025}(n_1, n_2)$	Validation
Model I					
Validation/Identification	0.791	(3 ; 6)	0.112	4.757	Yes
Validation/Replication	0.917	(3 ; 3)	0.108	9.277	Yes
Identification /Replication	1.159	(6 ; 3)	0.210	8.941	Yes
Model II					
Validation/Identification	0.996	(4 ; 4)	0.157	6.388	Yes
Validation/Replication	1.240	(4 ; 3)	0.152	9.117	Yes
Identification /Replication	1.245	(4 ; 3)	0.152	9.117	Yes

Table 8.41: Apparent confidence interval of the initial model coefficients with a risk of 5% for stress at break of uncrosslinked specimens

Coefficients	Values of $\hat{a}$	$\hat{a}_{min}$	$\hat{a}_{max}$	$\hat{a}_{min}^{red}$	$\hat{a}_{max}^{red}$	Θ	Significant
Model I							
a_0	1258.8345	378.8627	2138.8062	873.9790	1643.6899	5.6453	Yes
a_1	43.1097	-829.6953	915.9147	-428.2400	514.4595	1.1039	Yes
a_2	-53.7458	-819.3427	711.8511	-498.1386	390.6470	1.1510	Yes
a_3	6.4399	-531.2687	544.1484	-464.9099	477.7896	1.0242	No
a_{11}	10.4229	-1136.5580	1157.4037	-460.9269	481.7726	1.0183	No
a_{22}	-50.2132	-1192.0779	1091.6515	-521.5630	421.1365	1.0920	Yes
a_{33}	-2.5623	-1099.0555	1093.9309	-473.9120	468.7875	1.0047	No
a_{12}	-14.2777	-618.1926	589.6372	-518.1718	489.6164	1.0484	No
a_{13}	77.1778	-869.8032	1024.1587	-467.0901	621.4456	1.1775	Yes
a_{23}	-49.6778	-996.6587	897.3032	-593.9456	494.5901	1.1107	Yes
Model II							
a_0	1209.2143	849.0649	1569.3637	1020.7956	1397.6329	1.8483	Yes
a_1	40.3690	-377.3083	458.0464	-157.2461	237.9842	1.2140	Yes
a_2	-29.2143	-389.3637	330.9351	-237.5190	179.0904	1.1766	Yes
a_3	-16.8810	-443.2336	409.4717	-237.8214	204.0595	1.0825	Yes
a_{12}	-1.2024	-418.8798	416.4750	-222.1428	219.7381	1.0058	No
a_{13}	53.1310	-387.3010	493.5629	-167.8095	274.0714	1.2744	Yes
a_{23}	-32.5714	-486.9021	421.7593	-287.6915	222.5486	1.1545	Yes
a_{123}	57.1548	-392.6769	506.9864	-197.9653	312.2748	1.2911	Yes

Table 8.42: Standard deviation and confidence interval of the polynomial model coefficients of both polynomial models with a risk of 5% for stress at break of uncrosslinked specimens

Coefficients	Values of $\hat{a}$	$\hat{a}_{min}$	$\hat{a}_{max}$	$\hat{a}^{red}_{min}$	$\hat{a}^{red}_{max}$
Model I: $y = a_0 + a_1Q + a_2T + a_{22}T^2 + a_{13}QN + a_{23}TN$					
a_0	1259.6894	1082.4473	1436.9315	1160.1161	1359.2627
a_1	52.3895	-116.2215	221.0004	-69.5624	174.3414
a_2	-61.1470	-221.1053	98.8114	-176.1243	53.8304
a_{22}	-50.2748	-273.3261	172.7765	-172.2267	71.6771
a_{13}	85.5182	-120.9657	292.0021	-55.2997	226.3361
a_{23}	-58.0182	-264.5021	148.4657	-198.8361	82.7997
Model II: $y = a_0 + a_1Q + a_2T + a_3N + a_{13}QN + a_{23}TN + a_{123}QTN$					
a_0	1208.426	1043.4490	1373.4031	1075.5581	1341.2940
a_1	41.1292	-187.0674	269.3259	-98.2239	180.4824
a_2	-29.7718	-243.8922	184.3485	-176.6629	117.1193
a_3	-17.8198	-211.4761	175.8366	-173.6213	137.9818
a_{13}	53.8175	-207.2975	314.9324	-101.9841	209.6190
a_{23}	-33.2395	-308.6713	242.1923	-213.1436	146.6646
a_{123}	58.1312	-150.2088	266.4712	-121.7729	238.0354

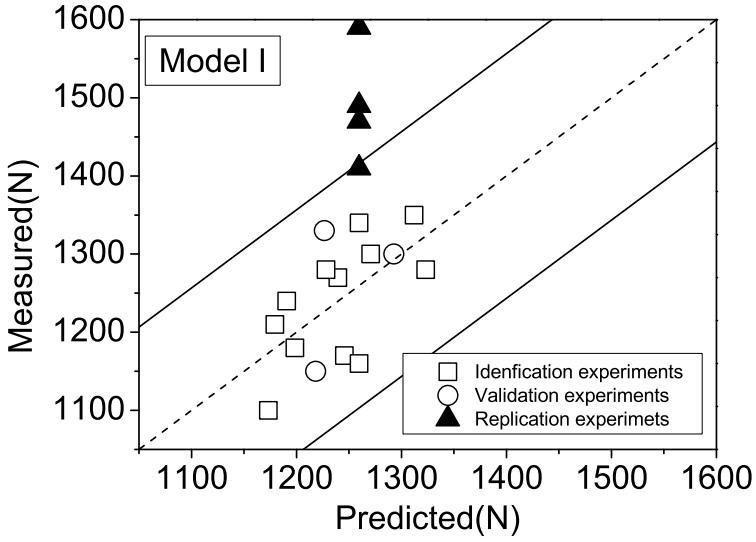

(a) model I

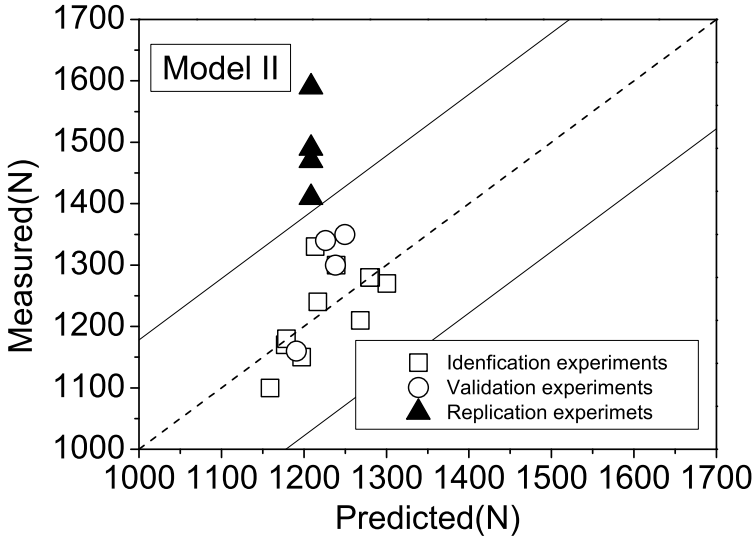

(b) model II

Figure 8.40: Comparison between experimental and calculated stress at break of uncrosslinked specimens

Table 8.43: Fisher-Snedecor test for stress at break of crosslinked specimens

Ratio	$F = \sigma_1^2/\sigma_2^2$	$(n_1; n_2)$	$1/F_{0.025}(n_2, n_1)$	$F_{0.025}(n_1, n_2)$	Validaiton
Model I					
Validation/Identification	2.097	(4 ; 4)	0.157	6.388	Yes
Validation/Replication	5.732	(4 ; 3)	0.152	9.117	Yes
Identification /Replication	2.733	(4 ; 3)	0.152	9.117	Yes
Model II					
Validation/Identification	3.433	(5 ; 4)	0.193	6.256	Yes
Validation/Replication	4.382	(5 ; 3)	0.185	79.014	Yes
Identification /Replication	1.276	(4 ; 3)	0.152	9.117	Yes

Table 8.44: Apparent confidence interval of the initial model coefficients with a risk of 5% for stress at break of crosslinked specimens

Coefficients	Values of $\hat{a}$	$\hat{a}_{min}$	$\hat{a}_{max}$	$\hat{a}_{min}^{red}$	$\hat{a}_{max}^{red}$	Θ	Significant
Model I							
a_0	1448.0313	637.3512	2258.7113	1102.7482	1793.3143	3.5439	Yes
a_1	-59.5000	-686.7377	567.7377	-458.1985	339.1985	1.2096	Yes
a_2	44.5938	-647.0504	736.2379	-354.1047	443.2922	1.1378	Yes
a_3	29.0469	-533.3645	591.4582	-423.0347	481.1285	1.1089	No
a_{11}	24.1563	-890.1920	938.5045	-374.5422	422.8547	1.0543	No
a_{22}	90.9375	-1067.1769	1249.0519	-331.9461	513.8211	1.1704	Yes
a_{33}	-64.0781	-1034.7549	906.5986	-516.1597	388.0035	1.1414	Yes
a_{12}	-59.5937	-606.8973	487.7098	-511.6753	392.4878	1.2444	Yes
a_{13}	-85.7969	-879.0559	707.4622	-574.1008	402.5070	1.2425	Yes
a_{23}	98.2969	-694.9622	891.5559	-390.0070	586.6008	1.2829	Yes
Model II							
a_0	1542.4286	1271.7244	1813.1327	1400.8048	1684.0523	1.4257	Yes
a_1	-57.4286	-371.3733	256.5161	-205.9648	91.1077	1.4478	Yes
a_2	27.5714	-243.1327	298.2756	-128.9995	184.1424	1.2268	Yes
a_3	51.5714	-268.8940	372.0368	-114.4971	217.6400	1.3836	Yes
a_{12}	-102.5714	-416.5161	211.3733	-268.6400	63.4971	1.9705	Yes
a_{13}	-76.5714	-407.6194	254.4766	-242.6400	89.4971	1.6018	Yes
a_{23}	88.8571	-252.6378	430.3521	-102.9023	280.6166	1.7034	Yes
a_{123}	-13.8571	-351.9704	324.2561	-205.6166	177.9023	1.0855	No

Table 8.45: Standard deviation and confidence interval of the polynomial model coefficients of both polynomial models with a risk of 5% for stress at break of crosslinked specimens

Coefficients	Values of $\hat{a}$	$\hat{a}_{min}$	$\hat{a}_{max}$	$\hat{a}^{red}_{min}$	$\hat{a}^{red}_{max}$
Model I: $y = a_0 + a_1Q + a_{22}T^2 + a_{33}N^2 + a_{12}QT + a_{13}QN + a_{23}TN$					
a_0	1468.0732	1189.6824	1746.464	1317.2027	1618.9436
a_1	-49.2683	-310.0519	211.5153	-223.4785	124.9419
a_2	32.4634	-251.8471	316.7739	-141.7467	206.6736
a_{22}	71.9512	-381.2729	525.1754	-112.8266	256.7290
a_{33}	-54.7561	-470.9440	361.4318	-252.2919	142.7797
a_{12}	-47.4634	-263.5412	168.6144	-244.9992	150.0723
a_{13}	-74.6159	-408.4779	259.2462	-287.9789	138.7471
a_{23}	87.1159	-246.7462	420.9779	-126.2471	300.4789
Model II: $y = a_0 + a_1Q + a_2T + a_3N + a_{12}QT + a_{13}QN + a_{23}TN$					
a_0	1534.0235	1407.9711	1660.076	1432.9922	1635.0549
a_1	-50.9736	-244.7115	142.7643	-156.9361	54.989
a_2	22.6048	-150.0784	195.2881	-89.0895	134.2992
a_3	41.4790	-104.8196	187.7777	-76.9907	7159.9488
a_{12}	-92.8690	-239.9645	54.2264	-211.3388	25.6007
a_{13}	-70.6577	-283.2057	141.8904	-189.1274	47.8121
a_{23}	83.0787	-138.8033	304.9607	-53.7184	219.8758

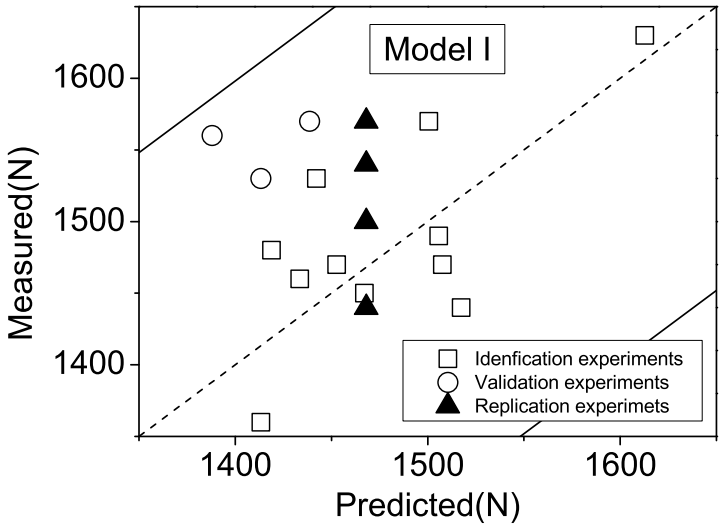

(a) model I

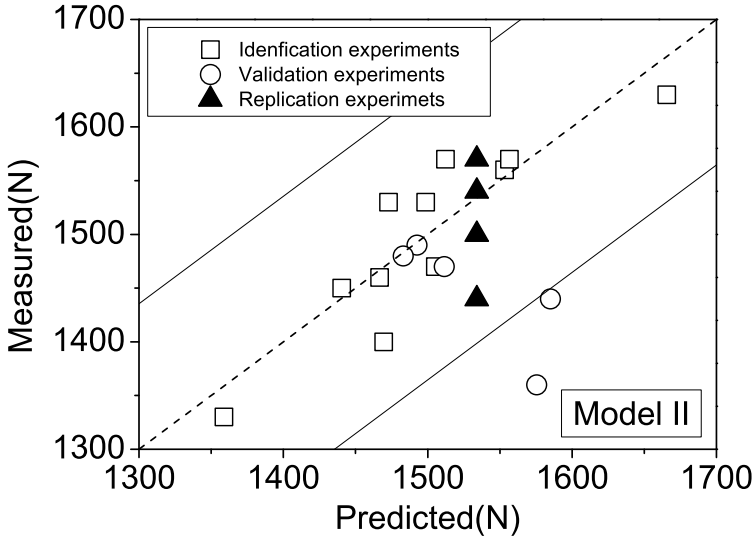

(b) model II

Figure 8.41: Comparison between experimental and calculated stress at break of crosslinked specimens

Table 8.46: Fisher-Snedecor test for Young's modulus of uncrosslinked specimens

Ratio	$F = \sigma_1^2/\sigma_2^2$	$(n_1; n_2)$	$1/F_{0.025}(n_2, n_1)$	$F_{0.025}(n_1, n_2)$	Validaiton
Model I					
Validation/Identification	27.947	(3 ; 6)	0.112	4.757	No
Validation/Replication	31.829	(3 ; 3)	0.108	9.277	No
Identification /Replication	1.139	(6 ; 3)	0.210	8.941	Yes
Model II					
Validation/Identification	1.146	(4 ; 5)	0.160	5.192	Yes
Validation/Replication	9.692	(4 ; 3)	0.152	9.117	No
Identification /Replication	8.454	(5 ; 3)	0.185	9.014	Yes

Table 8.47: Apparent confidence interval of the initial model coefficients with a risk of 5% for Young's modulus of uncrosslinked specimens

Coefficients	Values of $\hat{a}$	$\hat{a}_{min}$	$\hat{a}_{max}$	$\hat{a}_{min}^{red}$	$\hat{a}_{max}^{red}$	Θ	Significant
Model I							
a_0	1940.3749	574.0909	3306.6590	1342.8309	2537.9190	5.7598	Yes
a_1	-74.9880	-1430.1447	1280.1687	-806.8271	656.8510	1.1172	Yes
a_2	173.2810	-1015.4195	1361.9815	-516.7034	863.2655	1.3413	Yes
a_3	14.6550	-820.2157	849.5257	-717.1840	746.4940	1.0357	No
a_{11}	4.1291	-1776.7254	1784.9836	-727.7099	735.9682	1.0046	No
a_{22}	252.4221	-1520.4889	2025.3331	-479.4169	984.2612	1.3320	Yes
a_{33}	-16.9609	-1719.4261	1685.5042	-748.8000	714.8781	1.0201	No
a_{12}	-108.6548	-1046.3205	829.0109	-891.0236	673.7141	1.2621	Yes
a_{13}	-20.3845	-1490.7101	1449.9411	-865.4394	824.6704	1.0281	No
a_{23}	87.8845	-1382.4411	1558.2101	-757.1704	932.9394	1.1271	Yes
Model II							
a_0	2172.2857	534.0396	3810.5318	1315.2077	3029.3637	7.1353	Yes
a_1	102.7143	-1797.2148	2002.6434	-796.1967	1001.6253	1.1143	Yes
a_2	27.7143	-1610.5318	1665.9604	-919.8211	975.2497	1.0344	Yes
a_3	-130.2857	-2069.6769	1809.1055	-1135.2987	874.7273	1.1440	Yes
a_{12}	17.2857	-1882.6434	1917.2148	-987.7273	1022.2987	1.0184	No
a_{13}	5.2857	-1998.1491	2008.7205	-999.7273	1010.2987	1.0053	No
a_{23}	-28.4286	-2095.0862	2038.2290	-1188.9177	1132.0605	1.0279	Yes
a_{123}	43.4286	-2002.7637	2089.6208	-1117.0605	1203.9177	1.0434	Yes

Table 8.48: Standard deviation and confidence interval of the polynomial model coefficients of both polynomial models with a risk of 5% for Young's modulus of uncrosslinked specimens

Coefficients	Values of $\hat{a}$	$\hat{a}_{min}$	$\hat{a}_{max}$	$\hat{a}^{red}_{min}$	$\hat{a}^{red}_{max}$
Model I: $y = a_0 + a_1Q + a_2T + a_{22}T^2 + a_{12}QT + a_{23}TN$					
a_0	1932.5008	1658.0684	2206.9332	1778.3195	2086.6822
a_1	-58.3331	-271.1532	154.4869	-247.1659	130.4997
a_2	158.3298	-45.9005	362.5602	-19.7034	336.3631
a_{22}	240.8012	-103.0804	584.6829	51.9684	429.634
a_{12}	-101.4236	-313.0127	110.1655	-303.2943	100.4472
a_{23}	70.5543	-173.9268	315.0354	-147.4910	288.5997
Model II: $y = a_0 + a_1Q + a_2T + a_3N + a_{23}TN + a_{123}QTN$					
a_0	2183.2827	1611.9888	2754.5766	1720.0713	2646.4942
a_1	94.7818	-433.2256	622.7891	-391.0385	580.6020
a_2	33.2638	-530.1362	596.6637	-478.8357	545.3633
a_3	-117.0019	-790.8092	556.8054	-660.1654	426.1616
a_{23}	-22.1727	-714.8257	670.4803	-649.3639	605.0186
a_{123}	29.5731	-695.8465	754.9926	-597.6182	656.7643

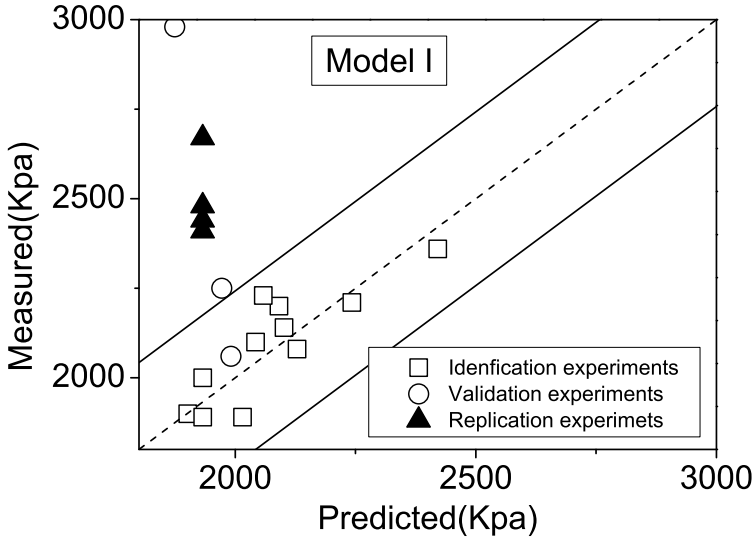

(a) model I

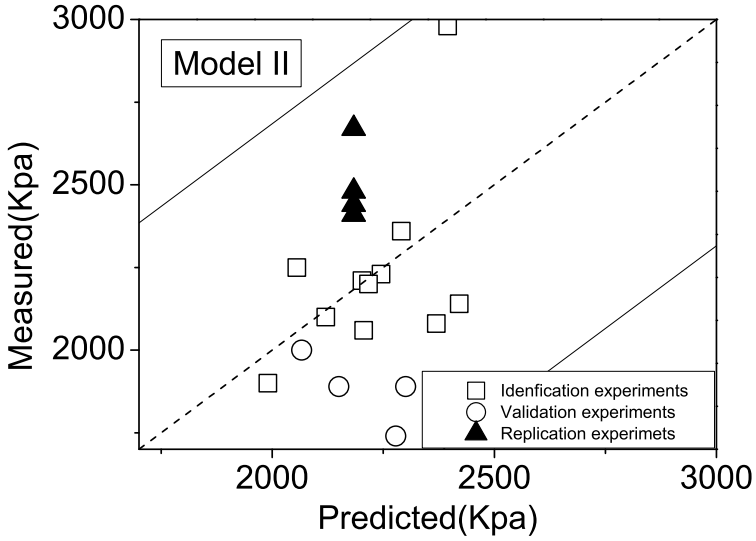

(b) model II

Figure 8.42: Comparison between experimental and calculated Young's modulus of uncrosslinked specimens

Table 8.49: Fisher-Snedecor test for Young's modulus of crcrosslinked specimens

Ratio	$F = \sigma_1^2/\sigma_2^2$	$(n_1; n_2)$	$1/F_{0.025}(n_2, n_1)$	$F_{0.025}(n_1, n_2)$	Validation
Model I					
Validation/Identification	20.545	(4 ; 4)	0.157	6.388	No
Validation/Replication	11.562	(4 ; 3)	0.152	9.117	No
Identification /Replication	0.563	(4 ; 3)	0.152	9.117	Yes
Model II					
Validation/Identification	5.775	(5 ; 4)	0.193	6.256	Yes
Validation/Replication	4.935	(5 ; 3)	0.185	9.014	Yes
Identification /Replication	0.855	(4 ; 3)	0.152	9.117	Yes

Table 8.50: Apparent confidence interval of the initial model coefficients with a risk of 5% for Young's modulus of crosslinked specimens

Coefficients	Values of $\hat{a}$	$\hat{a}_{min}$	$\hat{a}_{max}$	$\hat{a}^{red}_{min}$	$\hat{a}^{red}_{max}$	Θ	Significant
Model I							
a_0	2366.4375	1022.5123	3710.3627	1794.0360	2938.8390	3.6287	Yes
a_1	137.7500	-902.0690	1177.5690	-523.2024	798.7024	1.3054	Yes
a_2	90.8125	-1055.7779	1237.4029	-570.1399	751.7649	1.1720	Yes
a_3	131.9063	-800.4452	1064.2577	-617.5433	881.3558	1.3296	Yes
a_{11}	-60.8125	-1576.5962	1454.9712	-721.7649	600.1399	1.0836	No
a_{22}	185.6250	-1734.2681	2105.5181	-515.4208	886.6708	1.2141	Yes
a_{33}	-276.8438	-1886.0074	1332.3199	-1026.2933	472.6058	1.4156	Yes
a_{12}	67.9375	-839.3686	975.2436	-681.5120	817.3870	1.1619	Yes
a_{13}	17.2188	-1297.8263	1332.2638	-792.2793	826.7168	1.0265	No
a_{23}	150.2812	-1164.7638	1465.3263	-659.2168	959.7793	1.2580	Yes
Model II							
a_0	2601.2143	1823.4295	3378.9991	2194.3021	3008.1264	1.8531	Yes
a_1	174.6190	-727.4042	1076.6423	-252.1540	601.3921	1.4801	Yes
a_2	-51.2143	-828.9991	726.5705	-501.0726	398.6440	1.1410	Yes
a_3	439.1190	-481.6395	1359.8776	-38.0277	916.2658	2.8234	Yes
a_{12}	-232.9524	-1134.9756	669.0708	-710.0992	244.1944	1.6963	Yes
a_{13}	103.3810	-847.7833	1054.5452	-373.7658	580.5277	1.2439	Yes
a_{23}	61.9286	-919.2518	1043.1089	-489.0331	612.8902	1.1347	No
a_{123}	-286.0952	-1257.5593	685.3689	-837.0569	264.8664	1.8349	Yes

Table 8.51: Standard deviation and confidence interval of the polynomial model coefficients of both polynomial models with a risk of 5% for Young's modulus of crosslinked specimens

Coefficients	Values of $\hat{a}$	$\hat{a}_{min}$	$\hat{a}_{max}$	$\hat{a}^{red}_{min}$	$\hat{a}^{red}_{max}$
Model I: $y = a_0 + a_1Q + a_2T + a_3N + a_{22}T^2 + a_{33}N^2 + a_{12}QT + a_{23}TN$					
a_0	2333.8204	1871.4508	2796.190	2089.6935	2577.9473
a_1	125.8522	-196.8764	448.5807	-156.0413	407.7456
a_2	102.6063	-247.8905	453.1031	-179.2872	384.4997
a_3	144.0085	-226.7812	514.7982	-175.6286	463.6457
a_{22}	184.5845	-528.2272	897.3961	-114.4087	483.5776
a_{33}	-291.8963	-925.2382	341.4456	-611.5334	27.7408
a_{12}	61.5167	-310.1262	433.1595	-258.1205	381.1538
a_{23}	163.918	-227.4684	555.3045	-181.3295	509.1656
Model II: $y = a_0 + a_1Q + a_2T + a_3N + a_{12}QT + a_{13}QN + a_{123}QTN$					
a_0	2579.0372	2076.2858	3081.7885	2284.2147	2873.8596
a_1	218.7641	-193.9379	631.466	-90.4483	527.9765
a_2	-87.6182	-465.6843	290.4478	-413.5567	238.3202
a_3	414.4313	-189.5035	1018.3661	68.7213	760.1413
a_{12}	-203.8711	-765.7246	357.9825	-549.581	141.8389
a_{13}	150.0366	-283.6553	583.7285	-195.6734	495.7466
a_{123}	-260.7798	7-901.8483	380.2886	-659.9713	138.4116

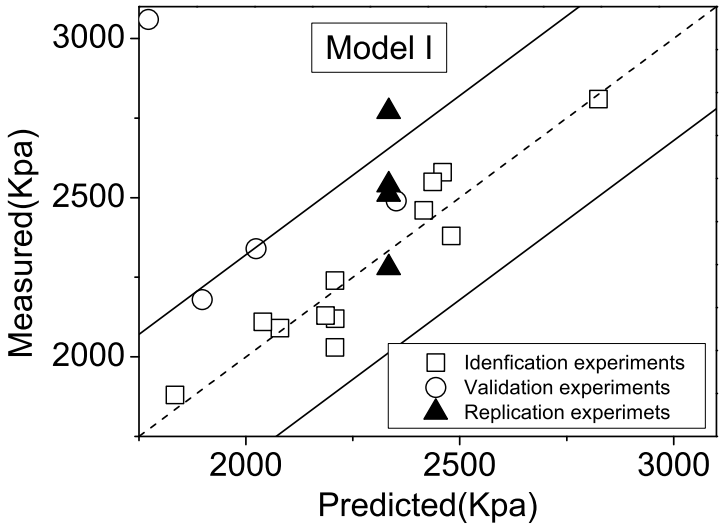

(a) model I

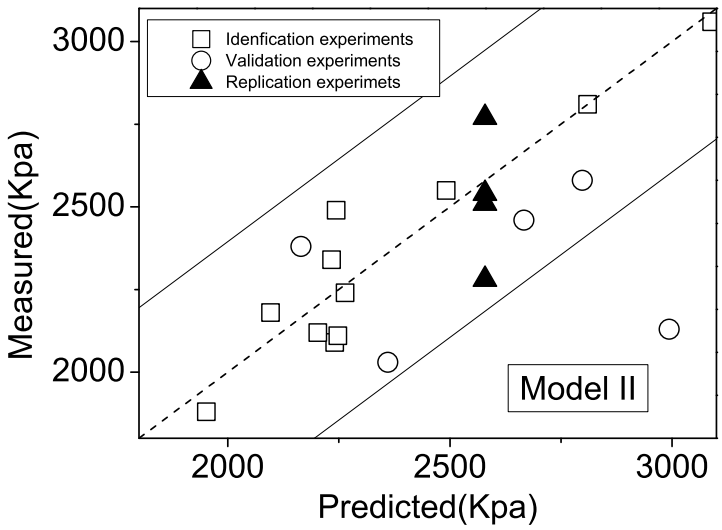

(b) model II

Figure 8.43: Comparison between experimental and calculated Young's modulus of crosslinked specimens

Table 8.52: Fisher-Snedecor test for elongation at break of uncrosslinked specimens

Ratio	$F = \sigma_1^2/\sigma_2^2$	$(n_1; n_2)$	$1/F_{0.025}(n_2, n_1)$	$F_{0.025}(n_1, n_2)$	Validation
Model I					
Validation/Identification	5.293	(3 ; 6)	0.112	4.757	No
Validation/Replication	6.368	(3 ; 3)	0.108	9.277	Yes
Identification /Replication	1.203	(6 ; 3)	0.210	8.941	Yes
Model II					
Validation/Identification	1.077	(4 ; 5)	0.160	5.192	Yes
Validation/Replication	1.641	(4 ; 3)	0.152	9.117	Yes
Identification /Replication	1.525	(5 ; 3)	0.185	9.014	Yes

Table 8.53: Apparent confidence interval of the initial model coefficients with a risk of 5% for elongation at break of uncrosslinked specimens

Coefficients	Values of $\hat{a}$	$\hat{a}_{min}$	$\hat{a}_{max}$	$\hat{a}_{min}^{red}$	$\hat{a}_{max}^{red}$	Θ	Significant
Model I							
a_0	19.1085	-43.8556	82.0726	-8.4288	46.6458	1.8714	Yes
a_1	-1.4986	-63.9499	60.9527	-35.2248	32.2276	1.0492	No
a_2	1.0756	-53.7047	55.8559	-30.7218	32.8730	1.0401	No
a_3	0.1200	-38.3544	38.5943	-33.6062	33.8462	1.0063	No
a_{11}	-7.2860	-89.3553	74.7832	-41.0122	26.4402	1.1949	Yes
a_{22}	5.7910	-75.9122	87.4941	-27.9352	39.5172	1.1526	Yes
a_{33}	-1.2125	-79.6692	77.2443	-34.9387	32.5137	1.0314	No
a_{12}	-2.0290	-45.2405	41.1826	-38.0838	34.0259	1.0985	Yes
a_{13}	-3.0496	-70.8084	64.7092	-41.9933	35.8941	1.0943	Yes
a_{23}	2.7246	-65.0342	70.4834	-36.2191	41.6683	1.0838	Yes
Model II							
a_0	16.6364	-14.2862	47.5591	0.4587	32.8142	3.3290	Yes
a_1	-1.4406	-37.3026	34.4215	-18.4080	15.5268	1.0837	No
a_2	1.9636	-28.9591	32.8862	-15.9216	19.8487	1.1356	Yes
a_3	-1.8431	-38.4500	34.7638	-20.8132	17.1270	1.1060	Yes
a_{12}	-0.6677	-36.5298	35.1943	-19.6378	18.3024	1.0379	No
a_{13}	-4.4944	-42.3102	33.3214	-23.4645	14.4757	1.2698	Yes
a_{23}	3.4829	-35.5263	42.4920	-18.4219	25.3876	1.1961	Yes
a_{123}	4.0630	-34.5599	42.6858	-17.8418	25.9678	1.2351	Yes

Table 8.54: Standard deviation and confidence interval of the polynomial model coefficients of both polynomial models with a risk of 5% for elongation at break of uncrosslinked specimens

Coefficients	Values of $\hat{a}$	$\hat{a}_{min}$	$\hat{a}_{max}$	$\hat{a}^{red}_{min}$	$\hat{a}^{red}_{max}$
Model I: $y = a_0 + a_{11}Q^2 + a_{22}T^2 + a_{12}QT + a_{13}QN + a_{23}TN$					
a_0	18.572	5.3200	31.8240	11.4499	25.6941
a_{11}	-7.988	-27.3555	11.3795	-16.7107	0.7348
a_{22}	5.5120	-13.8555	24.8795	-3.2107	14.2348
a_{12}	-1.7566	-11.1725	7.6594	-11.0816	7.5684
a_{13}	-1.7625	-12.4456	8.9206	-11.8346	8.3096
a_{23}	1.4375	-9.2456	12.1206	-8.6346	11.5096
Model II: $y = a_0 + a_2T + a_3N + a_{13}QN + a_{23}TN + a_{123}QTN$					
a_0	16.1152	5.2089	27.0214	7.2746	24.9558
a_2	1.0391	-9.8671	11.9453	-8.7346	10.8128
a_3	-2.4176	-15.2785	10.4433	-12.7842	7.9489
a_{13}	-3.2415	-14.7725	8.2895	-13.608	7.1251
a_{23}	2.2769	-11.1726	15.7264	-9.6934	14.2471
a_{123}	4.6508	-9.1949	18.4965	-7.3195	16.6211

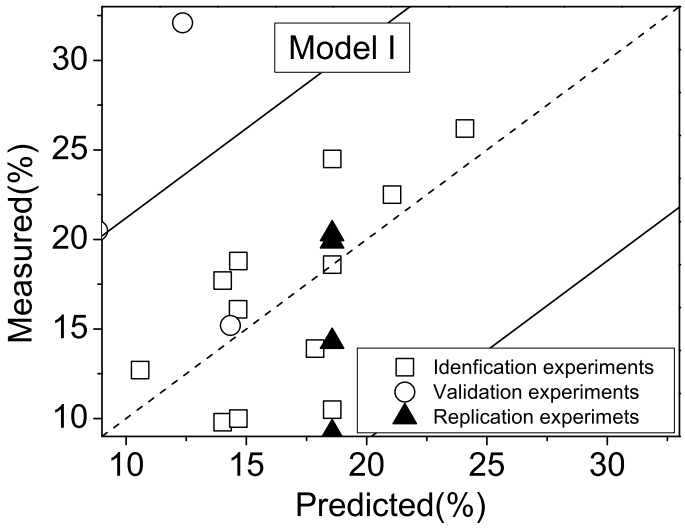

(a) model I

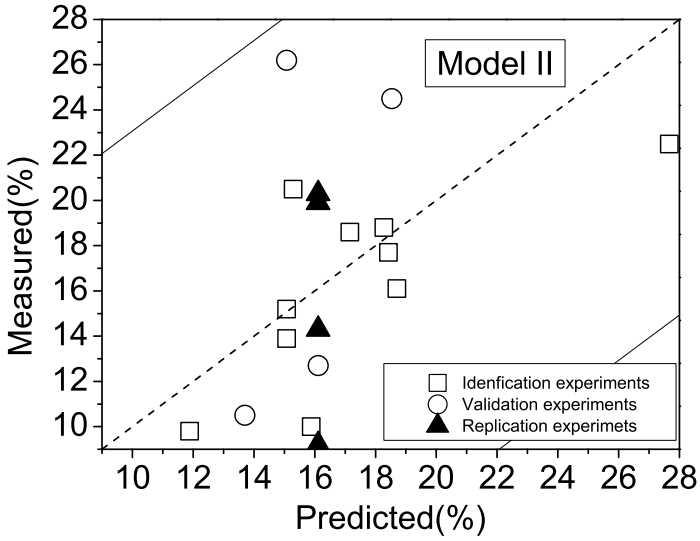

(b) model II

Figure 8.44: Comparison between experimental and calculated elongation at break of uncrosslinked specimens

Table 8.55: Fisher-Snedecor test for elongation at break of crosslinked specimens

Ratio	$F = \sigma_1^2/\sigma_2^2$	$(n_1; n_2)$	$1/F_{0.025}(n_2, n_1)$	$F_{0.025}(n_1, n_2)$	Validation
Model I					
Validation/Identification	3.842	(4 ; 5)	0.160	5.192	Yes
Validation/Replication	6.402	(4 ; 3)	0.152	9.117	Yes
Identification /Replication	1.666	(5 ; 3)	0.185	9.014	Yes
Model II					
Validation/Identification	0.447	(5 ; 4)	0.193	6.256	Yes
Validation/Replication	2.205	(5 ; 3)	0.185	9.014	Yes
Identification /Replication	4.930	(4 ; 3)	0.152	9.117	Yes

Table 8.56: Apparent confidence interval of the initial model coefficients with a risk of 5% for elongation at break of crosslinked specimens

Coefficients	Values of $\hat{a}$	$\hat{a}_{min}$	$\hat{a}_{max}$	$\hat{a}_{min}^{red}$	$\hat{a}_{max}^{red}$	Θ	Significant
Model I							
a_0	13.6644	-21.6560	48.9847	-1.3792	28.7079	2.2619	Yes
a_1	1.4775	-25.8505	28.8055	-15.8933	18.8483	1.1143	Yes
a_2	0.8081	-29.3260	30.9422	-16.5627	18.1789	1.0551	No
a_3	-2.4184	-26.9220	22.0852	-22.1151	17.2782	1.2190	Yes
a_{11}	-2.0081	-41.8452	37.8289	-19.3789	15.3627	1.1062	Yes
a_{22}	3.3563	-47.1014	53.8139	-15.0683	21.7808	1.1425	Yes
a_{33}	-0.9309	-43.2222	41.3603	-20.6276	18.7657	1.0450	No
a_{12}	-0.4206	-24.2660	23.4247	-20.1173	19.2760	1.0359	No
a_{13}	-2.3153	-36.8767	32.2460	-23.5901	18.9595	1.1436	Yes
a_{23}	-1.3347	-35.8960	33.2267	-22.6095	19.9401	1.0803	Yes
Model II							
a_0	14.1071	-11.7104	39.9247	0.6002	27.6141	3.4093	Yes
a_1	3.5554	-26.3861	33.4969	-10.6108	17.7215	1.2695	Yes
a_2	-2.5071	-28.3247	23.3104	-17.4396	12.4253	1.2151	Yes
a_3	-4.3071	-34.8705	26.2563	-20.1454	11.5311	1.3281	Yes
a_{12}	1.5696	-28.3719	31.5111	-14.2686	17.4079	1.1106	Yes
a_{13}	1.9696	-29.6030	33.5423	-13.8686	17.8079	1.1331	Yes
a_{23}	-4.5607	-37.1297	28.0083	-22.8492	13.7278	1.3257	Yes
a_{123}	0.1732	-32.0733	32.4197	-18.1153	18.4617	1.0108	No

Table 8.57: Standard deviation and confidence interval of the polynomial model coefficients of both polynomial models with a risk of 5% for elongation at break of crosslinked specimens

Coefficients	Values of $\hat{a}$	$\hat{a}_{min}$	$\hat{a}_{max}$	$\hat{a}^{red}_{min}$	$\hat{a}^{red}_{max}$
Model I: $y = a_0 + a_1Q + a_3N + a_{11}Q^2 + a_{22}T^2 + a_{13}QN + a_{23}TN$					
a_0	13.8253	2.9029	24.7476 78.9474	18.7031	
a_1	2.0460	-4.4094	8.5014	-3.5865	7.6785
a_3	-2.7527	-9.6876	4.1822	-9.1394	3.6339
a_{11}	-2.2242	-14.8840	10.4356	-7.8566	3.4083
a_{22}	2.2769	-9.3394	13.8933	-3.6972	8.2511
a_{13}	-1.6270	-9.6241	6.3701	-8.5253	5.2713
a_{23}	-2.0230	-10.0201	5.9741	-8.9213	4.8753
Model II: $y = a_0 + a_1Q + a_2T + a_3N + a_{12}QT + a_{13}QN + a_{23}TN$					
a_0	14.2122	2.3269	26.0975	4.6861	23.7383
a_1	3.4747	-14.7926	21.7420	-6.5164	13.4657
a_2	-2.4451	-18.7271	13.8370	-12.9766	8.0865
a_3	-4.1810	-17.9753	9.61330	-15.3513	6.9894
a_{12}	1.4484	-12.4211	15.3178	-9.7220	12.6187
a_{13}	1.8957	-18.1452	21.9366	-9.2746	13.0661
a_{23}	-4.4885	-25.4094	16.4325	-17.3869	8.4099

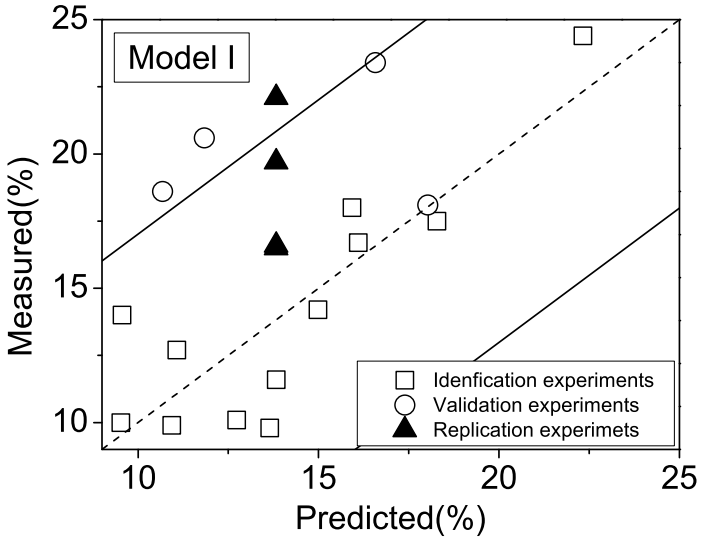

(a) model I

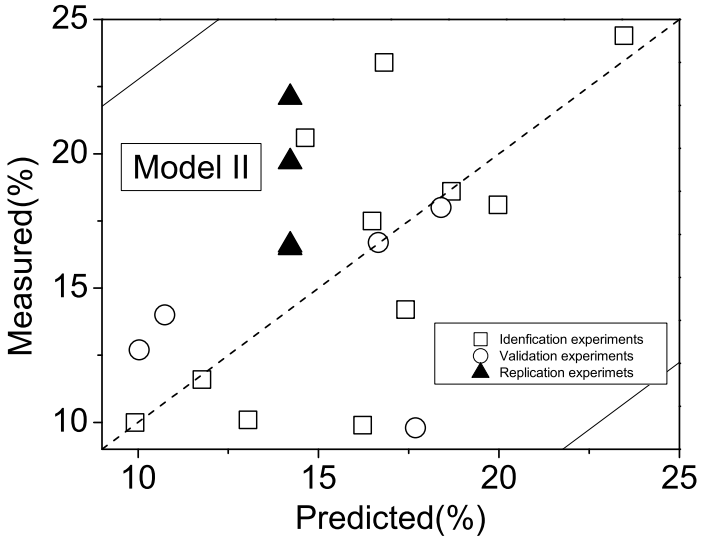

(b) model II

Figure 8.45: Comparison between experimental and calculated elongation at break of crosslinked specimens

8.4.5 Final models

Using the certqin two polynomial models, four significant equations based on the statistics points can be obained.They are:
1) Model I for percentage of grafted silane

$$\begin{aligned} Silane\%_{grafted} = \quad & 0.2755 - 0.0195Q - 0.0255T - 0.0353N \\ & +0.06517T^2 - 0.1124N^2 - 0.0249QT - 0.0573QN \end{aligned} \tag{8.12}$$

2) Model II for percentage of polymerized silane

$$Silane\%_{polymerized} = 0.272 - 0.058Q + 0.020N + 0.045QT + 0.028QN - 0.042QTN \quad (8.13)$$

3) Model II for percentage of complex viscosity of extracted samples

$$\eta_{0.063-ex} = 0.3051 + 0.0491Q + 0.0514T - 0.0360N - 0.0202QT + 0.0348QN - 0.0638QTN \quad (8.14)$$

4) Model II for torque

$$Torque = 67.3125 + 14.9655Q - 3.0625T - 6.9375N - 8.2069QN \quad (8.15)$$

It should be noted that the bad replication is due to abnormal operating conditions during the extrusion process. In the present study, after obtaining 15-20 samples from the extruder, some parts of the injection pump were dissolved by silane, which caused a bad control of the injection rate of the liquid. This abnormal working condition caused a bad replication. Thus the models established for prediction and optimization are not convincing.

For the tensile strength, these two models cannot be used, a new model should be searched.

8.5 Optimization

The aim of industrial production of silane grafting onto polypropylene by reactive extrusion is to obtain high grafting ratio, and high mechanical properties, meanwhile, to restrain side reaction, silane polymerization and polypropylene degradation, etc. Traditionally, optimizing this process has been done by minimizing an objective cost function made up of the weighted sum of all individual criteria. However, this approach often fails because of the difficulty to attribute a relative weight to individual criteria and because of the large number of local minima inherent in these complex systems. Recent progress in multicriteria optimization has led to methods for obtaining a solution to these complex problems using the knowledge of a human expert in a natural way. Most of these techniques require a priori that the domain of non-dominated solutions, known as the Pareto domain, be established. One multicriteria optimization technique, called the rough set method proposed by Pawlak in the early 1980s ([Pawlak, 1982, 1997]), has been widely studied in recent years ([Polkowski and Skowron, 1998]). This procedure is able to transform the preferences of a human expert, who ranks a small set of possible solutions extracted from different regions of the Pareto domain, to a simple set of rules for ranking the entire Pareto domain.

8.5.1 Generating the Pareto domain

The Pareto domain represents the collection of solutions taken from the total solution set that are not dominated by any other solution within this set. In this respect, one member in the set is said to be dominated by another if its values for all the optimization criteria are worst than those of the second member. The solution domain may then be divided into two groups: a set consisting of dominant solutions and another containing those points that are dominated by at least another solution.

While, in principle at least, one could generate the entire solution set and then determine the Pareto domain from this set, in practice this is infeasible. Instead, various algorithms have been developed that seek a reasonable representation of the Pareto domain from a finite set of solutions. One such method, referred to as the evolutionary genetic algorithm and described below, was used here to determine a finite representation of the Pareto domain ([Bicking et al., 1994, Viennet et al., 1996]).

The first step of the evolutionary genetic algorithm consists in generating an initial number of possible solutions. This is done by randomly selecting values for each of the six process inputs that lie within their acceptable ranges. The process outputs in each case are then determined using the stacked neural networks. (For example, 7000 unique solutions are calculated to represent a first approximation to the solution set). Further, each point in the solution set is initially assigned a domination number equal to 0.

Next, each unique pair of points from the solution set is compared to determine if one of the two points dominates the other. When a point is dominated by its partner, its domination number is incremented by 1. Upon completing the comparison, the entire solution set is sorted in ascending order according to the domination number. All of the dominant points (those with a domination number of 0) and a predetermined percentage of the dominated points having the lowest domination number are selected to form part of the new solution set. In other words, if M represents the total number of points in the original set (i.e. 7000) and N_0 represents the number of dominant points, the number of selected points, N, is given by

$$N = N_0 + INT(F_s(M - N_0)) \tag{8.16}$$

where F_S, referred to as the survival fraction, lies between 0 and 1 and where $INT(X)$ returns the integer value of X.

This subset of N points forms part of the next generation estimate of the Pareto domain. Meanwhile, those dominated points eliminated from the set are replaced by new points generated through the evolutionary genetic algorithm as follows. For each eliminated point, a random pair of points is selected from amongst the vector of N points that were retained from the previous generation. A new set of inputs I_p^{k+1} (input variable $p = 1...6$; generation $= k + 1$) is then determined from this pair, where each new input I_p^{k+1} is a weighted average of the inputs, $I_{p,i}^k$ and $I_{p,j}^k$, from the two parent points, i and j:

$$I_p^{k+1} = D_p I_{p,i}^k + (1 - D_p) I_{p,j}^k \tag{8.17}$$

where the variable D_p is a randomly selected number lying between 0 and 1 which takes a different value for each input and each generation. This derived set of inputs is then used to generate a new candidate for the solution set, replacing the eliminated ancestor.

Having replaced the eliminated members with this new generation of points, the domination ranking, solution set reduction and replacement process can be repeated to determine the next generation of solution set members. This is repeated until 6000 points contained within the solution set are dominant points. This final data set of 6000 points is then assumed to approximate the true Pareto domain. It was necessary to generate approximately 100000 points before obtaining the desired 6000 non-dominated points using the evolutionary algorithm whereas 10 times more iterations were necessary when purely random generation was used.

8.5.2 Planification for multicriteria optimization in the process of silane grafting onto polypropylene

The complex reactions and operating conditions in the process of silane grafting onto polypropylene by reactive extrusion in the extruder causes a poor repeatability of experiments, which is the main reason why almost all of the polynomial models established above cannot be used. In order to optimize this process, operating conditions should be improved to make the extrusion process more stable to get good repeatability of experiments. This is the work we will do next.

8.6 Conclusion

Silane grafted PP was prepared by reactive extrusion using a free radical mechanism. First, it was shown by FTIR spectroscopy that silane was indeed grafted on PP and that cross-linking did not happen during the reactive extrusion process. Furthermore, a quantitative analysis method of the silane grafting degree on PP was developed using FTIR spectroscopy. The grafting of silane on PP and/or blends of silane grafted PP, homo-polymerized silane and PP can improve the material tensile strength, and this property can be further increased by forming the cross-linked network structure by water-cross-linking. According to GPC with a RALS detector and the dynamic melt rheological measurements, homo-polymerization of silane and PP chain scission are the two main competitive side reactions in the extruder.

During the process, silane is grafted onto PP, on one hand, and polymerized, on the other hand. The PP is also subjected to chain scission, as revealed by its complex viscosity at a very low frequency. Therefore, the quality of the silane grafted PP depends very much on the percentages of grafted and polymerized silane as well as the complex viscosity at a very low frequency. For a given composition for the grafting system, it may be affected by the screw profile of the twin screw extruder, feed rate, screw speed, and barrel temperature. The screw profile should ensure good mixing between the PP melt and the small molecule reagents (silane and free radical initiator) at the location at which the small molecule reagents are injected. Residence time is also an important process parameter. For a given screw profile, the effects of feed rate, screw speed and barrel temperature are complex and are highly coupled. A simple relation between the product properties and the operating conditions (feed rate Q, screw speed N, barrel temperature T) could not be established just by experimental means. The modeling and optimization method was attempted to help to solve this multi-objective decision problem. Black box and two polynomial models were attempted to simulate this process. However, due to the abnormal working of injection of the liquid, which causes bad replication, significant models established based on the statistical tests cannot be used for predication and optimization. For this extrusion polymerization, an improved operating process should be developed to get a good repeatability of experiments. Then, polynomial models and multi-objective optimization can be used for further study.

Bibliography

G. S. Ahmed, M. Gilbert, S. Mainprize, and M. Rogerson. Ftir analysis of silane grafted high density polyethylene. *Plastics, Rubber and Composites*, 38:13–20, 2009.

F. Bicking, C. Fonteix, J. P. Corriou, and I. Marc. Global optimization by artificial life: a new technique using genetic population evolution. *RAIRO-Operation Research*, 28: 23–36, 1994.

R. A. Fisher, editor. *Statistical Methods for Research Workers.* Oliver and Boyd, Edinburgh, 1970.

C. Fonteix, F. Bicking, E. Perrin, and I. Marc. Haploid and diploid algorithms, a new approach for global optimization: compared performances. *Int. J. Syst. Sci.*, 26:1919–1933, 1995.

S. Jain, J. G. P. Goossens, and M. van Duin. Synthesis, characteriztion and properties of (vinyl triethoxy silane-grafted pp)/silica nanocomposites. *Macromol. Symp.*, 233: 225–234, 2006.

A. I. Khuri. A measure of rotabability for response-surface designs. *Technometrics*, 30: 95, 1988.

Z. Pawlak. Rough sets. *International Journal of Computer and Information Sciences*, 11: 341–356, 1982.

Z. Pawlak. Rough set approach to knowledge-based decision support. *European Journal of Operational Research*, 99:48–57, 1997.

L. Polkowski and A. Skowron, editors. *Rough Sets in Knowledge Discovery.* Physica-Verlag, Heidelberg, 1998.

F. Pukelsheim, editor. *Optimal design of experiments.* Wiley, New York, 1993.

R. Rached, R. Rahouadj, C. Fonteix, S. Hoppe, F. Pla, and C. Cunat. Mechanical behaviour modelling of a nanostructured polyamide blends obtained by reactive extrusion process. *Chem. Eng. Sci.*, 63:3843–3857, 2008.

G. W. Snedecor and W. G. Cochran, editors. *Statistical Methods.* Iowa State University Press, Ames, 1989.

R. Viennet, C. Fonteix, and I. Marc. Multicriteria optimization using a genetic algorithm for determining a pareto set. *International Journal of Systems Science*, 27:255–260, 1996.

E. Walter and L. Pronzato, editors. *Identification of Parametric Models from Experimental Data.* Springer, London, 1997.

Chapter 9

Conclusion

The thesis is composed by two parts:
- Part I. Two theoretical models were established in order to compare macro- and mini-emulsion polymerization. A validation with respect to experimental data was performed.
- Part II. The improvement of polypropylene properties was experimentally investigated by reactive extrusion. Statistical models of experimental design were searched for and an optimization study conclude that part.

In part I, the main conclusion is that the differences between macro- and mini- emulsion polymerization are related to the nucleation mechanism. Micelle nucleation is the dominant particle nucleation process in macro-emulsion polymerization, and by comparison, doplet nucleation is the dominant one in mini-emulsion polymerization. The establishment of a model in mini-emulsion polymerization is more difficult than that in macro-emulsion polymerization, as in mini-emulsion polymerization, the number of the nuclei places is more complex to be calculated. A model of macro-emulsion polymerization has been established based on 0-1 model, and by comparison, a model of mini-emulsion polymerization has been established, based on the balance of chemical potentials of the monomer in the reactor. In general, a good agreement is observed between models and experimental data taken from the literature. The model of macro-emulsion polymerization allows us to predict the radical chain size distribution for a given class of particle sizes and the particle size distribution, whereas the model of mini-emulsion polymerization allows us to predict the particle size distribution and the change of the droplets sizes. However, to obtain a more precise radical chain size distribution, the models involving both transfer of polymeric radical to the monomers in the particles and desorption of monomeric radicals in the particles into the aqueous phase should be developed.

In part II, reactive extrusion is proved a effective method to obtain grafted polypropylene (PP). Two kinds of monomers, maleic anhydride (MAH) and silane, were used to improve the properties of PP. To improve the grafting degree of MAH on PP, organically modified montmorillonite (MMT) was used as a nanoreactor. The effects of the amounts of MAH and of the initiator were studied. Strong interactions between MAH and MMT surface and the encapsulation of active species improve the grafting degree. With excessive MAH, a cage around MMT will be formed to prevent the formation of $PP^{\bullet}$ and reduce the grafting degree. To improve the grafting degree of silane on PP, the operating conditions were studied. The good mixing between the PP melt and the liquid small molecules (mainly silane and initiator) after the injection is a key to the grafting reaction. Moreover, the residence time is also an important process parameter. A long

residence time, a high barrel temperature and/or a strong mixing intensity will enforce the PP chain degradation. However, a simple relation between the product properties and the operating conditions (feed rate Q, screw speed N, barrel temperature T could not be found. To obtain the highest amount of silane grafted on PP, and simultaneously, restrain the two side reactions, i.e. polymerization of silane and PP chain degradation, the multi-objective optimization method was tried. However, because of the poor repeatability of experiments caused by the complex reactions and the operating conditions in the extruder, the polynomial models established could not well simulate the process. In order to correctly perform the multi-objective optimization of this system, a more stable extrusion process should be developed.

UNIVERSITÉ DE LORRAINE

AUTORISATION DE SOUTENANCE
DU DOCTORAT DE L'UNIVERSITE DE LORRAINE

o0o

VU LES RAPPORTS ETABLIS PAR :
Monsieur PUAUX Jean-Pierre, Professeur, PolytechLyon, Université de Lyon,
Madame OTHMAN Nida, Chargé de Recherche HDR, LAGEP, Université de Lyon 1.

Le Président de l'Université de Lorraine, autorise :

Monsieur LI Zheng-Hui

à soutenir devant un jury de l'UNIVERSITE DE LORRAINE, une thèse intitulée :

"Modélisation des procédés de polymérisation en émulsion et d'extrusion réactive"

en vue de l'obtention du titre de :

DOCTEUR DE L'UNIVERSITE DE LORRAINE

Intitulé du doctorat : **"Génie des Procédés et des Produits"**

Fait à Vandoeuvre, le **17 juillet 2012**
Le Président de l'Université de Lorraine,
Pierre MUTZENHARDT

Université de Lorraine
Le Président

UNIVERSITÉ DE LORRAINE
34 COURS LÉOPOLD - CS 25233
54052 NANCY CEDEX
TÉL : 03 54 50 54 00
CONTACT@UNIV-LORRAINE.FR
WWW.UNIV-LORRAINE.FR

Modélisation des Procédés de Polymérisationen Émulsion et d'Extrusion Réactive pour le Greffage sur Polypropylène

Résumé

Cette thèse se compose de deux parties. Dans la partie I, nous avons comparé les différences entre les polymérisations en macro- et mini- émulsion. Nous avons établi un modèle de polymérisation en macro-émulsion. Ce modèle peut prédire la distribution de la taille de la chaîne radicalaire pour une classe donnée de tailles des particules. Par comparaison, nous avons établi un modèle de polymérisation en mini-émulsion. Ce modèle peut fournir la distribution des tailles des particules et l'évolution des tailles des gouttelettes. Dans la partie II, afin d'améliorer les propriétés du PP, deux types de monomères ont été utilisés pour être greffés sur PP par extrusion réactive. Ces monomères sont l'anhydride maléique MAH et le silane. Pour améliorer le degré de greffage de MAH sur PP, la montmorillonite organiquement modifiée o-MMT a été utilisée comme un nanoréacteur. Les influences des quantités de MAH et d'initiateur ont été étudiées. Afin d'améliorer le degré de greffage du silane sur PP, les conditions opératoires ont été étudiées. Toutefois, une relation simple entre les propriétés du produit et les conditions de fonctionnement n'a pas pu être trouvée. Pour obtenir le montant le plus élevé de silane greffé sur PP, et en même temps, restreindre les deux réactions secondaires, c'est à dire la polymérisation du silane et la dégradation de la PP chaîne, modèles polynomiaux ont été tentées pour décrire ce processus.

Mots-Clefs: émulsion, polymérisation, mini-émulsion, modélisation, extrusion réactive, nanoréacteur, optimisation multi-objectif

Modelling of Emulsion Polymerization and a Reactive Extrusion Process of Grafting of Polypropylene

Abstract

This thesis consists of two parts: In Part I, the differences between macro-and mini-emulsion polymerization were compared. A model on macro-emulsion polymerization has been established. This model can predict the radical chain size distribution for a given class of particle sizes. By comparison, a model on mini-emulsion polymerization has been established. This model can provide the particle size distribtution and the change of droplets size. In Part II, in order to improve the properties of PP, two kinds of monomers were used to be grafted on PP by reactive extrusion. These monomers were maleic anhydride (MAH) and silane. To improve the grafting degree of MAH on PP, organically modified montmorillonite (MMT) was used as a nanoreactor. The effects of the amounts of MAH and the initiator was studied. In order to improve the grafting degree of silane on PP, the operating conditions were studied. However, a simple relation between the product properties and the operating conditions could not be found. To obtain the highest amount of silane grafted on PP, and meanwhile, restraining the two side reactions, i.e. the polymerization of silane and the PP chain degradation, polynomial models were attempted to describe this process.

Keywords: emulsion polymerization, mini-emulsion polymerization, modelling, reactive extrusion, nanoreactor, Multi-objective optimization